Depletion of the RNA Helicase SKIV2L2 Impedes Mitotic Progression and Histone mRNA Turnover in Murine Cell Lines

Alexis Marie Onderak
Marquette University

DEPLETION OF THE RNA HELICASE SKIV2L2 IMPEDES MITOTIC PROGRESSION AND HISTONE MRNA TURNOVER IN MURINE CELL LINES

By

Alexis M. Onderak

B.S. 2012, Marquette University

A Dissertation submitted to the Faculty of the Graduate School,

Marquette University,

in Partial Fulfillment of the Requirements for

the Degree of Doctor of Philosophy

Milwaukee, Wisconsin

December 2016

ABSTRACT
DEPLETION OF THE RNA HELICASE SKIV2L2
IMPEDES MITOTIC PROGRESSION AND
HISTONE MRNA TURNOVER IN
MURINE CELL LINES

Alexis M. Onderak

Marquette University, 2016

RNA surveillance via the nuclear exosome requires cofactors such as the helicase SKIV2L2 to process and degrade certain noncoding RNAs. This dissertation aimed to characterize the phenotype associated with RNAi knockdown of SKIV2L2 in two murine cancer cell lines: Neuro2A and P19. *Skiv2l2* knockdown in Neuro2A and P19 cells induced changes in gene expression indicative of cell differentiation and reduced cellular proliferation. Analysis of the cell cycle revealed defective progression through mitosis following SKIV2L2 depletion. These results indicate that SKIV2L2 enhances mitotic progression, thereby maintaining cancer cell proliferation and preventing differentiation. Indeed, SKIV2L2 levels were found to be downregulated during chemically induced differentiation, further implicating SKIV2L2 in maintaining proliferation and multipotency in cancer cell lines.

Because SKIV2L2 targets RNAs for processing and degradation via the nuclear exosome, it was hypothesized that with SKIV2L2 depletion, the accumulation of some RNA target triggers mitotic arrest. In search of such a target, RNA-seq was utilized to identify RNAs that were elevated in *Skiv2l2* knockdown cells. SKIV2L2 depletion resulted in the accumulation of non-coding RNAs, intergenic RNAs, ribosomal protein mRNAs, and replication-dependent histone mRNAs. Given that the regulation of histone mRNAs is tightly linked to the cell cycle, further experiments were conducted to confirm SKIV2L2 targets histone mRNAs for degradation. RNA immunoprecipitation demonstrated direct binding between SKIV2L2 and histone mRNAs, and RNA degradation assays showed that the half-life of histone mRNAs doubles with SKIV2L2 depletion. The resulting histone imbalance following loss of SKIV2L2-directed RNA surveillance could impede mitotic progression, resulting in mitotic defects and indirectly triggering differentiation

ACKNOWLEDGMENTS

Alexis M. Onderak

I would like to first and foremost thank my advisor, Dr. Anderson, for his guidance and support throughout my dissertation research. He played such an important role in helping me develop as a scientist. I appreciated all his help and patience along the way. During my time in the Anderson laboratory, I lost both my grandfather and godfather, and I am grateful for Dr. Anderson's compassion during those tough times.

I would also like to thank my committee members: Dr. Abbott, Dr. Maki, Dr. Petrella, and Dr. Schlappi. I thoroughly enjoyed learning from each one in the classroom, and I appreciated their criticisms and suggestions for my research. Each committee member pushed me to see things in a different light and more importantly instilled in me a great enthusiasm for biology, for which I am very grateful.

My research would not have been possible without the support of my fellow members of the Anderson laboratory: Dr. Jane Dorweiler, Yan Li, and Fengchao Wang. They helped me navigate and learn about both benchwork and genomic data analysis. Also, much gratitude is extended to the undergraduates Ryan O'Toole and Oleg Nagorny.

I would also like to thank the Hristova laboratory members for technical support and use of their qPCR machine, the Schlappi laboratory for use of the UVP imaging system, the Yang laboratory for instruction on use of their GFP microscope, and the Petrella laboratory for help with the inverted microscope. I am also appreciative of all the faculty, students, and staff that not only help the Marquette Biological Sciences Department run smoothly but also make it an enjoyable workplace.

Finally, I would like to thank my family and friends for their never-ending love and support. My family served as my rock throughout graduate school, always willing to listen and offer reassurance, and I am thankful to be surrounded by such kind and loving individuals.

TABLE OF CONTENTS

LIST OF TABLES

LIST OF FIGURES

LIST OF ABBREVIATIONS

ΔCq- change in quantification cycle

μM- microMolar

μm- micrometer

A- adenosine

ActB- β-actin

ATRA- all-trans retinoic acid

bp- base pair

cAMP/PKA- cyclic adenosine monophosphate/protein kinase A

Cdk-cyclin dependent kinase

ChAT- acetylcholine transferase

CHIP- chromatin immunoprecipitation

CLIP- cross-linked immunoprecipitation

CRAC- Cross-linking and analysis of cDNA

CUT- cryptic unstable transcript

DMSO- dimethyl sulfoxide

DNA- deoxyribonucleic acid

eRNA- enhancer RNA

ES cell- embryonic stem cell

Fabp3- Fatty acid binding protein 3

FACs- fluorescent activated cell sorting

FBS- fetal bovine serum

FSC-A- forward scatter area

G0-Gap 0

G1- Gap 1

G2- Gap 2

H3pS10- histone H3 phosphorylated at serine 10

IgG- immunoglobulin G

iPSCs- induced pluripotent stem cells

JAK/STAT-Janus kinase/signal transducers and activators of transcription pathway

kD- kilo Dalton

lncRNA- long non-coding RNA

M- $\log_2$(fold change)

miRNA- microRNA

M phase- Mitosis

MPP6- mitotic phosphoprotein 6

mRNA- messenger RNA

MTT- Thiazolyl Blue Tetrazolium Blue

n-number of biological replicates

N2a- neuro2A

ncRNA- non-coding RNA

NEXT complex- **N**uclear **ex**osome **t**argeting complex

nm- nanometer

NMD- nonsense mediated decay

NPAT- Nuclear Protein, Ataxia-Telangiectasia Locus

Oligo-dT- oligonucleotide deoxy-thymidine

PAPD5-PAP Associated Domain Containing 5

PCNA- profilerating cell nuclear antigen

PI- propidium iodide

piRNA- piwi-interacting RNA

PROMPT- promoter upstream transcript

q- q-value (false discovery rate)

qRT-PCR- quantitative Real-Time reverse transcription-polymerase chain reaction

RefSeq- NCBI Reference Sequence

RIP- RNA immunoprecipitation

RNA- ribonucleic acid

RNAi- RNA interference

RNAse- ribonuclease

RNA-seq- RNA sequencing

rRNA- ribosomal RNA

Rrp6/40- ribosomal RNA processing 6/40

S- Synthesis

SD- standard deviation

siRNA- silencing RNA

SKIV2L2- Superkiller viralicidic activity 2-like 2

SLBP- stem-loop binding protein

snoRNA- small nucleolar RNA

snRNA- small nuclear RNA

Sox2-SRY (sex determining region Y)-box 2

SSC-H- side scatter height

TA- transcript abundance

TH- tyrosine hydroxylase

TRAMP complex- **Tr**f4/**A**ir2/**M**tr4 **p**olyadenylation complex

$tRNA_i^{MET}$- initiator transfer RNA methionine

Tubb3- β-tubulin-III

UCSC Genome Browser- University of California, Santa Cruz Genome Browser

UTR- untranslated region

UV-ultraviolet

CHAPTER I: INTRODUCTION

1.1 RNA surveillance

During the course of transcription and post-transcriptional processing, certain aberrant RNAs arise in the cell, being expressed at the wrong time or the wrong form. With the cell depending on the expression of coding and non-coding RNAs, several quality control mechanisms exist within the cell to ensure that each RNA transcript is expressed in the correct cell type at the proper time, localized to the appropriate subcellular locale, and correctly processed to aid in the function of the RNA. RNA surveillance directs RNA processing and degradation to prevent the detrimental accumulation of incorrectly processed or expressed RNAs in the cell. To accomplish the quality control of RNAs, RNA surveillance detects, tags, and directs RNAs to nucleases for processing or degradation (Andersen, 2008). While RNA surveillance mechanisms have been characterized, and complications in RNA surveillance are linked to disease states, the importance of these mechanisms in cellular processes and overall health has not been clearly defined. This dissertation investigates the role of RNA surveillance in proliferating cells and establishes which RNAs are targeted for processing and degradation to maintain cell health and function.

RNA surveillance consists of multiple types of quality control mechanisms and protein complexes within the cell (Schmidt, 2013). Types of RNA surveillance can be characterized by the location and class of RNA targeted for processing and degradation. While similar in overall function, the detailed mechanisms behind RNA surveillance are

different for nuclear versus cytoplasmic RNAs and coding RNAs versus non-coding RNAs. Much of mRNA surveillance occurs in the cytoplasm and depends on translation (J Lykke-Andersen, 2014). As the ribosome translates mRNAs, nonsense mediated decay recognizes premature stop codons, which often arise during splicing, and degrade the mRNA so that it will not be translated into a potentially deleterious truncated protein (Chang, 2007). Other mRNA surveillance mechanisms, such as nonstop decay and no-go decay, trigger the degradation of transcripts that cause the ribosome to stall (J Lykke-Andersen, 2014). Certain mRNAs utilize these pathways so that the mRNA is degraded under specific conditions. For example, replication-dependent histones are transcribed at high levels during S phase but are rapidly turned over upon entry into G2 phase (Marzluff, 2008). This turnover at the end of S phase has been previously linked to the translational machinery and the nonsense-mediated decay factor Upf1 (Kaygun, 2005). Researchers have found that at the end of S-phase, histone mRNAs are oligouridylated, and SLBP, a protein bound to the 3' stem loops of histone mRNAs, associates with the decay factor Lsm1 (Zhang, 2012; Mullen, 2008). As a result, the histone mRNAs are de-capped and degraded by the exoribonuclease Xrn1 and the cytoplasmic exosome (Kaygun, 2005).

Because non-coding RNAs differ from mRNAs in structure and function, non-coding RNA surveillance requires unprocessed or aberrant RNAs to be detected, tagged, and directed to nucleases for processing or degradation without the assistance of translational machinery (Andersen, 2008). More recently, non-coding RNAs, such as microRNAs, long non-coding RNAs, and spurious transcripts, have been discovered to arise from what was previously characterized as “junk DNA.” The majority of these non-

coding RNAs are processed in the nucleus, with many functioning in the nucleus as well. Because understanding how, when, and why these RNAs are degraded offers insight into their regulation and function, RNA surveillance mechanisms that target non-coding RNAs for processing and degradation within the nucleus are of particular interest and are highlighted in this dissertation.

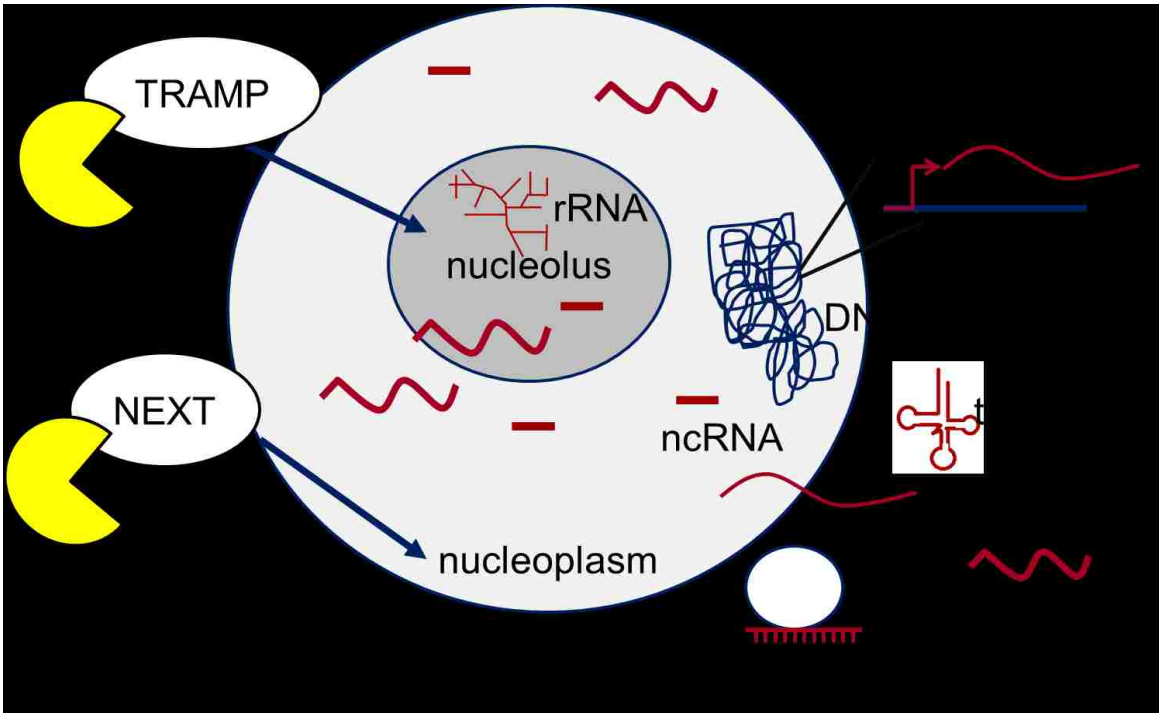

Fig 1.1. Mammalian nuclear RNA surveillance. In the mammalian nucleus, RNA surveillance influences the turnover and processing of RNAs. Two complexes, the TRAMP and the NEXT complex, partner with the nuclear exosome (yellow) to target various classes of RNAs for degradation in the nucleolus and nucleoplasm, respectively.

1.2 The nuclear TRAMP Complex

In the nucleus and nucleolus, RNA surveillance centers on targeting RNAs to the nuclear exosome (Fig 1.1). Highly conserved, the eukaryotic nuclear exosome consists of

a 9-subunit catalytically inactive core, a trimeric cap that binds RNA, and accessory proteins consisting of both endonucleases and exonucleases, such as Rrp44 and Rrp6 (Lykke-Anderson, 2009). The 3'→5' exoribonucleolytic activity of the nuclear exosome requires a series of cofactors for preparation and delivery of RNA substrates to facilitate their processing and degradation (Houseley, 2006). One such complex of cofactors, the Trf4/Air2/Mtr4 polyadenylation (TRAMP) complex, was first discovered in *Saccharomyces cerevisiae* (Houseley, 2006; La Cava, 2005). The yeast TRAMP complex consists of the non-canonical poly-A-polymerase Trf4/5p, the RNA binding protein Air1/2p, and the helicase Mtr4p. The TRAMP complex exists in two forms, TRAMP4 (Trf4p/Air1/2p/Mtr4p) and TRAMP5 (Trf5p/Air1p/Mtr4p).

While the mechanism behind TRAMP complex recognition of target RNAs remains elusive, the action of the TRAMP complex on such targets has been extensively studied (Fig 1.2). The TRAMP complex tags the 3' end of nuclear RNAs to be degraded with adenosines, guides those RNAs to the exosome, and then activates the exonucleolytic activity of the exosome (Lykke-Anderson, 2009; Houseley, 2006; La Cava, 2005). More specifically, Air1/2p binds RNA substrates through a series of five zinc knuckles, and Trf4/5p, which lacks an RNA binding domain, adenylates the RNA transcript (La Cava, 2005). The short A-tail added by Trf4/5p not only allows for exosome substrates to be distinguished from RNAs stabilized by a longer poly-A-tail (Andersen, 2008) but also creates a 5-6 nucleotide overhang on the 3' end that is preferentially bound by the helicase Mtr4p (Anderson, 2008; Jia, 2012). Mtr4p is necessary to unwind any secondary structure that would impede entry into the nuclear exosome (La Cava, 2005; Jia, 2012), and the binding of the TRAMP complex to the

nuclear exosome stimulates exonucleolytic activity to promote 3'end trimming or degradation of the transcript (Andersen, 2008). In yeast, the TRAMP complex has been found to be essential in RNA surveillance of several transcripts, including the turnover of hypomodified $tRNA_i^{MET}$ (Wang, 2007), 3' end trimming of the 5.8S rRNA (de la Cruz, 1998) and processing of the 7S rRNA precursor (Callahan, 2009), degradation of cryptic unstable transcripts (CUTs) arising from heterochromatic regions (Thiebaut, 2006), and efficient splicing and intron degradation (Kong, 2013; Nag, 2012).

The TRAMP complex components are found across the domain Eukarya, with extensive studies on their function being done in yeast, *Arabidopsis*, and teleost fish (La Cava, 2005; Lange, 2011; Cox, 2011). Recently, the homologs of the yeast TRAMP complex were found to be highly conserved in mammals (Fig 1.3), with the poly-A-polymerase PAPD5 having 37% amino acid sequence identity to Trf4p in its catalytic domain, ZCCHC7 showing similarity to Air1p in its five zinc knuckles, and SKIV2L2 retaining 51% amino acid sequence identity with the helicase Mtr4p (Schmidt, 2013; Norbury, 2011). This mammalian TRAMP complex is hypothesized to target RNAs for degradation and processing through adenylation, similar to its yeast counterpart. However, in addition to the TRAMP complex, mammalian SKIV2L2 interacts with the zinc knuckle protein ZCCHC8 and the putative RNA binding protein RBM7 to form the Nuclear Exosome Targeting (NEXT) Complex (Norbury, 2011; Lubas, 2011), which lacks a poly-A-polymerase and therefore must target RNAs through a unique mechanism (Fig 1.3). Studies suggest that the TRAMP complex's location and RNA targets may be primarily nucleolar, while the NEXT complex appears to be located in the nucleoplasm and targets nuclear RNAs (Lubas, 2011).

Research focused on identifying substrates of the mammalian nuclear exosome has demonstrated that SKIV2L2 is necessary for the maturation of ribosomal RNA precursors, including 3' end trimming of 5.8S rRNA (Schilders, 2007; Lubas, 2015), and facilitates the degradation of PROMPTs (promoter upstream transcripts) in concert with the NEXT complex (Tiedje, 2014). Furthermore, PAPD5 has been shown to bind RNA independent of the TRAMP complex (Rammelt, 2011) and modify miRNAs in vivo to alter their stability (Boele, 2014). The evolution of the mammalian TRAMP complex to perform functions beyond those seen in yeast suggests that RNA surveillance may have many roles to play in multicellular organisms, particularly in coordinating changes in the expression of RNAs involved in mammalian development.

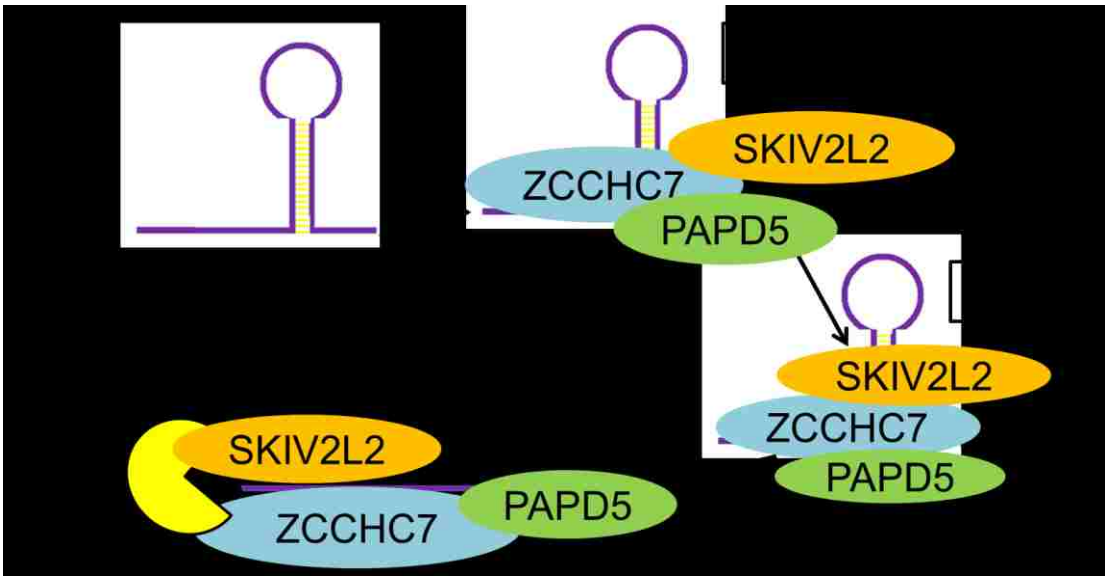

Fig 1.2. Predicted TRAMP complex mechanism of action. The TRAMP complex is thought to target RNAs to the nuclear exosome in three steps: first (1), the RNA is bound by the TRAMP complex members, second (2), PAPD5 adenylates the 3' end of the RNA, and third (3), SKIV2L2 unwinds the RNA and delivers the RNA to the nuclear exosome.

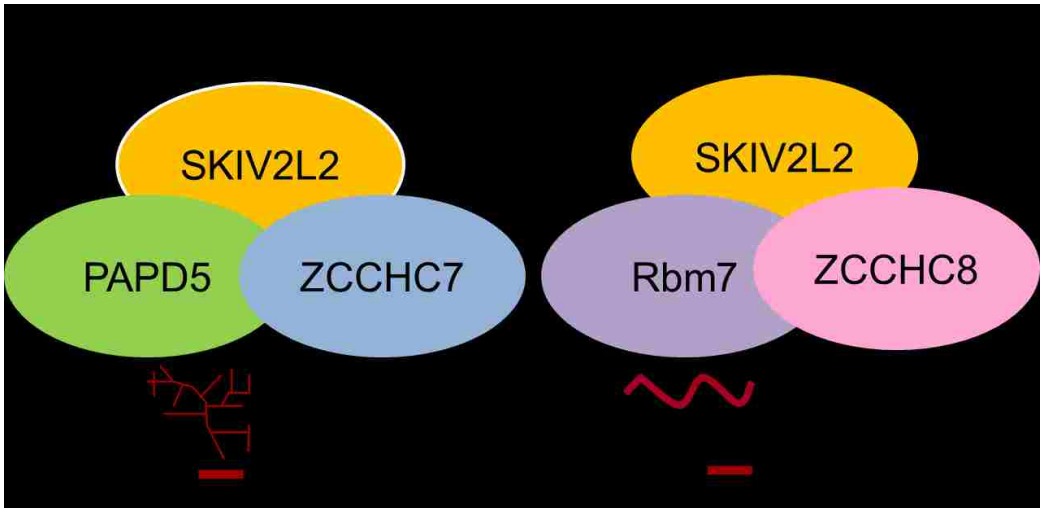

Fig 1.3. Mammalian nuclear RNA surveillance requires two complexes. SKIV2L2 functions in two known complexes: the TRAMP complex in the nucleolus and the NEXT complex in the nucleoplasm. Verified TRAMP RNA targets include rRNA and snoRNAs, while verified NEXT RNA targets include lncRNAs and PROMPTs.

1.3 SKIV2L2 functions as a helicase in RNA decay pathways

Because the helicase SKIV2L2 plays a central role in both the TRAMP and the NEXT complex, it acts as the key player in mammalian nuclear RNA surveillance. SKIV2L2, and its yeast homolog Mtr4p, both are categorized as SF2 helicases (Johnson, 2013). The SF2 superfamily helicases share two RecA domains that are essential for the core helical function (Johnson, 2013). The SF2 superfamily contains many different RNA and DNA helicases that vary widely based on their function in the cell and their mechanism of action. Despite large differences between the helicases, the SF2 superfamily is divided into families of helicases based on structure and unwinding mechanism. The DExD/H helicase family consists of three types of SF2 helicases: DEAD box helicases, DEAH helicases, and Ski2 helicases. While SKIV2L2 and Mtr4p fall

under the Ski2 helicase category, they also share properties with other DEAD box helicases, making both groups of helicases relevant to understanding how SKIV2L2 functions in nuclear RNA surveillance. (Johnson, 2013)

DEAD-box helicases are unique from other SF2 helicases in that they contain the amino acid sequence DEAD (Jarmoskaite, 2011). The yeast Mtr4p and human homolog SKIV2L2 function similar to DEAD-box helicases, as they both have ATPase-dependent 3'→5' RNA helicase activity (Norbury, 2011; Weir, 2010). DEAD-box helicases bind to ssRNA or dsRNA tightly when bound to ATP, but as ATP is hydrolyzed to ADP, the affinity of the helicase for RNA decreases, and the helicase "translocates" along the RNA (Jarmoskaite, 2011). As ATP is bound, hydrolyzed, and released, strand separation occurs, coupling RNA unwinding with ATP hydrolysis. However, DEAD-box helicases are not very processive and only unwind or remodel short RNA duplexes (Jarmoskaite, 2011). With both DEAD-box and Ski2 helicases, the helicase binds non-specifically to the sugar-phosphate backbone of the RNA, and binding specificity comes from the interaction of the helicase with other proteins or RNPs (Jarmoskaite, 2011). More specifically, Mtr4p and SKIV2L2 are classified as members of the Ski2 helicase family. Ski2 helicases have two additional domains, the winged helix domain and the ratchet domain, which along with the two RecA domains form a unique ring-like tertiary structure (Johnson, 2013). This unique structure allows for single stranded RNA to be fed through the core of the helicase. Ski2 helicases, which function primarily in RNA decay, are usually part of protein complexes that help mediate specific binding of RNAs (Johnson, 2013).

There are two major Ski2 family helicases, Ski2 and Mtr4p/SKIV2L2, and both are required for exosome activation. Both Ski2 and Mtr4p/SKIV2L2 separate RNA duplexes, and the resulting 3' end of the ssRNA is actively fed into the exosome as the helicase translocates along the RNA (Johnson, 2013). In the cytoplasm, Ski2 complexes with Ski3 and Ski8, and the Ski complex directs the degradation of RNAs via the exosome in the cytosol (Johnson, 2013). In the nucleus, Mtr4p/SKIV2L2 interacts with different proteins to form the TRAMP complex, common to most eukaryotes, and the NEXT complex found in mammals (Fig 1.3). While Ski2 does not interact directly with the exosome, SKIV2L2 directly binds to two nuclear exosome components in humans: MPP6 and PM/Scl-100 (Rrp6) (Johnson, 2013; Lubas, 2011). SKIV2L2 and the yeast Mtr4p both contain a distinguishing arch domain thought to facilitate this interaction (Johnson, 2013). In humans, this arch domain is necessary for the degradation of RNAs via Rrp6 but not for the degradation of RNAs via Rrp44 (Johnson, 2013). This essential arch domain, which is similar to that found in ribosomal proteins, results in a preference for binding RNA with a short 3' overhang (Jackson, 2010; Weir, 2010). Together, these properties define SKIV2L2 as a helicase that has uniquely evolved to unwind short duplexes in RNA, feed the RNA directly into the nuclear exosome, and activate the degradation or 3' end trimming of that RNA.

1.4 Stem cells are maintained through a variety of mechanisms

This dissertation evaluates SKIV2L2, and therefore nuclear RNA surveillance, as a potential factor in stem cell maintenance. Before delving deeper into the role of RNA surveillance in stem cells, it is necessary to understand what characterizes stem cells and

how stem cells are maintained. Stem cells have the potential to develop into multiple cell lineages. Stem cells can be further classified into totipotent, pluripotent, or multipotent. Totipotent cells can differentiate into all embryonic and extraembryonic tissue types, pluripotent cells can differentiate into embryonic endoderm, mesoderm, and ectoderm tissues, and multipotent cells can give rise to multiple, but not all, cell types (He, 2009). This totipotency and pluripotency is essential during development because one fertilized zygote must give rise to all the cells in the body through cell division and subsequent differentiation. In addition to maintaining pluripotency in the developing embryo, adult organisms have stem cell pools, which mostly contain multipotent stem cells that produce new cells to replenish old cells. For example, bone marrow contains stem cells that produce new blood cells, and stem cells located near hair follicles produce new epithelial cells. These stem cells are located in particular niches, which maintain the stem cell's ability to proliferate and differentiate into multiple lineages. (Morrison, 2008)

Various mechanisms are involved in stem cell maintenance, and each stem cell niche is unique. However, commonalities exist in stem cell maintenance, including cell signaling, transcription factors, and epigenetic factors, which work together to control the expression of genes necessary for self-renewal. Self-renewal means that as the cell divides, the cell maintains the potential to differentiate into multiple lineages. With asymmetric self-renewal, one cell retains pluripotency and continues to proliferate, while the other daughter cell leaves the stem cell niche and receives signals to differentiate into a specific cell type (He, 2009; Morrison, 2008). Self-renewal requires that extracellular signals from the niche regulate the expression of different proto-oncogenes, which support proliferation and pluripotency, and tumor-suppressors, which limit self-renewal

and protect against propagating DNA damage to daughter cells (He, 2009). The JAK/STAT, BMP, Wnt, Notch, CXCL12, and Hedgehog signaling pathways work in different stem cell niches to maintain self-renewal (Morrison, 2008). These signaling pathways regulate the expression of proto-oncogenes and tumor-suppressors. The most well-characterized instance of this is that signaling pathways regulate the expression of the pluripotency transcription factors Oct4, Sox2, Klf4, c-Myc, and Nanog. In turn, these transcription factors repress developmental genes and activate the expression of genes necessary for pluripotency and self-renewal (Liu, 2013a). For example, during reprogramming of iPSCs, Nanog directs Tet1 and Tet2 to pluripotency genes, where Tet1 and Tet2 remove cytosine methylation to epigenetically reactivate genes necessary for self-renewal (Costa, 2013). In stem cells, these signaling pathways must also activate tumor suppressors that prevent damaged stem cells from self-renewing, such as p53 and Rb, which trigger cell senescence and death in response to DNA damage (Morrison, 2008).

Stem cell maintenance must be tightly regulated throughout each developmental stage of life. Premature loss of stem cell pools negatively impacts development, and stem cell pools diminish as self-renewal decreases with age (He, 2009). On the other hand, cancer cells inappropriately express pluripotency and self-renewal factors, and some cancer cells take on the proliferative and multipotent nature of stem cells. In certain tumors, cancer stem cells express pluripotency factors like Nanog, Sox2, and Oct4, which drive self-renewal and tumorigenesis (Liu, 2013a). These cancer stem cells, which are found in mouse tumors like those that are immortalized into cell lines, approximate the behavior of stem cells because cancer stem cells are self-renewing, proliferative, and

multipotent. Therefore, understanding which factors are necessary for stem cell maintenance is important for the study of developmental diseases and aging-associated diseases, where stem cell pools may be diminished, and cancer, where cells take on stem cell characteristics.

This dissertation explores the possibility that RNA surveillance influences stem cell maintenance. In human cells, cytoplasmic NMD factor Upf1 must be downregulated during differentiation, and NMD influences both the TGF-β and BMP signaling pathways involved with maintaining stem cell niches and directing differentiation of daughter cells (Lou, 2016). However, it is unclear why nonsense-mediated decay must be downregulated during differentiation or if the regulation of other RNA surveillance pathways differs between stem cell niches and differentiated cells. This dissertation centers on the hypothesis that SKIV2L2-mediated RNA surveillance might also have a role to play in stem cell maintenance and differentiation.

1.5 The potential role of SKIV2L2 in development

In support of a role in stem cell maintenance and differentiation, SKIV2L2 has been implicated in animal development. Forward genetic screens in zebrafish identified SKIV2L2 as a possible factor in stem cell maintenance, as mutant zebrafish have reduced eye and brain size and lack the ability to regenerate melanocytes after cell ablation or regrow tails after surgical removal (Cox, 2011; Yang, 2007; Hultman, 2010). In the closely related medaka fish, *Skiv2l2* mutants fail to develop the thymus or spleen (Iwanami, 2009), suggesting that SKIV2L2-directed RNA surveillance may be of significance to immune system development. In zebrafish, *Skiv2l2* mRNA co-localizes

with the cell proliferation marker PCNA (Yang, 2007), indicating that *Skiv2l2* expression is enhanced in actively dividing populations of stem cells. Taken together, the phenotype associated with loss of SKIV2L2 in fish indicates that SKIV2L2 may help maintain stem cell populations. In mammals, large-scale RNAi screens identified a possible correlation between SKIV2L2 depletion, impaired cell division, and death of embryonic stem cells (ES cells). However, the results of these studies were preliminary, often inconsistent, and not explored in depth (Fazzio, 2008; Neumann, 2010).

Additionally, an extensive bioinformatic study used microarray data from stem cells before and after differentiation to determine genes in the mouse genome whose expression correlates with pluripotent embryonic stem cells. It was found that *Skiv2l2* falls within the top 2% of genes whose expression is positively correlated with pluripotent embryonic stem cells and negatively correlated with differentiated cells (Cinghu, 2014). Developmental downregulation of *Skiv2l2* has also been observed in the testes where SKIV2L2 levels decline in response to testosterone during spermatogenesis (Osman, 2011). Because *Skiv2l2* expression and function appear to be important in development, this dissertation focuses on discerning how SKIV2L2, and therefore RNA surveillance, might affect pluripotency and differentiation in mammalian cancer cell lines.

Stem cell maintenance requires that cell signaling pathways regulate the expression of genes necessary for pluripotency and self-renewal. During differentiation, the transcriptome changes so that pluripotency and proliferation genes are repressed and one set of cell-fate specific genes are activated (Guttman, 2011; Choi, 2013). The ability of the stem cell to maintain expression of pluripotency and proliferation genes while

repressing differentiation genes often depends on microRNAs (Wang, 2008), long noncoding RNAs (lncRNAs) (Guttman, 2011), and other noncoding RNAs, which may be targets of nuclear RNA surveillance. If these RNAs are targets of nuclear RNA surveillance, SKIV2L2 may help regulate their steady-state levels in the cell and influence stem cell maintenance and differentiation.

1.6 Aims and Hypotheses

Because the TRAMP and NEXT complexes target specific nucleolar and nuclear RNAs to the exosome (Lubas, 2011; Lubas, 2015), these RNA surveillance complexes also determine which RNAs persist in the cell. This notion led to the hypothesis that RNA surveillance may play a role in cell proliferation or pluripotency by altering the stability and/or processing of nuclear RNAs. To study this, cancer cell lines, which consist of cancer stem cells that exhibit stem cell like properties, were used to define the phenotype associated with *Skiv2l2* knockdown, and consequently depletion of SKIV2L2-mediated RNA surveillance. Neuro2a (N2a) cells derived from a murine neuroblastoma (Nilbratt, 2009; Tremblay, 2010; Zhi, 2012) and P19 cells derived from a murine embryonic teratocarcinoma (Jasmin, 2010) were used to investigate the role of SKIV2L2 in proliferation and differentiation. These mammalian cancer cell lines provide a system to investigate cell proliferation and model differentiation, as chemicals induce the differentiation of N2a cells into neurons (Nilbratt, 2009; Tremblay, 2010) and P19 cells into either neurons or myocytes (Jasmin, 2010; Dong, 2012). To classify the phenotype associated with loss of SKIV2L2-mediated RNA surveillance, both N2a and P19 cells

were treated with *Skiv2l2* siRNA and compared to both control cells and chemically differentiated cells.

1.7 Summary of Findings

This dissertation characterizes the anti-proliferative effects associated with SKIV2L2 depletion and identifies RNA substrates of SKIV2L2 which could be responsible for mediating developmental changes. *Skiv2l2* knockdown cells were found to exhibit changes in cell morphology and gene expression associated with cellular differentiation, including an increase in cell-fate specific gene expression and a decrease in the expression of pluripotency genes. *Skiv2l2* knockdown via RNAi also reduced cellular proliferation, which was found to be particularly attributed to defective progression through mitosis.

Little is known about the mammalian TRAMP complex are still in their infancy, and no previous studies have analyzed the role of SKIV2L2 in mammalian cells. By coupling large-scale RNA-seq with molecular techniques targeting specific RNA transcripts, this research defined the phenotype associated with loss of SKIV2L2 in mammalian cells, determined which cellular processes are controlled by RNA surveillance, and identified novel RNA targets of SKIV2L2. Following observation of mitotic arrest after SKIV2L2 depletion, RNA-seq was performed to identify RNAs accumulating in *Skiv2l2* knockdown cells that could impede progression through mitosis. While previous research has uncovered non-coding RNAs targeted for processing and degradation by the TRAMP and NEXT complexes, this research uncovered both non-coding and coding RNAs to be targets of nuclear RNA surveillance. Previous classes of

non-coding RNAs known to be TRAMP and NEXT complex targets were investigated in mouse and human cells, with this research detecting miRNA 5' leader sequences (Dorweiler, 2014), snoRNAs (Berndt, 2012; Lubas, 2015), rRNAs (Schilders, 2007; Lubas, 2015), PROMPTs (Tiedje, 2014), and lncRNAs (Beaulieu, 2012) targeted by SKIV2L2 for degradation or processing. While non-coding RNAs represent one class of nuclear RNA surveillance targets, elevated levels of replication-dependent histone mRNAs following loss of SKIV2L2-directed RNA surveillance suggest that SKIV2L2 mediates the turnover of certain mRNAs as well. Because histone mRNAs lack a poly-A-tail like many non-coding RNAs (Marzluff, 2008), it reasons that the nuclear turnover of histone mRNAs may be similar to that seen for non-coding RNAs. While the cytoplasmic turnover of histones via nonsense mediated decay has been extensively studied (Kaygun, 2005; Mullen, 2008), this dissertation presents evidence that SKIV2L2 is involved with nuclear turnover of histone mRNAs. SKIV2L2 directly binds histone mRNAs, as demonstrated through RNA immunoprecipitation (RIP), and SKIV2L2 depletion leads to a doubling of histone mRNA half-life. With *Skiv2l2* knockdown, histone mRNAs fail to be properly turned over at the end of S phase, leading to a histone imbalance, which has previously been shown to disrupt mitosis (Singh, 2010; Meeks-Wagner, 1986; Günesdogan, 2014). This study presents novel findings that link RNA surveillance via SKIV2L2 to mammalian cellular proliferation.

1.8 Significance of Findings

By exploring which RNAs are targeted by SKIV2L2 for processing and degradation and how loss of SKIV2L2 affects cellular health, RNA surveillance was

found to be an integral part of maintaining cell proliferation in two murine cancer cell lines. While the techniques utilized are not exceptionally novel, this dissertation offers an in-depth characterization of SKIV2L2 function in a mammal, which has not previously been accomplished, and presents evidence supporting a nuclear pathway for the degradation of histone mRNAs, a process once thought to only occur in the cytoplasm. Additionally, investigating the function of the TRAMP complex in cell proliferation and differentiation has implicated SKIV2L2 and RNA surveillance in stem cell maintenance and tumor growth, with possible implications on cancer treatment, adult neurogenesis, and stem cell therapy.

CHAPTER II: DIFFERENTIATION OF MURINE CELL LINES IS ASSOCIATED WITH DOWNREGULATION OF SKIV2L2 EXPRESSION

2.1 Introduction

Hypothesis: *Skiv2l2* is downregulated in murine cancer cell lines following chemical differentiation.

In light of a previous bioinformatic study drawing a positive correlation between *Skiv2l2* expression and pluripotency in ES cells (Cinghu, 2014), it was hypothesized that *Skiv2l2* was actively downregulated during differentiation. Pluripotent cells have the potential to differentiate into ectoderm, endoderm, or mesoderm cells and can self-renew. Pluripotent cells, such as ES cells and iPSCs, express a series of pluripotency factors that support self-renewal and a chromatin landscape that represses differentiation genes while still allowing for their future activation (Maden, 2007; Guttman, 2011). Pluripotency factors include Oct4, Sox2, Klf4, and c-Myc, which serve as transcriptional activators of genes necessary to maintain pluripotency and self-renewal, including genes involved in signaling pathways and chromatin remodeling (Takahashi, 2006). More recent studies have identified miRNAs and non-coding RNAs that function in maintaining pluripotency (Anokye-Danso, 2011). As pluripotent cells begin to differentiate, there are significant changes in gene expression due to epigenetic, transcriptional, and post-transcriptional changes. For example, a proportion of development genes in ES cells have bivalent promoters with both repressive (H3K27me3) and activating (H3K4me3) chromatin marks (Bird, 2007). Upon differentiation, genes to be expressed will retain the activating H3K4me3 modification, while other genes will maintain the H3K27me3 mark and be

silenced (Bird, 2007). These changes in gene expression also coordinate the upregulation of genes specific to one developmental pathway with the permanent silencing of both pluripotency genes and genes specific to different developmental pathways (Chen, 2008). This silencing can be accomplished through miRNAs, such as let-7, epigenetic silencing via the Polycomb complex, and CpG methylation (Bird, 2007). Given that *Skiv2l2* shares a CpG island promoter with the neighboring gene, Dhx29, *Skiv2l2* could be silenced in a developmental manner during differentiation.

In support of the hypothesis that *Skiv2l2* might be associated with pluripotency and is downregulated during differentiation, co-immunoprecipitation studies have demonstrated protein-protein interactions between *SKIV2L2* and the pluripotency factors Nanog and Sox2 (Cox, 2013; Costa, 2013; Engelen, 2011). Sox2 and Nanog activate the transcription of genes necessary to maintain pluripotency, and Sox2 drives the reprogramming of differentiated cells into induced pluripotent stem cells, as it works in concert with Oct4, c-myc, and Klf4 to upregulate genes necessary for epigenetic reprogramming and maintaining pluripotency (Takahashi, 2006). This establishes a physical connection between SKIV2L2 and pluripotency factors. Transcription factors like Nanog and Sox2 bind to DNA to regulate transcription and epigenetic changes, and it is possible that the physical interaction between Nanog, Sox2, and SKIV2L2 coordintaes their binding to a given location on the genome. Because RNA surveillance often occurs as RNAs are being transcribed, RNA surveillance factors such as SKIV2L2 bind nascent transcripts, tethering the RNA surveillance machinery to a specific genomic location (Lubas, 2015). The association between Sox2, Nanog, and SKIV2L2 could target RNA

surveillance factors to genes bound by Sox2 and Nanog to direct RNA turnover and processing events essential for pluripotency.

Evidence also supports the hypothesis that *Skiv2l2* may be regulated both transcriptionally and post-transcriptionally through signaling pathways known to support cell proliferation or trigger cell differentiation. Chromatin immunoprecipitation coupled with DNA sequencing (ChIP-seq) suggests that multiple transcription factors such as STAT3 (Hutchins, 2013; Chen, 2008), CREB (Lesiak, 2013), E2F1 (Chen, 2008), and Myc (Chen, 2008; Sabo, 2014) bind to the *Skiv2l2* promoter, and a microarray study demonstrated that *Skiv2l2* mRNA increases with cAMP/PKA activation (Guo, 2012). Additionally, the *SKIV2L2* protein has been previously found to be a target of the MAPK-ERK signaling cascade in mice (Sundaram, 2013), and the transcription factor Smad4 has been shown to regulate *Skiv2l2* transcription (Fei, 2010). However, seeing as the majority of these studies were large scale screens, the transcriptional regulation of *Skiv2l2* by these signaling pathways was not investigated in depth. Nevertheless, these findings connect *Skiv2l2* expression signaling pathways that control transcription in pluripotent and differentiating ES cells. Under specific conditions, these signaling pathways are activated to modulate the expression of genes involved in cell proliferation, pluripotency, self-renewal, and differentiation. These signaling pathways all work in different ways to closely regulate stem cell maintenance and properly direct differentiation and development. Additionally, knockdown of mir-297, a miRNA that is depleted in colon cancer (K Xu, 2012), has been shown to result in *Skiv2l2* upregulation (Parikh, 2010), suggesting that *Skiv2l2* is targeted by at least one miRNA necessary to prevent tumor cell proliferation. Given that *Skiv2l2* expression has been linked to

proliferation or pluripotency genes, the possibility that *Skiv2l2* could be downregulated during differentiation was investigated in the following experiments.

2.2 Approach and Results

To determine whether *Skiv2l2* is downregulated upon differentiation, it was first necessary to implement a model for pluripotent cells and differentiating cells. Two murine cancer cell lines were selected for this purpose. Neuro2a (N2a) cells and P19 cells are derived from a male mouse neuroblastoma (Zhi, 2012) and a male mouse embryonic teratocarcinoma of the testes (Dong, 2012), respectively. Both N2a and P19 cells are considered to be multipotent, meaning that they can differentiate into many cell types but not all germ layers. Fetal bovine serum (FBS) is used in culture medium to flood N2a and P19 cells with various growth factors required to sustain this multipotency and keep cells proliferating. Over time, the components of the FBS are exhausted or degraded, leading to differentiation and ultimately cell death (Phillips, 2006). This requires the cells to be passaged periodically into new growth medium with fresh FBS. However, the natural ability of N2a and P19 cells to mirror the physiological differentiation of neuronal stem cells and embryonic stem cells allows them to serve as a model in differentiation studies. The expression of *Skiv2l2* following differentiation was monitored following chemical differentiation using Western blotting to measure protein levels and quantitative RT-PCR (qRT-PCR) to measure mRNA steady-state levels.

Differentiation of N2a and P19 cells can be augmented using both serum starvation and chemical treatment, which result in exit from the cell cycle at G1 phase and terminal differentiation (Tremblay, 2010; Dong, 2012). However, terminally

differentiated N2a and P19 cells cannot be maintained indefinitely in culture, ultimately leading to differentiated cells detaching from the tissue culture plate and undergoing apoptosis. Nevertheless, N2a and P19 cells serve as an excellent model for studying changes in gene expression during differentiation. Treatment of N2a cells with all-trans retinoic acid (ATRA) alone induces differentiation into cholinergic neurons (Tremblay, 2010; Sun, 2010). Additionally, serum starvation where the FBS content is reduced from 10% to 2% of culture volume also triggers N2a cell differentiation, resulting in multiple neuronal cell types (Tremblay, 2010). Growing cells in 20 μM ATRA with 2% FBS enhances N2a cell differentiation, leading to the terminal differentiation of N2a cells into cholinergic neurons (Figure 2.1a). N2a cell differentiation into neurons is readily observed as the extension of neuronal processes. Counting the number of cells exhibiting axon and dendrite extension allows for easy quantification of differentiation (Sun, 2010). Both differentiation and pluripotency markers can also be measured to assess the extent of N2a cell differentiation. For example, proliferating N2a cells express Sox2 at high levels, while terminally differentiated N2a cells express very little Sox2 (Liu, 2013b). During N2a cell differentiation, the axon specific tubulin Tubb3 is upregulated (F Zhi, 2012), and either acetylcholinesterase (ChAT) or tyrosine hydroxylase (TH) are upregulated for cholinergic and dopaminergic neuronal function, respectively (Sidiropoulou, 2008; Tremblay, 2010).

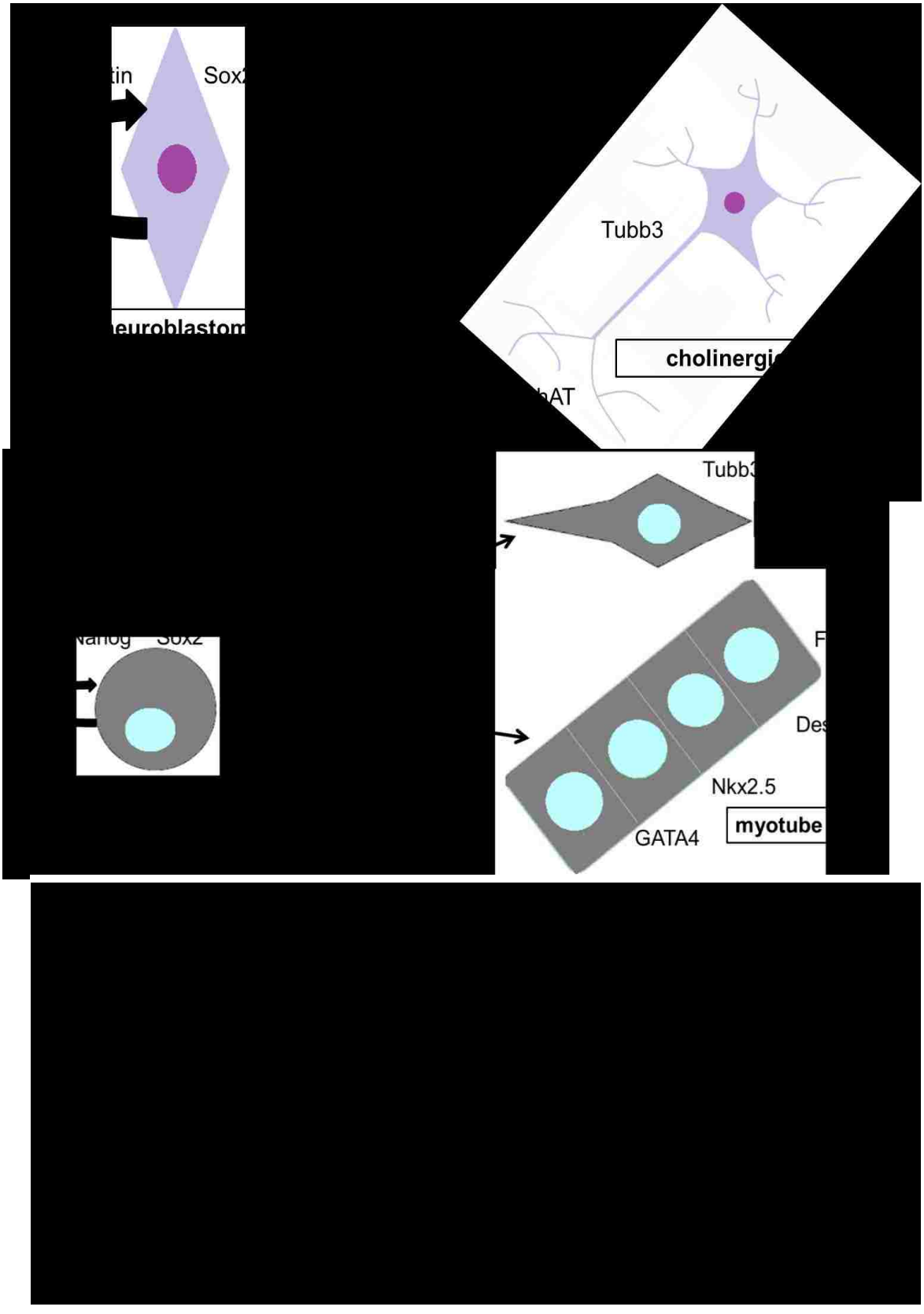
Sox2
Tubb3
cholinergic
ChAT
Tubb3
Nkx2.5
GATA4
myotube

Because cancer cell lines only approximate the behavior of stem cells, both N2a and P19 cells were used to study *Skiv2l2* expression to ensure results were not specific to any one cell line. P19 cells are unique in that they are able to differentiate into a vast array of cell types, including cardiac, skeletal, and smooth muscle myocytes, and multiple neuronal cell types including cholinergic, dopaminergic, and GABAergic neurons (Dong, 2012). Differentiation of P19 cells is accomplished through chemical treatment only, as serum starvation leads to apoptosis (Fig.2.1b). P19 cells can be forced to form embryoid bodies in solution by plating the cells on untreated, polystyrene petri dishes, and treatment of these embryoid bodies with 0.1% DMSO induces terminal differentiation into cardiomyocytes (Jasmin, 2010). P19 cells will also form embryoid bodies during natural differentiation on adherent tissue culture plates in certain conditions such as the natural depletion of FBS (Jasmin, 2010; Dey, 2010). Additionally, P19 cell treatment with ATRA can be utilized to force differentiation into the neuronal cell fates (Dong, 2012). While embryoid body formation is observable, the presence of mixed cell populations makes quantification of differentiation based on cell morphology difficult. For these reasons, measuring differentiation in P19 cells depends on monitoring the pluripotency marker Sox2, which is downregulated during terminal differentiation into all cell types (Dong, 2012). Desmin, an intermediate filament specific to all muscle cell types, and Fabp3, a cardiac muscle marker, are upregulated in P19 cells following differentiation into cardiomyocytes (Choi, 2004; Dey, 2010; Zhu, 2011). The measurement of neuronal differentiation in P19 cells proves more difficult, as P19 cells express Tubb3 due to their testicular origin, and differentiation with ATRA produces an assortment of neuronal cell types. It is worth noting that not all P19 cell lines retain the

ability to be chemically induced to differentiate into all possible cell fates due to the high rate of mutation in cancer cells. Pilot studies demonstrated that ATRA cannot be used to effectively differentiate the P19 cell line utilized in these experiments because ATRA treatment led to substantial cell death. For these reasons, P19 cell differentiation was induced by 0.1% DMSO to form cardiomyocytes. Regardless, N2a and P19 cells provided a model where two different cancer cell lines were differentiated into two different cell types: neurons and myocytes.

2.2.1 N2a and P19 cells differentiate into cholinergic neurons and cardiomyocytes following chemical treatment

To validate the established model for differentiation, the ability to differentiate N2a and P19 cells via chemical treatment was first confirmed. N2a cells were grown in either 10% FBS (control) or 20 μM ATRA with 2% FBS for forty-eight hours, at which point the cells were either observed for changes in cell morphology or harvested for the isolation of protein and RNA (Fig 2.1a). Differentiation was first verified by the extension of axons and dendrites. To better visualize axons and dendrites, N2a cells were stained with the Neuronal Outgrowth Staining Kit®, which stained cell membranes bright orange and viable cell bodies green (Fig 2.2). Neuronal processes were readily seen as bright orange extensions on an inverted microscope. Viable cells (appearing yellow with the overlay of orange and green) extending neuronal processes that were two times the diameter of the cell body in length were considered to exhibit a neuronal cell phenotype. Compared to 1% of cells grown in 10% FBS, 19% of cells grown in 2% FBS, 20 μM ATRA were found to extend neuronal processes (two proportion Z-score= -11.8, p-

value< 0.0001, Fig 2.2). Approximately 1% of both control and chemically differentiated cells were non-viable, as these cells failed to stain with the green viability marker and appeared red. Extending the duration of treatment to 72 hours increased the percentage of cells with neuronal processes in both control cells and chemically treated to 40% and 73%, respectively. Although differentiation at 48 hours was not complete, this time point was selected throughout further studies. Growth past 48 hours without refreshing the medium resulted in significant differentiation of control cells and cell death in chemically treated cells. Therefore, in subsequent RNAi experiments cells were grown for 48 hours to limit cell death.

To determine if chemical treatment of N2a and P19 cells induced changes in gene expression indicative of cell differentiation, RNA isolated from N2a cells grown either in 10% FBS or 20 μM ATRA with 2% FBS was reverse transcribed using oligo-dT to generate cDNA for quantitative PCR analysis. The differentiation markers ChAT and Tubb3 were quantified using ActB as a control (Fig 2.3a). Compared to cells grown in 10% FBS, ChAT and Tubb3 mRNA levels in chemically treated cells increased by 4.3 and 1.9 fold, respectively (p-values< 0.006, 0.01), indicative of increased differentiation. The pluripotency marker Sox2 was found to decrease 2.8 fold in mRNA levels (p-value< 0.002), demonstrating both an upregulation of cholinergic neuron markers and a downregulation of pluripotency markers following serum starvation and ATRA treatment (Fig 2.3a).

P19 cells were analyzed in a similar manner following growth in either 10% FBS or 0.1% DMSO. Cells grown in 0.1% DMSO were found to express 3.3 fold more Fabp3 and 2 fold more Desmin than cells grown in 10% FBS alone, as measured via qRT-PCR

(Fig 2.3b, p-values< 0.0001, 0.02). P19 cells grown in 0.1% DMSO also exhibited a 1.3 fold decrease in Sox2 mRNA levels (Fig 2.3b, p-value< 0.05). Together, these results indicate that DMSO treatment successfully induced differentiation into cardiomyocytes, as demonstrated through the downregulation of Sox2 and the upregulation of Fabp3 and Desmin.

A.

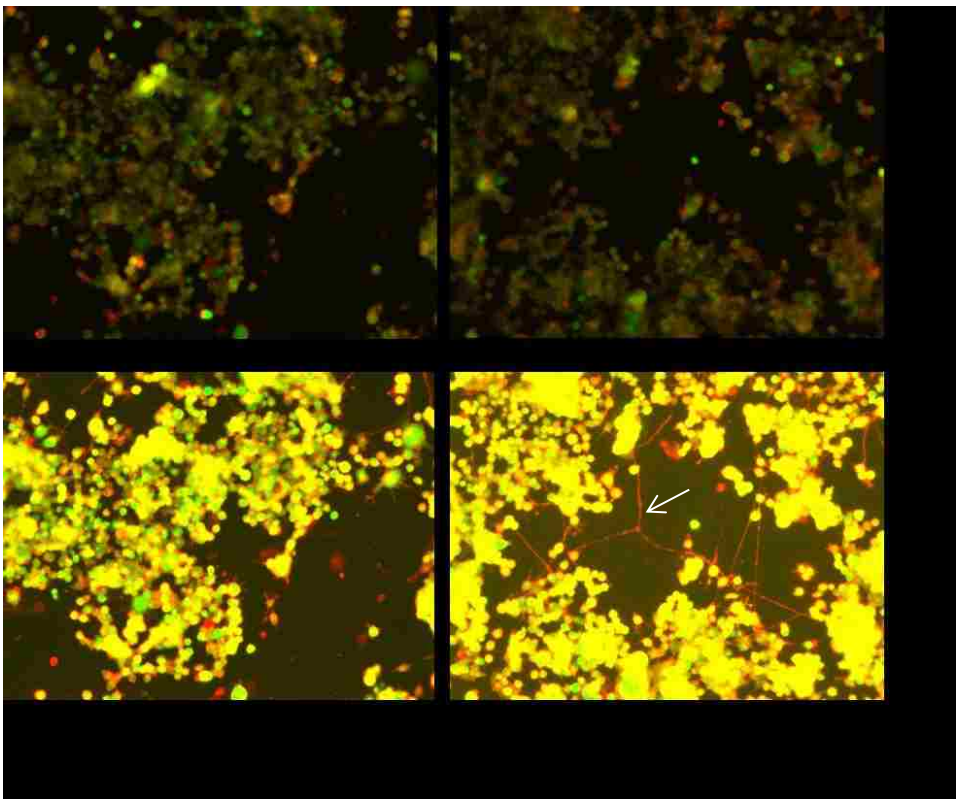

B.

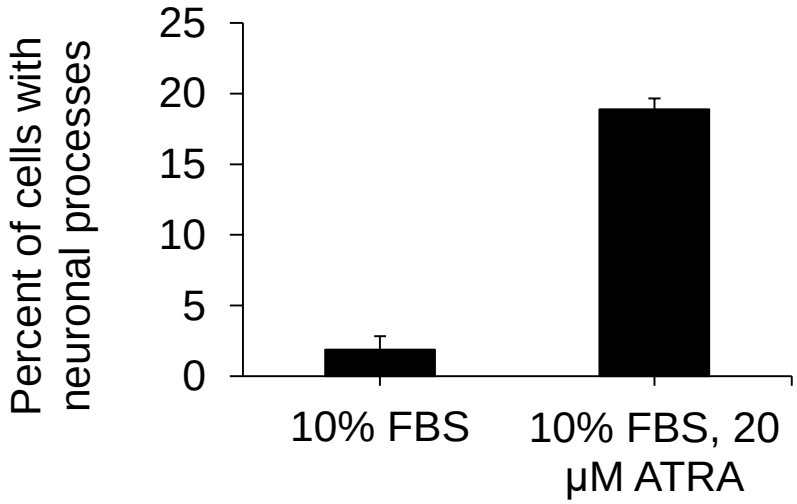
Percent of cells with neuronal processes
25
20
15
10
5
0
10% FBS
10% FBS, 20 μM ATRA

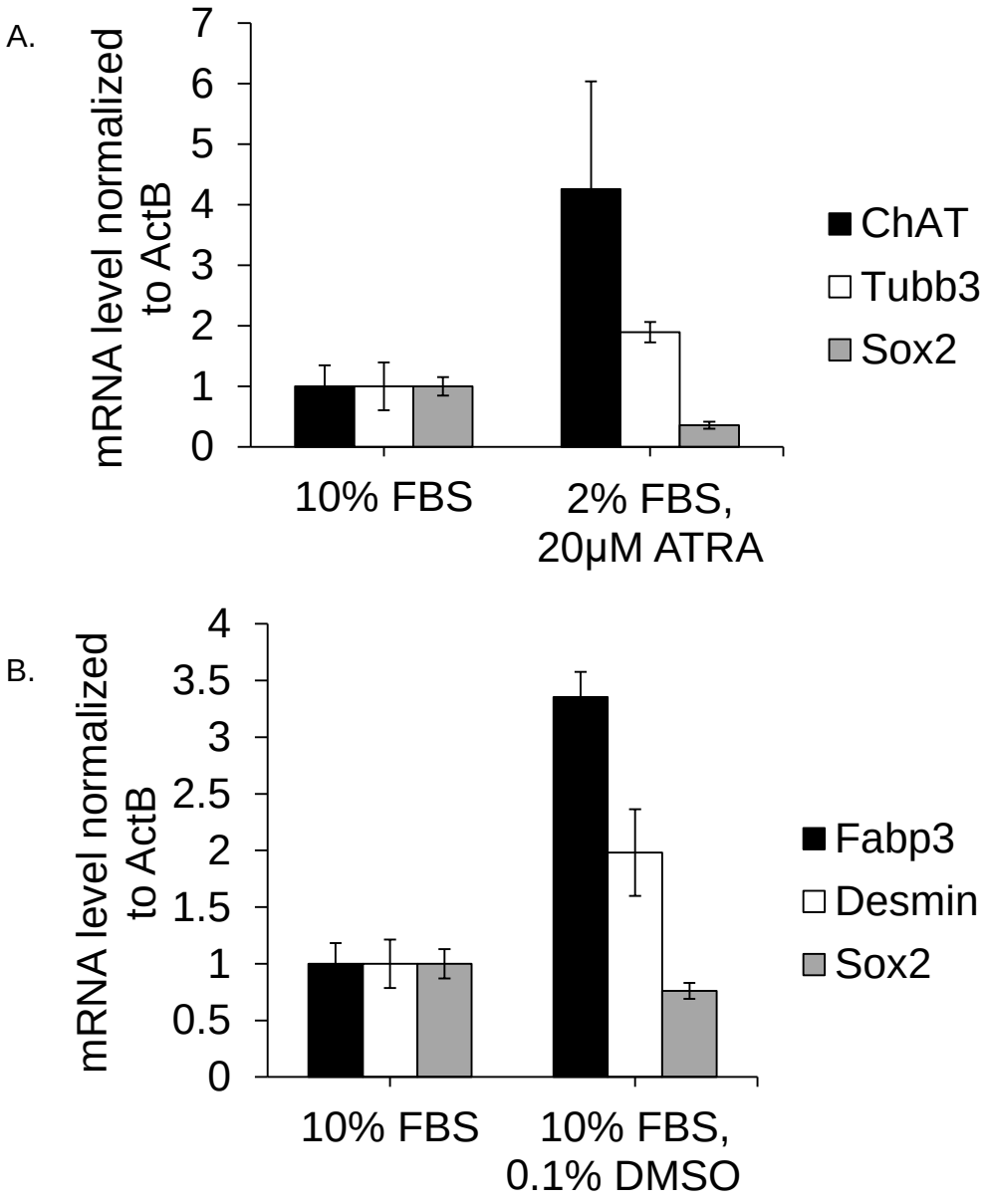

Fig 2.3: Chemical differentiation of N2a and P19 cells results in changes in gene expression. A. qRT-PCR of N2a cell markers. RNA isolated from N2a cells grown in either 10% FBS or 2% FBS with 20 μM ATRA was reverse transcribed and amplified. *ChAT, Tubb3,* and *Sox2* expression were calculated from ΔCq values and normalized to *β-actin* expression and control siRNA levels (n=3, p-values< 0.006, 0.01, 0.002, respectively). F. qRT-PCR of P19 cell markers. RNA isolated from P19 cells grown in either 10% FBS or 10% FBS with 0.1% DMSO was reverse transcribed and amplified. Performed as stated above, *Fabp3, Desmin,* and *Sox2* expression were calculated from ΔCq values and normalized to *β-actin* expression and control siRNA levels (n=3, p-values< 0.0001, 0.02, 0.05, respectively).

2.2.2 *Skiv2l2* is downregulated during chemically induced differentiation of N2a and P19 cells

Following chemical differentiation of P19 and N2a cells, total protein and RNA were isolated to measure *Skiv2l2* levels within the cell. With the hypothesis that *Skiv2l2* is downregulated during differentiation, it was expected that Western blotting against *SKIV2L2* would show high levels of *SKIV2L2* in cells grown in 10% FBS, with lower levels found in chemically treated cells. This would demonstrate that *SKIV2L2* protein levels decrease as cells differentiate. However, lower protein levels could be attributed to decreased protein stability, post-transcriptional silencing, or decreased transcription. To ascertain at what level *Skiv2l2* expression is affected, RNA extracted from the cells was reverse transcribed, and *Skiv2l2* was amplified using qRT-PCR.

N2a cells were first grown in either 10% FBS or 20 μM ATRA with 2% FBS to induce differentiation. Western blots were utilized to measure *SKIV2L2* protein levels in both samples after 48 hours. N2a cells induced to differentiate with ATRA and serum starvation were found to express approximately 50% less *SKIV2L2* protein when compared to N2a cells grown in 10% fetal bovine serum (p-value< 0.0001, Fig 2.4a). Western blots were quantified using ImageJ software and normalized to ActB protein levels to calculate SKIV2L2/β-actin levels with 10% FBS control levels set to one. To investigate whether *Skiv2l2* mRNA levels were also reduced in chemically differentiated N2a cells, qRT-PCR was used to measure the steady-state level of *Skiv2l2* mRNA in differentiating cells. Results demonstrated that differentiation induced with ATRA and serum starvation downregulates *Skiv2l2* mRNA levels by 4.3 fold (Figure 2.4b, p-value< 0.003).

Repeating this process on P19 cells, cells were grown in either 10% FBS or 0.1% DMSO with 10% FBS. Differentiation of P19 cells with DMSO resulted in a significant 86% decrease in *SKIV2L2* protein levels (p-value< 0.04, Fig .2.5a) and a 3-fold decrease in *Skiv2l2* mRNA levels (Fig.2.5b, p-value< 0.03). This demonstrates that differentiation into multiple cell types, specifically cholinergic neurons and cardiomyocytes, correlates with a downregulation of *Skiv2l2* protein and mRNA. However, because qRT-PCR captures the steady-state levels of *Skiv2l2* mRNA, it does not distinguish between transcription versus post-transcriptional mechanisms that destabilize mRNAs, such as miRNAs or increased mRNA turnover. Therefore, although these experiments show that both *Skiv2l2* mRNA and protein are downregulated during differentiation, they offer little insight into whether *Skiv2l2* is transcriptionally or post-transcriptionally regulated.

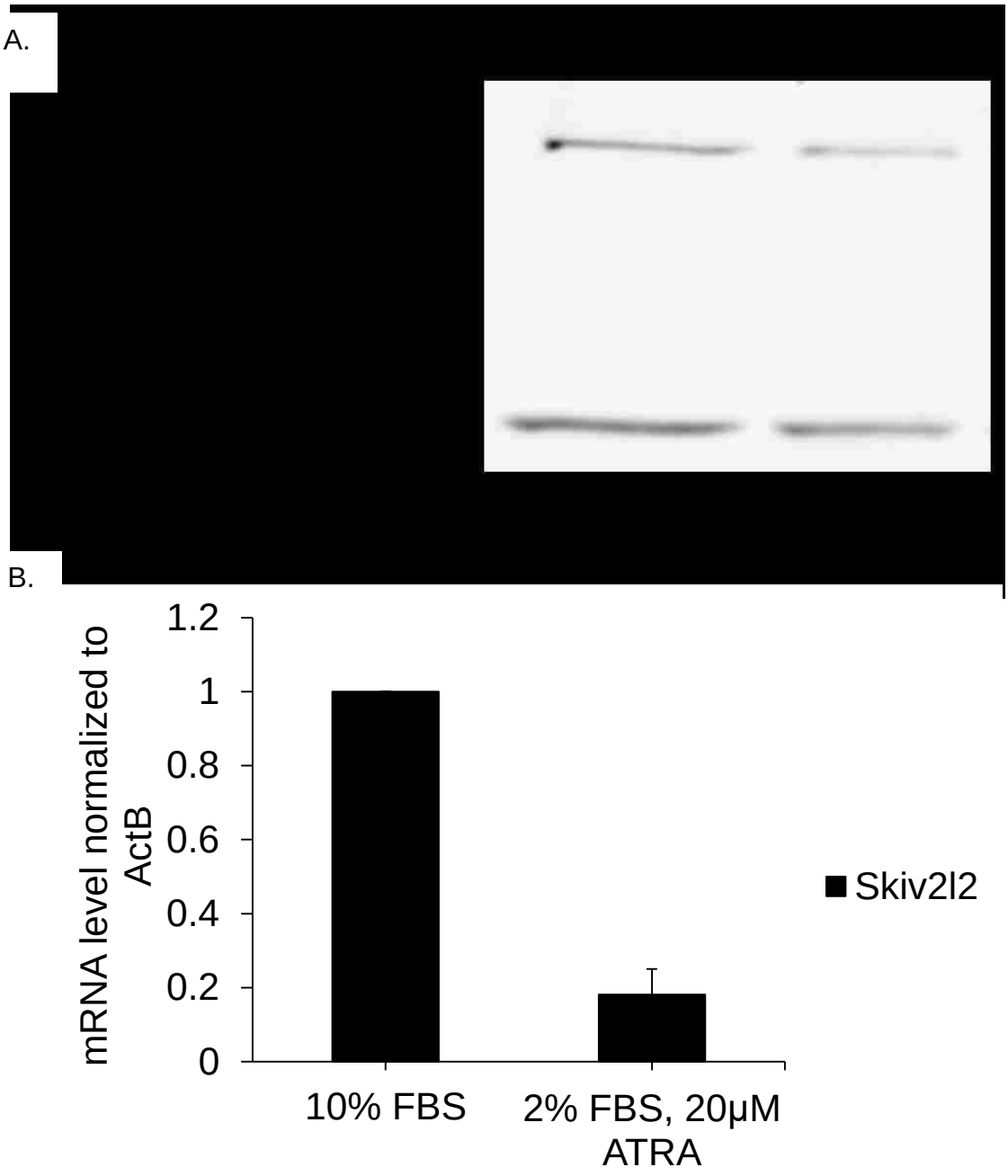

Fig 2.4: Chemical differentiation of N2a cells downregulates *Skiv2l2*. A. Western blots against *SKIV2L2* protein in N2a cells grown in 10% FBS or 2% FBS with ATRA. SKIV2L2 protein levels (118 kD) were quantified using ImageJ software and normalized to β-actin protein levels and 10% FBS levels (42 kD), with p-value< 0.001. B. qRT-PCR of *Skiv2l2* mRNA from cells grown in 10% FBS or 2% FBS with ATRA. *Skiv2l2* expression measured via ΔCq values was normalized to *β-actin* expression and control siRNA levels. Error bars represent ±SD for n=3, p-value< 0.003.

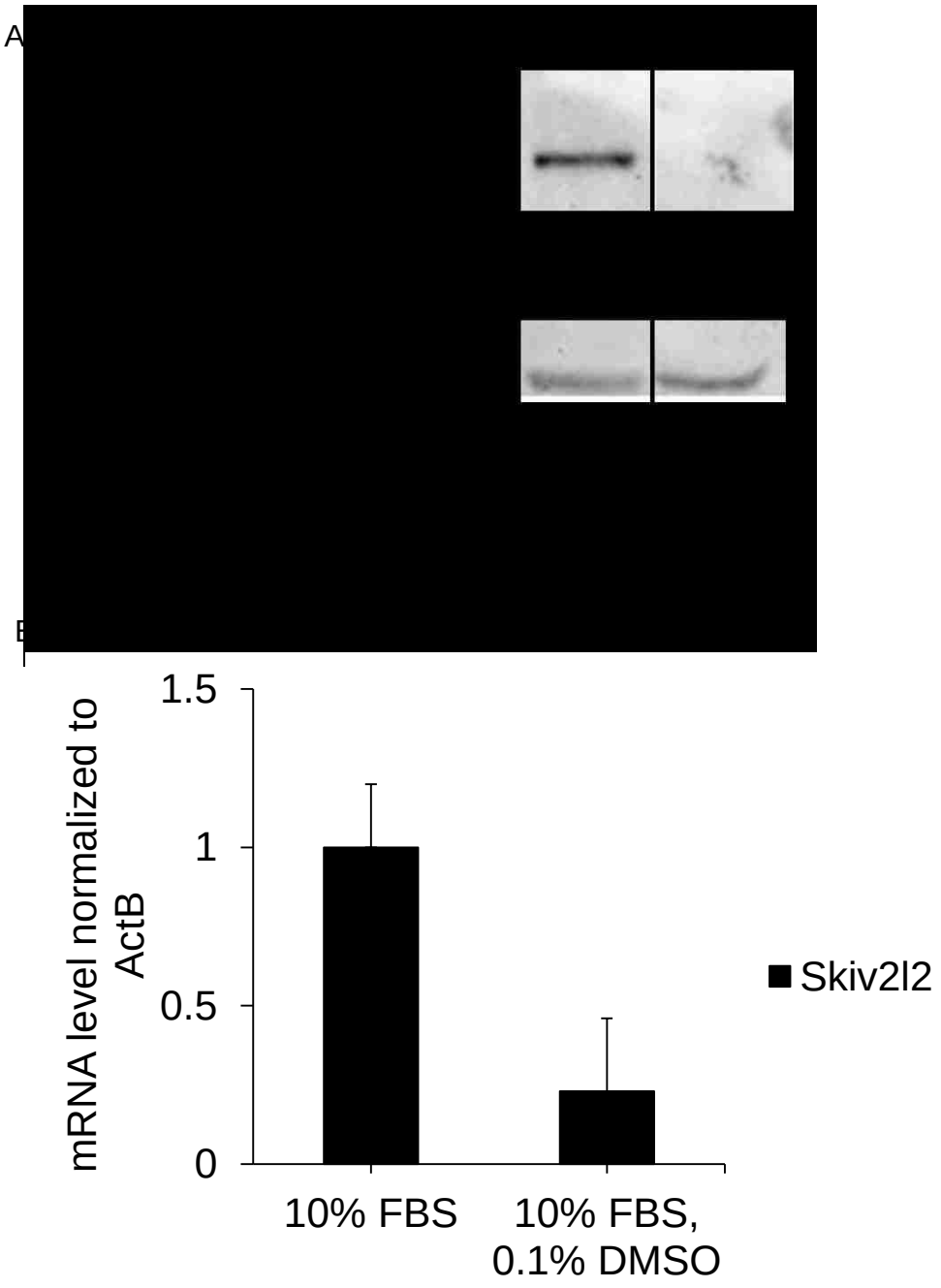

Fig 2.5: Chemical differentiation of P19 cells downregulates *Skiv2l2*. A. Western blots against *SKIV2L2* protein in P19 cells grown in 10% FBS or 10% FBS with 0.1% DMSO. *SKIV2L2*(118 kD) protein levels quantified via ImageJ software were normalized to β-actin protein levels and 10% FBS levels (42 kD), with p-value< 0.04. B. qRT-PCR of *Skiv2l2* mRNA from cells grown in 10% FBS or 10% FBS with 0.1% DMSO. *Skiv2l2* expression measured via ΔCq values was normalized to *β-actin* expression and 10% FBS levels. Error bars represent ±SD for n=3, p-value< 0.03.

2.2.3 Serum starvation is sufficient to downregulate *Skiv2l2* in N2a cells

Since N2a cells had been differentiated using serum starvation and retinoic acid treatment in the previous experiments, the next question addressed whether serum starvation or retinoic acid treatment alone were sufficient to downregulate *Skiv2l2* in N2a cells. Because the previous experiment revealed that both protein levels and mRNA could serve as an indicator of *Skiv2l2* downregulation during differentiation, Western blots were selected to measure *SKIV2L2* protein levels. Cells were either grown in 10% FBS, 10% FBS with 20 μM ATRA, or 2% FBS.

Western blotting demonstrated that cells treated with 20 μM ATRA in 10% FBA had *SKIV2L2* protein levels similar to those seen in cells grown in 10% FBS (p-value< 0.55, Fig 2.6a). While treatment with ATRA did not induce differentiation to the extent seen in cells grown in 2% FBS with 20 μM ATRA, these results seemed to suggest that ATRA was not sufficient to downregulate *Skiv2l2*, eliminating *Skiv2l2* as a potential transcriptional target of the ATRA-retinoic acid receptor transcriptional complex. However, treatment with 2% FBS alone did cause around a 40% decrease in *SKIV2L2* protein (p-value< 0.01, Fig 2.6b). This demonstrated that serum starvation alone is sufficient to downregulate *Skiv2l2* during differentiation. Due to the nature of FBS, this hints that a growth factor in the serum either directly or indirectly maintains *Skiv2l2* expression in N2a cells.

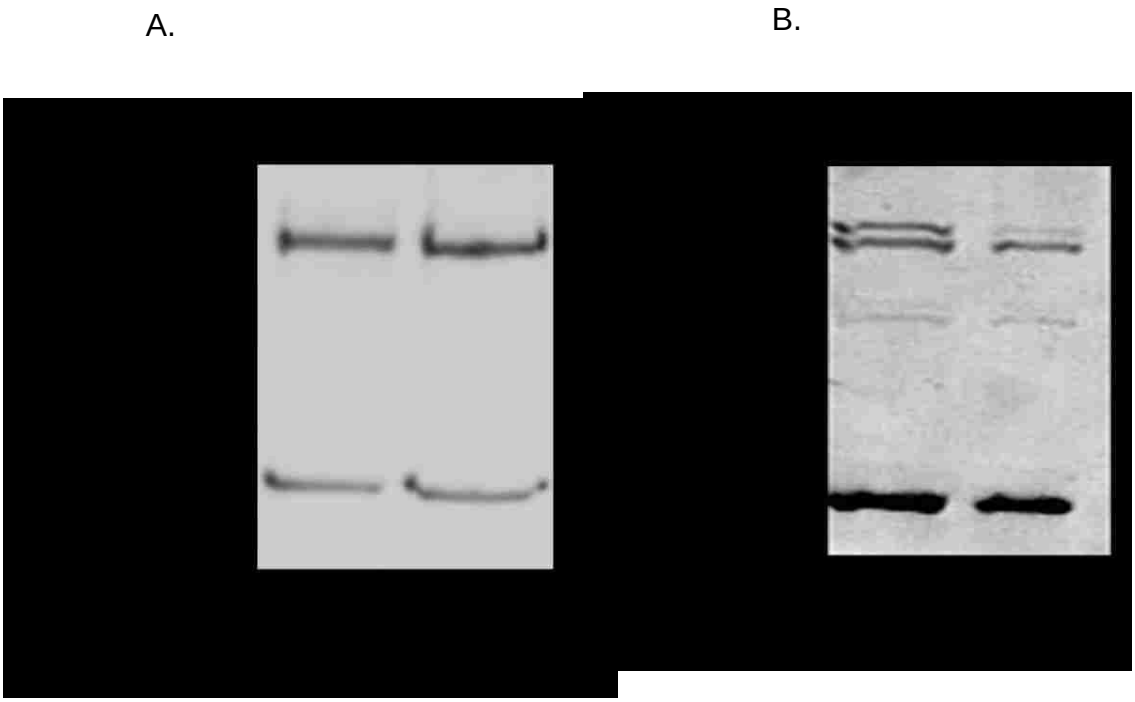

Fig 2.6: Serum starvation alone downregulated *SKIV2L2*. A. Western blots against *SKIV2L2* protein in N2a cells grown in 10% FBS or 10% FBS with ATRA. *SKIV2L2* protein levels (118 kD) were normalized to β-actin protein levels (42 kD) and 10% FBS levels following quantification with ImageJ software (p-value> 0.05). B. Western blots against *SKIV2L2* protein in N2a cells grown in 10% FBS with ATRA or 2% FBS. *SKIV2L2* protein levels (118 kD) were normalized to β-actin protein levels (42 kD) and 10% FBS levels quantified using ImageJ software, p-value< 0.01. Doublet represents slight protein degradation of SKIV2L2 and quantification included both bands.

2.2.4 *Skiv2l2* downregulation during N2a cell differentiation does not occur due to post-transcriptional regulation via *Skiv2l2*'s 3'UTR

Although *Skiv2l2* downregulation during differentiation was demonstrated through Western blotting and qRT-PCR, it was unknown whether this downregulation of *Skiv2l2* occurs transcriptionally or post-transcriptionally. Reasonably, lower steady-state *Skiv2l2* mRNA levels measured via qRT-PCR could be attributed to a decrease in transcription or a decrease in mRNA stability. Because miRNAs are responsible for many changes in cell expression during development, it was hypothesized that *Skiv2l2* could be directly downregulated by microRNA binding during differentiation. At least one miRNA, mir-297, targets *Skiv2l2* (Parikh, 2010), and miRANDA prediction tools demonstrated multiple putative miRNA binding sites in *Skiv2l2*'s short 200 base pair 3'UTR. To test whether miRNAs downregulate *Skiv2l2* during differentiation, N2a cells were transfected with a pMirGlo vector carrying *Skiv2l2*'s 3' UTR inserted at the 3' end of the firefly luciferase gene, allowing for firefly luciferase stability to be influenced by the 3'UTR of *Skiv2l2* (Fig 2.7). The expression of the luciferase gene off the PGK promoter correlates to the bioluminescence of the luciferase protein, which was measured using a luminometer.

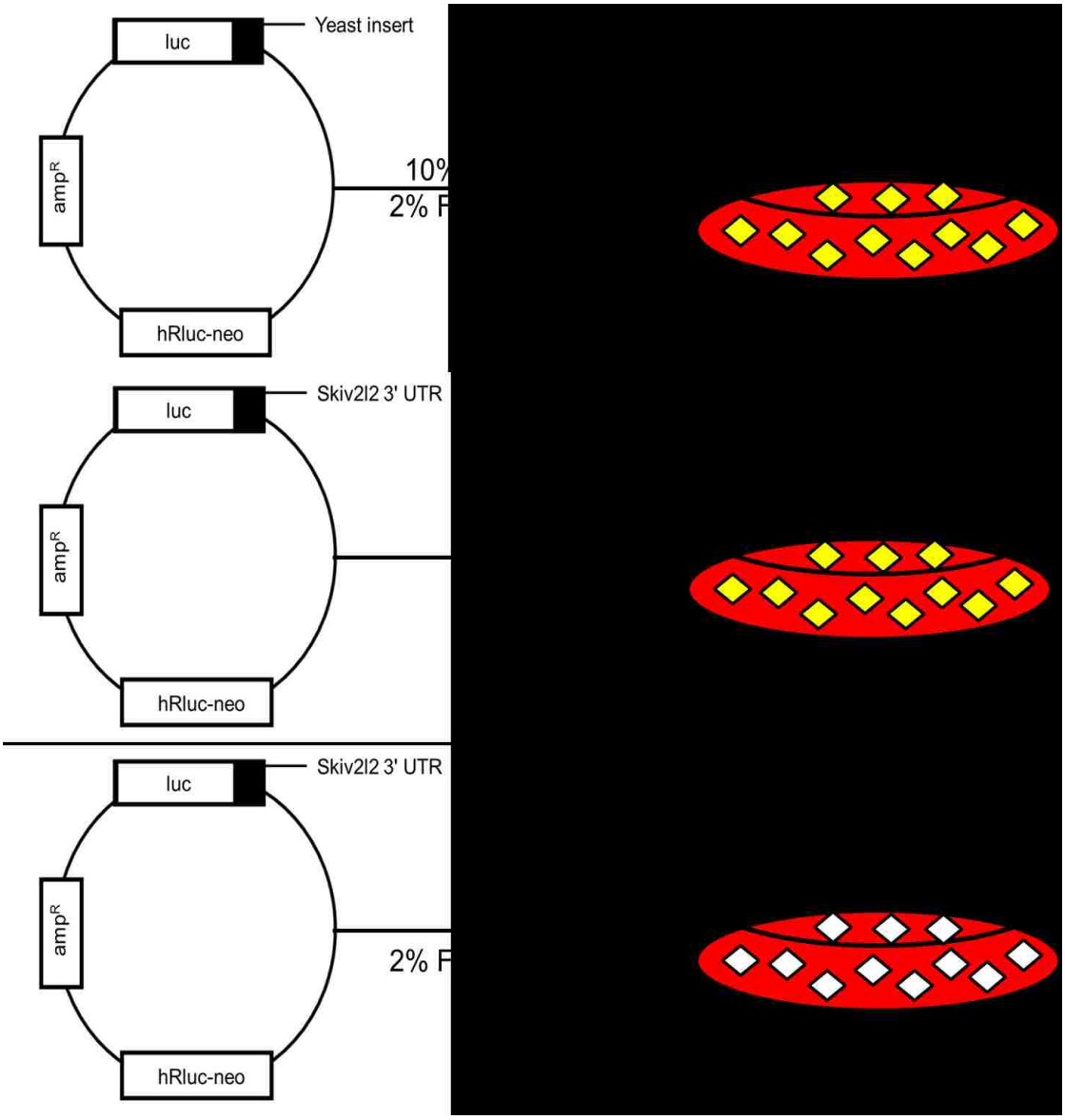

Fig 2.7: The pMirGlo vector provides a luminescent read-out of post-transcriptional regulation via the 3' UTR. The 200 bp 3' UTR of *Skiv2l2* was fused to the firefly luciferase gene. The vector also contains an ampicillin resistance gene for bacterial selection and a fusion gene consisting of renilla luciferase as a transfection control. A negative control vector (top) was constructed where 200 bp of yeast DNA with no putative miRNA binding sites was cloned into the multiple cloning site, producing no change in luciferase expression (yellow). However, with luciferase fused to the 3' UTR of *Skiv2l2* (middle) would be expected to decrease if miRNAs control *Skiv2l2* expression. If that were true, luciferase would be stable in cells grown in 10% FBS (yellow). However, upregulation of certain miRNAs during chemical treatment with 2% FBS and ATRA would result in downregulation of luciferase (white, bottom).

To account for differences in transfection efficiency and expression of the vector, the bioluminescence of firefly luciferase was normalized to the bioluminescence resulting from renilla luciferase also expressed off the same pMirGlo vector. Cells were also transfected with a negative control pMirGlo vector containing firefly luciferase with 200 base pairs of yeast *Skiv2l2* DNA taken from the 5' end of the open reading frame, which contains no putative miRNA binding sites. If miRNAs bind to the 3' UTR of *Skiv2l2* to downregulate its translation during differentiation, then inducing differentiation with serum starvation and retinoic acid treatment would upregulate those miRNAs (Fig 2.7). As a result, the miRNAs would repress the translation of firefly luciferase, and bioluminescence would decrease. Changes in luciferase translation were normalized to those seen in the negative control containing luciferase fused to the yeast genomic insert to affirm that any depression of bioluminescence was indeed due to the 3' UTR of *Skiv2l2*. This also was used to verify that miRNAs present in the multipotent, proliferating N2a cells did not downregulate *Skiv2l2* via the 3'UTR.

N2a cells were transfected with the following constructs under the following conditions: pMirGlo-yeast genomic DNA with growth in 10% FBS, pMirGlo-yeast genomic DNA with growth in 20 μM ATRA and 2% FBS, pMirGlo-*Skiv2l2* 3' UTR with growth in 10% FBS, and pMirGlo-*Skiv2l2* 3' UTR with growth in 20 μM ATRA and 2% FBS. Bioluminescence produced by firefly luciferase was measured using the Dual Stop and Glo Kit, and firefly luciferase was normalized to renilla luciferase to account for differences in transfection efficiency. There was no significant difference in firefly luciferase translation across the samples (Fig 2.8, p-values all >0.05). Because *Skiv2l2*'s 3' UTR did not destabilize luciferase mRNA under both growth conditions, it was

concluded that the 3' UTR of *Skiv2l2* does not account for the downregulation of *Skiv2l2* during N2a cell differentiation, meaning miRNAs are not directly involved in this downregulation, at least through binding of the 3' UTR.

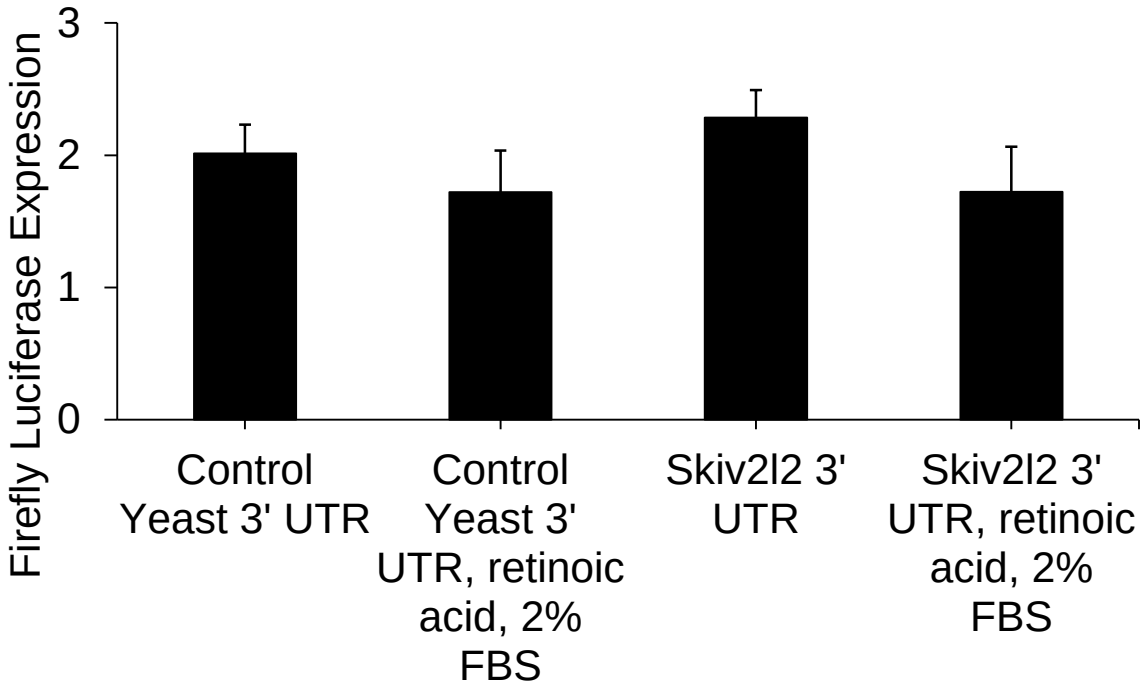

Fig 2.8: The 3'UTR of *Skiv2l2* does not affect gene expression. N2a cells were transiently transfected with either the control luc-yeast 3' UTR pMirGlo vector or the luc-*Skiv2l2* 3' UTR pMirGlo vector. Cells were then grown in either 10% FBS or 2% FBS with 20μM ATRA to induce differentiation. The DualGlo Stop ‘n Glo kit was used on harvested cells to measure luciferase expression. Firefly luciferase bioluminescence was normalized to renilla luciferase bioluminescence (n=3 biological replicates with 3 measurements per sample, p-values all> 0.05).

2.2.5 Multiple signaling cascades could indirectly or directly regulate *Skiv2l2* expression

Because serum starvation, but not miRNAs targeted to the 3' UTR, downregulated *Skiv2l2*, it was hypothesized that proliferative signaling cascades could transcriptionally upregulate *Skiv2l2*, and differentiation signaling cascades could downregulate *Skiv2l2*. Certain signaling pathways are known to support cell proliferation, such as the TGFβ and JAK/STAT signaling pathways, as improper activation of these pathways contributes to cancer (Chen, 2008). These pathways rely on a series of phosphorylation events that eventually lead to the activation of transcription factors. These transcription factors then activate the transcription of genes necessary for cell proliferation.

To determine if a specific signaling cascade involved in stem cell maintenance and differentiation might also regulate *Skiv2l2* expression, N2a cells were treated with small molecule inhibitors of certain kinases that lead to the phosphorylation of transcription factors supporting cell proliferation (Fig 2.9). ChIP data suggests that multiple transcription factors bind to the *Skiv2l2* promoter, and these transcription factors are controlled by the JAK/STAT, RAS/RAF/MAPK/ERK, cAMP/PKA, and the TGF-β/Smad/BMP4 signaling pathways (Hutchins, 2008; Chen, 2008; Sundaram, 2013; Guo, 2012; Fei, 2010). Respectively, these signaling pathways were inactivated in N2a cells through growth in the presence of the following drugs: JAK inhibitor I, AZD6244, H-89, and SB505124 (Table 2.1). In an attempt to establish a negative control whose transcription factor is not predicted to bind the *Skiv2l2* promoter, cells were treated with FAK inhibitor IV. However, FAK inhibitor IV proved to be an effective anti-cancer agent, inducing differentiation and cell death within hours of treatment. This failed

attempt demonstrated a flaw in this experimental design: the inhibition of these signaling pathways could downregulate *Skiv2l2* directly or indirectly through crosstalk with other pathways that promote differentiation. For this reason, these drug treatments served as a putative screen for pathways that could potentially regulate *Skiv2l2*, and cells were harvested within three hours of treatment before significant differentiation could take place. 30 μL of the vehicle DMSO served as the control treatment.

Fig 2.9: Experimental design to test if signaling cascades control *Skiv2l2* expression. *Skiv2l2* levels may be maintained through a signal transduction pathway activated by a growth factor in FBS. Loss of those growth factors (removal of FBS) would result in decreased *Skiv2l2* expression. To determine what signal transduction pathway might account for increased *Skiv2l2* expression in stem cells, cells were treated with kinase inhibitors that target specific growth pathways. If the inhibitor blocks the pathway involved in maintaining *Skiv2l2* expression, then *Skiv2l2* expression would decrease.

N2a cells were grown in the presence of the drugs listed in Table 2.1 to inhibit the binding of STAT, Myc, Creb, and Smad transcription factors to target genes (Fig 2.9). If the signaling pathways targeted by these drug inhibitors activate *Skiv2l2* transcription, either directly or indirectly, then treatment with these drugs would trigger a decrease in *Skiv2l2* levels. *Skiv2l2* mRNA levels were assessed using qRT-PCR as outlined above, with changes in *Skiv2l2* mRNA levels attributed to transcriptional control of *Skiv2l2*.

Finally, SKIV2L2 protein levels were measured via Western blotting to confirm changes seen in mRNA levels.

Inhibitor	Target	Pathway inhibited	Transcription Factor Family	Treatment
AZD6244	MEK1, MEK2	ERK/MAPK	Myc	75 μM
SB505124	ALK4, ALK5, ALK7	TGF-β	Smad	75 μM
H-89	PKA	PKA	CREB	25 μM
JAK inhibitor I	JAK I, JAKII, JAKIII	JAK/STAT	STAT	0.375 μM

Treatment of N2a cells with drugs resulted in mixed results that were difficult to replicate. This is not surprising because the effect of anti-cancer drugs on cancer cells can vary widely as certain cells are more or less drug sensitive (Yang, 2010). Also, anti-cancer drugs often compromise RNA integrity, making qRT-PCR difficult (Narendrula, 2016). Treatment with SB505124 to inhibit TGF-β signaling pathways had no effect on *SKIV2L2* protein levels, with a slight but variable increase in *Skiv2l2* mRNAs levels (Fig 2.10a). Cells treated with AZD6244 expressed both *Skiv2l2* mRNA and protein levels equivalent to those seen in control cells (Fig 2.10). Two drug treatments did downregulate *Skiv2l2* mRNA and protein levels in a reproducible manner: JAK inhibitor I and H-89. JAK inhibitor I treatment decreased *Skiv2l2* mRNA levels by 57% (Fig 2.10a, p-value< 0.003) and *SKIV2L2* protein levels by 65% (Fig 2.10b, p-value< 0.02).

Treatment with H-89 did cause a decrease in *Skiv2l2* mRNA (Fig 2.10a, 70% decrease, p-value< 0.08) and protein (Fig 2.10b, 34% decrease, p-value< 0.07), although these results were not statistically significant. However, further experimentation with dosage, length of treatment, and increased replicates could reveal H-89 as a disruptor of *Skiv2l2* expression via PKA signaling. Previous research found that *Skiv2l2* expression is responsive to cAMP, a PKA activator, and is downregulated following siRNA knockdown of PKA (Guo, 2012). While these results are suggestive that *Skiv2l2* could be a target of the JAK/STAT and PKA signaling pathway, they are not definitive due to the complex effects of cancer drugs on N2a cells. Further experimentation could investigate *Skiv2l2* transcriptional control via RNAi against STAT3 and CREB to eliminate off-target effects. However, these experiments were not performed as they were beyond the scope of this study.

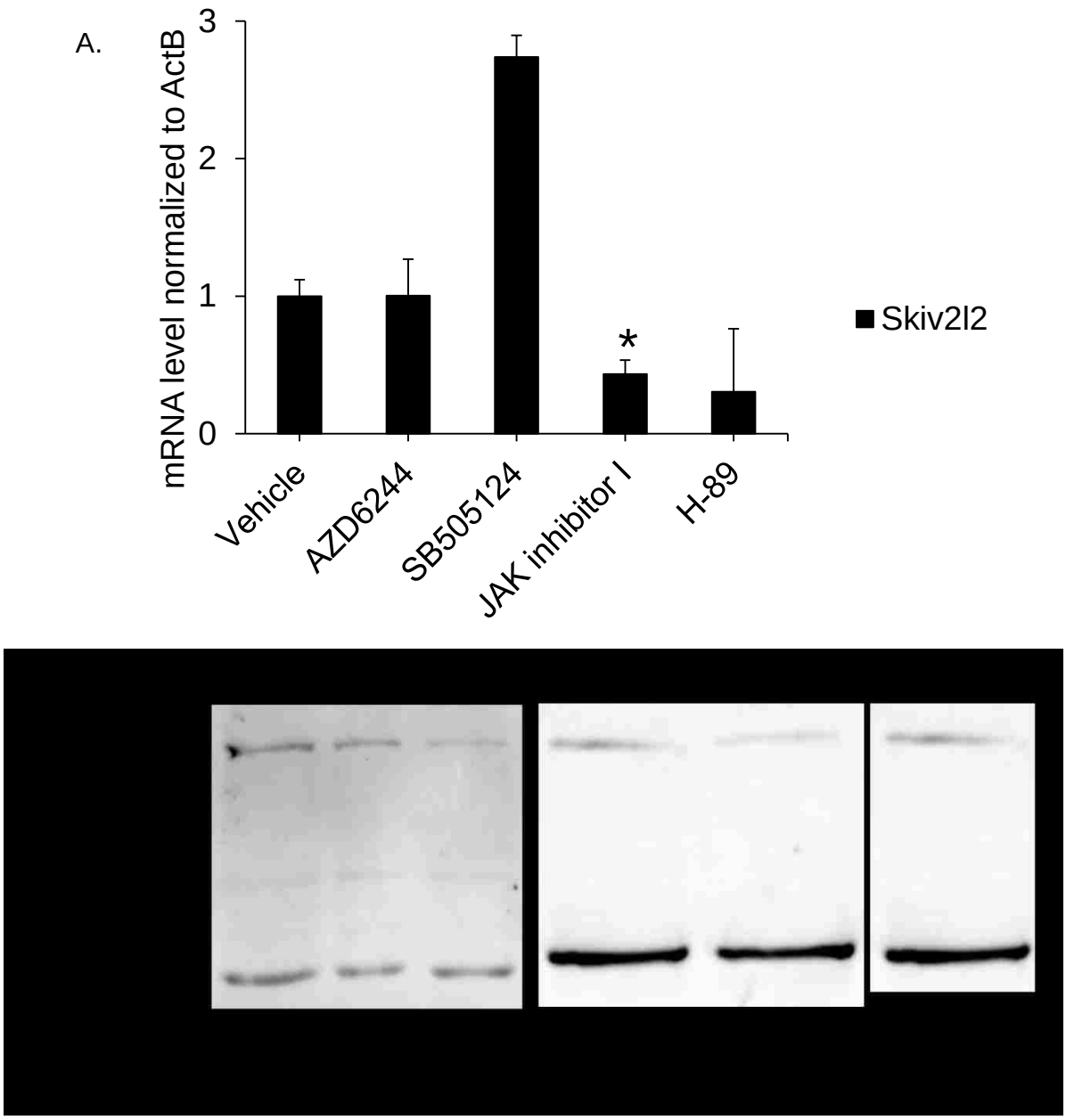

Fig 2.10: Treatment of N2a cells with JAK inhibitor I significantly downregulates *Skiv2l2*. A. qRT-PCR of *Skiv2l2* mRNA from cells treated with various kinase inhibitors. *Skiv2l2* expression measured via ΔCq values was normalized to *β-actin* expression and vehicle levels. Error bars represent ±SD for n=3. Statistically significant values are denoted with an asterisk (*), where p-value< 0.003, and all other values have p-value> 0.05. B. Western blots against *SKIV2L2* protein in N2a cells treated with various kinase inhibitors. *SKIV2L2* protein levels (118 kD) were normalized to β-actin protein levels (42 kD) and vehicle levels. Statistically significant values are denoted with an asterisk (*), where p-value< 0.02.

2.3 Discussion

These experiments prove that *Skiv2l2* is downregulated in both N2a and P19 cells following chemically induced differentiation. Decreases in *SKIV2L2* can be correlated to decreases in *Skiv2l2* mRNA. Although there is a slight discrepancy between *Skiv2l2* mRNA and protein levels, this is predicted to be due to differences in experimental methods or the high stability of *SKIV2L2* protein when in complex with other RNA surveillance components. Because the 3' UTR of *Skiv2l2* does not destabilize transcripts during differentiation, *Skiv2l2* is not likely to be regulated by miRNAs and instead could be transcriptionally downregulated during differentiation. In support of this hypothesis, ChIP studies conducted in other laboratories show the binding of multiple proliferative transcription factors to the *Skiv2l2* promoter (Hutchins, 2008; Chen, 2008; Sundaram, 2013; Guo, 2012; Fei, 2010). Removing growth factors contained in FBS and inhibiting JAK kinases that support proliferation both resulted in the downregulation of *Skiv2l2*. Together, this suggests that transcription factors activate the expression of *Skiv2l2* in proliferative N2a cells and that *Skiv2l2* levels decline as these transcription factors are inactivated during differentiation (Fig 2.11).

These findings offer an in-depth analysis of *Skiv2l2* expression using molecular techniques. While previous studies used bioinformatics to correlate lower *Skiv2l2* levels with cell differentiation, the experiments outlined above demonstrate that *Skiv2l2* is downregulated at the transcriptional level during the chemically induced differentiation of two murine cell lines into two different cell types. Confirming that *Skiv2l2* is downregulated during differentiation establishes a temporal link between RNA

surveillance and development, meaning that RNA surveillance activity may change in response to developmental changes. The finding that *Skiv2l2*'s expression changes in during differentiation prompts questions into its role in development, namely why *Skiv2l2* expression is elevated in pluripotent, proliferative cells, how Skiv2l2 expression changes after differentiation, and how RNA surveillance is maintained in differentiated cells with lower levels of *SKIV2L2*. Interestingly, analysis of expression shows a high level of *SKIV2L2* in immune cells (Iwanami, 2009), hinting at a possible correlation between immune cell proliferation and nuclear RNA surveillance.

Skiv2l2 expression changes have been linked to different disease states. *Skiv2l2* expression is upregulated in the blood serum of amyotrophic lateral sclerosis patients (Baciu, 2012), and RNAi screens have determined that *Skiv2l2* is a metastatic-essential gene in breast cancer, as its knockdown impairs cancer cell metastasis (Wang, 2012). In light of these studies, establishing that *Skiv2l2* is downregulated during differentiation could contribute to a better understanding of how RNA surveillance contributes to these diseases. Potentially, future studies on *Skiv2l2* could focus on utilizing high levels of *Skiv2l2* as a diagnostic marker in cancer and other proliferative diseases.

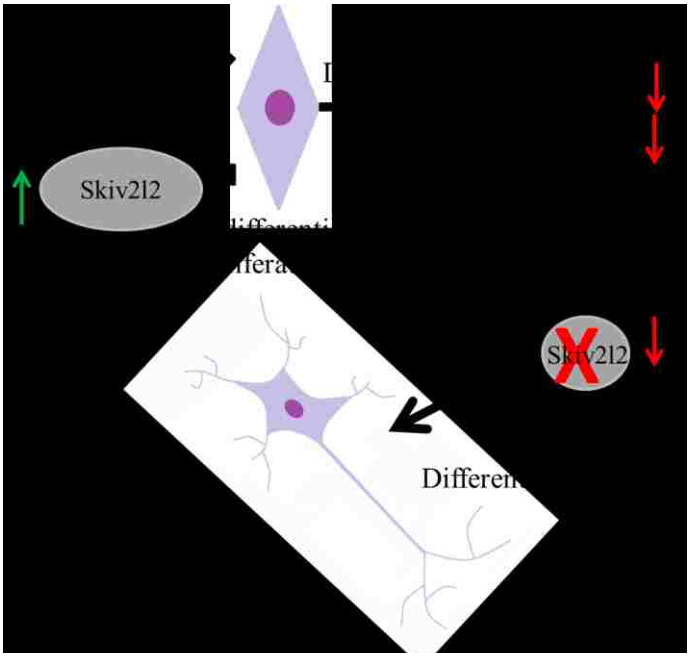

Fig 2.11: Cells downregulate *Skiv2l2* as they differentiate. Following chemically induced differentiation, *Skiv2l2* mRNA and protein levels drop. Given that this reduction in SKIV2L2 also occurs with inhibition of JAK/STAT growth signaling, it can be concluded that factors that maintain cells in their proliferative, undifferentiated state also promote *Skiv2l2* expression.

CHAPTER III: KNOCKDOWN OF *SKIV2L2* VIA RNAI ENHANCES P19 CELL AND N2A CELL DIFFERENTIATION

3.1 Introduction

Hypothesis: RNAi knockdown of *Skiv2l2* promotes P19 and N2a cell differentiation

Upon observation that chemically induced differentiation in N2a and P19 cells leads to the downregulation of *Skiv2l2*, it was hypothesized that low levels of SKIV2L2 might promote differentiation. In support of this hypothesis, RNA surveillance mechanisms have been previously shown to impact differentiation in both yeast and murine cells (Hiriart, 2011; Tinguely, 2012). In *Schizosaccharomyces pombe*, the Mmi1 RNA surveillance machinery, which includes the nuclear exosome component Rrp6, mediates the degradation and RNAi-directed silencing of transcripts that direct sexual differentiation. To prevent the expression of sexual differentiation genes during vegetative growth, Mmi1 recruits the RNA-induced transcriptional silencing complex (RITs) to loci that drive sexual differentiation, leading to the formation of heterochromatin and silencing of these regions. During sexual differentiation, this repression is relieved to allow yeast to express genes necessary for meiosis. (Hiriart, 2011). This provides one example where RNA surveillance helps regulate changes in gene expression during differentiation.

In addition to RNA surveillance preventing premature sexual differentiation in yeast, mRNA surveillance has been found necessary to promote proper differentiation in murine immune cells. During B-cell differentiation, the production of diverse Ig transcripts depends on error-prone V(D)J recombination, which often results in premature

stop codons. These nonsense Ig transcripts accumulate in primary B cells, but the increased efficiency of nonsense-mediated decay (NMD) pathways during B cell activation results in the degradation of these transcripts and promotes terminal differentiation (Tinguely, 2012). Furthermore, NMD guided by Smg6 has been found to be necessary to downregulate the pluripotency factor c-Myc, making NMD essential for the differentiation of murine embryonic stem cells and iPSCs (T Li, 2015).

While mRNA surveillance mechanisms have dissimilar effects on differentiation in yeast and mice, the established link between mRNA surveillance and differentiation lends credence to the hypothesis that nuclear RNA surveillance may also play a role in cell differentiation. Converse to how increased NMD activity is necessary to enhance differentiation in mouse cells, the timing of *Skiv2l2* downregulation suggests that high levels of nuclear RNA surveillance activity might prevent differentiation. SKIV2L2 and nuclear RNA surveillance have been primarily implicated in the processing and turnover of non-coding RNAs. Given that non-coding RNAs, such as miRNAs and lncRNAs, play an important role in mammalian pluripotency and stem cell maintenance (Meza-Sosa, 2014; Ghosal, 2013), it reasons that TRAMP-mediated RNA surveillance could regulate the steady-state levels of these non-coding RNAs involved with pluripotency. In stem cells, SKIV2L2-mediated RNA surveillance might to target non-coding RNAs that function in pluripotency or differentiation to the nuclear exosome for processing and turnover. Loss of SKIV2L2-mediated RNA surveillance could cause these pluripotency and differentiation RNAs to aberrantly accumulate, triggering changes in differentiation.

3.2 Approach and Results

3.2.1 RNAi knockdown reduces SKIV2L2 levels to negligible amounts in N2a and P19 cells

To test the hypothesis that *Skiv2l2* downregulation promotes differentiation, experimentation began by using RNAi to reduce *Skiv2l2* levels in both N2a and P19 cells. Following transfection with siRNA ID #177475 complementary to *Skiv2l2* sequence (*Skiv2l2* siRNA), western blotting and qRT-PCR were used to confirm knockdown of *Skiv2l2* levels. When compared to N2a cells transfected with non-targeting control siRNA, N2a cells transfected with *Skiv2l2* siRNA expressed 97% less SKIV2L2 protein (p-value< 0.0004, Fig 3.1a). The knockdown of *Skiv2l2* mRNA levels was confirmed via qRT-PCR, where *Skiv2l2* mRNA levels normalized to the expression of β-Actin (ActB) showed that *Skiv2l2* siRNAs reduced *Skiv2l2* mRNA levels by 86% (Fig 3.1b, p-value< 0.008). *Skiv2l2* knockdown was repeated in P19 cells, although this knockdown was slightly less efficient than in N2a cells. RNAi against *Skiv2l2* in P19 cells led to a 70% reduction in SKIV2L2 protein levels compared to control siRNA treated cells when measured through western blotting (p-value< 0.0001, Fig 3.2a). SKIV2L2 protein levels could be consistently reduced by 70-80%, with a consistent 87% decrease in *Skiv2l2* mRNA levels (Fig 3.2b, p-value< 0.01).

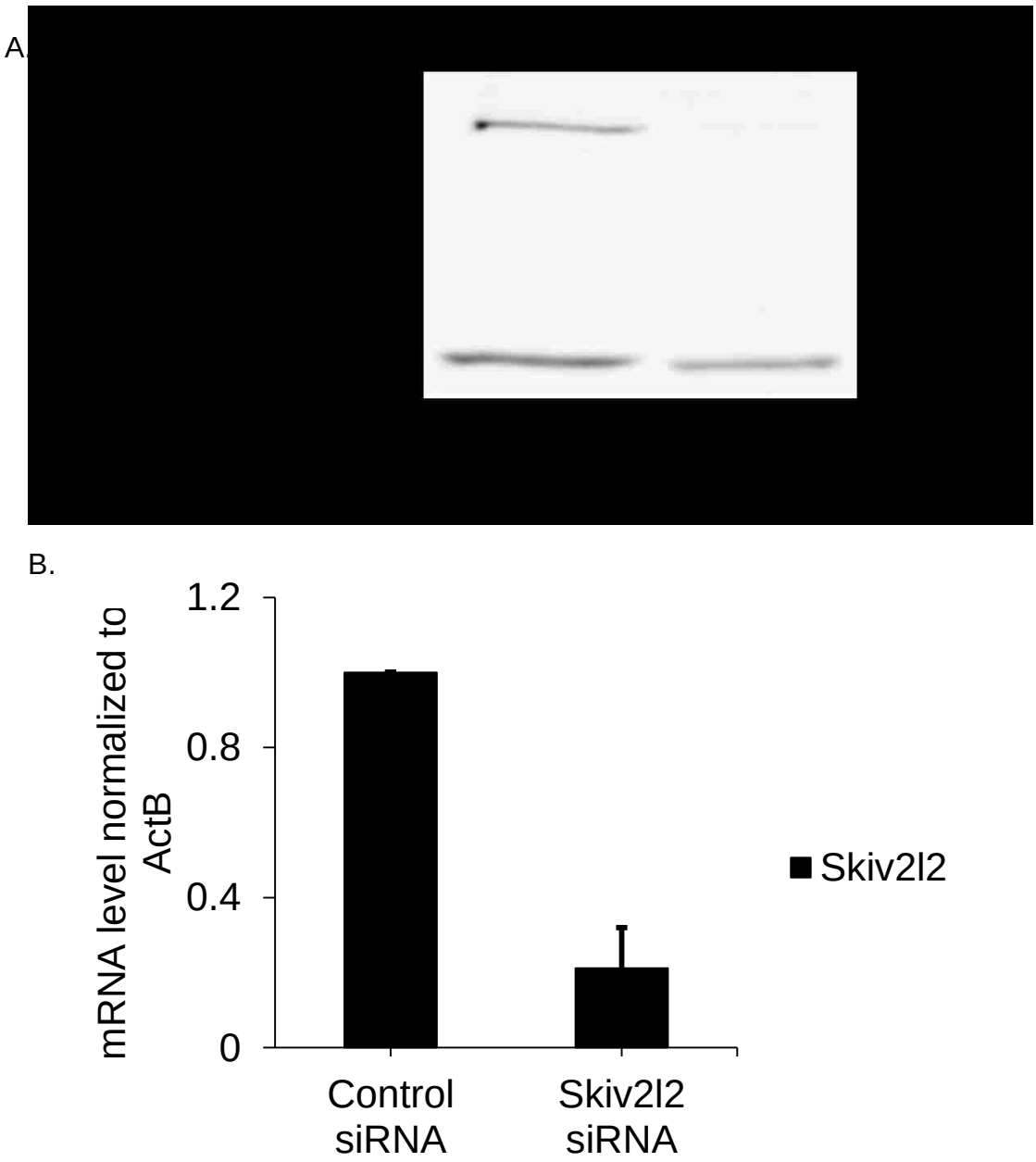

Fig 3.1: Verification of *Skiv2l2* knockdown in N2a cells. A. Western blots against SKIV2L2 protein in cells transfected with non-targeting control siRNA or *Skiv2l2* siRNA. N2a cells transfected with siRNA were grown in 10% FBS. *SKIV2L2* protein levels (118 kD) were normalized to β-actin protein levels and control siRNA levels (42 kD), p-value< 0.004. B. qRT-PCR of *Skiv2l2* mRNA from N2a cells transfected with non-targeting control siRNA or *Skiv2l2* siRNA. *Skiv2l2* expression measured via ΔCq values was normalized to *β-actin* expression and control siRNA levels. Error bars represent ±SD for n=3, p-value< 0.0080.

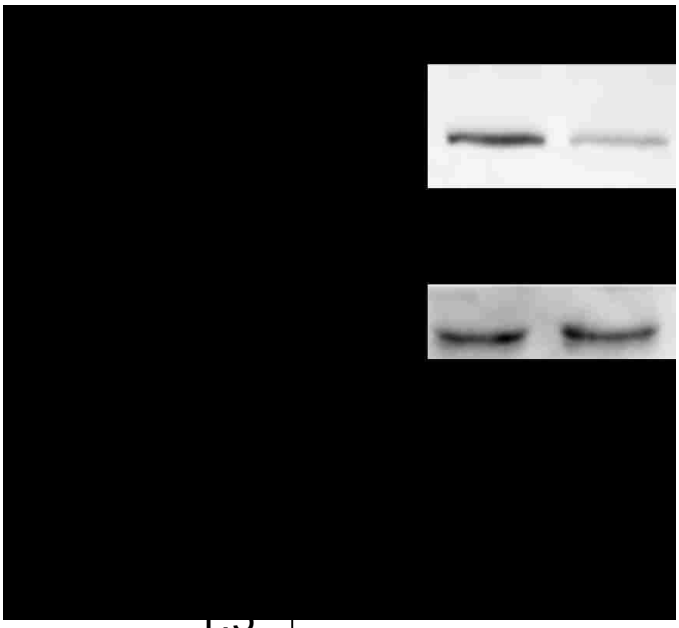

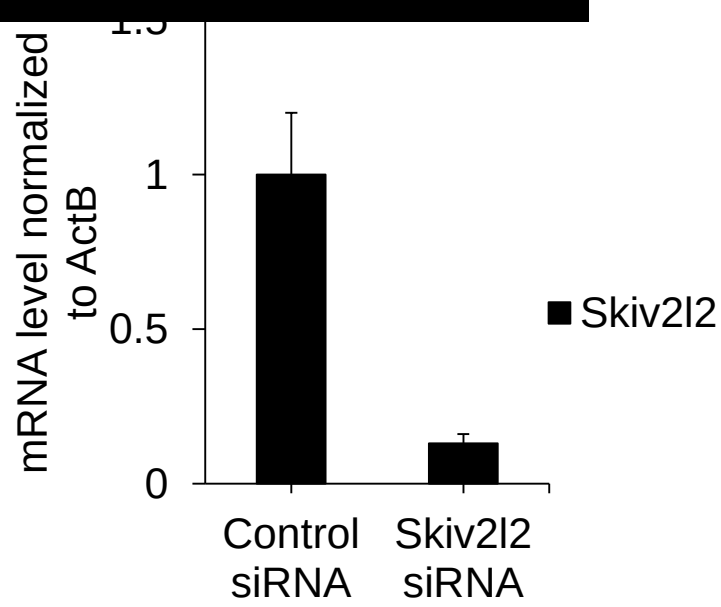
mRNA level normalized to ActB
1
0.5
0
Skiv2l2
Control siRNA
Skiv2l2 siRNA

3.2.2 SKIV2L2 depletion enhances morphological changes consistent with differentiation

Initial observations revealed that following treatment with siRNAs directed against *Skiv2l2*, N2a cells failed to grow to 100% confluency, unlike N2a cells treated with the non-targeting control siRNA. Further inspection revealed increased extension of axons and dendrites following SKIV2L2 depletion, hinting that SKIV2L2 may play a role in maintaining cancer cell proliferation or preventing differentiation. These observations led to experiments to characterize the phenotype associated with *Skiv2l2* knockdown in regards to increased cell differentiation.

Because N2a cell differentiation is readily visualized by the formation of axons and dendrites, N2a cells transfected with either control siRNA or *Skiv2l2* siRNA were analyzed using an inverted microscope to better visualize axons and dendrites stained with the Neurite Outgrowth Staining Kit® (Fig 3.3a). Neuronal processes were readily seen as bright orange following staining of the cell membrane, and cells extending processes two times the diameter of cell body were considered to exhibit a neuronal cell phenotype. Because cell morphology can be quantified to reflect the extent of N2a cell differentiation, an increase in cells extending neuronal processes following *Skiv2l2* knockdown would indicate enhanced terminal differentiation upon SKIV2L2 depletion. Cells were counted and scored based on the extension of neuronal processes. Accordingly, *Skiv2l2* knockdown resulted in a 20% increase in the number of cells extending long neuronal processes over control cells (two-proportion Z-score= -14.3, p-value< 0.0001, Fig 3.3b). This increase in neuronal phenotype following *Skiv2l2* knockdown suggests that loss of SKIV2L2 enhances the differentiation of N2a cells into

neurons. P19 cell differentiation is not easily quantified by morphological changes, as P19 cells grow in clusters and differentiate into multiple cell types. However, *Skiv2l2* knockdown was qualitatively observed to increase embryoid body formation. Embryoid body formation occurs in response to DMSO or cellular senescence and correlates with increased differentiation into muscle tissue (Jasmin, 2010). The increase in the appearance of embryoid bodies with SKIV2L2 depletion is consistent with P19 cell differentiation into a variety of myocytes, but it is not a reliable marker for differentiation as it occurs under various conditions.

A.

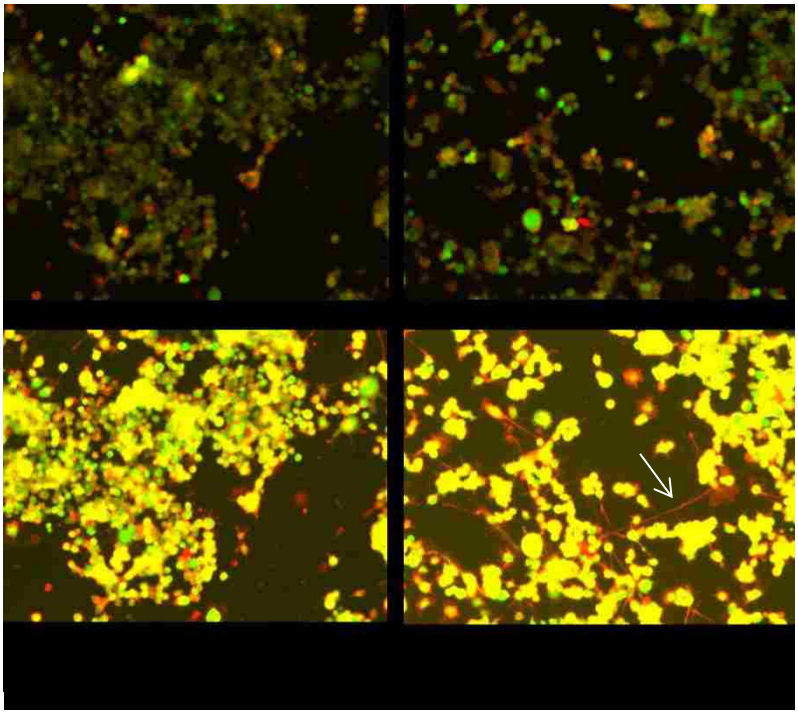

B.

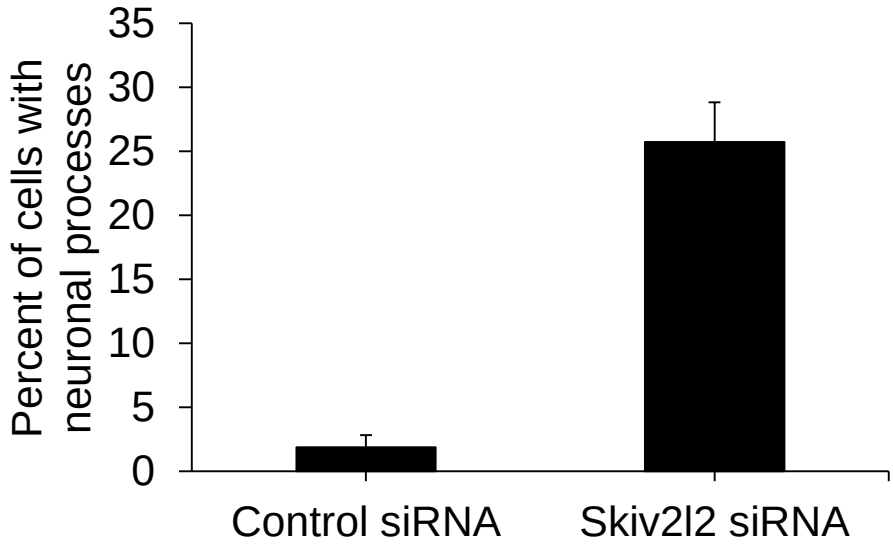
Percent of cells with neuronal processes
35
30
25
20
15
10
5
0
Control siRNA
Skiv2l2 siRNA

[redacted]

3.2.3 Gene expression changes in *Skiv2l2* knockdown cells reflect increased differentiation

While morphological changes were consistent with enhanced differentiation following *Skiv2l2* knockdown, it was also necessary to establish that SKIV2L2 depletion induces changes in gene expression indicative of differentiation. In both N2a and P19 cells, differentiation can be characterized by an upregulation of differentiation markers and a downregulation of pluripotency markers. As N2a cells differentiate, genes specific to neurons, such as ChAT and Tubb3, are transcribed, while pluripotency genes such as Sox2 and Nestin are silenced (Zhi, 2012; Tremblay, 2010; Liu, 2013b). An increase in ChAT and Tubb3 transcripts, coupled with a decrease in the pluripotency transcripts Sox2 and Nestin would reflect cell differentiation following SKIV2L2 depletion.

Due to the ability of P19 cells to form cardiac muscle, skeletal muscle, and various neurons (Dong, 2012; Jasmin, 2010), the phenotype of P19 cells following SKIV2L2 depletion could only be examined through qRT-PCR of cardiac myocyte markers and pluripotency markers, as cell morphology is not a reliable measurement of differentiation into multiple cell types. Gene transcripts selected to screen for differentiation included the cardiac muscle transcription factors GATA4 and Nkx2.5 (Choi, 2004), fatty-acid binding protein 3 (Fabp3) specific to cardiac muscle (Zhu, 2011), and the intermediate filament Desmin expressed in all muscle cell types (Dey, 2010). High levels of the transcription factors Nanog (Zhu, 2011) and Sox2 (Dong, 2012) characterize P19 cell pluripotency (Xie, 2010). While P19 cells can also differentiate into neurons, the neuronal cell fate was not examined due to the inability to drive P19 cell differentiation using retinoic acid, suggesting that the P19 cell line utilized in these

studies has not retained the ability to differentiate into neurons. However, increased levels of GATA4, Nkx2.5, Fabp3, and Desmin would indicate P19 cell differentiation into myocytes following *Skiv2l2* knockdown, and a decrease in Nanog and Sox2 would reflect a loss of pluripotency (Xie, 2010).

qRT-PCR was performed on total RNA isolated from N2a cells transfected with control siRNA or *Skiv2l2* siRNA, and ChAT, Tubb3, Sox2, and Nestin mRNA expression was quantified relative to ActB. Following *Skiv2l2* knockdown, Tubb3 expression increased 2.0 fold (p-value< 0.048), and ChAT mRNA levels increased 3.2 fold above those levels seen in control cells (p-value< 0.0001) (Fig 3.4a). This increase in Tubb3 and ChAT mRNA levels, representative of axon structure and function, is consistent with the enhanced neuronal cell morphology in *Skiv2l2* knockdown cells. Furthermore, the expression of pluripotency markers Nestin and Sox2 was found to exhibit a 2.97 fold decrease (p-value< 0.03) and a 2.98 fold decrease (Fig 3.4b, p-value< 0.01), respectively, in *Skiv2l2* knockdown cells when compared to control siRNA treated cells. The increase in neuronal cell morphology, elevated Tubb3 and ChAT expression, and decrease in Sox2 and Nestin indicate that SKIV2L2 depletion results in a loss of multipotency and enhance cell differentiation in N2a cells.

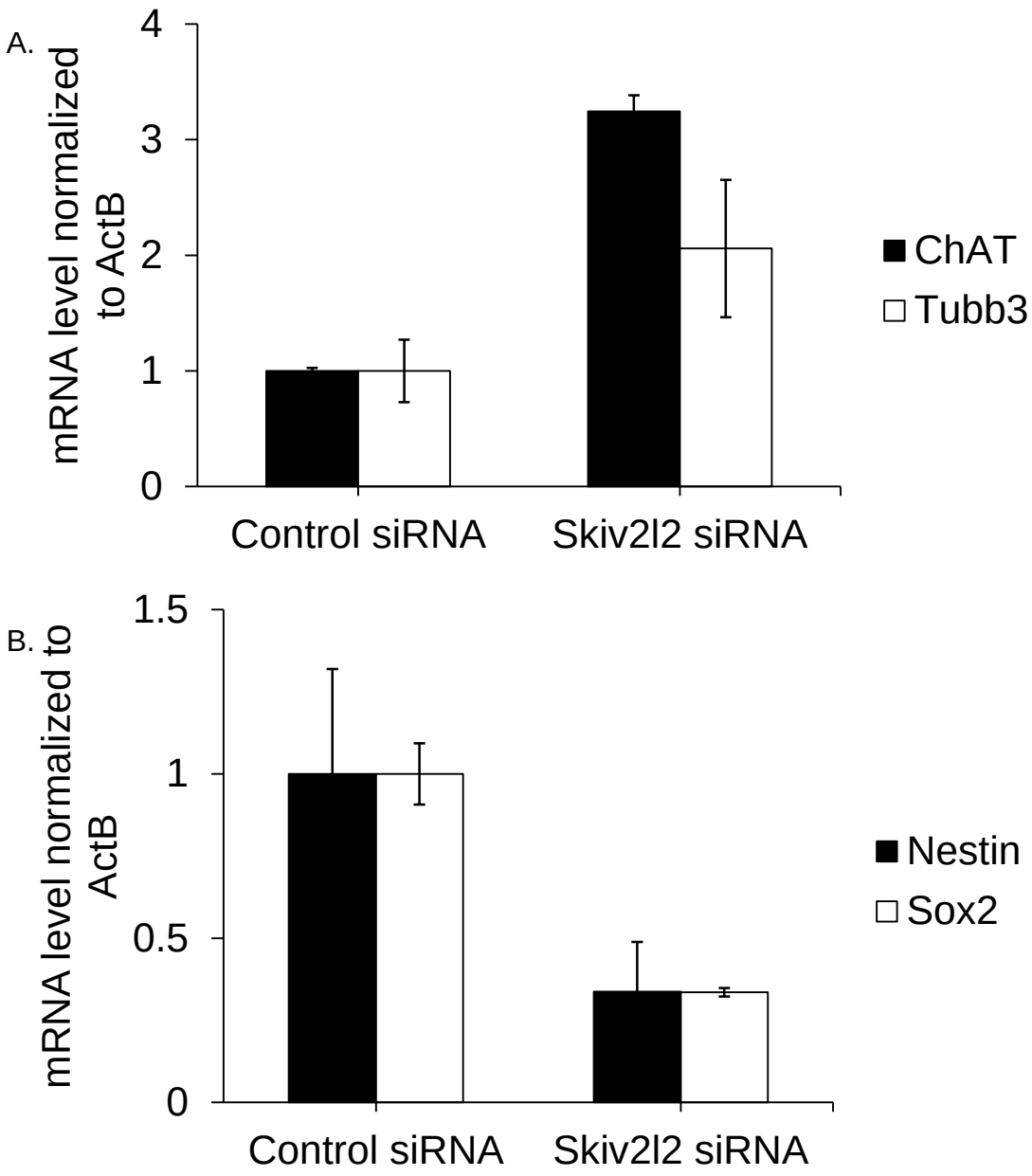

Fig 3.4: N2a cells exhibit changes in gene expression indicative of differentiation following *Skiv2l2* knockdown. A. qRT-PCR of Neuronal Differentiation Markers. RNA isolated from N2a cells transfected with either non-targeting control siRNA or *Skiv2l2* siRNA was reverse transcribed and amplified. *Tubb3* and *ChAT* expression were calculated from ΔCq values and normalized to ActB expression and control siRNA levels (error bars represent ±SD, n=3, p-values< 0.05, 0.0001). B. qRT-PCR of Pluripotency markers *Nestin* and *Sox2*. Performed as stated above, *Nestin* and *Sox2* expression were calculated from ΔCq values and normalized to ActB expression and control siRNA levels(error bars represent ±SD for n=3, p-values< 0.03, 0.01).

Following *Skiv2l2* knockdown, both GATA4 and Nkx2.5 mRNA levels increased 3.9 fold above those found in control P19 cells (Fig 3.5a, p-values< 0.0008, 0.008, respectively). Fabp3 mRNA levels were elevated 1.8 fold (p-value< 0.02), and Desmin mRNA levels increased 2.6 fold (p-value< 0.04) following SKIV2L2 depletion (Fig 3.5b). Overall, the expression pattern after *Skiv2l2* knockdown in P19 cells indicates enhanced differentiation into cardiomyocytes. Downregulation of the pluripotency transcription factors Nanog by 2.3 fold (p-value< 0.04) and Sox2 by 50 fold (p-value< 0.00001), respectively, denotes a shift in P19 cells from multipotent to differentiated following *Skiv2l2* knockdown (Fig.3.5c). Therefore, SKIV2L2 depletion promotes differentiation into both neurons in N2a cells and cardiac myocytes in P19 cells.

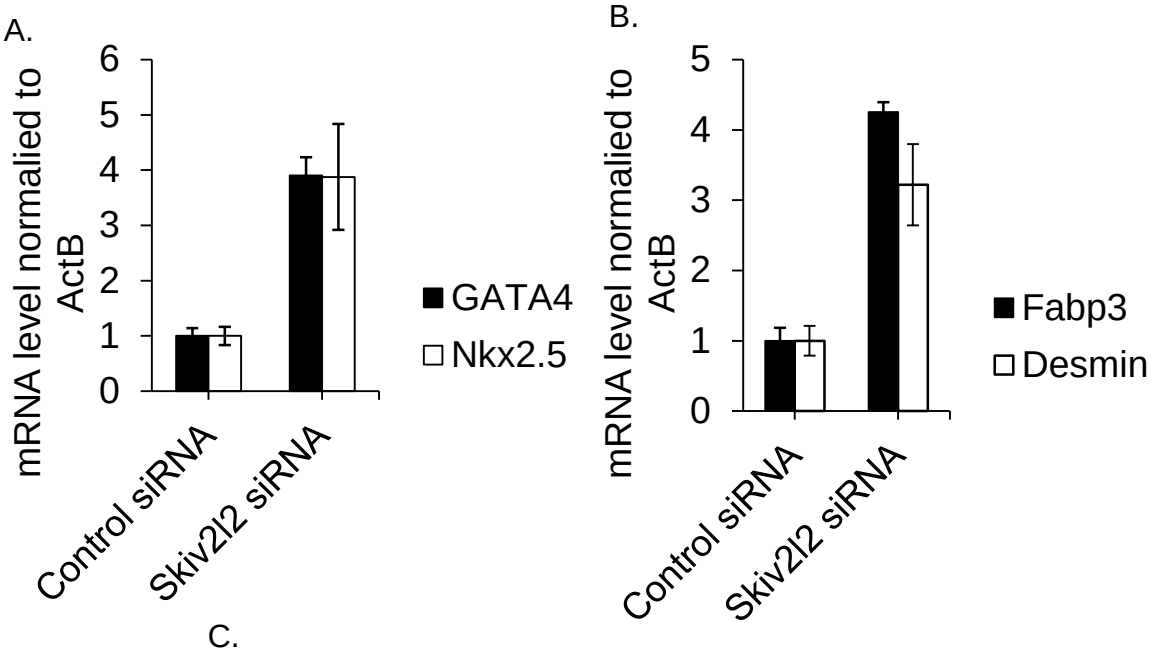
A.
mRNA level normalied to ActB
6
5
4
3
2
1
0
GATA4
Nkx2.5
Control siRNA
Skiv2l2 siRNA
B.
mRNA level normalied to ActB
5
4
3
2
1
0
Fabp3
Desmin
Control siRNA
Skiv2l2 siRNA

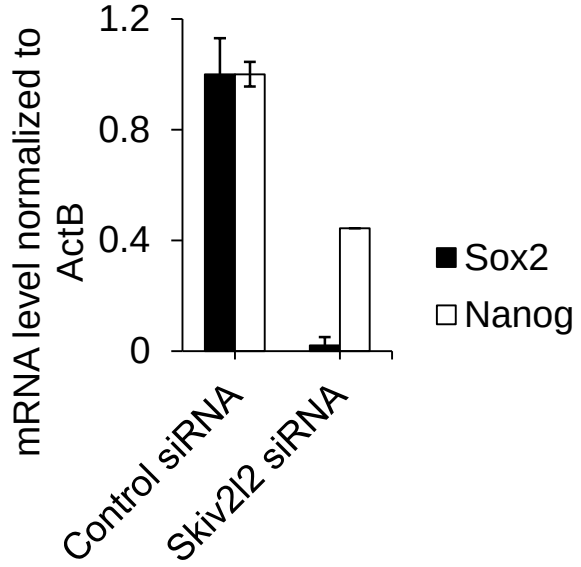
C.
mRNA level normalized to ActB
1.2
0.8
0.4
0
Sox2
Nanog
Control siRNA
Skiv2l2 siRNA

3.2.4 SKIV2L2 depletion does not restrict differentiation to one cell type

To see if SKIV2L2 is involved with repressing any one cell-fate, the cell fates in the population of *Skiv2l2* knockdown cells were monitored. If SKIV2L2 depletion results in differentiation into a single preferred cell fate, SKIV2L2 may be involved in repressing particular differentiation pathways (Fig 3.6). N2a cells have the ability to differentiate into both cholinergic neurons that express ChAT (Niblratt, 2009; Tremblay, 2010; Sidiropoulou, 2008) and dopaminergic neurons that express tyrosine hydroxylase (TH) (Tremblay, 2010; Sidiropoulou, 2008) . Retinoic acid treatment induces differentiation into cholinergic neurons, while dopaminergic neurons are produced following treatment with dibutyryl cyclic adenosine monophosphate (Tremblay, 2010; Sidiropoulou, 2008). To determine if SKIV2L2 depletion promotes differentiation into cholinergic neurons, dopaminergic neurons, or both cell types, qRT-PCR was performed to measure the relative abundance of ChAT and TH. As controls, cells were treated with control siRNA or ATRA, which were expected to trigger no differentiation and differentiation into cholinergic neurons, respectively. *Skiv2l2* knockdown cells were grown in either 10% FBS or 10% FBS supplemented with ATRA (which was not found to significantly alter SKIV2L2 levels).

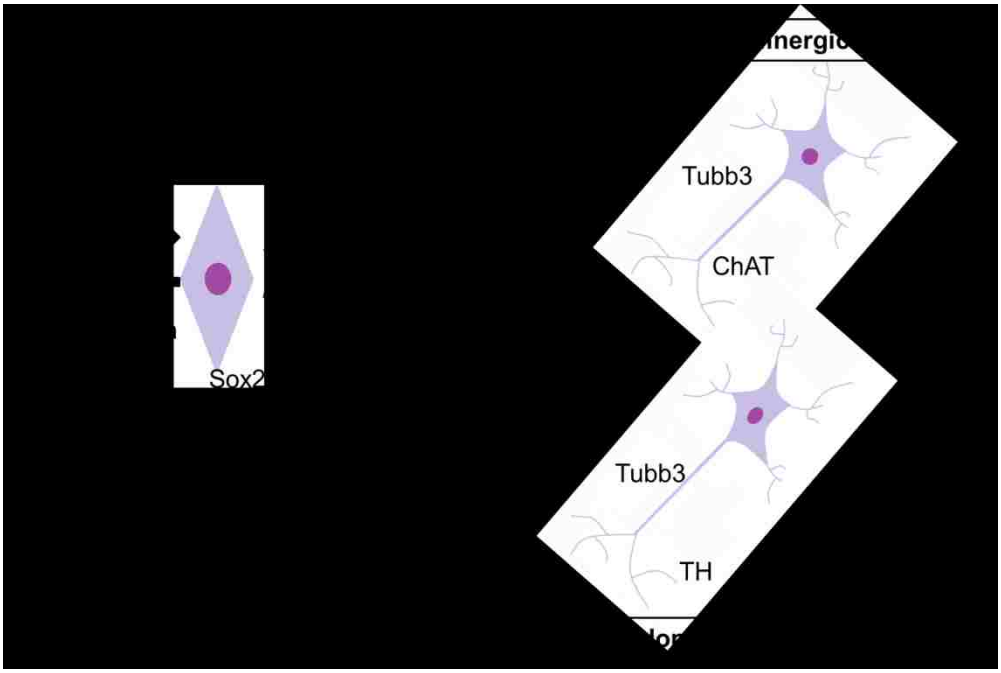
Tubb3
ChAT
Sox2
Tubb3
TH

qRT-PCR was employed to measure ChAT and TH mRNA levels among the cell population following either 20 μM ATRA treatment or *Skiv2l2* knockdown to assess the fates of differentiated cells. As expected, ATRA treatment alone caused a 4.2 fold increase in ChAT mRNA levels, with a 3.2 fold decrease in TH mRNA levels (Fig 3.7, p-value< 0.0001). This confirmed that ATRA drives N2a cell differentiation toward the cholinergic fate and away from the dopaminergic fate. However, in *Skiv2l2* knockdown cells, ChAT mRNA levels were elevated as previously described, but no decrease in TH was observed compared to control cells (Fig 3.7, p-value< 0.7). This suggests that following *Skiv2l2* knockdown, cells express both ChAT and TH, representing a pool of differentiated cells with mixed cell fates. Treating *Skiv2l2* knockdown cells with ATRA caused a significant 10 fold increase in ChAT expression (Fig. 3.7, p-value< 0.001), with a 1.2 fold decrease in TH levels (Fig. 3.7, p-value< 0.03). This effect suggests that treating *Skiv2l2* knockdown cells with ATRA restricts cells to differentiate into cholinergic neurons. Taken together, SKIV2L2 depletion alone does not drive differentiation into any one neuronal cell type. Instead, *Skiv2l2* knockdown cells appear to be poised to differentiate into multiple lineages, and differentiation can be directed down a certain pathway with chemical treatment.

A.

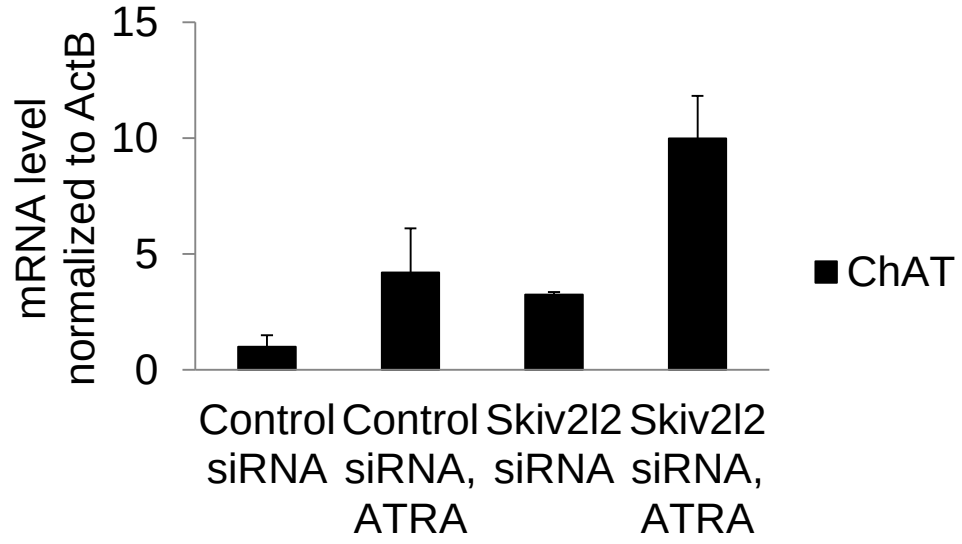
15
10
5
0
mRNA level normalized to ActB
ChAT
Control siRNA
Control siRNA, ATRA
Skiv2l2 siRNA
Skiv2l2 siRNA, ATRA

B.

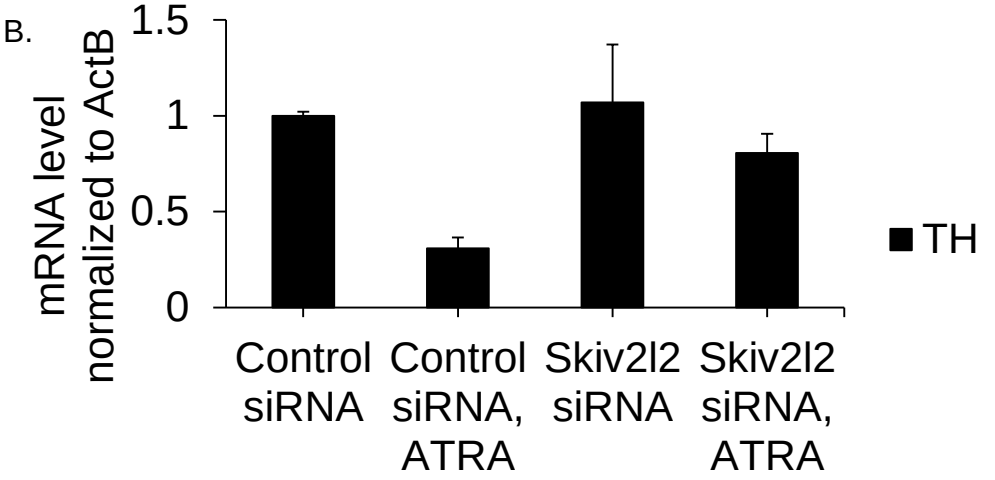
1.5
1
0.5
0
mRNA level normalized to ActB
TH
Control siRNA
Control siRNA, ATRA
Skiv2l2 siRNA
Skiv2l2 siRNA, ATRA

3.2.5 Differentiation cannot be directly attributed to the loss of the TRAMP or NEXT complexes

After discovering that *Skiv2l2* was downregulated during differentiation and lower levels of SKIV2L2 enhance differentiation into multiple cell types, experimentation focused on deciphering whether the function of SKIV2L2 in the TRAMP complex or the NEXT complex served to block differentiation. To address this question, the TRAMP complex member PAPD5 and NEXT complex member ZCCHC8 were each knocked down using siRNA. Differentiation was then defined through morphological and gene expression changes as outlined previously. If the TRAMP complex prevented cell differentiation, it was predicted that PAPD5 depletion would replicate the enhanced differentiation phenotype seen with *Skiv2l2* knockdown. Conversely, if the NEXT complex prevented differentiation, then ZCCHC8 depletion would enhance differentiation. It is also possible to get different phenotypes when knocking down different complex members because different proteins within the complex have different functions. For example, the adenylation of TRAMP targets has been shown to be nonessential in targeting certain RNAs to the exosome (Schilders, 2007), PAPD5 adenylates miRNAs independent of the TRAMP complex (Rammelt, 2011), and the role of ZCCHC8 in the NEXT complex is not well characterized, as all three components (Rbm7, *Skiv2l2*, and *Zcchc8*) have RNA binding capabilities. Given this, it was possible that PAPD5 and ZCCHC8 depletion could have no effect on differentiation or influence differentiation in a way distinct from SKIV2L2 function. After testing two commercially available antibodies against PAPD5 with no success, knockdown efficiency was measured via qRT-PCR for both *Papd5* and *Zcchc8*, as

mRNA levels were previously found to be comparative to protein levels following *Skiv2l2* knockdown. Due to reduced transfection efficiency in P19 cells, RNAi against *Papd5* and *Zcchc8* was performed in N2a cells. qRT-PCR was used to verify knockdown efficiency, and *Papd5* and *Zcchc8* mRNA levels were each reduced by 85% and 55%, respectively (Fig. 3.8, p-values< 0.05). Following RNAi treatment, differentiation was measured as previously outlined.

Papd5 knockdown cells were visualized using the same neuron outgrowth staining kit, and increased neuronal cell morphology was observed, with a 10% increase in cells extending neuronal processes (two proportion Z-score=-8.3, p-value< 0.05, Fig 3.9a,b). The mRNA levels of differentiation markers were quantified using qRT-PCR (Fig. 3.9c). PAPD5 depletion resulted in a 2.5 fold increase in ChAT mRNA levels (p-value< 0.02) and a 1.5 fold increase in Tubb3 mRNA levels (p-value< 0.001). These results appear to indicate that PAPD5 depletion replicated the phenotype observed with *Skiv2l2* knockdown.

However, *Zcchc8* knockdown cells were also characterized by a slight but insignificant increase in ChAT, Tubb3, and TH (Fig 3.10a, p-values< 0.20, 0.06, 0.080, respectively), with a statistically significant 3.6 fold decrease in Sox2 and a 2.7 fold decrease in Nestin (Fig 3.10b, p-values< 0.002, 0.02). This led to the conclusion that either loss of the TRAMP complex or loss of the NEXT complex could trigger reduced pluripotency, but that loss of ZCCHC8 alone does not promote terminal differentiation into neurons to the same extent seen in *Papd5* and *Skiv2l2* knockdown cells.

A.

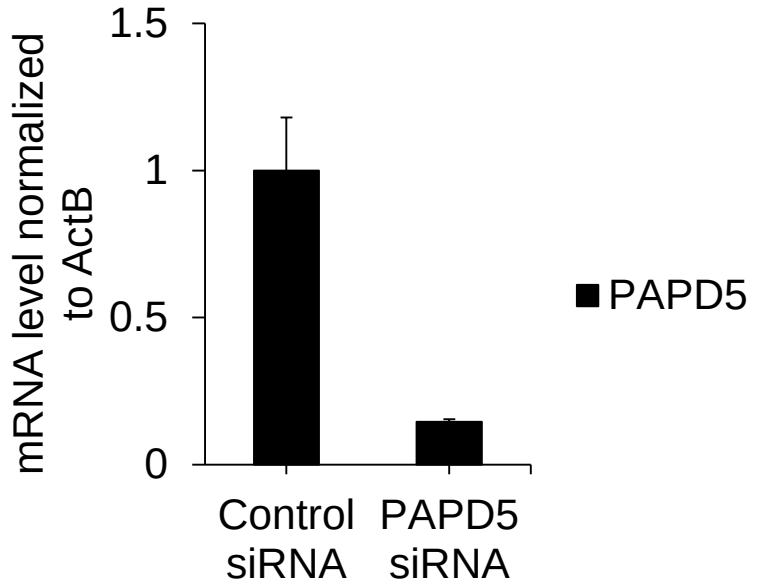

B.

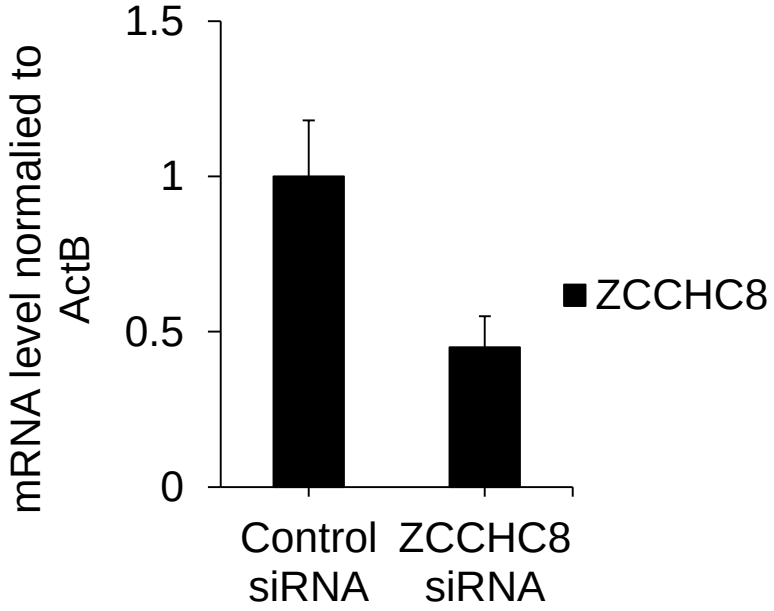

Fig 3.8: Verification of *Papd5* and *Zcchc8* knockdown in N2a cells. A. qRT-PCR of *Papd5*. RNA isolated from N2a cells transfected with either non-targeting control siRNA or *Papd5* siRNA was reverse transcribed and amplified. *Papd5* expression was calculated from ΔCq values and normalized to ActB expression and control siRNA levels (error bars represent ±SD for n=3, p-value< 0.05). B. qRT-PCR of the *Zcchc8*. *Zcchc8* expression was calculated from ΔCq values and normalized to ActB expression and control siRNA levels (error bars represent ±SD for n=3, p-value< 0.05).

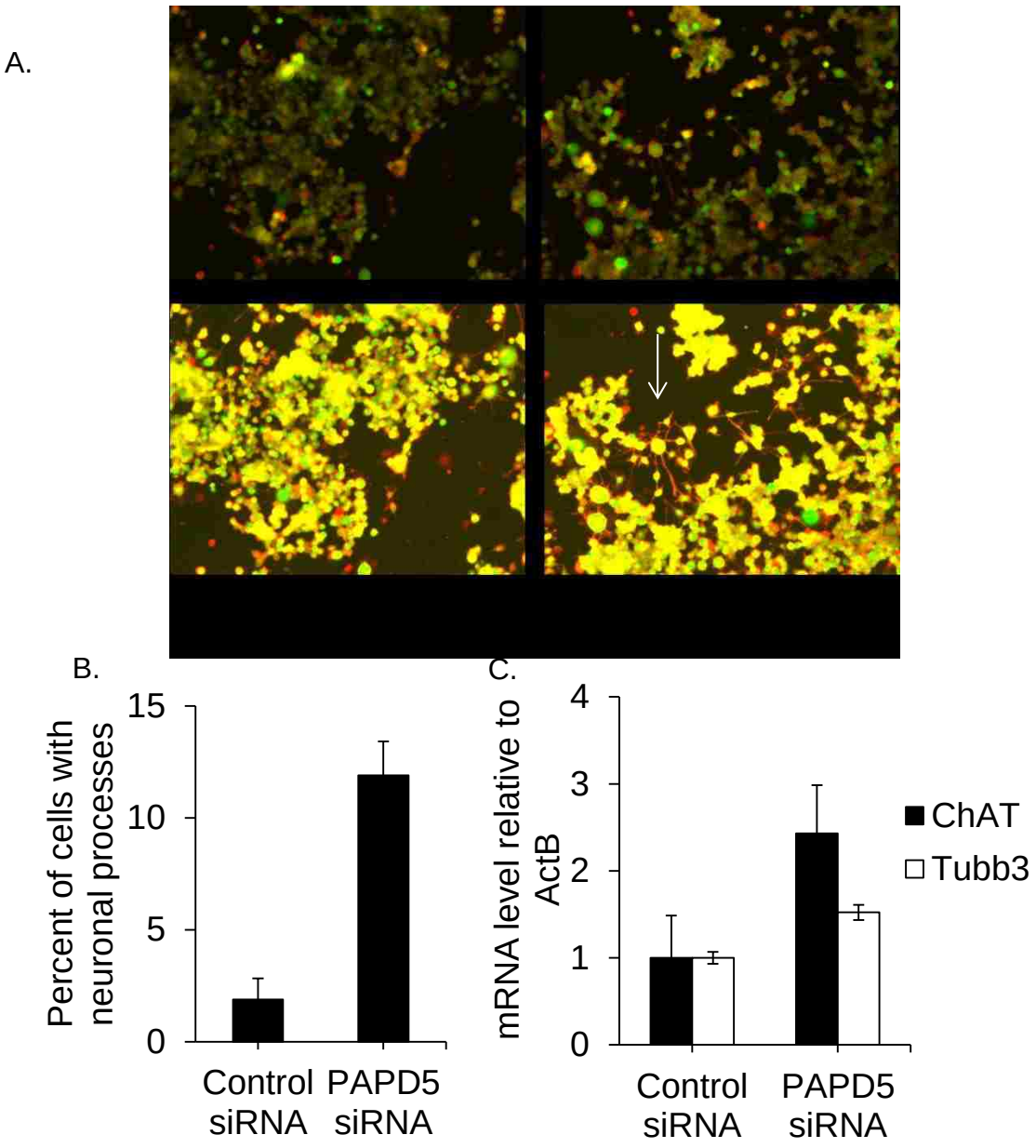

Fig 3.9: *Papd5* knockdown induces N2a cell differentiation. A. Fluorescent imaging. N2a cells stained with the neurite outgrowth staining kit, where green is a cell viability stain, orange is a cell membrane stain, and the overlay appears in yellow. Scale bar = 250 μm. Neuronal processes seen as red extensions were observed following *Papd5* knockdown. B. Quantification of neuronal processes. Cells extending neuronal processes longer than twice the diameter of the cell were counted for both samples. C. qRT-PCR of differentiation markers ChAT and Tubb3. RNA isolated from N2a cells transfected with either non-targeting control siRNA or *Papd5* siRNA was reverse transcribed and amplified. *ChAT* and *Tubb3* expression were calculated from ΔCq values and normalized to ActB expression and control siRNA levels (error bars represent ±SD for n=3, p-values< 0.02, 0.001).

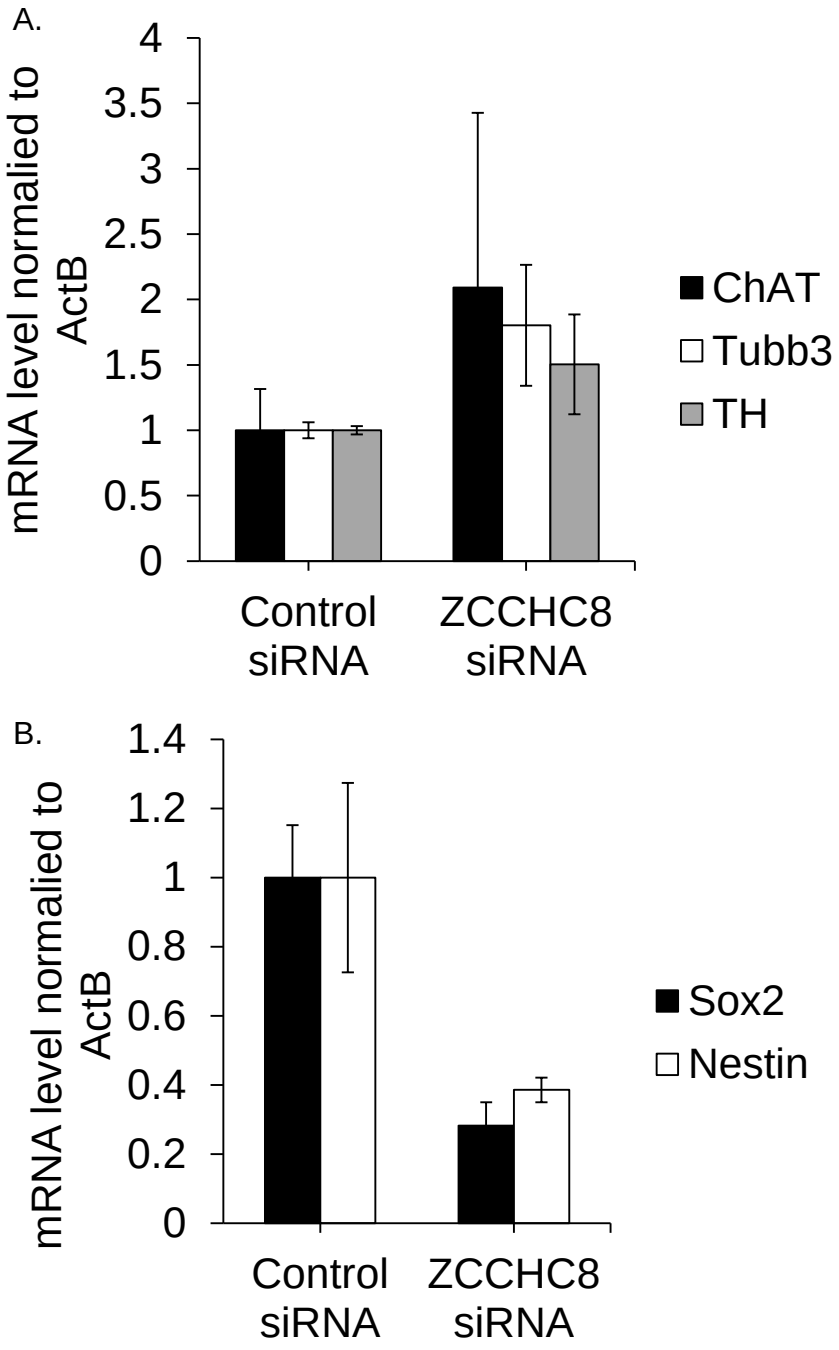

Fig 3.10: *Zcchc8* knockdown reduces pluripotency in N2a cells. A. qRT-PCR of differentiation markers. RNA isolated from N2a cells transfected with either non-targeting control siRNA or *Zcchc8* siRNA was reverse transcribed and amplified. *ChAT, Tubb3, and TH* expression were calculated from ΔCq values and normalized to ActB expression and control siRNA levels (error bars represent ±SD for n=3, p-values>0.05). B. qRT-PCR of pluripotency markers. *Sox2* and *Nestin* expression were calculated from ΔCq values and normalized to ActB expression and control siRNA levels (error bars represent ±SD for n=3), p-values< 0.002, 0.02.

In an attempt to explain this result, the expression of *Skiv2l2* was examined in *Papd5* and *Zcchc8* knockdown cells. Western blots demonstrated that *Papd5* knockdown resulted in a 42% decrease in SKIV2L2 protein levels (p-value< 0.002, Fig 3.11a). In agreement with these results, *Papd5* knockdown caused a 43% reduction in *Skiv2l2* mRNA levels (Fig.3.11b, p-value< 0.001). This reflects about a 50% destabilization of SKIV2L2 following PAPD5 depletion, a member of the TRAMP complex. Conversely, *Papd5* mRNA levels remained stable following *Skiv2l2* knockdown (p-value< 0.52). However, *Zcchc8* knockdown caused a slight but insignificant 1.7 fold increase in SKIV2L2 levels (Fig 3.11a, p-value< 0.2). SKIV2L2 levels remain stable following *Zcchc8* knockdown, suggesting that the expression of at least one NEXT complex component does not affect *Skiv2l2* expression.

Given that both *Zcchc8* and *Papd5* knockdown impacted differentiation and multipotency, the differentiation phenotype associated with SKIV2L2 depletion cannot be directly attributed to its function in either the TRAMP or NEXT complexes. It is possible that SKIV2L2 could influence differentiation through either the TRAMP or NEXT complex, or neither, but the redundancy and intricate relationships between nuclear surveillance components make it difficult to decipher which complex is involved. One way to address this would be to look at phenotypes following knockdown of different combinations of nuclear RNA surveillance proteins. For example, a *Papd5* and *Zcchc7* double knockdown would target the TRAMP complex, while a *Rbm7* and *Zcchc8* double knockdown would target the NEXT complex. Following both single and double knockdown experiments, the phenotype could be observed and compared to that seen with *Skiv2l2* knockdown. Finally, RNA-sequencing would identify RNAs accumulating

under each condition to see which RNAs are targeted by the NEXT complex, the TRAMP complex, or SKIV2L2 alone.

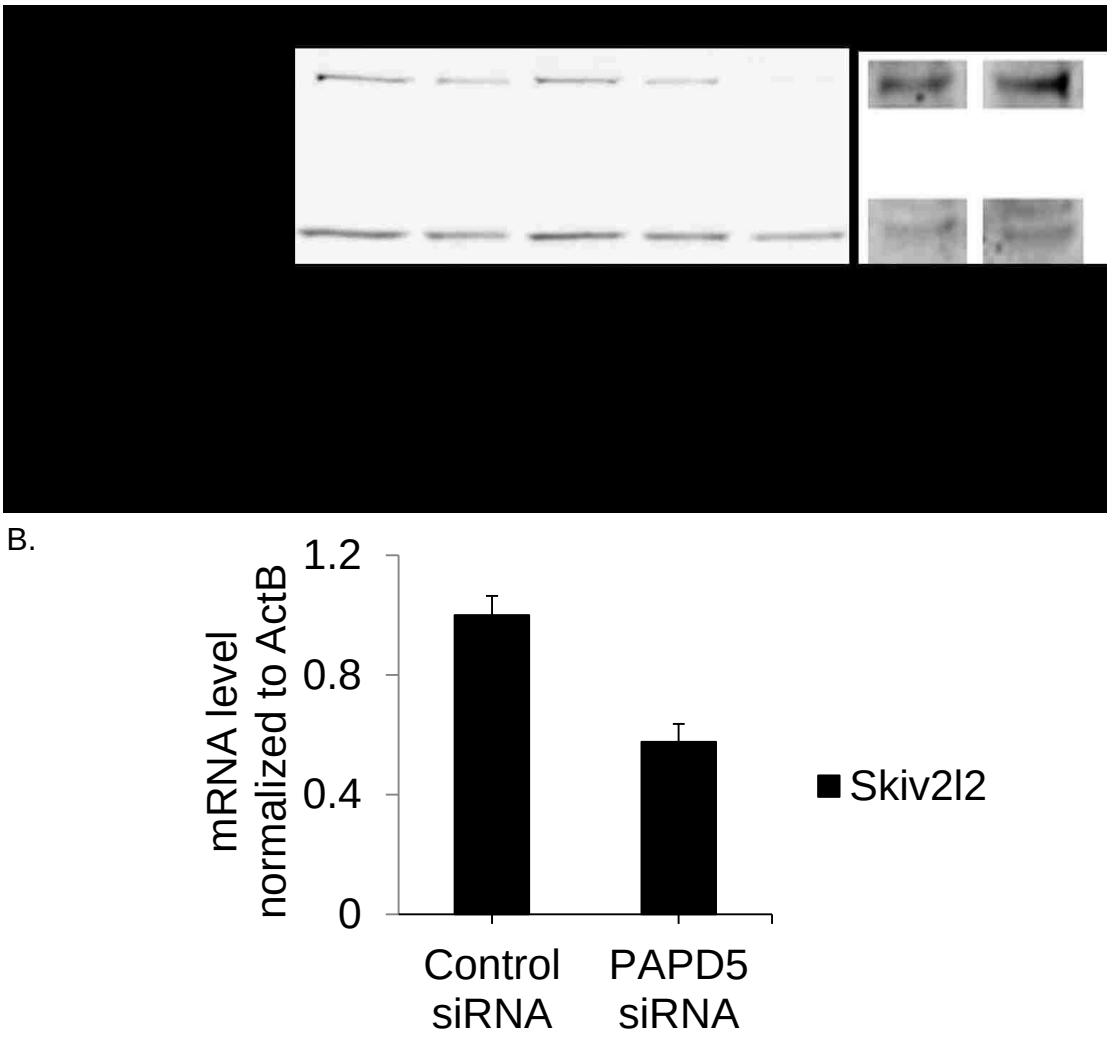

Fig 3.11: *Skiv2l2* expression decreases following *Papd5* knockdown. A. Western blots against SKIV2L2 protein in cells transfected with non-targeting control siRNA, *Skiv2l2* siRNA *Papd5* siRNA, or *Zcchc8* siRNA. N2a cells transfected with siRNA were grown in 10% FBS or 2% FBS, 20μM ATRA. SKIV2L2 protein levels (118 kD) were normalized to β-actin protein levels and control siRNA levels (42 kD). Experiment was run on two separate gels. B. qRT-PCR of *Skiv2l2* mRNA from cells transfected with non-targeting control siRNA or *Papd5* siRNA. *Skiv2l2* expression measured via ΔCq values was normalized to β-actin expression and control siRNA levels. Error bars represent ±SD for n=3, p-value< 0.001.

3.3 Discussion

Through these experiments, it was demonstrated that RNAi knockdown of *Skiv2l2* is sufficient to trigger the loss of pluripotency and induce differentiation in both P19 and N2a cells. Seeing as SKIV2L2 depletion promoted differentiation into both neurons and cardiomyocytes, this differentiation is not restricted to a single cell fate. In N2a cells, *Skiv2l2* knockdown resulted in both cholinergic and dopaminergic neurons, further supporting the conclusion that this effect on differentiation is not specific to a single differentiation pathway. *Papd5* knockdown alone enhanced differentiation, and *Zcchc8* knockdown reduced the expression of pluripotency markers. However, the complicated nature of the relationship between the NEXT and TRAMP complex components muddled any conclusion about whether the differentiation phenotype observed following SKIV2L2 depletion is due to either the TRAMP complex or the NEXT complex. It is possible that multiple SKIV2L2 target RNAs are responsible for the increased differentiation observed with SKIV2L2 depletion. These RNAs may each be targeted by a different complex, making the loss of one complex insufficient to drive differentiation. In addition, Papd5 and Zcchc8 may complex with SKIV2L2 but may not be essential to the turnover or processing of these specific RNAs.

These findings indicate that not only is decreased *Skiv2l2* expression indicative of differentiated cells, but SKIV2L2 depletion is sufficient to induce cell differentiation. This directly links RNA surveillance with differentiation and suggests that high SKIV2L2 levels impede differentiation. Pluripotent cells may require high levels of nuclear RNA surveillance. Similar to how autophagy pathways are upregulated in stem

cells due to increased translation (Phadwal, 2012), stem cells may also upregulate nuclear RNA surveillance pathways in response to the high levels of transcription and protein synthesis required for pluripotency and cell division (Boisvert, 2007). During differentiation, nuclear RNA surveillance mechanisms may be downregulated to change the steady-state levels of certain RNAs, leading to decreased pluripotency and allowing for differentiation to proceed.

While the differentiation phenotype could not be definitively linked to the TRAMP or NEXT complexes, the experiments did reveal insight into nuclear RNA surveillance. PAPD5 appears to be necessary for the stability of SKIV2L2 in the TRAMP complex. Differentiation following *Papd5* knockdown could be attributed to downregulation of SKIV2L2, loss of the TRAMP complex, or loss of PAPD5 function outside the TRAMP complex. Because *Zcchc8* knockdown alone reduced the expression of pluripotency markers but did not induce terminal differentiation, it is possible that the reduction in ZCCHC8 was not sufficient to replicate the differentiation associated with SKIV2L2 depletion, or that the differentiation seen following *Skiv2l2* knockdown is a complex phenotype resulting from the loss of both TRAMP and NEXT complex functions. The finding that *Papd5* knockdown led to a consistent 40% decrease in SKIV2L2 levels has two implications. First, differentiation seen in *Papd5* knockdown cells could be attributed to lower levels of SKIV2L2. Second, SKIV2L2 levels seem to be regulated based on its function in the TRAMP complex because loss of another TRAMP complex component, but not a NEXT complex component, led to *Skiv2l2* downregulation.

While these results definitively indicate that SKIV2L2 is necessary to maintain pluripotency in murine cancer cell lines, it is unclear whether differentiation is directly inhibited by SKIV2L2 or differentiation results indirectly from decreased pluripotency or increased cell stress. It is worth noting that N2a and P19 cell growth depends on confluency and contact inhibition. Plate overcrowding can lead to detachment, apoptosis, and cell death. Also, cells grown at increased confluency cannot differentiate due to contact inhibition (Zhi, 2012). Because cells were not grown past confluency, overcrowding did not occur. However, *Skiv2l2* knockdown plates were not as confluent as control plates, meaning that decreased contact inhibition could contribute to increased levels of differentiation. One way to address this would be to closely look at changes in gene expression and cell confluency over time to see if decreased confluency is the cause or result of differentiation.

Therefore, while these experiments established SKIV2L2 as necessary to maintain multipotency in cancer cell lines, they do not offer conclusive proof that SKIV2L2 directly represses differentiation pathways, as opposed to maintaining proliferation and indirectly blocking differentiation. On the contrary, the seemingly poised status of N2a cells to undergo differentiation into either cholinergic or dopaminergic neurons following *Skiv2l2* knockdown implicates SKIV2L2 in maintaining proliferation and pluripotency as opposed to repressing a single differentiation pathway. The next chapter addresses this hypothesis in further detail. Nevertheless, the conclusion that loss of SKIV2L2 leads to cell differentiation offers unique insight into the role of RNA surveillance in stem cell maintenance. Coupled with the downregulation of *Skiv2l2* during differentiation, discovering that this downregulation is sufficient to induce differentiation gives a better

understanding of how and why RNA surveillance changes upon cell differentiation. Focusing on specific RNA surveillance targets that are necessary to maintain pluripotency will not only expand knowledge of RNA surveillance mechanisms but also will help advance understanding of stem cell maintenance. Given that many anti-cancer drugs focus on triggering apoptosis or differentiation, and stem cell therapy requires cell differentiation, the downregulation of *Skiv2l2* can be potentially utilized to enhance cell differentiation in future cancer and stem cell research.

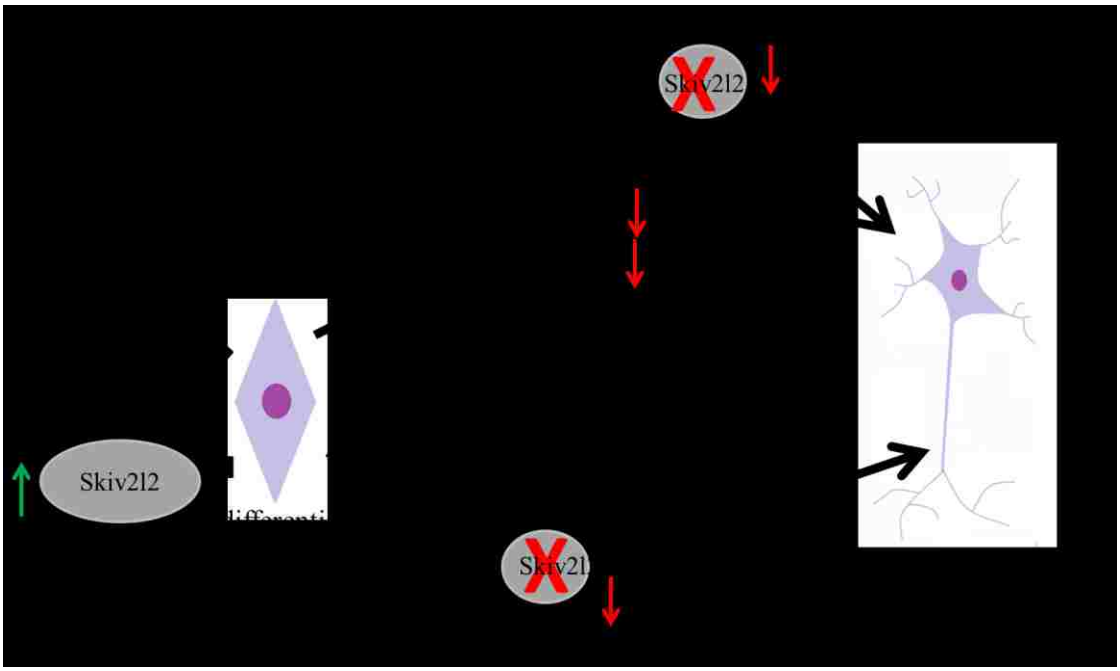

Fig 3.12: Model depicting the relationship between SKIV2L2 and differentiation. Decreases in SKIV2L2 levels are correlated with increased differentiation. This decrease in SKIV2L2 can be accomplished through chemically induced differentiation, which leads to decreased growth signaling, or through RNAi. Higher levels of SKIV2L2 maintain pluripotency and proliferation in cancer cell lines.

CHAPTER IV: SKIV2L2 DEPLETION INDUCES A SLIGHT BUT SIGNIFICANT MITOTIC ARREST IN MURINE CELL LINES

4.1 Introduction

Hypothesis: SKIV2L2 depletion via RNAi results in reduced proliferation in murine cell lines.

In the previous chapter, experiments demonstrated that *Skiv2l2* knockdown via RNAi enhanced differentiation in N2a and P19 cells and that the differentiation resulting from reduced SKIV2L2 levels was not restricted to one cell type or one differentiation pathway. Because differentiation and cancer stem cell maintenance are affected in multiple cell types, it is unlikely that RNA surveillance specifically represses one cell fate, which would be more likely result in ectopic expression of lineage-specific genes with loss of SKIV2L2. The maintenance of stem cells and cancer stem cells depends on both the expression of pluripotency genes and high levels of proliferation. With no evidence that SKIV2L2 represses specific differentiation pathways, it was hypothesized that SKIV2L2 instead enhances proliferation to maintain pluripotency. In support of the hypothesis that SKIV2L2 enhances cell proliferation, studies in zebrafish found that SKIV2L2 is necessary to maintain stem cell pools and colocalizes with PCNA, a marker of cells in S phase (Yang, 2007; Hultman, 2010). *Skiv2l2* mutant zebrafish not only have underdeveloped brains and immune systems, but the mutants also cannot regenerate melanocytes or tails normally derived from stem cell pools (Yang, 2007; Iwanami, 2009). While the experiments outlined in Chapter 3 demonstrated that SKIV2L2 depletion results in reduced expression of pluripotency markers, such as Sox2 and Nanog, it was

necessary to also investigate how *Skiv2l2* knockdown influences cellular proliferation to understand the effect of SKIV2L2 on cancer stem cell maintenance.

SKIV2L2's localization to the nucleoplasm and nucleolus bolsters the hypothesis that SKIV2L2 functions as a regulator of cell division (Osman, 2011; Lubas, 2011). In particular, the nucleolus regulates certain stages in cell growth and division, and other nucleolar proteins have been shown to be downregulated during differentiation (Boisvert, 2007; Tsai, 2014; Yang, 2011). DNA helicases in the nucleolus influence the timing of S phase, and the nucleolar sequestration of different proteins like HDM2 regulates growth arrest (Boisvert, 2007; Phillips, 2006). Because SKIV2L2 functions in nucleolar RNA surveillance, and the nucleolus helps regulate cell division (Boisvert, 2007; Tsai, 2014; Yang, 2011), SKIV2L2 may also play a role in cell division. Interestingly, ZCCHC8, a NEXT complex member, is phosphorylated during the G2/M phase spindle assembly checkpoint, suggesting RNA surveillance is regulated in a cell cycle dependent manner (Gustafson, 2007). Overall, the cellular location of SKIV2L2 and the G2-specific phosphorylation of ZCCHC8 lend credence to the hypothesis that RNA surveillance is necessary for cell proliferation.

Differentiation and proliferation are often viewed as antagonistic processes because cells proliferate prior to differentiation, but cells arrest in G1 phase just before differentiation (Liu, 2013b). Therefore, proliferative cells usually do not differentiate, and differentiation requires proliferation to halt. The majority of terminally differentiated cells lose the ability to divide, with new cells coming only from a stem cell pool. Additionally, many cancer cell lines, including N2a cells, differentiate following serum starvation, indicating that the growth factors that keep cancer cells proliferating are

necessary to prevent differentiation (Phillips, 2006). Slowed cellular proliferation could result in the increased differentiation seen with *Skiv2l2* knockdown, as SKIV2L2 depletion caused reduced confluency, which could induce differentiation by relieving contact inhibition. Because N2a and P19 cells are immortalized cell lines derived from cancer cells, it was also possible that differentiation could result from cell cycle stress (Smith, 1998). Genetic mutations in cancer cells can prevent apoptosis that would be triggered in healthy cells experiencing cell cycle arrest (Freije, 2014). This phenomenon often leads to "slippage" through cell cycle checkpoints, followed by cellular senescence, necrosis, or differentiation (Freije, 2014; Dikovskaya, 2015; Sato, 1994; Rieder, 2004). This occurs as cells cannot hold the spindle assembly checkpoint indefinitely, as cyclin B is degraded over time. This causes the cell to progress through mitosis, generating a tetraploid cell. Tetraploid cells then either exit the cell cycle, followed by senescence or differentiation, or continue through the cell cycle, ultimately dying through necrosis (Freije, 2014; Dikovskaya, 2015; Sato, 1994; Rieder, 2004). In light of this, it was hypothesized that reduced SKIV2L2 levels impede progression through the cell cycle, ultimately causing cellular differentiation. To investigate this hypothesis, multiple experiments were performed to see how SKIV2L2 depletion affects cell proliferation (Fig 4.1).

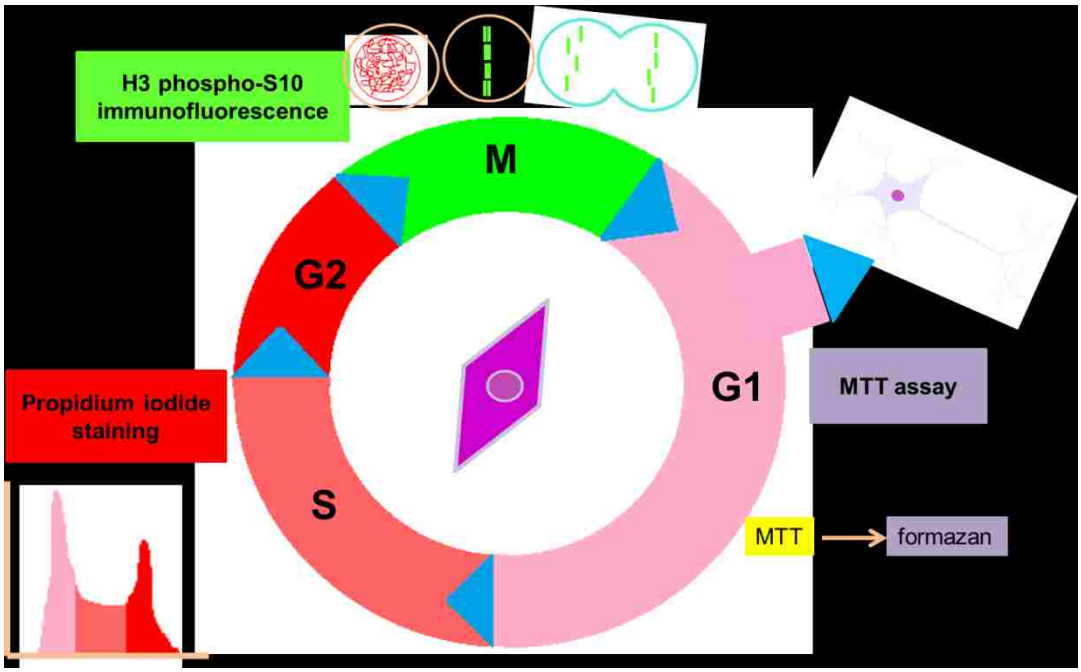

Fig 4.1: Experimental method to determine how *Skiv2l2* knockdown via RNAi influences proliferation. Three major experiments were performed: MTT assays, propidium iodide staining, and H3 phospho-S10 immunofluorescence. MTT assays gave a colorimetric readout of overall proliferation, propidium iodide staining monitored the percent of cells in G1, S, and G2/M based on DNA content, and H3 phospho-S10 immunofluorescence measured the amount of cells undergoing mitosis.

4.2 Approach and Results

4.2.1 SKIV2L2 depletion reduces the total number of proliferating cells by approximately 30%

To test the hypothesis that SKIV2L2 maintains cell proliferation in cancer stem cells, MTT assays were used to quantify the proliferation of both N2a and P19 cells transfected with either control or *Skiv2l2* siRNA. MTT assays estimate the relative amount of proliferating cells. The mitochondrial reductases in proliferating cells reduce MTT 3-(4,5-dimethylthiazol-2-yl)-2,5-diphenyltetrazolium bromide to the purple formazan crystal, making formazan production a readout of metabolic activity (Xie,

2010; Gui, 2014). Lower levels of MTT reduction into the purple formazan product correspond to a decrease in the number of proliferating cells, which could be due to cell death, cell differentiation, or slower progression through the cell cycle (Xie, 2010; Gui, 2014). MTT reduction is easily quantified using a spectrophotometer to measure the absorbance of the formazan crystal, with higher absorbance correlating with both increased formazan production and more proliferating cells. Cell proliferation was measured by comparing the absorbance at 570 nm of the dissolved formazan from *Skiv2l2* knockdown cells to control cells.

In both N2a cells and P19 cells, SKIV2L2 depletion resulted in a decrease in formazan production. Transfection of N2a cells with *Skiv2l2* siRNA resulted in a 38% (p-value< 0.0001, Fig.4.2a, b) overall decrease in formazan reduction. Capturing this in a time course experiment revealed that proliferation of both retinoic acid treated cells and *Skiv2l2* knockdown cells slowed similarly over time when compared to control cells (Fig. 4.2c). Twenty-eight hours following transfection, *Skiv2l2* siRNA resulted in a 22% (p-value< 0.002) reduction in proliferation, and at thirty-two hours, *Skiv2l2* knockdown cell proliferation was 27% less than that seen in control cells (p-value< 0.002). The experiment was repeated following *Skiv2l2* siRNA transfection of P19 cells, with P19 cells showing a similar 30% decrease in formazan production after 32 hours (p-value< 0.0001, Fig. 4.2d). This result demonstrates a 22-38% reduction in the number of proliferating cells following SKIV2L2 depletion.

A.

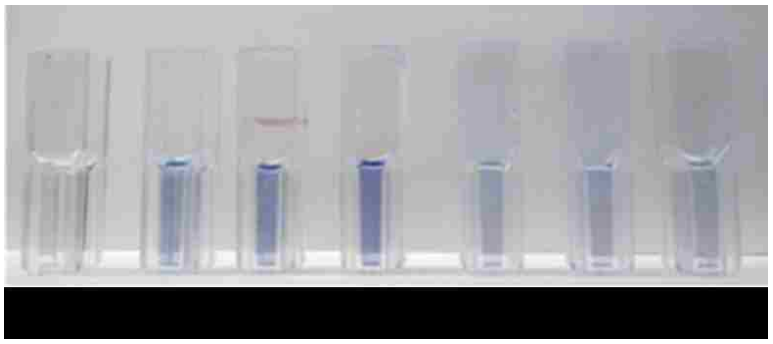

C.

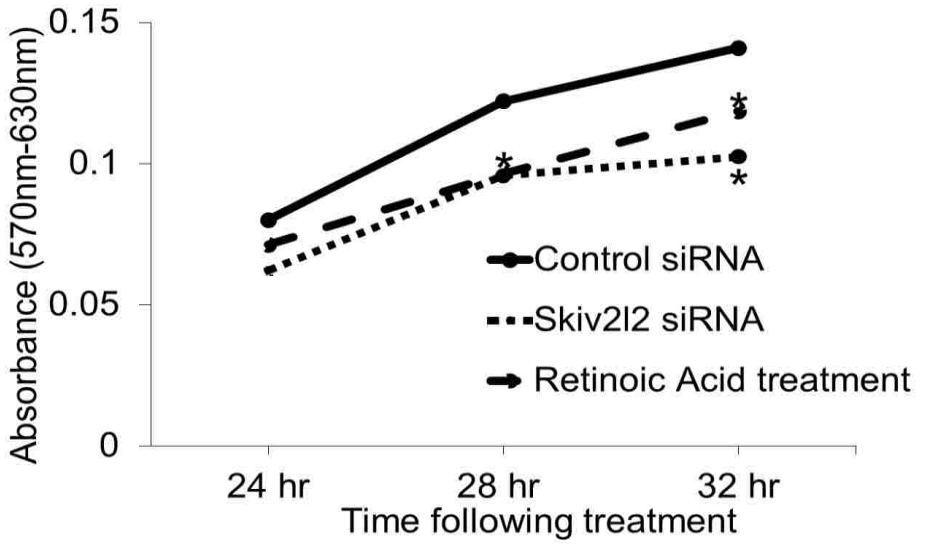
0.15
0.1
0.05
0
Absorbance (570nm-630nm)
Control siRNA
Skiv2l2 siRNA
Retinoic Acid treatment
*
*
*
24 hr
28 hr
32 hr
Time following treatment

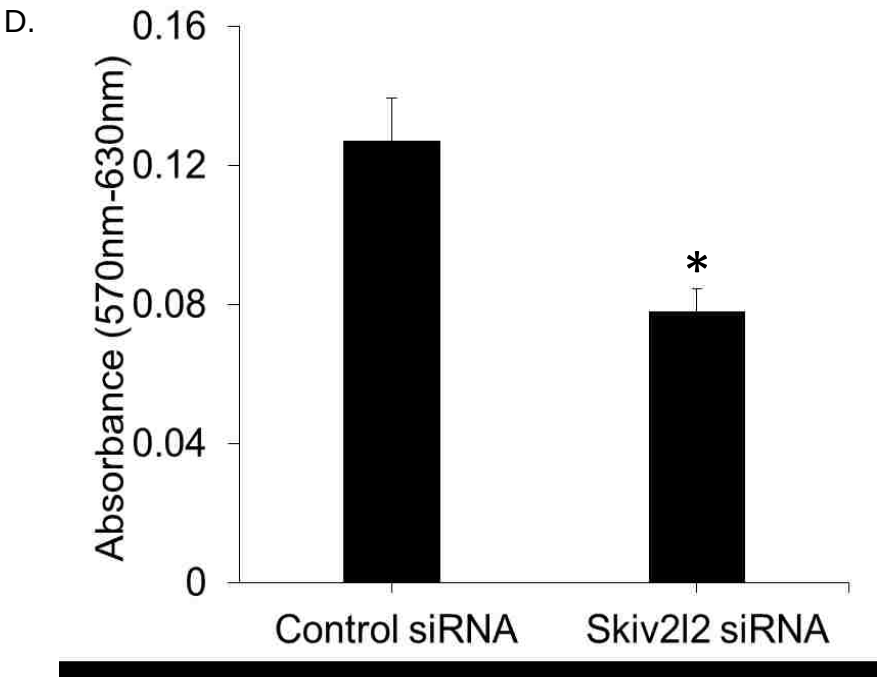

Fig 4.2: MTT assays demonstrated reduced overall proliferation following *Skiv2l2* knockdown. A. MTT Assay in N2a cells. Cells were treated with MTT 48 hours following transfection of N2a cells with non-targeting control siRNA or *Skiv2l2* siRNA. Cuvette 1 contains N2a cells that were not treated with MTT as a negative control, cuvettes 2-4 contain control siRNA cells treated with MTT, and cuvettes 5-7 contain *Skiv2l2* siRNA cells treated with MTT. B. Quantification of formazan absorbance from MTT assay in A. Background absorbance at 630nm was subtracted from 570nm formazan absorbance to determine the total level of MTT reduction (error bars represent ±SD for n=9, p-value< 0.0001). C. MTT Time point Assay in N2a cells. Absorbance of formazan was recorded at 6 hour time points before harvesting cells transfected with non-targeting control siRNA or *Skiv2l2* siRNA (n=4 for each time point, * represents p-value< 0.05 compared to control cells). D. MTT Assay in P19 cells. MTT Assay performed in P19 cells as stated in A and B, where p-value< 0.0001.

4.2.2 *Skiv2l2* knockdown does not induce cell death in cancer cell lines

Because the MTT assay measures overall proliferation, the reduced proliferation of *Skiv2l2* knockdown cells could be due to cell death. To examine this possibility, N2a cells were stained with propidium iodide, which passes through the compromised membranes of dead cells and binds to DNA. This allows cells to be sorted through fluorescent activated cell sorting (FACs) and quantified based on cell viability: dead or dying cells stain with propidium iodide, while live cells do not (Lima, 2008). In addition to propidium iodide staining, FACs analysis sorts cells based on forward scatter and side scatter. Forward scatter measures size, allowing smaller cellular debris and larger clumps to be excluded from the cell population to be analyzed. Side scatter measures the granularity of the cells, and apoptotic, necrotic, and dead cells generally have increased side scatter (Lima, 2008). Measuring the proportion of cells with increased side scatter serves as a way to both confirm the percentage of dead cells measured via propidium iodide staining and measure the percentage of apoptotic cells with intact cellular membranes that do not stain with propidium iodide.

Because P19 cells grow in clusters as myocytes or embryoid bodies, it was impractical to subject these cells to FACs analysis as the large clumps of cells would make data analysis difficult. Instead, N2a cells were stained with propidium iodide to investigate cell viability following *Skiv2l2* knockdown (Fig 4.3a). Quantifying the percentage of total cells staining with propidium iodide revealed that transfection of N2a cells with control siRNA and differentiation with all-trans retinoic acid resulted in identical 14% cell death rates (p-value< 0.7, $n=3$). SKIV2L2 depletion, however,

significantly decreased the number of dead cells, as only 5% of *Skiv2l2* knockdown cells stained with propidium iodide (p-value< 0.0001, n=3, Fig 4.3b). This denotes that the reduced levels of proliferation following SKIV2L2 depletion seen in the MTT assay could not be attributed to increased cell death. To confirm this result, side scattering was examined through FACs analysis (Fig 4.4). Control cells and *Skiv2l2* knockdown cells exhibited comparable proportions of cells with increased side scatter (7.6% and 4.9%, respectively, p-value< 0.2). Retinoic acid treatment had a higher proportion of cells exhibiting side scatter (13.9%, p-value< 0.01), suggesting that a higher proportion of chemically differentiated cells undergo apoptosis. Seeing as SKIV2L2 depletion did not increase the proportion of granule cells, it was concluded that loss of SKIV2L2 does not result in increased cell death or trigger apoptosis.

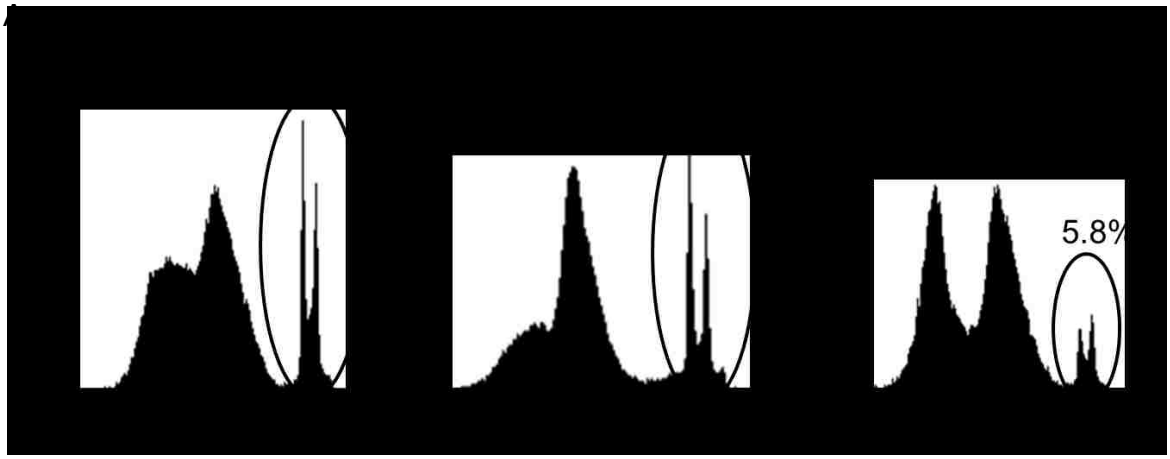
5.8%

B.

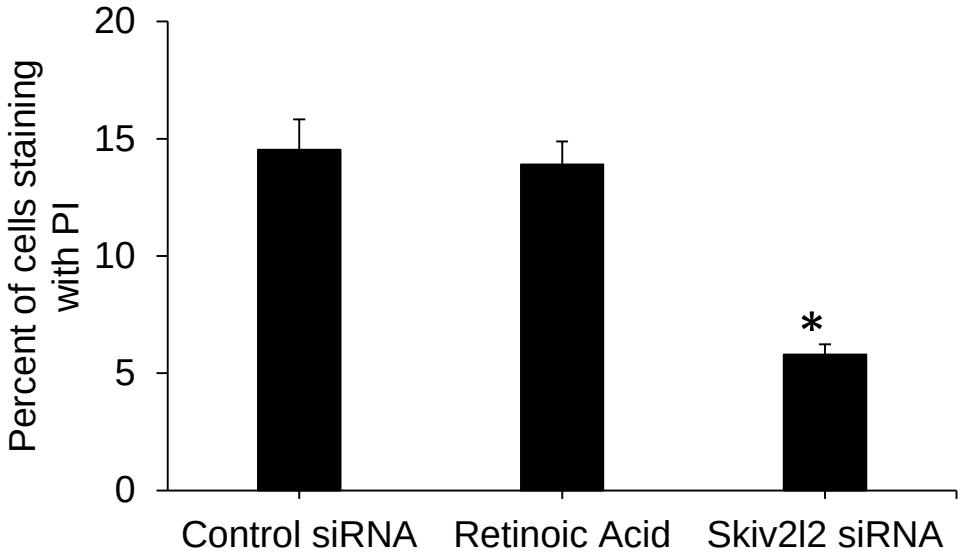
Percent of cells staining with PI
20
15
10
5
0
*
Control siRNA
Retinoic Acid
Skiv2l2 siRNA

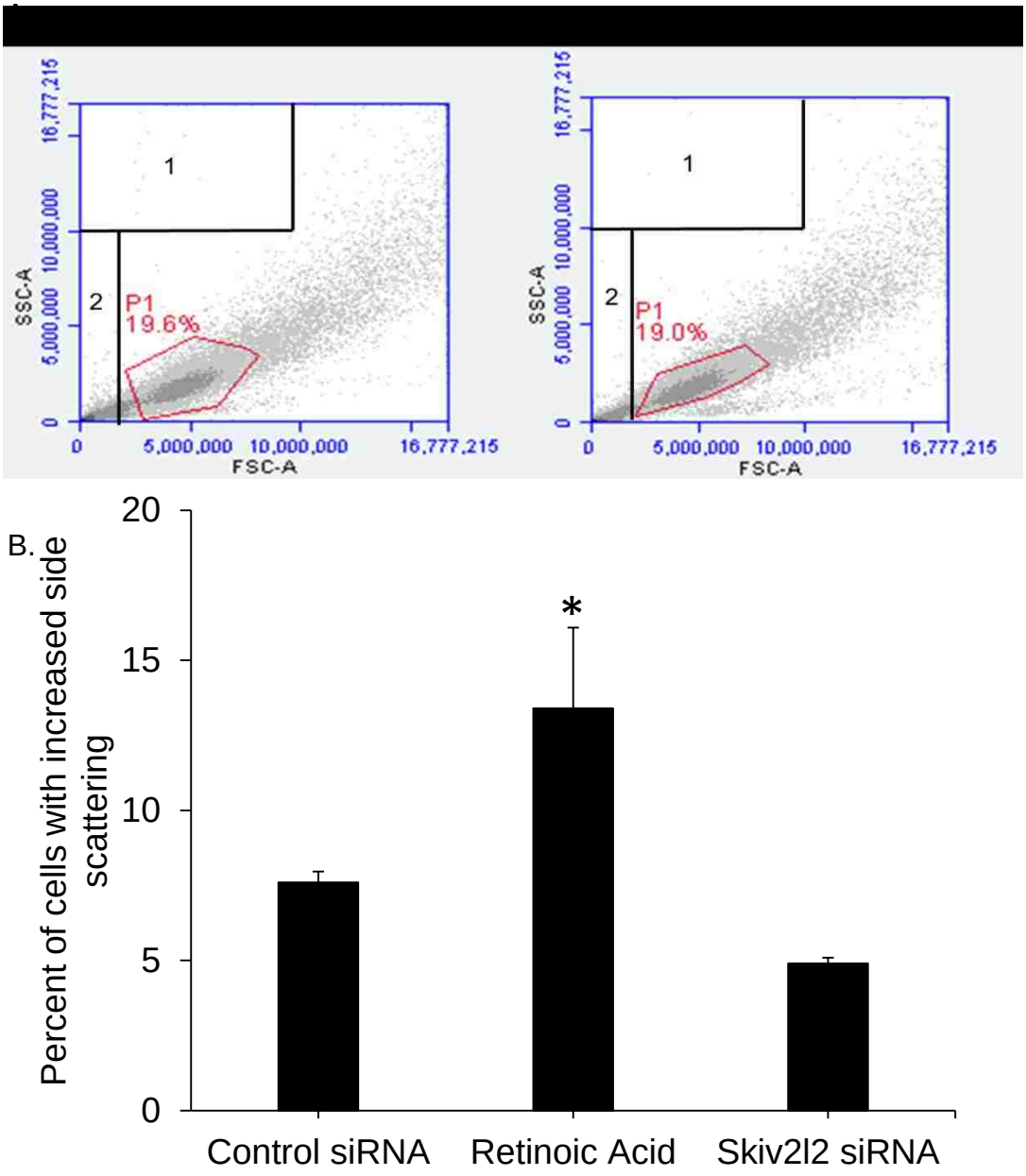

Fig 4.4: *Skiv2l2* knockdown does not trigger cell death according to side scattering. A. FACs analysis of side scatter. N2a cells stained with propidium iodide were excited at 488nm and sorted using the Accuri C6. Cells were initially sorted based on forward scatter (FSC-A) vs. side scatter (SSC-H). Cells with increased side scatter are in quadrant (1), with debris in quadrant (2). Single live cells ideal for analysis are circled. B. Quantification of dead cells based on side scatter. To approximate the percentage of dead, apoptotic, and necrotic cells, cells in quadrant (1) were selected using the Accuri C6 software. No significant change was observed with Skiv2l2 siRNA (p-value< 0.2), while retinoic acid increased apoptotic cells (p-value< 0.01).

4.2.3 SKIV2L2 depletion triggers a modest but statistically significant increase in G2/M phase cells

Because SKIV2L2 depletion results in increased differentiation, it was hypothesized that loss of SKIV2L2 would first cause G1 arrest and then differentiation like that seen in N2a cells treated with ATRA (F Zhi, 2012; Wesley, 2015). To test this hypothesis, the cell cycle was examined through FACs analysis of fixed N2a cells stained with propidium iodide. Propidium iodide passes through the permeabilized membranes of fixed cells and binds to DNA. Gating based on forward and side scatter allows cell debris, cell clumps, and dead cells to be excluded from the analysis. The amount of propidium iodide fluorescence correlates to DNA content, and FACs sorts the cells based on the intensity of propidium iodide fluorescence (Krishan 1975). Given that DNA content is replicated in S phase, cells in G1 phase possess half the DNA content of cells in G2 phase and therefore half the intensity of propidium iodide fluorescence. For example, ATRA treatment induces G1 phase arrest followed by cell cycle exit and differentiation (F Zhi, 2012), which would lead to the majority of cells staining with propidium iodide at a lower intensity. If SKIV2L2 depletion induced differentiation in a similar manner, the cell cycle profile would be similar to ATRA treated cells and indicate G1 phase arrest. A different landscape would suggest that SKIV2L2 depletion disrupts the cell cycle in a way distinct from natural or chemically induced differentiation.

For N2a cells transfected with negative control siRNA, the majority of cells were found to be in G1 phase, with smaller proportions of cells observed in S phase and G2/M phase. As expected, differentiation of N2a cells with ATRA induced a small but significant 11% increase in the proportion of cells in G1 phase compared to control cells

(p-value< 0.003, Fig 4.5). Low levels of G1 differentiated cells were most likely due to the use of ATRA alone with 10% FBS, which is less effective at inducing differentiation but does not induce changes in *Skiv2l2* expression. Surprisingly, SKIV2L2 depletion did not cause G1 arrest as expected. Instead, the highest proportion of *Skiv2l2* knockdown cells appeared to have doubled their DNA content, indicative of G2/M phase. This modest but statistically significant 23% increase (p-value< 0.00001, Fig 4.6a) in G2/M phase cells implies that SKIV2L2 depletion hinders the progression of cells through G2/M phase. Additionally, when compared to control cells, *Skiv2l2* knockdown cells showed a marked 23% reduction in G1 phase cells (p-value< 0.000001, Fig 4.5). The increase in G2/M phase cells following SKIV2L2 depletion indicates impaired cell cycle progression distinct from the G1 phase arrest seen in chemically differentiating N2a cells. FACS analysis of propidium iodide-stained cells implicates SKIV2L2 in G2/M phase progression, as reduced SKIV2L2 levels cause an increase in the percent of cells in G2/M phase. This finding hints that while SKIV2L2 is necessary to prevent cell differentiation, the differentiation that occurs following *Skiv2l2* knockdown is an indirect effect of loss of RNA surveillance. With direct induction of differentiation pathways, G1 arrest would be expected, similar to that seen with ATRA treatment. Because *Skiv2l2* knockdown does not increase the number of G1 phase cells, differentiation is not likely to occur in the same manner.

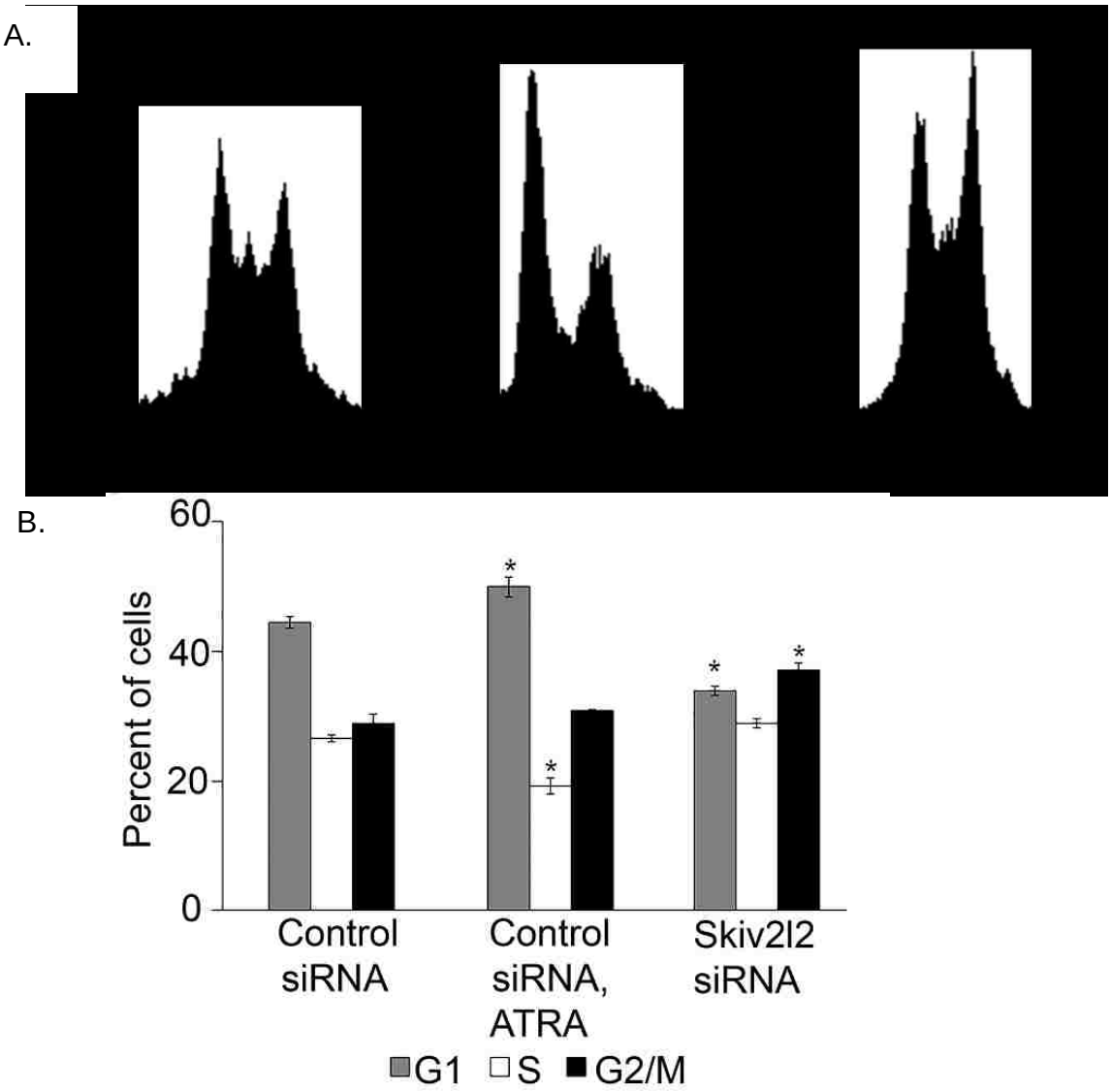

Fig 4.5 SKIV2L2 depletion induces a modest but significant G2/M phase arrest. A. Cell Cycle Analysis with Propidium Iodide Staining of Fixed N2a Cells. N2a cells transfected with non-targeting control siRNA, *Skiv2l2* siRNA, or all-trans retinoic acid were fixed in ethanol and stained with propidium iodide. Cells were excited at 488 nm, and sorted using FL-2 on the Accuri C6 based on propidium iodide fluorescence. The sorted cells corresponded to G1, S, and G2/M phase as denoted. B. Quantification of Cell Cycle Profile. Based on the cell cycle landscapes generated in D, the Accuri C6 software was used to calculate the percentage of cells in G1, S, and G2/M phase, where n=3 sets of 50,000 cells from each treatment. Comparison of the percentage of cells in each phase was performed, with statistically significant differences compared to control siRNA treated cells (p-value< 0.003) denoted with an asterisk (*).

4.2.4 SKIV2L2 depletion results in mitotic arrest as demonstrated through increased H3 phospho-S10 levels

Following the observance of a modest G2/M phase arrest following *Skiv2l2* knockdown (Fig 4.6a), further experiments were aimed at deciphering whether SKIV2L2 depletion impaired G2 phase or mitosis. Phosphorylation of serine 10 on histone H3 is a well-accepted marker of mitosis that increases with mitotic chromosome condensation (Crosio, 2002). The H3 phospho-S10 marker was monitored in two ways to determine whether *Skiv2l2* knockdown causes mitotic arrest. First, cells were stained with the H3 phospho-S10 antibody, which was then detected using a secondary anti-rabbit antibody conjugated to AlexaFluor488. The cells were sorted based on green fluorescence using the Accuri C6, and the percentage of cells immunostained with H3 phospho-S10 were quantified. A larger proportion of stained cells would indicate mitotic arrest following *Skiv2l2* knockdown. Second, western blots to detect phosphorylated H3 (H3 phospho-S10) were performed on histones acid-extracted from control and *Skiv2l2* knockdown cells. This results in a measurement of the total amount of H3 phospho-S10, which correlates to the proportion of cells in M phase.

The number of cells in G2/M phase (Fig. 4.6a) was compared to the number of cells in mitosis (Fig. 4.6b). Following treatment with control siRNA, 6.8% of cells stained with H3 phospho-S10, and ATRA treatment resulted in a similar percentage of H3 phospho-S10 positive cells (8.4%, p-value< 0.4, Fig 4.6b). This suggests that approximately 20% of G2/M phase cells detected by propidium iodide are in mitosis. 15.5% of *Skiv2l2* knockdown cells were positive for H3 phospho-S10 as measured through FACs analysis (p-value< 0.007, Fig 4.6b). This correlates to approximately 40%

of the cells detected as G2/M phase cells using propidium iodide are undergoing mitosis. Western blots were used to detect overall H3 phospho-S10 levels, with β-actin as a loading control. *Skiv2l2* knockdown cells exhibited an average 2.5 fold increase in H3 phospho-S10 compared to control cells (n=8, p-value< 0.007, Fig 4.7a). Figure 4.7a demonstrates one such Western blot for H3 phospho-S10 depicting a 1.9 fold increase in cells treated with *Skiv2l2* siRNA. The experiment was replicated in P19 cells, where an 80% reduction in SKIV2L2 resulted in a 4-fold increase in H3 phospho-S10 (p-value< 0.04, Fig 4.7b). With both a 2.5 fold increase in overall H3 phospho-S10 levels and a 1.8 fold increase in the total number of cells staining with H3 phospho-S10, it was concluded that an approximate doubling in H3 phospho-S10, which corresponds to more cells in mitosis, characterizes *Skiv2l2* knockdown cells.

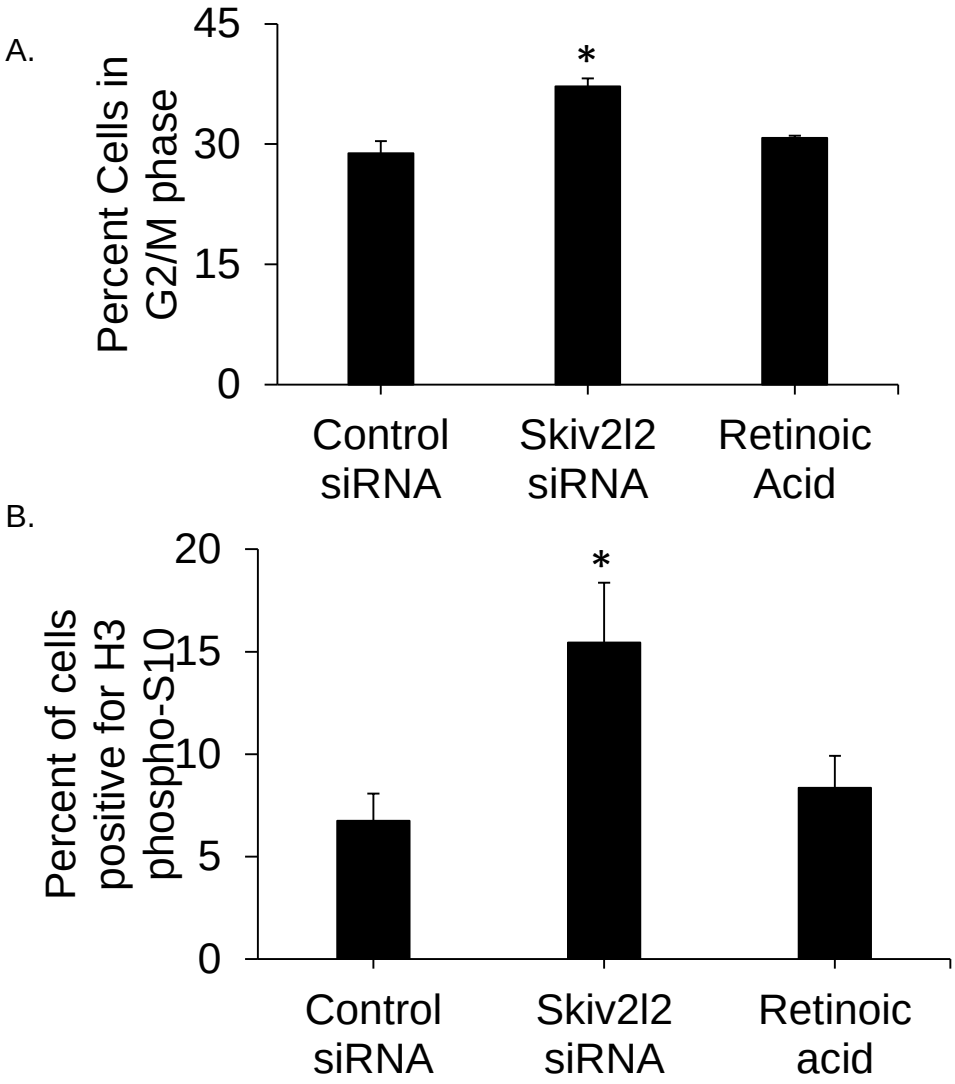

Fig 4.6: *Skiv2l2* knockdown cells arrest in M-phase. A. Quantification of G2/M phase N2a cells based on propidium iodide staining. Fixed N2a cells stained with propidium iodided were excited at 488 nm, and 50,000 cells per sample were sorted using FL-2 on the Accuri C6 based on propidium iodide fluorescence. The percentage of cells in G2/M phase was averaged for three biological replicates with statistically significant differences (p-value< 0.00001) denoted by an asterisk. B. FACs analysis of H3 phospho-S10 cells. Fixed N2a cells were incubated with primary antibody against H3 phospho-S10 and anti-rabbit conjugated to AlexaFluor®-488. Cells were excited at 488 nm, and 50,000 cells per sample were sorted using the FL-1 filter on the Accuri C6 based on AlexaFluor fluorescence. The percentage of cells fluorescing over background (no primary antibody control) was quantified for three biological replicates to determine the percentage of cells positive for the mitotic marker H3 phospho-S10. Statistically significant differences (p-value< 0.007) denoted by an asterisk.

A.

B.

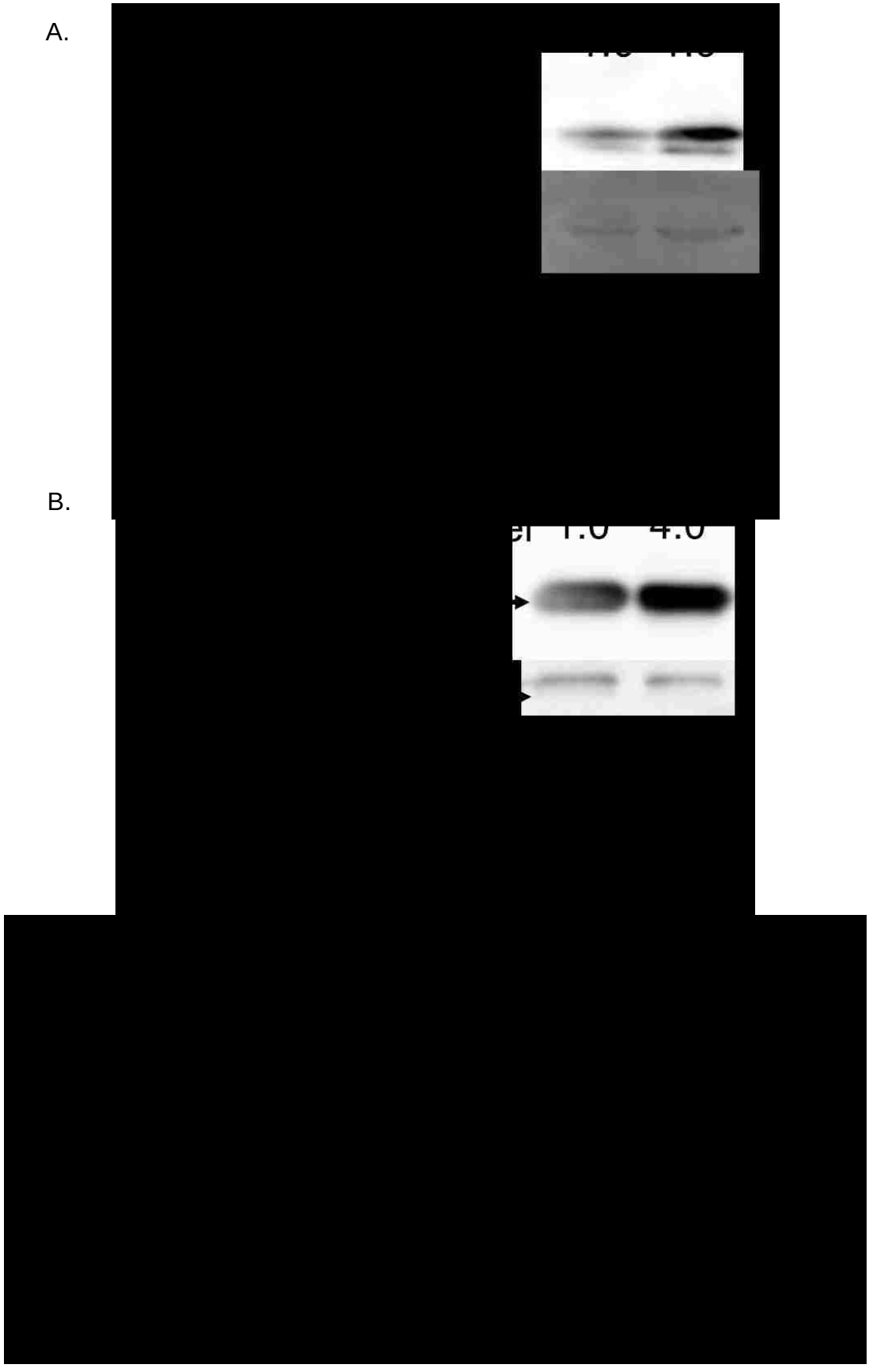

4.2.5 Binuclear cells were detected following SKIV2L2 depletion

To confirm the increased H3 phospho-S10 levels observed with SKIV2L2 depletion, the H3 phospho-S10 mitotic marker was also utilized to visualize N2a cells using immunofluorescence microscopy. Cells immunostaining with H3 phospho-S10 were counted to determine if reduced SKIV2L2 levels increased the proportion of mitotic cells. Visualization of the cells allowed for observation of the intensity of H3 phospho-S10 staining and verified the nuclear colocalization of the mitotic marker with propidium iodide. Because FACs analysis gates out binuclear cells and clumps, visualization also captured a more complete picture of the cell population. However, once again, immunostaining of P19 cells was not practical due to the formation of embryoid bodies and myocytes.

Viewing and counting N2a cells immunostained for H3 phospho-S10 on the Nikon Eclipse E600 microscope confirmed that more *Skiv2l2* knockdown cells stained positive for H3 phospho-S10 compared to control cells (Fig 4.8). Images were obtained from control siRNA and *Skiv2l2* siRNA treated cells stained with both propidium iodide and H3 phospho-S10 antibody. In control cells, cells densely staining with H3 phospho-S10 appeared most often as mononucleated cells. Approximately 10.7% (± 4.3% SD) cell nuclei staining with propidium iodide also expressed H3 phospho-S10 in control siRNA treated samples (Fig 4.7b). Comparatively, SKIV2L2 depletion resulted in 20.1% (± 4.3% SD) of cell nuclei staining with the mitotic marker H3 phospho-S10 antibody (Fig 4.8). This represents nearly a 2 fold increase in cells expressing H3 phospho-S10 following *Skiv2l2* knockdown (n=four biological replicates, 150 nuclei counted per

replicate, p-value< 0.01), which correlates to the observed 2.5 fold increase seen via Western blotting. Interestingly, binucleated cells were observed in *Skiv2l2* knockdown samples (Fig 4.8a), denoted by arrows, while no binucleated cells were observed among control cells. These observed binucleated cells depict a failure to undergo cytokinesis following SKIV2L2 depletion (Rieder, 2004). Together, reduced SKIV2L2 levels increased both the number of mitotic cells, suggesting mitotic arrest, and resulted in binucleation in a subset of cells expressing the mitotic marker H3 phospho-S10.

A.

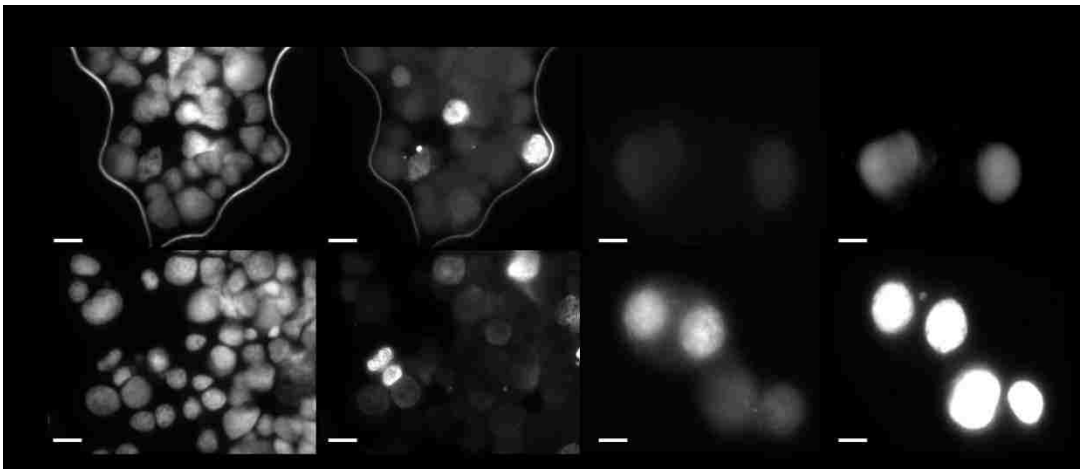

B.

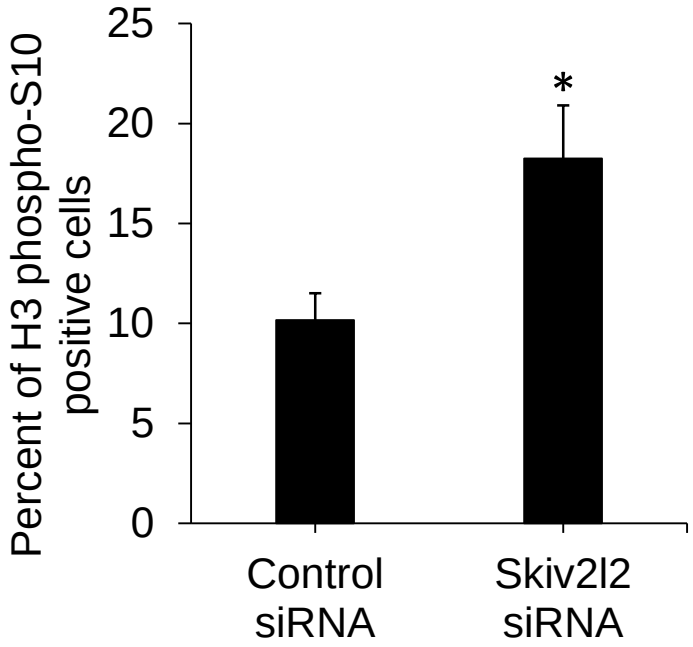

Fig 4.8: *Skiv2l2* knockdown results in mitotic arrest and binuclear cells detected via H3 phospho-S10 immunostaining. A. Immunofluorescent staining of H3 phospho-S10 in N2a cells. N2a cells were stained with propidium iodide for nuclei visualization. Incubation with H3 phospho-S10 antibody followed by anti-rabbit AlexaFluor488 stained mitotic cells green. Scale bar is 15 µM for the four leftmost panels and 20 µM scale bar for the four rightmost panels. B. Quantification of H3 phospho-S10 staining nuclei. Nuclei densely staining with H3 phospho-S10 were divided by the number of nuclei staining with propidium iodide to obtain the percentage of nuclei undergoing mitosis. 150 propidium iodide-stained nuclei were counted for control and *Skiv2l2* siRNA transfected N2a cells in two distinct knockdown experiments (* marks p-value< 0.05).

4.2.6 Cell cycle genes are dysregulated following SKIV2L2 depletion

To better understand this mitotic arrest, RNA-seq data obtained from P19 cells following treatment with control or *Skiv2l2* siRNA was probed to identify changes to the transcriptome indicative of proliferation defects. GO-ontology analysis of mRNAs dysregulated in *Skiv2l2* knockdown cells revealed genes involved in positively regulating cell proliferation were downregulated (p-value< 0.03), while anti-apoptotic genes were upregulated (p-value< 0.001). Genes found to be dysregulated following SKIV2L2 depletion included those involved in the DNA damage response, signaling-induced cell proliferation, mitotic cyclins, chromatin remodeling, and mitotic spindle assembly. Multiple protein-coding mRNAs that could cause changes in cells proliferation or indicate cell division defects were dysregulated with *Skiv2l2* knockdown, including 26 cytoskeletal and spindle genes, 125 known oncogenes, tumor suppressors, and differentiation markers, and 29 chromatin modification and remodeling genes. A subset of these genes is depicted in Fig 4.9, with a false discovery rate of less than 5%. Of particular interest, *Skiv2l2* knockdown cells showed higher expression of cyclin-G1, which accumulates in G2/M phase arrested cells (Kimura, 2011), and lower expression of both the G1-S phase transition cyclin-D1 and the mitotic progression cyclin-B2 (Wu, 2002; Matsuura, 2004). This result is consistent with fewer cells in G1 and more cells arrested in mitosis. Together, this affirmed that mRNA levels reflected the observed defects in cell proliferation, as genes involved with cell division were dysregulated.

Fig 4.9: Graph of select genes involved in cell cycle control with differential expression in *Skiv2l2* knockdown cells. RNA-seq was performed in triplicate on control and *Skiv2l2* siRNA transfected P19 cells. Upregulated and downregulated genes following loss of SKIV2L2 were found to be involved in cell cycle control, with an emphasis on cyclin, mitotic spindle assembly, and the DNA damage response. All changes in RNA levels depicted have a q-value of less than .05.

4.3 Discussion

These experiments demonstrated that SKIV2L2 depletion results in decreased cellular proliferation, specifically attributed to failed progression through mitosis. The proliferation defect in *Skiv2l2* knockdown cells was first identified through MTT assays, which reported that loss of SKIV2L2 causes an approximate 30% reduction overall

metabolic activity. This decrease in metabolically active cells was attributed to decreased proliferation and increased differentiation because FACs analysis showed no increase in dead cells as measured by propidium iodide staining and side scatter. Because SKIV2L2 depletion resulted in increased differentiation and decreased proliferation similar to ATRA treated cells, it was hypothesized that SKIV2L2 depletion would cause the G1 arrest characteristic of both natural and chemically induced differentiation (Zhi, 2012). However, FACs analysis of the cell cycle through the staining of fixed N2a cells with propidium iodide demonstrated an 8% increase in mitotic cells following *Skiv2l2* knockdown, with a sharp decrease in G1 cells and a slight increase in S phase cells. This suggests SKIV2L2 depletion triggers a G2/M phase block, with a slight impairment in DNA replication. Mitotic arrest was found to be responsible for this disruption in the cell cycle. Both the total amount of the mitotic marker H3 phospho-S10 and the number of cells staining with H3 phospho-S10 increased with *Skiv2l2* knockdown. Coupled with the observance of binuclear cells that fail to undergo cytokinesis, this evidence suggests that SKIV2L2 depletion hinders progression through mitosis.

At first glance, the observance of mitotically arrested and binuclear cells following SKIV2L2 depletion appears to conflict with the differentiation phenotype originally observed, as cells usually arrest in G1 prior to differentiation, not in G2/M phase. However, mitotic arrest could trigger differentiation in two possible ways. First, the overall decrease in proliferation caused by mitotic arrest would relieve contact inhibition, resulting in the differentiation of neighboring cells in G1 phase. A second explanation for increased differentiation would be mitotic slippage. Mitotic slippage occurs as a result of activation of the spindle assembly checkpoint and temporary mitotic

arrest. If the cell fails to undergo apoptosis as a result of this mitotic arrest, the checkpoint cannot be maintained indefinitely, causing the cell to aberrantly continue through mitosis in a phenomenon termed mitotic slippage (Rieder, 2004; Dikovskaya, 2015; Freije, 2014). Mitotic slippage can occur in N2a and P19 cells because the spindle assembly checkpoint is impaired. Failed cytokinesis following mitotic slippage generates one 4N G1 cell (binuclear or tetraploid) that can undergo apoptosis, enter S phase with significant genomic damage, or arrest in G1 to either senesce or differentiate (Freije, 2014; Rieder, 2004; Dikovskaya, 2015; Zanet, 2010). One mediator of apoptosis, p53, is not expressed in N2a or P19 cells according to both our RNA-seq data and other sources (Chang, 2010). Given that p53 functions to trigger apoptosis in response to DNA damage following mitotic slippage, the lack of p53 in P19 and N2a cells could lead to cellular senescence, differentiation, or necrosis in tetraploid cells (Zanet, 2010; Freije, 2014). The gene expression patterns captured using RNA-seq in P19 cells following SKIV2L2 depletion are consistent with induction of the spindle assembly checkpoint, followed by mitotic slippage and failed cytokinesis. Further experiments could be aimed at deciphering whether differentiated cells are binuclear to clarify how mitotic perturbations cause differentiation following SKIV2L2 depletion.

Overall, cell proliferation genes were downregulated following SKIV2L2 depletion, and anti-apoptotic genes were upregulated. Genes involved with DNA damage and spindle assembly were dysregulated in *Skiv2l2* knockdown cells. The mitotic arrest observed in *Skiv2l2* knockdown cells could result from activation of the DNA damage response or the spindle assembly checkpoint. Kinetochores can fail to attach to the chromosomes as a result of DNA damage or improper chromatin compaction, and DNA

damage can result from errors in replication, chromatin packaging, or chromosome segregation (Smith, 1998; Rieder, 2004; Meeks-Wagner 1986; Singh, 2010). Gross issues in chromosome segregation or DNA damage could explain the presence of binuclear cells, as both would cause failed cytokinesis. In totality, the changes in gene expression following SKIV2L2 depletion support the hypothesis that loss of SKIV2L2 triggers mitotic arrest, probably due to DNA damage, followed by mitotic slippage, failed cytokinesis, and ultimately differentiation. However, further investigation into this hypothesis would require looking at phosphorylation events indicative of the spindle assembly checkpoint.

Still, the results of these experiments are significant in that they show SKIV2L2 to be necessary for proper mitotic progression in cancer cell lines. Because SKIV2L2 depletion impairs mitotic progression, RNA surveillance may have an important role to play in development, stem cell maintenance, and proliferative diseases such as cancer. By demonstrating that SKIV2L2 depletion reduces cancer cell proliferation, this research reinforces previous RNAi screens that found SKIV2L2 necessary for breast cancer metastasis (Wang, 2012). Future research focusing on how SKIV2L2 and RNA surveillance may promote tumor growth and metastasis could have possible implications on cancer treatment.

While previous studies have hinted at RNA surveillance supporting cell proliferation, these experiments validate these results in mammals and specifically implicate SKIV2L2 in mitosis. Extrapolating from the effect of *Skiv2l2* knockdown on cancer cell lines, a model can be generated to explain a potential role for SKIV2L2 in development: SKIV2L2 is necessary to maintain efficient proliferation in stem cells. As

these stem cells differentiate, the cell cycle slows and eventually halts. During differentiation, SKIV2L2 is downregulated as high levels of proliferation no longer need to be sustained. In an effort to establish a definitive link between RNA surveillance and stem cell maintenance, the experiments outlined in the subsequent chapters focus on identifying RNAs that could be processed or turned over via SKIV2L2-mediated RNA surveillance to prevent mitotic arrest in stem cells.

CHAPTER V: SKIV2L2 TARGETS SPECIFIC NON-CODING RNAs FOR PROCESSING AND DEGRADATION

5.1 Introduction

Hypothesis: Unique RNA targets of SKIV2L2 can be identified among those transcripts accumulating upon *Skiv2l2* knockdown.

To date, studies on mammalian nuclear RNA surveillance have focused on identifying which classes of RNAs are targeted by the TRAMP and NEXT complexes for processing and degradation. These studies generally use high throughput sequencing and have been successful in discovering key roles for RNA surveillance in ribosomal RNA processing, promoter upstream transcript (PROMPT) and enhancer RNA (eRNA) turnover, and snoRNA processing (Tiedje, 2014; Lubas, 2015; Dorweiler, 2014). While a list of putative target RNAs have been identified in different organisms, particularly yeast and humans, it is believed that many RNA surveillance targets remain to be discovered, as different RNAs are expressed under certain conditions and in different cell types. Additionally, the biological importance of processing and turnover of RNA surveillance targets has not been investigated in depth. This research aimed to expand on previous studies by characterizing RNA surveillance targets of the helicase SKIV2L2, which functions in both the TRAMP and NEXT complexes, in N2a and P19 cells.

Initially, RNA surveillance studies focused on identifying targets of the TRAMP complex in yeast, which functions in both the nucleus and nucleolus. In *Saccharomyces cerevisiae*, the TRAMP complex was found to degrade hypomodified $tRNA_i^{MET}$. Mutation of Mtr4p suppresses the temperature sensitive growth phenotype associated

with low $tRNA_i^{MET}$ following Trm6 mutation (Kadaba, 2004). This discovery allowed for characterization of the TRAMP complex. High throughput sequencing of targets accumulating following TRAMP complex depletion and methods crosslinking TRAMP proteins to RNAs have resulted in identification of other TRAMP targets in yeast, including 5.8s rRNA, the 7s rRNA precursor, snRNAs arising from splicing, snoRNAs, and cryptic unstable transcripts transcribed from heterochromatin (CUTs) (de la Cruz, 1998; Callahan, 2009; Kong, 2013; Thiebaut, 2006). The TRAMP complex has been found to be important in gene expression, as degradation of antisense CUTs can impact transcriptional silencing and prevent loss of repeats during recombination (Thiebaut, 2006). In *Schizosaccharomyces pombe*, the TRAMP complex prevents endogenous antisense RNAs from activating RNAi silencing pathways (Bühler, 2008).

With the recent discovery of the mammalian homologs, the NEXT and TRAMP complexes, current research focuses on characterizing RNA surveillance targets in mammals as it is applicable to human disease. Currently, the NEXT complex is thought to function in the degradation of PROMPTs and eRNAs (Lam, 2014; Lubas, 2015; Tiedje, 2014). In the NEXT complex, Rbm7 was found to preferentially bind U-rich RNAs and target uridylated snRNAs for degradation (Lubas, 2015; Tiedje, 2014). This finding illustrates that the three distinct RNA binding domains found in the NEXT (Rbm7, ZCCCH8, and SKIV2L2) and TRAMP (PAPD5, ZCCHC7, and SKIV2L2) may each recognize and bind unique classes of RNAs, allowing for many types of RNAs to be processed and degraded via nuclear RNA surveillance. For example, the TRAMP complex has been found to target different snoRNAs and rRNA precursors for 3' end processing and degradation (Lubas, 2015; Schilders, 2007), while the NEXT complex

was thought to target PROMPTs for degradation (Tiedje, 2014; Lubas, 2015). However, the discovery of certain PROMPTs adenylated by PAPD5 does hint at some overlap between TRAMP and NEXT complex targets (Preker, 2011). Indeed, the distinction between the two complexes might prove more complex. Understanding which RNAs are targeted by the TRAMP and NEXT complexes in mammals proves to be even more difficult due to certain members acting independent from the complex or being nonessential for targeting certain RNAs. For example, PAPD5 has been found to be necessary for the 3' end trimming of H/ACA box snoRNAs and involved in the processing of rRNA precursors in concert with the TRAMP complex (Berndt, 2012; Sloan, 2014; Schilders, 2007). However, PAPD5 adenylation is not necessary for the turnover of long non-coding RNAs via SKIV2L2, the nuclear exosome, and PABPN1 (Beaulieu, 2012). While the yeast Trf4p lacks an RNA binding domain and therefore cannot function independent from the TRAMP complex (La Cava, 2005), PAPD5 possesses an RNA binding domain and has been found to adenylate certain mature miRNAs to alter their stability (Rammelt, 2011; Boele, 2014). PAPD5 adenylates the oncogenic mir-21, resulting in poly (A) specific ribonuclease (PARN)-mediated turnover of mir-21, which ultimately prevents tumor formation (Boele, 2014). Together, these suggest a layer of complexity in identifying RNA surveillance complex targets not seen in yeast. Because the relationships between the protein members of the TRAMP and NEXT complex are poorly understood, this research attempted to characterize RNA targets of SKIV2L2, which is presumed to be essential for both TRAMP and NEXT complex function because it is the only helicase in both complexes. Recently, human SKIV2L2 was shown to complex with PABPN1 and ZCF3H1 for the turnover of

adenylated RNAs (Beaulieu, 2012; Meola, 2016). Studies have also shown that SKIV2L2 functions with MPP6 to degrade unidentified, nuclear RNAs adenylated by poly-A-polymerase (Fujiwara, 2016). These preliminary studies hint at a role for SKIV2L2 in nuclear RNA surveillance independent from both the TRAMP and NEXT complexes as well, truly making it the cornerstone in nuclear RNA surveillance.

Previous work in the Anderson laboratory has focused on sequencing RNA targets of SKIV2L2 in N2a cells. After *Skiv2l2* knockdown, TRAMP targets are thought to be adenylated by PAPD5 but accumulate because they cannot be degraded by the exosome. Using oligo-dT to select for adenylated RNAs, the total RNA from *Skiv2l2* knockdown cells was reverse-transcribed and sequenced, and putative TRAMP targets were identified, including the 5' leader released by Drosha cleavage of primary miRNAs, the 5'ETS cleaved during ribosomal RNA processing, the small nucleolar RNA U3, and the mRNA VGF (Dorweiler, 2014). Following poly-A-seq, molecular techniques verified RNA targets to better understand processing and degradation via the TRAMP complex. In addition, it was necessary to repeat the high throughput sequencing of RNAs following *Skiv2l2* knockdown to identify NEXT complex targets and potential TRAMP complex targets not detected in the original poly-A-sequencing data. The oligo-dT to reverse transcribe was thought to only capture TRAMP targets adenylated by PAPD5. However, the efficiency of oligo-dT priming off of the short A-tails added by PAPD5 (assuming PAPD5 efficiently adenylates TRAMP targets in the absence of SKIV2L2) calls this method into question. To combat this, RNA-sequencing was performed on both control siRNA and *Skiv2l2* siRNA treated P19 cells to detect accumulating RNAs that could be either TRAMP or NEXT complex targets. In addition to detecting and classifying unique

RNA surveillance targets via high throughput sequencing, molecular techniques were again utilized to verify these targets in P19 cells (Fig 5.1).

Finally, a system to verify RNA binding to SKIV2L2 was instituted based on UV-crosslinking of RNA and proteins followed by immunoprecipitation of endogenous SKIV2L2 (Fig 5.2). Previous CLIP (Cross-linked immunoprecipitation) and CRAC (Cross-linking and analysis of cDNA) methods depend on overexpression of the target protein fused to a tag (Tiejde, 2014; Bohnsack, 2012). Both protein overexpression and fusion tags can affect RNA binding, calling the validity of these results into question. In this chapter, RNA immunoprecipitation (RIP) was performed on endogenous SKIV2L2 to detect RNAs bound to SKIV2L2 and therefore confirm those RNAs as direct targets of SKIV2L2-mediated RNA surveillance.

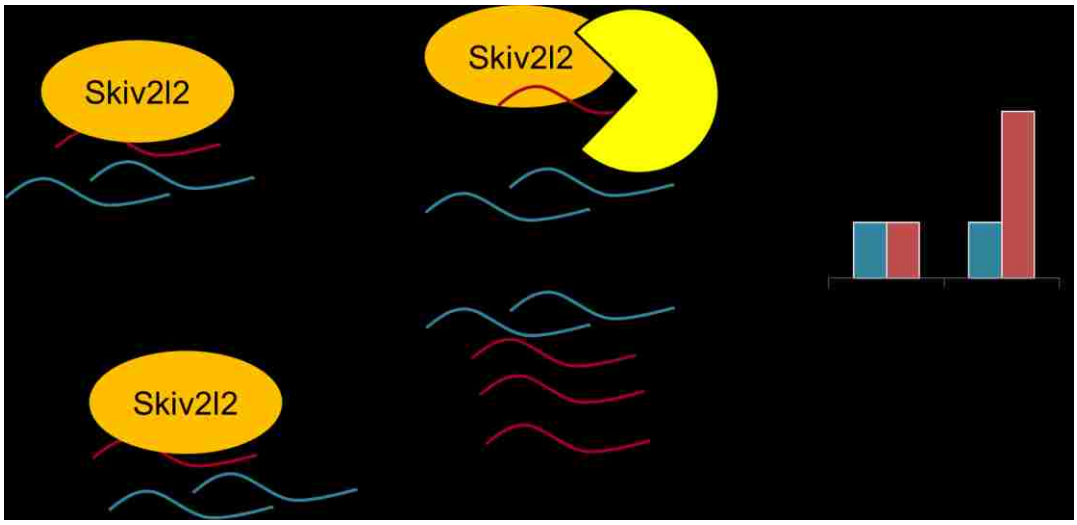

Fig 5.1: RNA-seq and qRT-PCR identify and verify RNA targets of SKIV2L2. In cells treated with control siRNA, SKIV2L2 targets in red would be turned over. However, with *Skiv2l2* knockdown, these targets would accumulate. These targets can be detected via qRT-PCR and RNA-seq. RNAs not targeted by SKIV2L2 (blue) would remain at similar levels under both conditions, while red target RNAs would accumulate in knockdown cells.

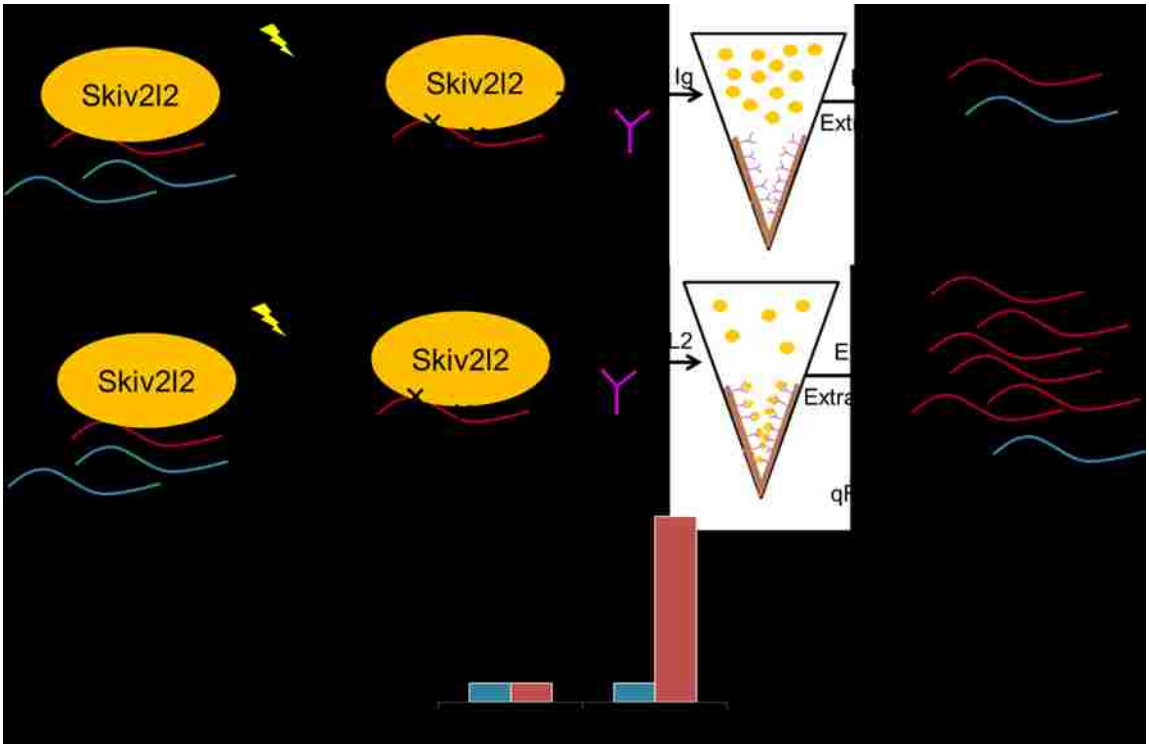

Fig 5.2: RIP-qRT-PCR identifies RNAs binding to SKIV2L2. In RNA immunoprecipitation, RNAs associated with SKIV2L2 (red) are covalently bound through UV crosslinking. Cell lysates are then applied to magnetic Dynabeads coated with either negative control anti-goat Ig or anti-SKIV2l2 antibodies. SKIV2L2 with its bound target RNAs would immunoprecipitate with anti-SKIV2L2. Using qRT-PCR, these bound RNAs (red) would be detected at higher levels in samples immunoprecipitated with anti-SKIV2L2 compared to anti-goat Ig. However, unbound RNAs (blue) would be immunoprecipitated at similar rates with both anti-SKIV2L2 and anti-goat Ig antibodies.

5.2 Approach and Results

5.2.1 TRAMP complex RNA targets possess short 3' tails consisting of three to six adenosines

The Anderson laboratory previously conducted a poly-A-seq experiment to detect polyadenylated RNAs that accumulate in *Skiv2l2* knockdown cells (Dorweiler, 2014). The rationale behind this experiment was that becauseSKIV2L2 aids in RNA turnover via the nuclear exosome, RNAi against SKIV2L2 would prevent the turnover and cause the accumulation of RNAs targeted for degradation by the TRAMP or NEXT complex. Given that PAPD5 adenylates TRAMP target RNAs, but the NEXT complex lacks a poly-A-polymerase (Lubas, 2011), oligo-dT primed reverse transcription would detect accumulating TRAMP target RNAs. Indeed, analysis of the resulting poly-A-seq data from N2a cells treated with either control siRNA or *Skiv2l2* siRNA revealed certain RNA classes as putative TRAMP targets. In particular, misprocessed U3 was found to be elevated in *Skiv2l2* knockdown cells. U3 undergoes 3' end trimming to form the mature snRNA, and the data suggests that aberrant U3 RNAs are degraded via SKIV2L2. Additionally, the poly-A-seq data from *Skiv2l2* knockdown cells detected an accumulation of 5' leader sequences of specific miRNAs (Fig 5.3). As the primary miRNA transcript is cleaved by Drosha, a 5' and 3' fragment are released to generate the pre-miRNA hairpin (Bartel, 2004). A subset of miRNA 5’ leader sequences, including mir-322, accumulates in *Skiv2l2* knockdown cells, suggesting that SKIV2L2 may aid in their turnover.

Given that the rationale behind the poly-A-seq data rests on the premise that PAPD5 adenylates TRAMP target RNAs, two questions were asked regarding the miRNA 5' leader and U3 snRNA transcripts. The first question asked was whether the RNAs were adenylated. Detecting adenylated miRNA 5' leader and U3 snRNA transcripts would not only verify that the poly-A-seq experiment selected for adenylated RNAs, but it would also suggest that these RNAs could be TRAMP complex targets. The second question addressed the length of the poly-A-tails on these transcripts. Because the yeast Trf4p adds three to five adenosines (Wlotzka, 2011; Jia, 2011), it was hypothesized that the mammalian homolog PAPD5 would add short poly-A-tails as well. However, with in vivo and in vitro experiments offering conflicting data on the length of poly-A-tails added by Trf4p (Schmidt, 2013; Nag, 2012; Jia, 2011), and the experiments never having been performed in mouse cells, the exact length of poly-A-tails in mice could not be estimated. Therefore, measuring the length of the poly-A-tails on TRAMP targets in mouse was important because it would reveal insight into whether oligo-dT is the best method to detect these RNAs, as priming efficiency would decrease for poly-A-tails less than 19 adenosines in length and structured 3' ends can interfere with oligo-dT primer hybridization (Bustin, 2004).

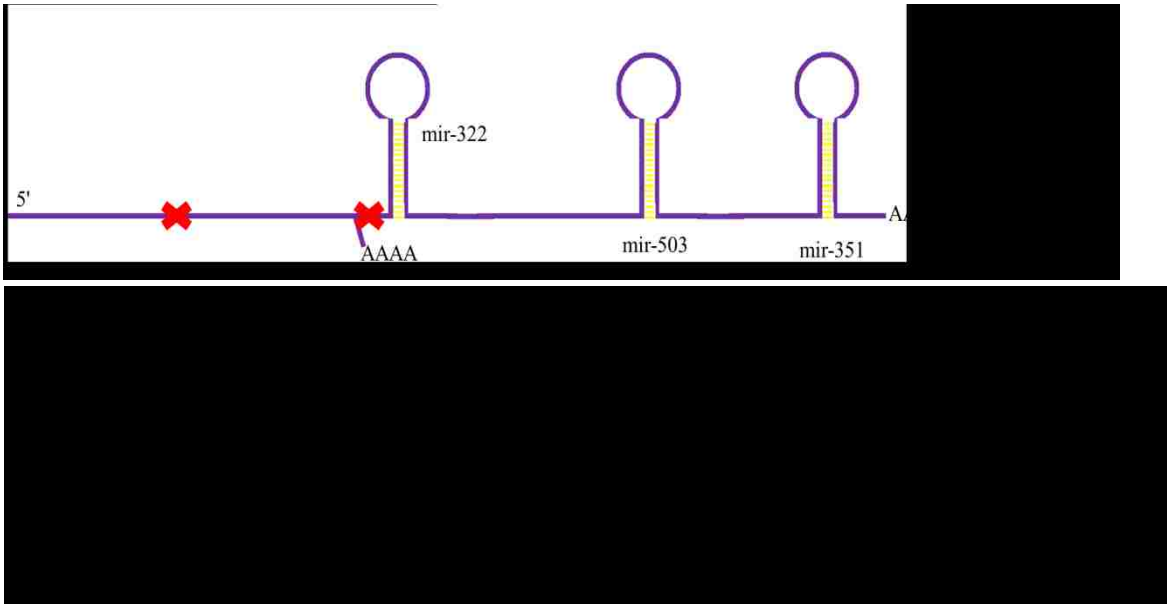

To detect poly-A-tails added to the 3' end of the mir-322 5' leader and U3, total RNA was isolated from *Skiv2l2* knockdown cells to enrich for these RNAs. RNA extracts were digested using RNaseH and primers specific to the 5' most end (first red X) of 5' leader of mir-322 and U3 (Fig.5.3). This digested both RNAs into similar sized fragments approximately 150-200 base pairs in length, which is the length at which RNAs undergo circular ligation with the most efficiency (Shore, 1981). These short RNAs were then treated with RNA ligase to circularly ligate the 3' and 5' ends to each other. This would fuse any adenosines at the 3' end to the 5' end. The circularly ligated RNA was then reverse transcribed into cDNA using a gene specific primer, and the cDNA was amplified across the 5'-3' junction. This technique resulted in an amplicon that was cloned into bacteria and sequenced to detect any untemplated adenosines between the 5' and 3' ends of the RNA.

This experimental method proved difficult due to low efficiency and low levels of the target RNA in respect to total RNA. The majority of cloned U3 was not adenylated,

which was expected given that only misprocessed U3 was elevated in the sequencing data. However, three U3 transcripts were found to be adenylated of the approximately thirty clones sequenced (Table 5.1). These three transcripts each had different defects in processing, including errors in 3' end trimming and an internal deletion. The number of untemplated adenosines spanning the 5'-3' junction ranged from three to six in number. For one of the transcripts, it was unclear whether the tail was four to six adenosines in length as two adenosines were predicted to occur at that position based on the U3 sequence. This suggests that misprocessed U3 is adenylated with three to six adenosines. Sequencing of the 5' leader of mir-322 yielded only one adenylated transcript. The majority of the thirty clones were retroelements expressed elsewhere in the genome with extensive sequence similarity to the mir-322 primary transcript. The one adenylated 5' leader sequence had an A-tail that was three adenosines in length. While four adenylated transcripts is not definitive proof, it does suggest that the A-tail of putative TRAMP targets is three to six adenosines in length. Indeed, two laboratories have confirmed that Trf4p, when acting with Mtr4p, adds three to five adenosines in yeast (Jia, 2011; Wlotzka, 2011). It is of note that this short tail that would not be as efficiently primed using oligo-dT as a longer poly-A-tail, suggesting that certain TRAMP targets might not be represented in the poly-A-seq data.

5.2.2 The 5' leader of mir-322 is a definitive TRAMP target

After detecting putative TRAMP targets using the poly-A-seq data, it was necessary to verify that these miRNA 5' leader sequences accumulate using another method. To do this, qRT-PCR was employed to detect the levels of the 5' leader sequence of mir-322 in control, *Skiv2l2*, and *Papd5* knockdown cells. A series of primers were designed to detect the 5' leader of mir-322. Total RNA from all three cell treatments was reverse transcribed using either a primer specific to miRNA 5' leader sequence or oligo-dT. By using two primers for reverse transcription, both adenylated 5' leader and total 5' leader levels could be detected and compared among the control, *Skiv2l2*, and *Papd5* knockdown cells. A single amplicon within the 5' leader sequence was amplified using qPCR to quantify the amount of mir-322 5' leader in each sample. Because NEXT complex targets are not adenylated, this experiment was designed to confirm SKIV2L2 depletion impairs mir-322 5' leader turnover while also deciphering whether PAPD5 and the TRAMP complex are responsible for mir-322 5' leader turnover.

The experiment was performed under two conditions. First, control cells were compared to *Skiv2l2* knockdown cells alone using ActB as an RNA loading control. Then, control cells were compared to both *Skiv2l2* and *Papd5* knockdown cells using CyphB as an RNA loading control. When comparing the overall mir-322 5' leader levels, there was a 5 fold increase following *Skiv2l2* knockdown (p-value< 0.04, Fig 5.4a). In the second set of experiments, overall levels of 5' leader were found to accumulate 11 fold in *Skiv2l2* knockdown and 6 fold in *Papd5* knockdown cells. Additionally, adenylated 5' leader transcripts were elevated 5 fold in *Skiv2l2* knockdown cells but were not

significantly detected in *Papd5* knockdown cells (Fig 5.4b). This data verifies that mir-322 is a direct TRAMP target, as it accumulates in both *Skiv2l2* and *Papd5* knockdown cells. The loss of adenylated 5' leader in *Papd5* knockdown cells confirms that PAPD5 is the poly-A-polymerase responsible for the observed adenylation. In addition to validating mir-322 5' leader as a direct TRAMP target, these experiments also established an experimental method that could be applied to other putative TRAMP target RNAs.

5.2.3 SKIV2L2 is necessary for processing snoRNA Z18 from the long non-coding RNA Gas5

In addition to identifying U3 and the 5' leader sequence of specific miRNAs as putative TRAMP targets, the poly-A-Seq data suggested an accumulation of the long non-coding RNA Gas5 following *Skiv2l2* knockdown. However, it was not clear whether SKIV2L2 targeted a portion or the entire transcript for degradation. Viewing the poly-A-Seq data converted into BigWig format on the IGV genome browser suggested a significant proportion of the accumulating transcripts covered the 3' end of the first intron. Gas5 lncRNA harbors multiple snoRNAs in its introns, and the fate of the lncRNA transcript changes based on cell stress (Wang, 2005). Without stress, spliced Gas5 is turned over via nonsense-mediated decay. Under conditions that induce growth arrest, including starvation, Gas5 undergoes an additional splicing event, is retained in the nucleus, and sequesters glucocorticoid hormone receptors so that genes responsive to glucocorticoid are silenced (Wang, 2005; Tani, 2013). The differential splicing of Gas5 releases certain introns containing snoRNAs, and the intronic snoRNAs are processed into mature snoRNAs. The first intron contains the snoRNA Z18, and it was

hypothesized that SKIV2L2 promotes the processing of the first intron to generate mature Z18 (Fig 5.5a).

To test this hypothesis, qRT-PCR was again utilized to determine whether the entire Gas5 transcript accumulates following *Skiv2l2* knockdown or if the accumulation is specific to the first intron containing Z18. Using total RNA extracted from control and *Skiv2l2* knockdown cells, Gas5 was reverse transcribed using two distinct primers: one that annealed to the 3' end of the long non-coding RNA and one that annealed to the first intron downstream of Z18's mature 3' end. After reverse transcription, qPCR was performed using one amplicon spanning the junction between exons 11 and 12 to detect full length Gas5 and a second amplicon detecting 3' extended Z18 (Fig 5.5a). SKIV2L2 could affect the stability of spliced Gas5 (detected through the amplicon spanning exons 11 and 12), unspliced Gas5 transcript (both exons and introns), or Z18 snoRNA (first intron). The use of multiple primer sets allowed each possibility to be explored.

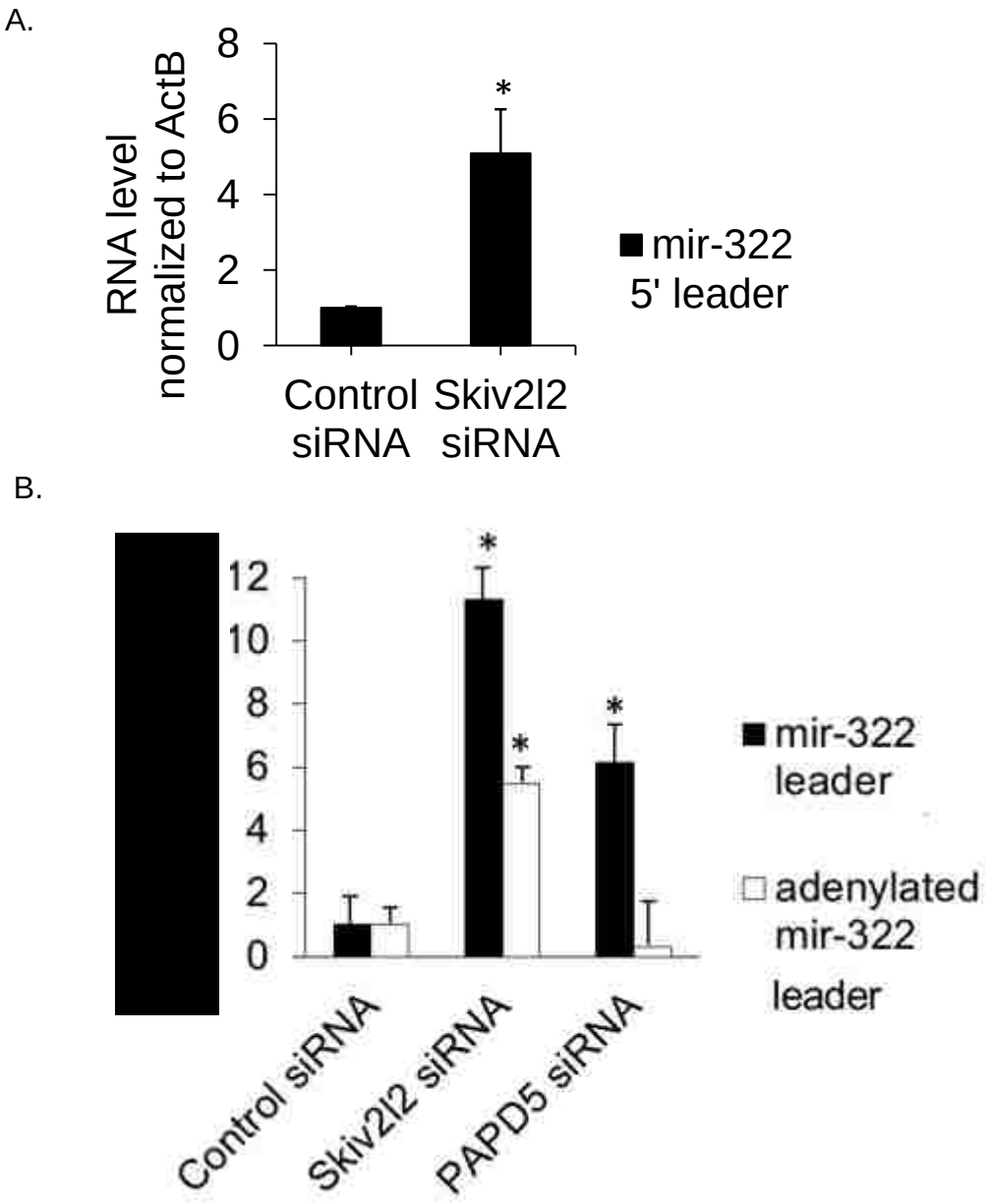

Fig 5.4: qRT-PCR verifies mir-322 5' leader sequence as a TRAMP complex target. A. mir-322 5' leader accumulates in *Skiv2l2* knockdown cells. Total RNA from control and *Skiv2l2* knockdown cells was reverse transcribed using gene specific primers. qPCR was then performed to measure the abundance of the 5' leader of mir-322 relative to ActB (n=3, * marks p-value< 0.05). B. Adenylated 5' leader of mir-322 accumulates in *Skiv2l2* knockdown cells but not *Papd5* knockdown cells. Total RNA was reverse transcribed using either gene specific primers or oligo-dT. qPCR was then performed to measure the abundance of total and adenylated mir-322 5' leader relative to CyphB (* marks p-value< 0.05 compared to control siRNA cells).

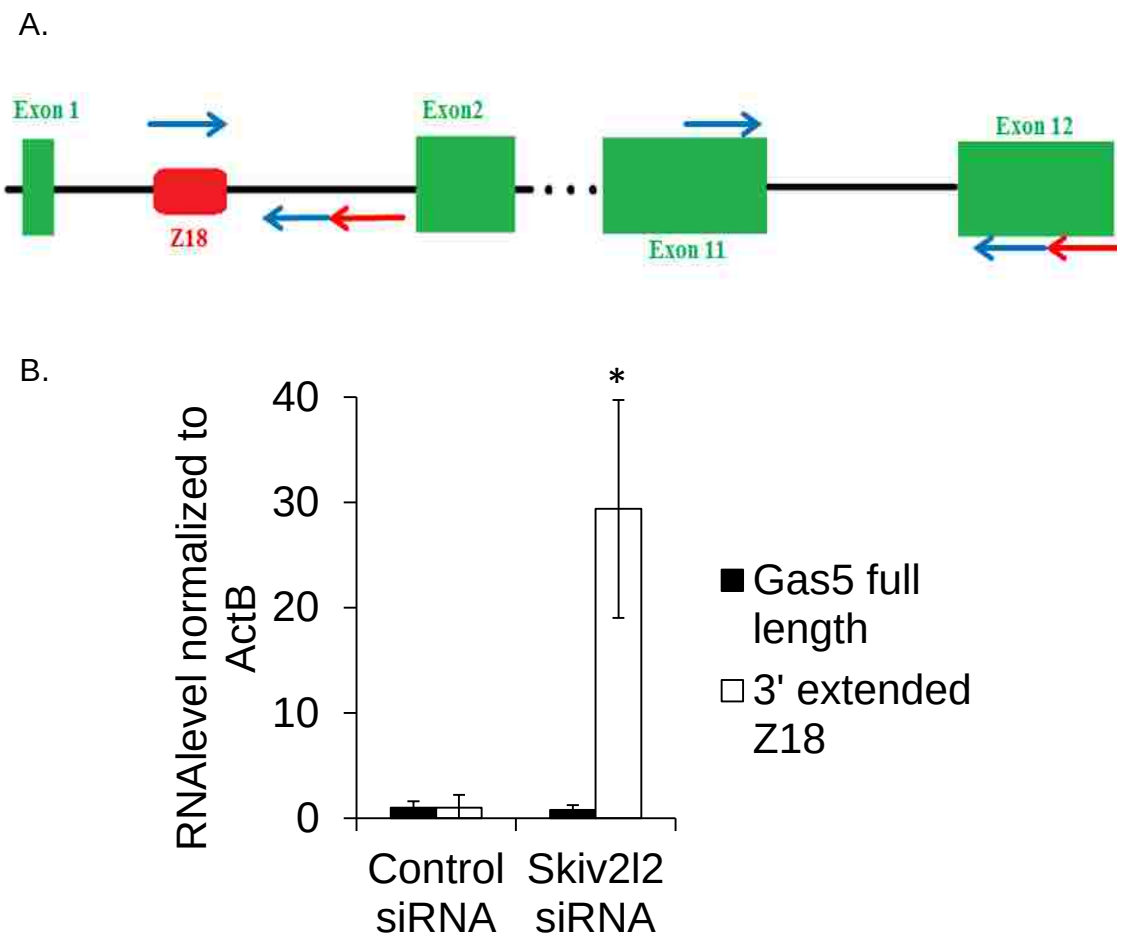

Fig 5.5: qRT-PCR verifies the snoRNA Z18 is a SKIV2L2 target. A. The snoRNA Z18 is processed from the first intron of the long non-coding RNA Gas5. Z18 is located in the first intron of Gas5. Primers for reverse transcription are in red, and primers for qPCR are in blue. Two primer sets were used to amplify either full length Gas5 (amplicon across exons 11 and 12) or 3' extended Z18 (forward primer within Z18, reverse primer downstream of the snoRNA). B. 3' extended Z18 accumulates in *Skiv2l2* knockdown cells. Control and *Skiv2l2* knockdown RNA was reverse transcribed using gene specific primers (red in A). qPCR was then performed to measure the abundance of the full length Gas5 and 3' extended Z18 relative to ActB (n=3, * marks p-value <0.05).

When comparing the levels of Gas5 between control and *Skiv2l2* knockdown cells, spliced Gas5 levels, detected at the exon11-exon12 junction, were equivalent between the two treatments. This demonstrated that *Skiv2l2* knockdown does not upregulate Gas5 transcription or influence the stability of spliced Gas5. Instead, qRT-PCR results demonstrated that the first intron containing Z18 accumulated nearly30 fold (p-value< 0.02, Fig 5.5b). Based on the use of two amplicons and location of the primers, this could not be attributed to an increase in Gas5 expression or an increase in mature Z18. Therefore, *Skiv2l2* knockdown leads to an accumulation of only the first intron of Gas5. Seeing as the overall transcript does not change following SKIV2L2 depletion, but the first intron is elevated, the conclusion is that SKIV2L2 is necessary for processing of the first intron, likely to generate mature Z18.

5.2.4 Forty seven non-coding RNAs accumulate in P19 cells following SKIV2L2 depletion

In light of both the analysis of TRAMP targets in N2a cells and the proliferation defect observed following SKIV2L2 depletion, an additional RNA-seq experiment was conducted in P19 cells to identify targets of SKIV2L2-mediated RNA surveillance that could influence mitotic progression. This experiment addressed two concerns with the poly-A-seq data obtained from N2a cells. First, by performing the RNA-seq in P19 cells following *Skiv2l2* knockdown, this experiment allowed for comparison between two cell lines and had the potential to reveal additional RNA transcripts as SKIV2L2-mediated RNA surveillance targets. Second, given that NEXT complex targets have no poly-A-tails (Lubas, 2011), and the adenosine tails on TRAMP complex targets are short, using

total RNA-seq circumvented inefficiency in priming with oligo-dT and allowed RNAs without poly-A-tails to be detected as well.

Similar to the poly-A-seq performed on N2a cells (Dorweiler, 2014), the purpose of this RNA-seq experiment was to identify potential RNAs that are turned over or processed via SKIV2L2. P19 cells were treated with control siRNA or *Skiv2l2* siRNA, and RNA was harvested, quantified, and checked for quality. Three biological replicates for each treatment were sent to the University of Wisconsin-Madison for preparation and sequencing. Using the online Galaxy platform, the resulting sequencing data was mapped to the mm10 mouse genome with tophat, transcript abundance was quantified with cufflinks, and changes between control and knockdown cells were identified with cuffdiff. Comparing control P19 cells with *Skiv2l2* knockdown cells detected changes in RNA steady-state levels between the two samples. For simplicity, transcripts that were detected at a higher rate in the *Skiv2l2* knockdown cells compared to control cells were considered to be upregulated, elevated, or accumulating, while transcripts detected at a lower rate in *Skiv2l2* knockdown cells were considered to be downregulated. In control cells, it was hypothesized that any RNA targets of SKIV2L2-mediated RNA surveillance would be turned over or processed. However, in *Skiv2l2* knockdown cells, these RNAs would fail to be turned over or processed by the nuclear exosome, leading to either an accumulation of the full-length transcript or an accumulation of an aberrant transcript. In both cases, these transcripts would appear to be "upregulated" in *Skiv2l2* knockdown cells based on the RNA-seq data. The list of "upregulated" genes in *Skiv2l2* knockdown cells contains RNA transcripts that are either directly targeted by RNA surveillance to the nuclear exosome or indirectly affected by changes in RNA surveillance. Conversely,

SKIV2L2 is presumed to indirectly affect the downregulated transcripts through a mechanism that does not depend on the nuclear exosome.

Based on the RNA-seq data obtained from P19 cells, 1473 RefSeq genes were misregulated in *Skiv2l2* knockdown cells. Of these, 585 genes were elevated following *Skiv2l2* knockdown, while 887 genes were downregulated with a false discovery rate of 5%. 337 elevated genes and 428 reduced genes showing greater than a 1.5-fold change were probed in further detail (Table 9.1). These transcripts were identified and classified into one of three groups: non-coding RNAs, replication-dependent histone mRNAs, and other mRNAs. RefSeq genes elevated following SKIV2L2 depletion included 36 replication-dependent histone mRNA transcripts, 47 non-coding RNAs, and 254 other mRNAs (Fig 5.6). Genes showing decreased steady-state RNA levels following SKIV2L2 depletion included 416 other mRNAs and only 10 non-coding RNAs and 2 non-canonical histone mRNA transcripts (Fig 5.7). Additionally, 772 intergenic transcripts (RNAs transcribed from regions of the mouse genome containing no annotated genes) were significantly elevated following SKIV2L2 depletion, while only 99 intergenic transcripts were downregulated (Table 9.2).

Previous research has demonstrated that the yeast TRAMP complex and the mammalian TRAMP and NEXT complexes primarily function in the processing and turnover of non-coding RNAs via the nuclear exosome (Andersen, 2008). Expanding off this research, the 47 non-coding RNAs identified as elevated in *Skiv2l2* knockdown cells were probed in further detail (Table 9.3). The non-coding RNAs were classified as miRNAs, snoRNAs, or lncRNAs. Twelve RNAs could not be grouped into these categories and are denoted as “other” in the pie chart showing the breakdown of non-

coding RNAs elevated following SKIV2L2 depletion (Fig 5.8). These twelve “other” non-coding RNAs include six small non-coding RNAs of unknown function, two non-coding pseudogenes, and the RNA components of two enzymes, ribonuclease P and mitochondrial RNA processing endoribonuclease. Additionally, the 45S ribosomal RNA precursor and the snRNA U12 were both elevated in *Skiv2l2* knockdown cells.

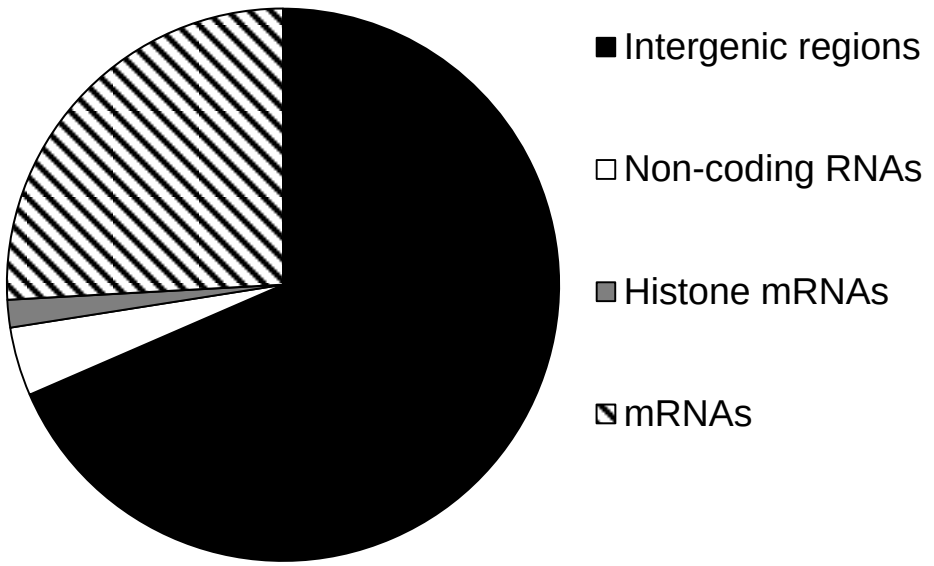

Fig 5.6: Various classes of RNAs accumulate in P19 cells following SKIV2L2 depletion. Following RNA-seq, sequences were mapped for three biological replicates using Tophat, and accumulating RNA sequences were sorted based in intergenic regions (no annotated genes) and annotated gene type ($q<0.05$, $M>0.58$).

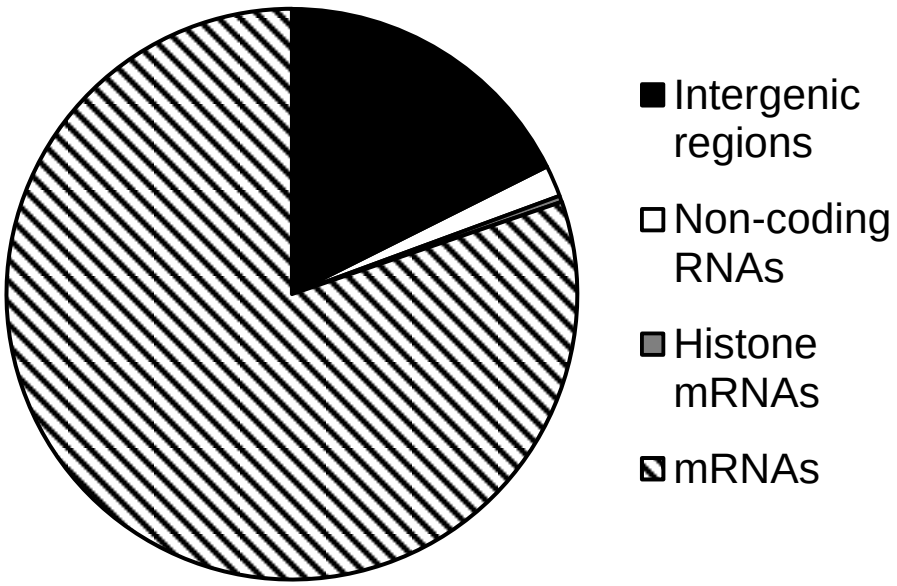

Fig 5.7: Transcripts downregulated in P19 cells following SKIV2L2 depletion. As identified through RNA-seq, those RNAs downregulated in knockdown cells by 1.5 fold or greater with a q-value <0.05 were included in analysis. Downregulated RNAs were then classified as coding, non-coding, or intergenic (no annotated genes).

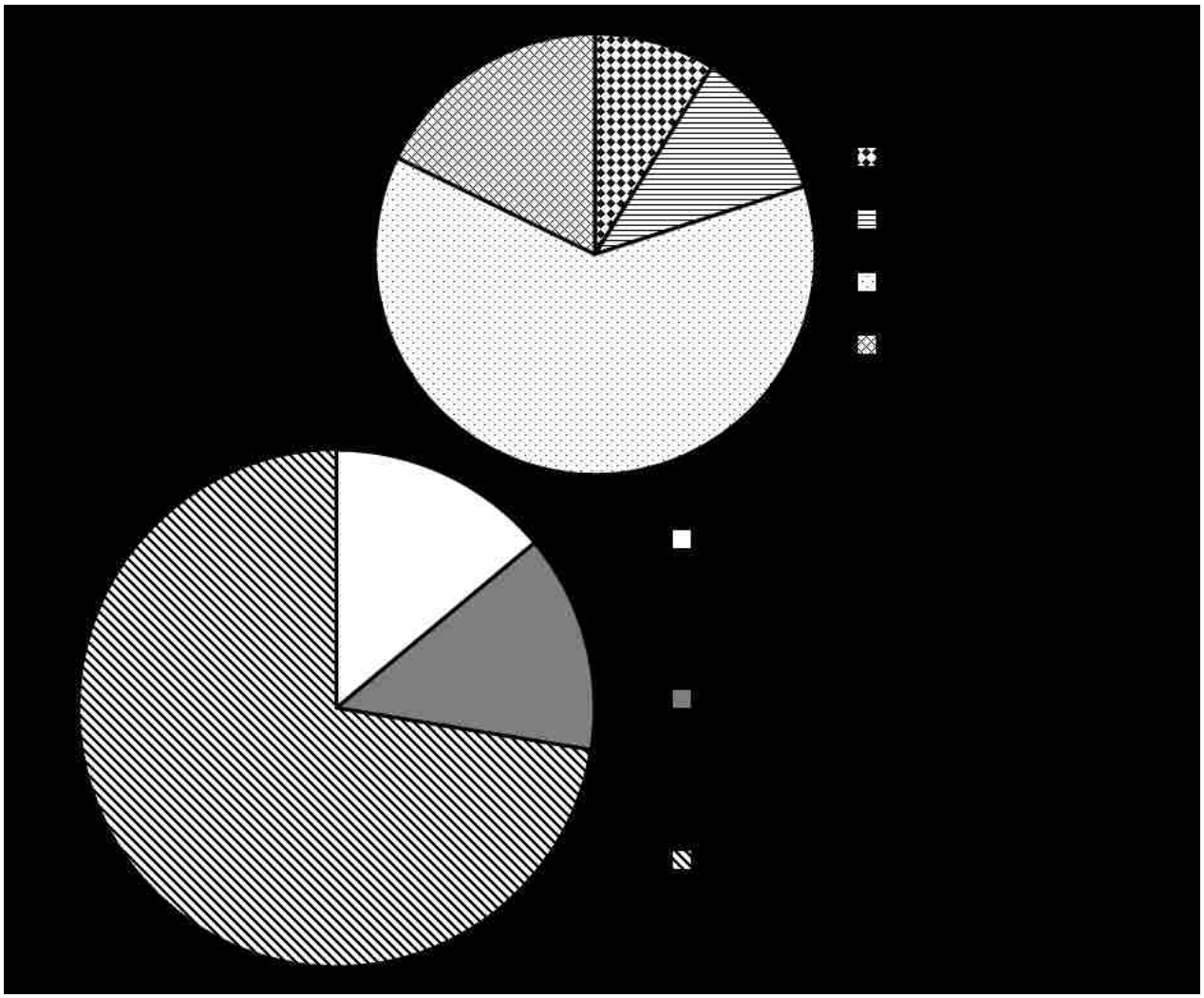

Fig 5.8: SKIV2L2 depletion leads to the accumulation of different types of non-coding RNAs. Annotated genes elevated in *Skiv2l2* knockdown cells were looked at in-depth. The non-coding RNAs identified from Table 9.1 were further categorized into the following groups: lncRNAs, miRNAs, snoRNAs, or other, with other RNAs including RNA components of enzymes, snRNAs, and non-coding RNAs of unknown class.

Twenty-seven of the non-coding RNAs were classified as long non-coding RNAs, the majority with unknown function. However, lncRNAs with at least some documentation included Snhg7 (a snoRNA host gene similar to Gas5), miRNA host genes (Snhg20, Mir22hg, and E130102H24 Rik), antisense transcripts (5031425E22Rik, RAB26os, Gt(ROSA)26Sor, and Fam120aos), one miRNA sponge lncRNA (Btbd19), and one lncRNA derived from the intron of an immunoglobulin gene (D430020J02Rik). Two of these lncRNAs were probed in further detail by looking at the Sashimi plot, which graphs the RNA-seq reads on the mouse genome and puts both samples side by side. Increased RNA-seq reads correlate to a larger peak amplitude at a given point, representing an increase in transcript abundance. For the antisense transcript Fam120aos, Sashimi plots revealed that the first exon of the gene was not detected in P19 cells, while the first intron and second exon were found to accumulate in *Skiv2l2* knockdown cells (Fig 5.9a). The slight upregulation of the Fam120 protein coding gene suggests that the expression and turnover of the coding and non-coding antisense transcripts may be linked. Conversely, the antisense transcript RAB26os appears to accumulate in *Skiv2l2* knockdown cells with little to no impact on the expression of the RAB26 protein coding gene (Fig 5.9b). Regardless, it is of note that SKIV2L2 depletion was found to impact three major types of lncRNAs: RNAs antisense to other genes, RNAs processed from host genes, and host genes that undergo post-transcriptional processing.

A.

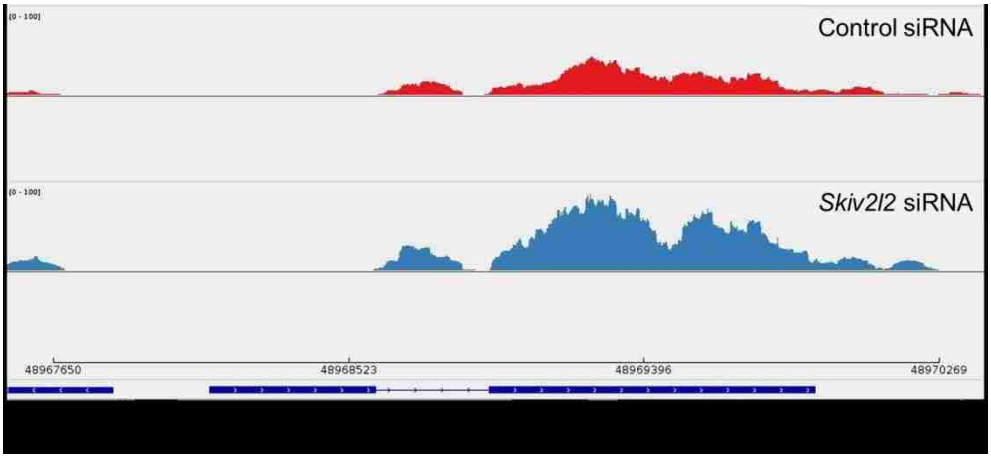

B.

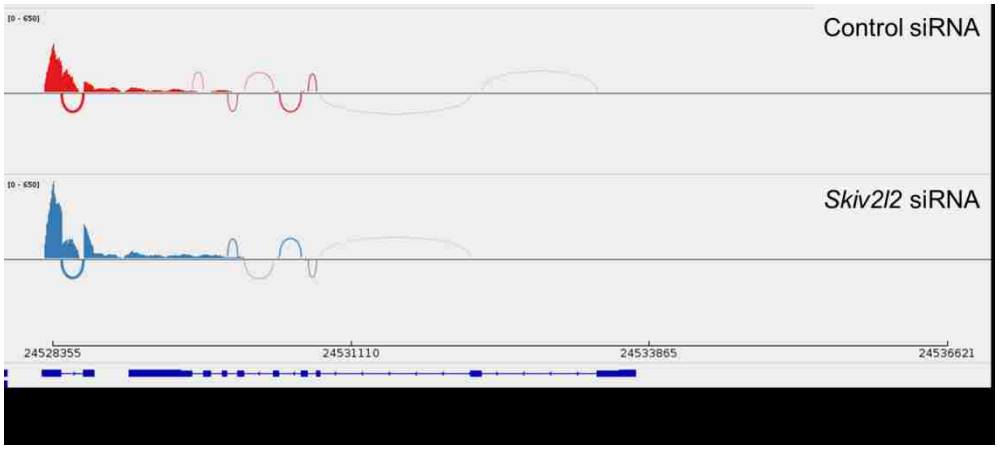

Fig 5.9: lncRNAs accumulate in *Skiv2l2* knockdown cells. A. Sashimi plot for Fam120aos. Fam120aos accumulates in *Skiv2l2* knockdown cells (blue) compared to control P19 cells (red) measured via RNA-seq analysis. Accumulation occurs over the first intron, second exon, and 3' end. B. Sashimi plot for Rab26os. Rab26os accumulates in *Skiv2l2* knockdown cells (blue) compared to control P19 cells (red) as measured via RNA-seq analysis. Accumulation is most pronounced over the first and second exons.

Five snoRNAs were elevated following SKIV2L2 depletion. These included snora65, snora70, snora64, snora21, and snord22, representing four H/ACA box snoRNAs and one C/D box snoRNA. Looking at the Sashimi plot for snora64, which is processed from the second intron of the Rsp2 host gene, accumulation only occurs over Rsp2's two introns, with the greatest increase in transcript abundance occurring over snora64 in *Skiv2l2* knockdown cells (Fig.5.10a). This result suggests that Rsp2 splicing, intron turnover, and snora64 processing may all depend on SKIV2L2. Additionally, one lncRNA that functions as a snoRNA host-gene was elevated following SKIV2L2 depletion. For the lncRNA Snhg7, the Sashimi plot shows that *Skiv2l2* knockdown induces only the accumulation of the intronic region that contains the H/ACA box snora78 (Fig. 5.10b). This result further implicates SKIV2L2 in the processing and turnover of intronic snoRNAs.

Attention was then focused on two "other" non-coding RNAs found to accumulate in *Skiv2l2* knockdown cells: Gm6548 and Gm6623. Both Gm6548 and Gm6623 are annotated as processed pseudogenes (expressed retrogenes). In Gm6548's Sashimi plot, only two small areas of the transcript are expressed in P19 cells, and the accumulating transcripts in *Skiv2l2* knockdown cells only occur at the 3' most peak (Fig 5.11a). According to the piRNABank database, this region is predicted to contain piRNAs, possibly implicating SKIV2L2 in piRNA turnover. The Sashimi plot for Gm6623 suggests expression of the entire predicted non-coding RNA, with the transcript accumulating in *Skiv2l2* knockdown cells along the entire gene (Fig. 5.11b). The piRNABank predicted no piRNAs over this gene, which is consistent with the transcript coverage on the Sashimi plot. Instead the predicted gene Gm6623 may be an example of

a longer non-coding RNA turned over via SKIV2L2 and the nuclear exosome. Probing into these two predicted genes further confirmed that SKIV2L2 functions in a wide range of non-coding RNA processing and turnover events.

Of the twelve non-coding RNAs that were downregulated following SKIV2L2 depletion, ten were lncRNAs, one was a non-coding transcript variant of Mphosph9 (mitotic phosphoprotein), and one was a non-coding RNA with little information (Table 9.3). The ten downregulated lncRNAs represented a broad range, with some being differentially expressed in cancer and others containing piRNAs and miRNAs. Because these non-coding RNAs were not predicted to be SKIV2L2 targets based on the experimental design, they were not investigated in greater detail. However, it is of note that the lncRNA Neat1 was downregulated following SKIV2L2 depletion. The observed downregulation of Neat1, which maintains paraspeckles, could be due changes in mitosis, as paraspeckles are not maintained during telophase (Wang, 2016). Seeing as Neat1 is upregulated in certain cancer cells (Wang, 2016), its downregulation with loss of SKIV2L2 offers some insight into the observed mitotic arrest phenotype and the SKIV2L2's role in maintaining cancer cell proliferation.

A.

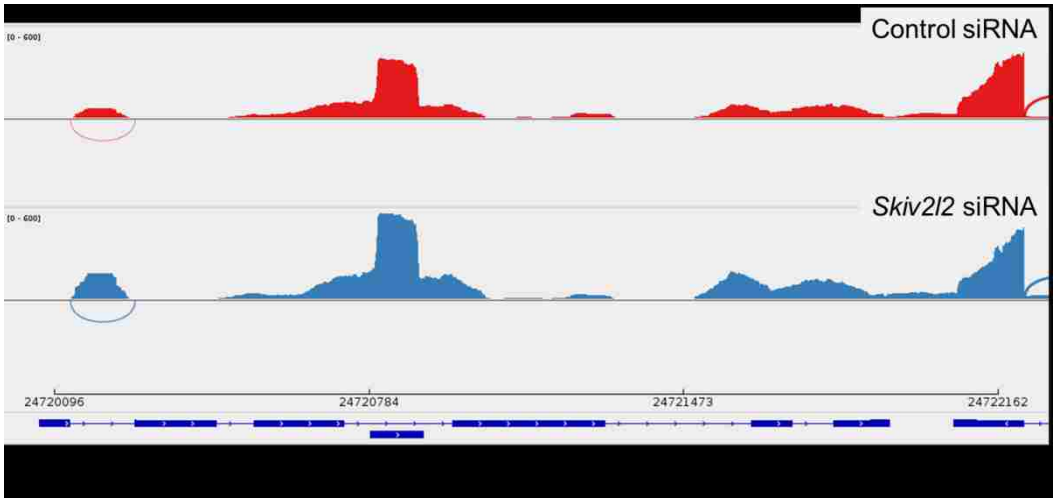

B.

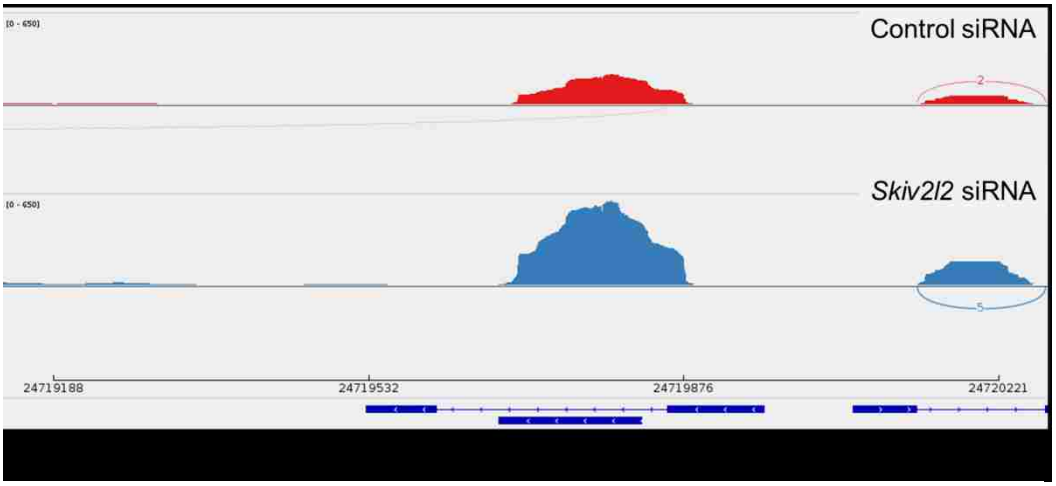

Fig 5.10: H/ACA box snoRNAs accumulate in *Skiv2l2* knockdown cells. A. Sashimi plot for snora64. Snora64 derived from the Rsp2 transcript accumulates in *Skiv2l2* knockdown cells (blue) compared to control P19 cells (red) as measured via RNA-seq analysis. Accumulation is mostly limited to the snoRNA itself with a slight accumulation of the 3' extended snoRNA. B. Sashimi plot for snora78. Snora78 derived from Snhg9 accumulates in *Skiv2l2* knockdown cells (blue) compared to control P19 cells (red) as measured via RNA-seq analysis. Accumulation only occurs over mature snora78.

A.

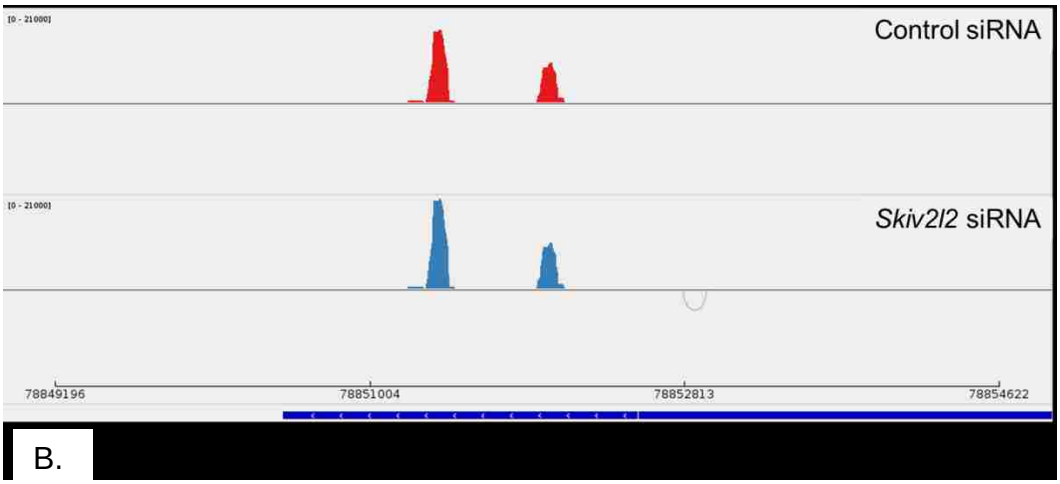

B.

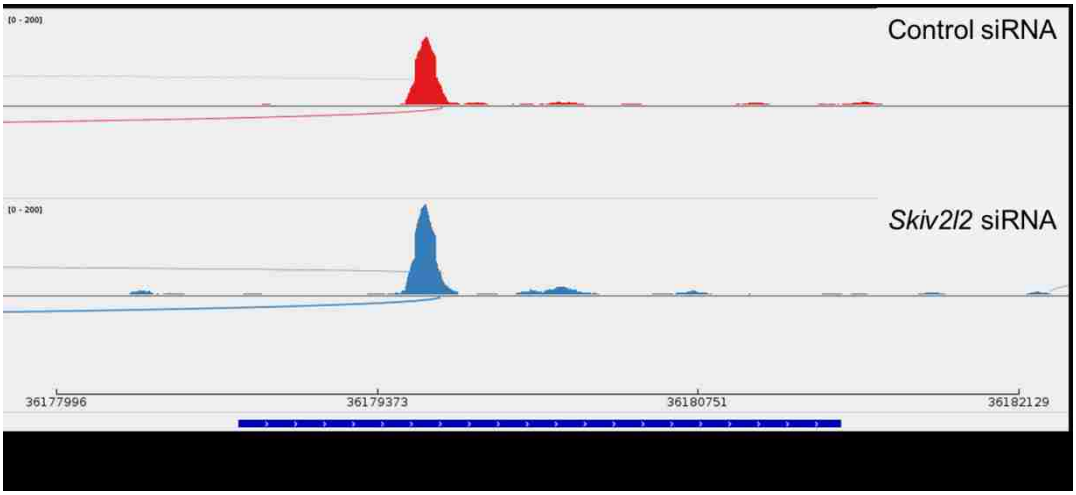

Fig 5.11: Processed pseudogenes accumulate in *Skiv2l2* knockdown cells. A. Sashimi plot for Gm6548. Gm6548 accumulates in *Skiv2l2* knockdown cells (blue) compared to control P19cells (red) as measured via RNA-seq analysis. Accumulation only occurs at the most 3' peak. B. Sashimi plot for Gm6623. Gm6623 accumulates in *Skiv2l2* knockdown cells (blue) compared to control cells (red) as measured via RNA-seq analysis in P19 cells. Accumulation occurs over the entire transcript but is most notable at the most 5' peak.

5.2.5 SKIV2L2 depletion results in the accumulation of transcripts expressed from intergenic regions

The RNA-seq data revealed that SKIV2L2 depletion induces a strong, directional trend toward the upregulation of transcripts arising from regions with no annotated genes (Table 9.2). Of these 772 upregulated intergenic transcripts, a fraction were found to contain retrogenes annotated on the UCSC genome browser, while some of these intergenic regions fall upstream of promoters, possibly representing PROMPTs (promoter upstream transcripts), a known target of nuclear RNA surveillance (Lubas, 2015; Tiedje, 2014). Interestingly, only 99 intergenic loci were reduced in *Skiv2l2* knockdown cells, suggesting that SKIV2L2 depletion causes a substantial increase in intergenic transcripts.

Because PROMPTs are a known NEXT complex target, research focused on processed pseudogenes (retrogenes) that were upregulated in *Skiv2l2* knockdown cells. Pseudogenes are defined as functional genes that have lost their protein-coding abilities. There are two types of pseudogenes: unprocessed, which are created due to gene duplication events followed by mutations, and processed pseudogenes. Processed pseudogenes, also called retrogenes, arise when mRNA from a functional gene is reverse-transcribed and inserted into the genome at a different location. Because they are formed from mRNA, these retrogenes are missing some or all introns and lack promoters and regulatory elements necessary to drive their transcription. (Pink, 2011) The majority of pseudogenes upregulated in *Skiv2l2* knockdown cells were found to be processed pseudogenes (retrogenes). Some of these processed pseudogenes are named as predicted genes (pseudogene Gm12611), while some are unnamed and referred to by their parental gene name (retro-Phgdh).

The Sashimi plot from processed pseudogene 9577 shows that only a small portion of the pseudogene is expressed (red block on the UCSC genome browser), with the accumulation in *Skiv2l2* knockdown cells restricted to two peaks, each covering approximately 100 base pairs (Fig 5.12a). Similarly, retro-Phdgh (Fig 5.12b) accumulates in *Skiv2l2* knockdown cells only at one 120 base pair region in the processed pseudogene. This result suggests that either SKIV2L2 is involved in the silencing of processed pseudogenes, the turnover and processing of small non-coding RNAs arising from these pseudogenes, or both.

To confirm that these processed pseudogenes accumulate in *Skiv2l2* knockdown cells, qRT-PCR was performed to look at the steady-state levels of the complete transcripts for retro-Phdgh and pseudogene Gm12611. These two processed pseudogenes were selected from the RNA-seq data because SKIV2L2 depletion triggered high levels of accumulation with minimal change in the expression of the original gene. Total RNA was reverse-transcribed using oligo-dT or gene specific primers to detect adenylated and unadenylated transcripts. A small segment was selected for amplification in qRT-PCR. This allowed for detection of processed pseudogenes, both unadenylated and adenylated, that accumulate following SKIV2L2 depletion.

Attempts to amplify these processed pseudogenes in N2a cells were unsuccessful, suggesting that their expression is specific to P19 cells. This is not surprising given that processed pseudogenes typically are expressed in a tissue-specific manner (Pink, 2011). In P19 cells, both retro-Phgdh and Gm12611 were elevated 1.3 fold following SKIV2L2 depletion (Fig 5.13a, p-values< 0.003 and 0.03, respectively). While adenylated retro-Phgdh was unchanged following SKIV2L2 depletion, adenylated Gm12611 increased 1.4

fold (Fig. 5.13b, p-value< 0.03). This suggests that accumulating Gm12611 is adenylated, whereas retro-Phgdh is not. The levels of retro-Phgdh and Gm12611 detected through qRT-PCR are significantly lower than those seen in the RNA-seq data. These low levels support the Sashimi plot data, which suggest that the accumulation occurs at small regions expressed from the processed pseudogene that are not efficiently detected through qRT-PCR.

Finally, RNA immunoprecipitation was utilized to see if processed pseudogene transcripts associate with SKIV2L2 in vivo. In this experiment (Fig. 5.2), proteins were UV crosslinked to RNAs bound to them and loaded onto Protein A-conjugated beads. These beads were pre-incubated with antibodies either specific to SKIV2L2 or to goat Ig. SKIV2L2 and its bound RNAs would be pulled down with anti-SKIV2L2. The anti-goat Ig would not capture SKIV2L2, serving as a negative control to ensure that the RNAs detected were specifically bound to SKIV2L2 and not to the magnetic beads. The immunoprecipitated RNAs in both samples were then reverse transcribed using gene-specific primers, and qRT-PCR was performed. RNAs bound to SKIV2L2 would be pulled down at a higher rate with anti-SKIV2L2 compared to anti-goat Ig. To ensure that the SKIV2L2 protein did not indiscriminately associate with RNA or DNA and skew the data, qRT-PCR values were normalized to *Skiv2l2* and *Tubb3* mRNA, which were not detected among the immunoprecipitate and served as background levels.

Fig 5.12: Specific segments of processed pseudogenes accumulate in *Skiv2l2* knockdown cells. A. Sashimi plot for Gm9577 shows an accumulation (red box on the UCSC genome browser) in the processed pseudogene. This accumulation occurs following *Skiv2l2* knockdown (blue) when compared to control cells (red) as measured via RNA-seq analysis in P19 cells. B. Sashimi plot for retro-Phgdh. Accumulation in *Skiv2l2* knockdown cells (blue) was limited to one small segment of retro-Phgdh, denoted by a red box on the UCSC genome browser.

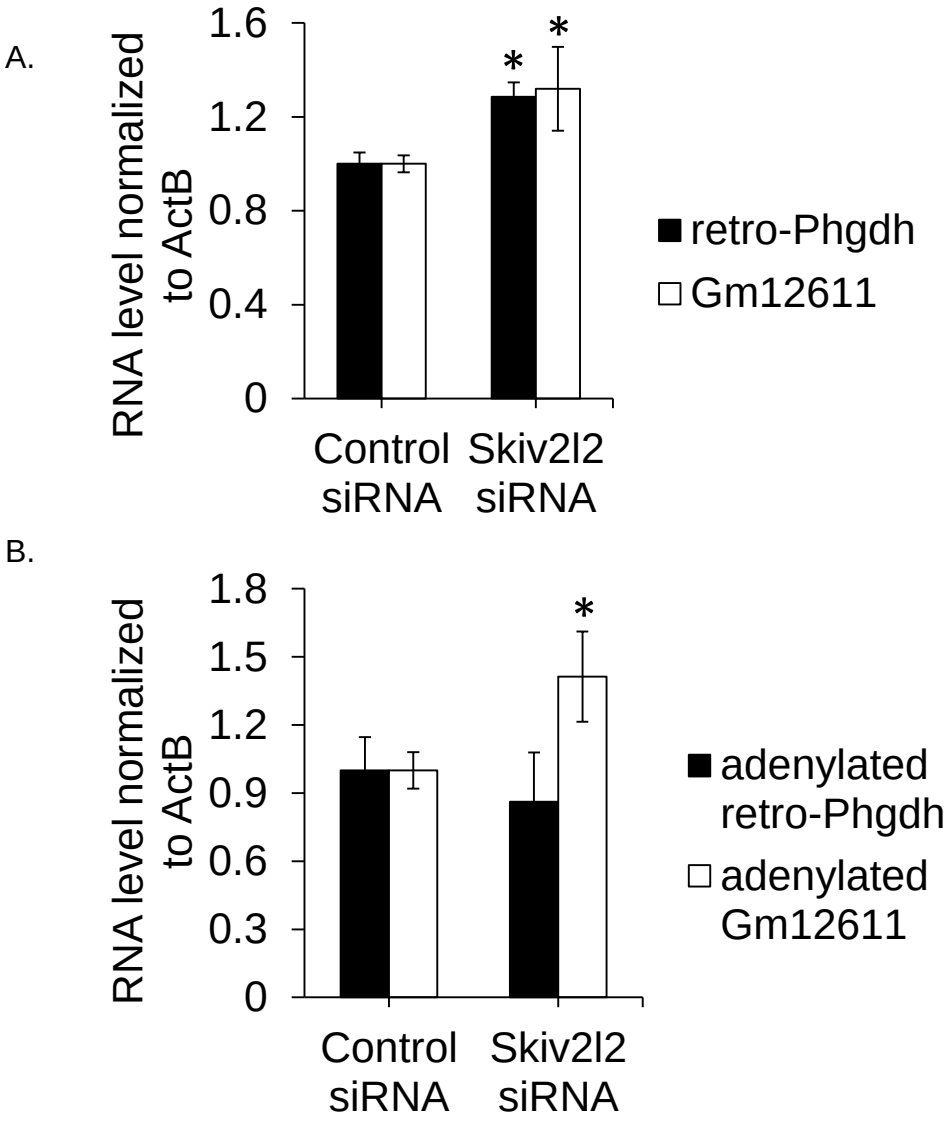

Fig 5.13: qRT-PCR verifies slight accumulation of processed pseudogenes following SKIV2L2 depletion in P19 cells. A. Unadenylated processed pseudogenes accumulate slightly with SKIV2L2 depletion. Total RNA extracted from control and *Skiv2l2* knockdown cells was reverse-transcribed with gene specific primers, with a segment amplified using qRT-PCR and normalized to ActB and control siRNA levels (n=3, * marks p-values <0.05) B. Only accumulating Gm12611 is adenylated. Total RNA extracted from control and *Skiv2l2* knockdown cells was reverse-transcribed with oligo-dT, with a segment amplified using qRT-PCR and normalized to ActB and control siRNA levels (n=3, * marks p-values <0.05).

Using this RNA immunoprecipitation protocol, qRT-PCR showed that retro-Phgdh and Gm12611 did not efficiently immunoprecipitate with anti-SKIV2L2 (p-values > 0.05, Fig. 5.14). While Gm12611 levels doubled in anti-SKIV2L2 samples, this increase was neither statistically significant (p-value> 0.05) nor on par with the increase expected to occur based on the detection of other target RNAs bound to SKIV2L2. Together, these results indicate that SKIV2L2 is not directly involved in the turnover of full-length retrogene transcripts.

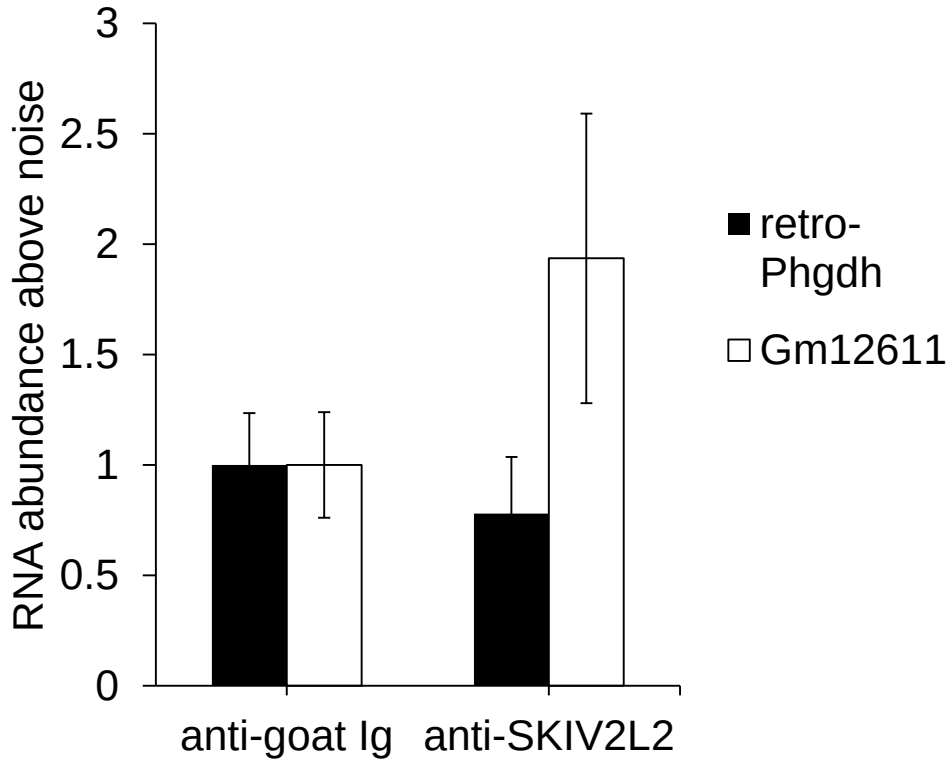

Fig 5.14: RNA immunoprecipitation does not detect significant association between processed pseudogenes and SKIV2L2. RNAs that co-precipitate with anti-goat Ig and anti-SKIV2L2 in P19 cells were reverse transcribed with gene specific primers and a segment was amplified using qRT-PCR to measure its abundance. Processed pseudogene transcript levels were normalized to *Skiv2l2* and *Tubb3* mRNAs to account for background noise and then normalized to anti-goat Ig levels (n=3, p-values >0.05).

5.2.6 SKIV2L2 depletion impacts the steady state levels of certain mRNAs

The majority of genes downregulated upon SKIV2L2 depletion were mRNAs. GO Ontology analysis established that a significant proportion of these downregulated mRNAs are positive regulators of cell proliferation (p-value< 0.03), while anti-apoptotic genes were upregulated (p-value< 0.001). The Sashimi plot for one mRNA, Neurog1, shows that the entire Neurog1 transcript is expressed at a lower level in *Skiv2l2* knockdown cells (Fig 5.15).

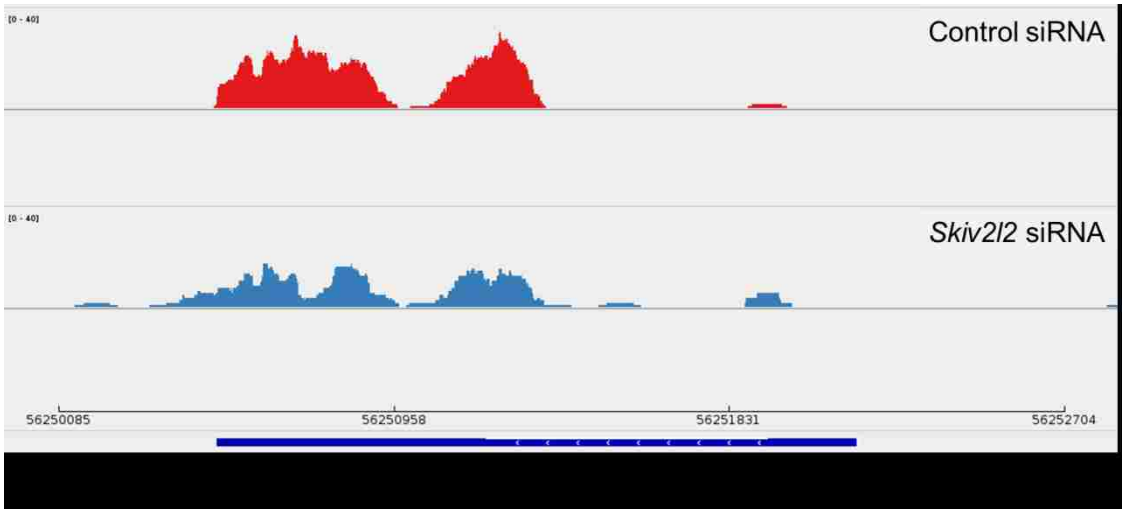

Fig 5.15: Developmental mRNAs are downregulated in P19 cells following SKIV2L2 depletion. The entire Neurog1 mRNA is downregulated following *Skiv2l2* knockdown (blue) when compared to control cells (red) as measured via RNA-seq analysis in P19 cells. Neurogenin1 triggers early stages of neuronal differentiation but is downregulated soon after.

Interestingly, certain trends emerged among the classes of mRNAs that were dysregulated in the RNA-seq data. While previous research focused on non-coding RNA targets of nuclear RNA surveillance, at least three types of coding RNAs were noticeably

dysregulated following SKIV2L2 depletion: imprinted genes, ribosomal protein mRNAs, and histone mRNAs (discussed in Chapter VI). First, imprinted genes were overrepresented among genes dysregulated following *Skiv2l2* knockdown. Out of the 129 imprinted genes in the mouse genome, 16 were found to change expression with SKIV2L2 depletion, which is statistically significant (p-value< 2.52E-06, Table 5.2). The majority of these genes were paternally expressed (maternally imprinted) and downregulated upon SKIV2L2 depletion. Grb10, Peg12, Inpp5f, Frat1, Igf2, and Gab1 are related to cell growth and cancer (Madon-Simon, 2014; Akamatsu, 2015; Jonkers, 1997; Montagener, 2005), and Lin28a and H19 are involved with the let-7 miRNA network (Piskounova, 2011; Kallen, 2014). While the nature of this trend is unknown, this finding at least alludes to a possible connection between imprinting and nuclear RNA surveillance.

In addition to imprinted genes, there also appeared to be a statistically significant change in ribosomal protein mRNAs in *Skiv2l2* knockdown cells. Approximately one-third of all ribosomal protein mRNAs accumulated in *Skiv2l2* knockdown cells (twenty-two mRNAs), with only six ribosomal protein mRNAs being downregulated (Table 9.4) This represents a statistically significant link between SKIV2L2 depletion and ribosomal protein mRNA regulation (p-value< 4.59E-20). Ribosomal protein mRNAs found to accumulate included one-fourth of the small subunit (40S) proteins and almost two-fifths of the large subunit (60S) proteins. Only one mitochondrial ribosomal protein mRNA accumulated in *Skiv2l2* knockdown cells. Sashimi plots for these upregulated ribosomal protein mRNAs (Fig 5.16) demonstrate that the exons accumulate in *Skiv2l2* knockdown

cells when compared to control cells. This implies that SKIV2L2 either directly or indirectly impacts the steady-state levels of ribosomal protein mRNAs.

Gene	Expression	$\log_2$ (fold change)	chromosome location	q-value
Grb10	Isoform Dependent	1.43	chr11	0.0014
Impact	Paternal	0.420	chr18	0.0026
Snrpn	Paternal	0.409	chr7	0.035
Lin28a	Paternal	0.373	chr4	0.020
Peg12	Paternal	-0.391	chr7	0.044
Inpp5f	Paternal	-0.408	chr7	0.016
Slc38a4	Paternal	-0.450	chr15	0.014
H19	Maternal	-0.482	chr7	0.050
Pigu	Paternal	-0.485	chr2	0.022
Frat1	Paternal	-0.521	chr19	0.39
Ppp1r9a	Maternal	-0.544	chr6	0.0014
Igf2	Paternal	-0.578	chr7	0.0055
Ocrl	Paternal	-0.844	chrX	0.0014
Gab1	Paternal	-0.909	chr8	0.049
Plagl1	Paternal	-1.17	chr10	0.0014
Zdbf2	Paternal	-1.38	chr1	0.039

Table 5.2: Imprinted gene expression changes with *Skiv2l2* knockdown. RNA-seq data demonstrated that a statistically significant number of known imprinted genes undergo changes in gene expression upon SKIV2L2 depletion. Genes with statistically significant changes in expression (q-value <0.05) included upregulated, downregulated, maternally expressed (pink), and paternally expressed (blue) genes. Genes highlighted in green are involved with growth signaling, and genes highlighted in orange are linked to the let-7 miRNA network.

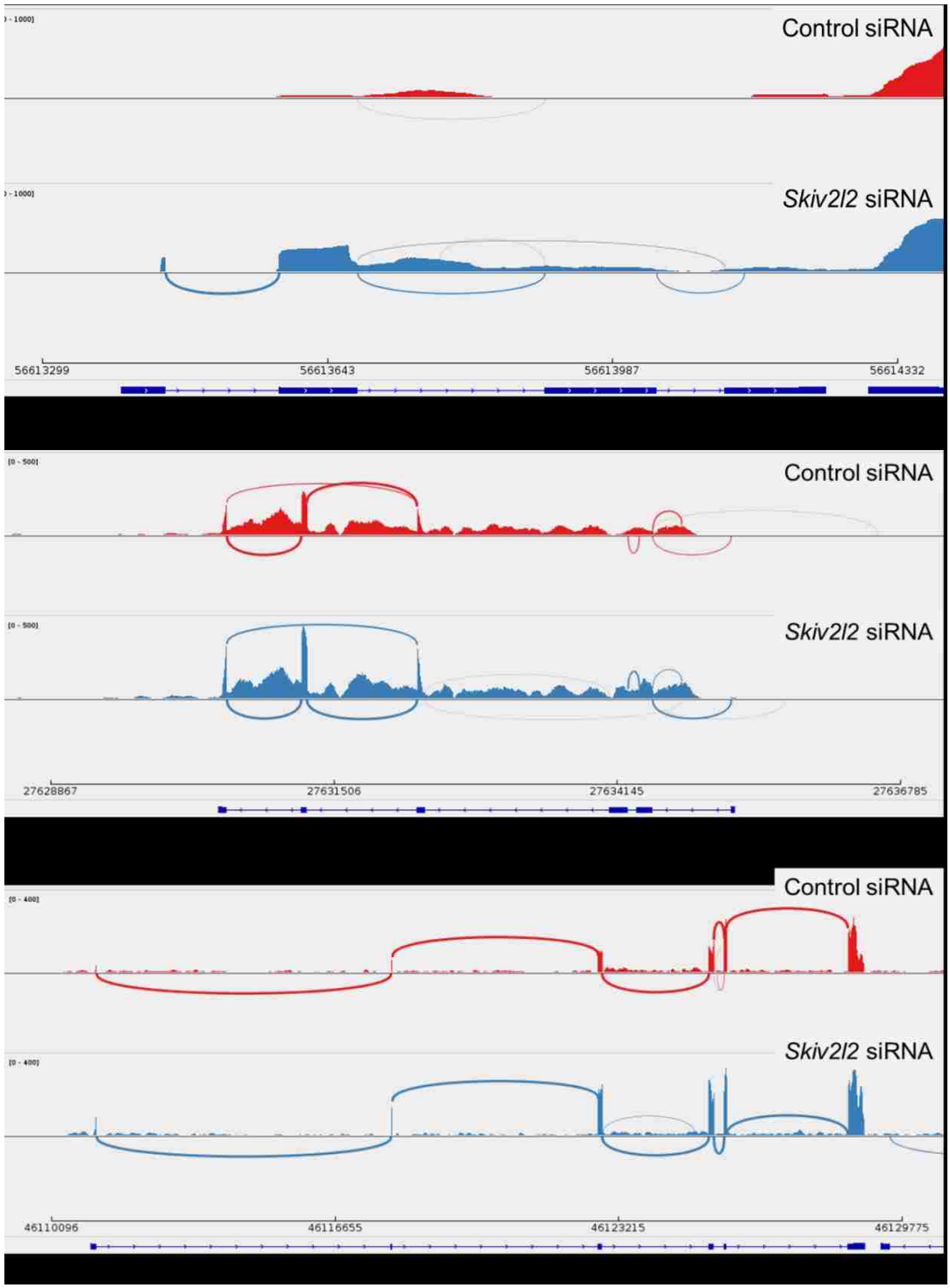

Fig 5.16: Ribosomal protein mRNAs accumulate in *Skiv2l2* knockdown cells. Sashimi plots for Rpl36 (A), Rps10 (B), and Mrps18a (C) show an accumulation of the entire mRNA in *Skiv2l2* knockdown cells (blue) when compared to control cells (red) as measured via RNA-seq analysis in P19 cells.

5.3 Discussion

Two RNA-seq studies were performed to identify potential SKIV2L2 target RNAs in mice. The first study in N2a cells relied on amplification with oligo-dT to detect only polyadenylated RNAs, which would include mRNAs and TRAMP complex targets. Non-coding RNAs found to accumulate following SKIV2L2 depletion were predicted to be potential targets of the TRAMP complex. However, these results needed to be verified at a molecular level. To accomplish this, qRT-PCR was employed to confirm the accumulation of these potential target RNAs, establish which part of the RNA was accumulating, and determine whether the TRAMP complex was involved. In addition to identifying U3, mir-322 5' leader, and the Z18 snoRNA as potential TRAMP targets, this method established a set protocol for verifying future targets of nuclear RNA surveillance.

In an effort to validate the poly-A-sequencing results, molecular cloning was performed to measure the length of A-tails on putative target RNAs. The finding that PAPD5 adds three to five adenosines to the 3' ends of target RNAs called into question the ability of oligo-dT to capture all potential TRAMP target RNAs (Wlotzka, 2011). For this reason, a second RNA-seq study was performed on total RNA to identify all potential SKIV2L2 target RNAs. By capturing the steady-state level of all RNAs, this RNA-seq study in P19 cells identified changes in gene expression and RNA accumulation following SKIV2L2 depletion. The resulting list of potential target RNAs included both targets of the TRAMP and NEXT complex, as polyadenylation was no longer required to detect target RNAs.

A significant number of non-coding RNAs were found among those RNAs accumulating in *Skiv2l2* knockdown cells, confirming previous studies centered on the role of SKIV2L2 in non-coding RNA processing and turnover. Long non-coding RNAs represented the majority of accumulating non-coding RNAs. lncRNAs have been linked to differentiation and pluripotency, with knockdown of 137 out of 147 lncRNAs inducing differentiation in mouse embryonic stem cells. These lncRNAs were found to regulate Nanog and Oct4 expression, repress specific cell-fates, and inhibit apoptosis (Guttman, 2011). As studies continue to uncover more information about lncRNA function, the processing, turnover, and regulation of these lncRNAs is of particular interest. Many lncRNAs are not adenylated and function in the nucleus (Ghosal, 2013; Dey, 2010), making them potential targets of nuclear RNA surveillance. Given the mitotic arrest phenotype associated with SKIV2L2 depletion, it is possible that SKIV2L2 aids in the processing or degradation of lncRNAs to promote cell pluripotency and proliferation.

Noticeably, many of the accumulating non-coding RNAs arise from introns or contain introns hosting smaller non-coding RNAs. For example both snoRNAs and miRNAs processed from lncRNAs, and the lncRNAs that contain such snoRNAs and miRNAs, were found to accumulate with SKIV2L2 depletion. This finding was not surprising, as the TRAMP complex promotes efficient pre-mRNA splicing in yeast (Kong KY, 2014), and human SKIV2L2 interacts with splicing factors (Lubas, 2011). Rbm7 proves necessary for splicing of intronic snoRNAs, possibly attributing the accumulation of intronic snoRNAs with SKIV2L2 depletion to the loss of NEXT complex function (Hrossova, 2015).

The majority of mRNAs dysregulated in *Skiv2l2* knockdown cells are not expected to be direct targets of nuclear RNA surveillance. However, ribosomal protein mRNAs and histone mRNAs may represent unique instances of SKIV2L2-mediated degradation of mRNAs. The yeast TRAMP complex has been linked to the processing and turnover of specific mRNAs (Milligan, 2005; Ciais, 2008), and Rbm7 binds pre-mRNAs and 3' extended replication dependent histone mRNAs (Lubas, 2015). Given the previously established association between pre-mRNAs and nuclear RNA surveillance, it is not surprising that ribosomal protein mRNAs and histone mRNAs were found to accumulate in SKIV2L2 knockdown cells. However, this finding does represent a unique instance of nuclear mRNA turnover attributed to SKIV2L2, which was thought to mainly aid non-coding RNA turnover.

The RNA-seq data also revealed a substantial change in the levels of intergenic transcripts. SKIV2L2 depletion resulted in the accumulation of over 700 transcripts arising from regions without annotated genes, while less than 100 were downregulated. This suggests that SKIV2L2 either directly or indirectly prevents the accumulation of spurious transcripts. Many of these regions contain processed pseudogenes containing repetitive elements. Because the RNA-seq data indicates only a subset of these regions accumulate, and the full-length pseudogenes do not bind SKIV2L2, it is hypothesized that piRNAs or other small RNAs arising from these regions might be processed or turned over through SKIV2L2-mediated RNA surveillance. Processed pseudogenes are known to harbor small regulatory RNAs (Pink, 2011), and the loss of SKIV2L2 may result in the accumulation of the small non-coding RNAs as opposed to the entire pseudogene. Small RNAs transcribed from processed pseudogenes in mouse oocytes

have been found to enter the siRNA pathway to regulate the expression of protein-coding genes. In addition, small RNAs that are antisense to pseudogenes regulate the expression of their protein-coding counterparts, particularly oncogenes such as Oct4 (Hawkins, 2010). In light of these findings, SKIV2L2 may mediate the turnover of small regulatory RNAs, such as siRNAs, piRNAs, or antisense RNAs, and modulate the expression of protein-coding genes. Alternatively, changes in chromatin compaction could account for the upregulation of these intergenic regions. If SKIV2L2 depletion induces a more open chromatin environment, spurious transcription from intergenic regions could occur. While attempts to visualize global changes in chromatin compaction were inconclusive, previous studies agree that histone overexpression often induces changes in the chromatin structure only in specific regions (Eberle, 2015; Singh, 2010). While it is unclear whether SKIV2L2 depletion affects processed pseudogene processing, siRNA/piRNA turnover, or chromatin compaction, this RNA-seq experiment does casually associate nuclear RNA surveillance with the regulation of processed pseudogene transcripts.

The two RNA-seq studies in N2a and P19 cells following SKIV2L2 knockdown established a pipeline for verifying SKIV2L2 target RNAs. This pipeline was used to identify multiple targets of SKIV2L2, both unique and previously known. Of note, SKIV2L2 was linked to the turnover of 5' leader sequences of miRNAs, ribosomal protein mRNAs, snoRNAs, and lncRNAs. In addition, nuclear RNA surveillance appears to play some role in the regulation of intergenic transcripts. The resulting list of both accumulating and downregulated genes was probed in light of the mitotic arrest phenotype observed following SKIV2L2 depletion. In particular, ribosomal protein mRNAs and lncRNAs of unknown function could be responsible for mitotic arrest. On

the other hand, aberrant transcription from intergenic regions could cause mitotic arrest or be symptomatic of changes in chromatin structure that can lead to chromosome nondisjunction. These possibilities will be discussed further in Chapter VII.

CHAPTER VI: SKIV2L2 TARGETS HISTONE MRNAS FOR DEGRADATION IN THE NUCLEUS

6.1 Introduction

Hypothesis: SKIV2L2 targets histone mRNAs for degradation.

Studies on nuclear RNA surveillance have focused on the turnover of non-coding RNAs that function in the nucleus (Andersen, 2008). Even though some mRNA processing has been linked to the TRAMP complex in yeast (Nag, 2012; Kong, 2013; Hiriart, 2012; Milligan, 2005), the majority of mRNA turnover is thought to be coupled to translation in the cytoplasm (Chang, 2007). However, RNA-seq analysis of P19 cells revealed an accumulation of replication-dependent histone mRNAs following SKIV2L2 depletion. Only two histone mRNAs were downregulated, both non-canonical, suggesting a strong connection between RNA surveillance and histone regulation. This finding led to further investigation into the role of SKIV2L2 in histone mRNA turnover.

Chromatin is composed of DNA wrapped around the nucleosome, an octamer of histones composed of two of each of the following histones: H2A, H2B, H3 and H4. The histone H1 binds to the linker DNA between nucleosomes. (Marzluff, 2008) Histone protein modifications change histone spacing and chromatin compaction, leading to areas of open euchromatin permissive to gene expression and closed heterochromatin containing transcriptionally silent genes (Bird, 2007). Because large quantities of histone proteins are necessary to package and maintain chromatin, mammalian genomes encode for over seventy-five replication-dependent histone genes (Marzluff, 2002). In mice, the replication-dependent histone genes are located in three genomic clusters containing

multiple genes encoding the H1, H2A, H2B, H3, and H4 histones. The Hist1 cluster contains over fifty histone transcripts, with additional histone genes found in the Hist2 and Hist3 clusters. H4 and H2A genes are also located outside of the histone clusters, and certain histone variants, including H2A.X, H2A.Z, and H3.3, are expressed from distinct loci and regulated differently from the replication-dependent histones. (Marzluff, 2002) The transcription of all these histone genes must be tightly regulated to ensure the correct stoichiometry of the histones in relation to each other and in relation to DNA (Gunjan, 2005).

During S phase, the replication of DNA must be coordinated with its packaging into chromatin (Gunjan, 2005; Günesdogan, 2014). This requires increased histone protein production only during S phase, with lower levels of histones being generated throughout the cell cycle to replace histones already incorporated into chromatin (Marzluff, 2008). To accomplish this, histone levels are regulated at both the transcriptional and post-transcriptional level. At the onset of S-phase, the cyclinE-Cdk2 complex phosphorylates the transcription factor NPAT located in Cajal bodies adjacent to the histone genomic clusters (Zhao, 2000). The phosphorylation of NPAT leads to its binding to the histone genes, enhancing histone transcription by 3-5 fold (Zhao, 2000). However, S phase requires 25-30 fold more histones than other phases of the cell cycle (Marzluff, 2008). This increase is accomplished through multiple post-transcriptional mechanisms that enhance the processing and translation of histone mRNAs.

Because replication-dependent histone mRNAs lack introns and poly-A-tails, their 3' end formation and translation require unique mechanisms (Marzluff, 2008). Histone mRNAs contain a 3' stem loop followed by a purine-rich histone downstream

element (HDE) (Zainer, 2002). Concurrent with transcription, SLBP, the major protein involved with histone mRNA processing and stabilization, binds to the stem loop and recruits the U7 snRNP (Zhao, 2004; Zhang, 2012). As U7 snRNA base-pairs with the HDE, multiple factors such as symplekin, CPSF100, and CPSF73 bind the histone mRNA and ultimately lead to cleavage of the 3' end of the histone mRNA via an unknown nuclease (Sullivan, 2009). This leads to the formation of the mature 3' end of the replication histones, which terminate in the stem loop. SLBP remains bound to the stem loop as it is required for export of the mRNA out of the nucleus (Sullivan, 2001; Zhang, 2002; Zhao, 2004; Marzluff, 2008). Circularization of the histone mRNA achieved through binding of the SLBP, SLIP, and EIF4G proteins then enhances the translation of the histone mRNA, making SLBP the key player in histone regulation (Ling, 2002). The downregulation of both SLBP and histone mRNAs at the end of S-phase is necessary for cell cycle progression because the expression of histone proteins outside of S-phase negatively impacts chromosome segregation during mitosis and may titrate histone modifiers away from chromatin (Groth, 2005; Günesdogan, 2014; Gunjan, 2005; Lanzotti, 2002; Meeks-Wagner, 1986; Singh, 2010). At the end of S phase, cyclin A-Cdk1 phosphorylates SLBP, leading to the proteolysis of SLBP (Koseoglu, 2008). Also, with the onset of G2 phase, histone mRNA stability decreases (Marzluff, 2008).

Previous research has shown that histone mRNA turnover is coupled to translation and nonsense mediated-decay proteins such as Upf1 (Kaygun, 2005ab). Cytoplasmic histone mRNA is uridylated by an unknown TUTase at the end of S phase or at the onset of DNA damage (Mullen, 2008; Schmidt, 2010). The poly(U) tail binds to Lsm proteins that recruit decapping enzymes (Kaygun, 2005ab; Mullen, 2008). This

ultimately results in the degradation of the histone mRNA in a 5' to 3' manner via the exonuclease Xrn1 (Kaygun, 2005ab; Mullen, 2008). However, in humans, the rapid degradation of histone mRNAs also depends on a different nuclease: PM/Scl100, the homolog of Rrp6 (Mullen, 2008). While Rrp6 in yeast is restricted to the nucle`ar exosome (Houseley, 2006), and initial studies on PM/Scl100 demonstrated its nuclear localization (Allmang, 2009), some researchers believe that a small fraction of PM/Scl100 functions in the cytoplasm in mammals (Lejeune, 2003). Initially, PAPD5 was identified as the TUTase that uridylates histone mRNAs (Mullen, 2008), while further studies eliminated PAPD5 as the responsible TUTase (Schmidt, 2010). However, the link between PAPD5, PM/Scl100, and histone mRNA turnover hints that nuclear RNA surveillance may be involved in regulating histone levels during the cell cycle.

The fact that Trf4p, the yeast homolog of PAPD5, and the TRAMP complex have been implicated in histone mRNA turnover in yeast (Reis, 2006) supports the possibility that SKIV2L2 mediates the degradation of mammalian histone mRNAs. In yeast, loss of Trf4p and the exosome component Rrp6 both lead to histone accumulation (Reis, 2006, Canavan, 2008). Similarly, knockdown of Rrp6 in Drosophila results in the accumulation of histone transcripts and inhibited cell cycle progression into M phase (Graham, 2009). In support of these studies, mature histone mRNAs accumulate following knockdown of human Rrp6 (PM/Scl100) but not Rbm7 in humans (Mullen, 2008). The RNA-seq experiment outlined in Chapter 5 identified replication-dependent mRNAs among RNAs accumulating following SKIV2L2 depletion. In regards to the mitotic arrest phenotype observed in *Skiv2l2* knockdown cells, both reduction in and the accumulation of histone mRNAs and proteins have been shown to induce mitotic arrest in eukaryotes (Graham,

2009; Groth, 2005; Gunjan, 2003; Gunjan, 2005; Lanzotti, 2002; Meeks-Wagner, 1986; Murillo-Pineda, 2014; Zhao, 2004). This incriminates histone mRNAs as a potential candidate responsible for the observed mitotic arrest in *Skiv2l2* knockdown cells. Indeed, Mtr4p depletion results in M phase arrest due to impaired microtubule spindle assembly (Smith, 2011), but it is unclear if this is due to a histone imbalance. The following research demonstrates that histone mRNAs are a unique mRNA target of the nuclear RNA surveillance in mammals. This finding is of significance for two reasons: it is the first finding of nuclear turnover of histone mRNAs, and histone mRNAs could be responsible for the activation of the spindle assembly checkpoint and resultant mitotic arrest following SKIV2L2 depletion.

6.2 Approach and Results

6.2.1 Histone mRNAs H1, H2A, H3, and H4 accumulate in P19 and N2a cells following SKIV2L2 depletion

In addition to imprinted genes and ribosomal protein mRNAs, histone mRNAs were significantly overrepresented in the RNA-seq data (p-value< 1.85E-57). Over 75% of histone mRNAs were dysregulated in *Skiv2l2* knockdown cells (Table 6.1). Of the sixty replication-dependent histone mRNAs, forty-six were found to accumulate following SKIV2L2 depletion, with greater than 1.5 fold accumulation occurring for 36 histone mRNAs. Multiple mRNAs encoding core histone proteins (H2A, H2B, H3, and H4) and the linker protein H1 accumulated with SKIV2L2 depletion, denoting a global change in histone regulation. Only two non-canonical histone mRNA transcripts, H2A.x and H2A.z, were downregulated. Notably, the spliced and polyadenylated mRNA encoding

the non-canonical histone H3.3 decreased slightly in abundance with SKIV2L2 depletion, although this downregulation was not statistically significant (q-value=.06). The replication-dependent histone mRNA accumulation seen with SKIV2L2 depletion suggests that nuclear RNA surveillance might influence histone mRNA turnover.

To examine the accumulation seen at replication-dependent histone mRNAs, the sequencing data from P19 cells was plotted into Sashimi plots. The histone cluster 1 on chromosome 13 was examined in detail. Histone cluster 1 contains 45 histone mRNAs, thirty-seven of which were significantly elevated in *Skiv2l2* knockdown cells. Histone cluster 1 consists of six H1 genes, nine H3 genes, five H2A genes, sixteen H2B genes, and nine H4 genes (Wang, 1996). Looking at the Sashimi plots, Hist1h1b accumulates in *Skiv2l2* knockdown cells (blue) when compared to control knockdown cells (red, Fig 6.1). In total, three out of six H1 histone mRNAs accumulate with SKIV2L2 depletion. The two non-canonical H1 histone mRNAs, H1f0 and Histh1t, do not change with *Skiv2l2* knockdown. In cluster 1, all five H2A mRNAs and eleven out of sixteen H2B mRNAs accumulate with SKIV2L2 depletion. As seen in the Sashimi plots (Fig 6.2), H2A and H2B genes are often located in clusters, with the genes transcribed in divergent directions. In these cases, mRNAs arising from both the H2A and H2B gene accumulate in *Skiv2l2* knockdown cells (blue) when compared to control knockdown cells (red). Similarly, all nine H3 and nine H4 mRNAs in cluster 1 accumulate with SKIV2L2 depletion. The Sashimi plot of Hist1h3a shows higher levels of histone mRNA in *Skiv2l2* knockdown cells (Fig 6.3), as does the Sashimi plot of Hist1h4d (Fig. 6.4).

Histone	Gene Name	log_2fold change	q-value
H3	Hist1h3e	3.422	0.0015
H2A	H2afj	2.8614	0.0015
H4	Hist1h4j	2.4992	0.0055
H2B	Hist1h2bc	1.7225	0.0015
H4	Hist1h4a	1.6044	0.0015
H2B	Hist1h2bn	1.5449	0.0015
H2B	Hist1h2bh	1.4328	0.0015
H2A	Hist1h2an	1.3952	0.0015
H4	Hist1h4f	1.3176	0.0015
H4	Hist1h4k	1.3143	0.0015
H4	Hist1h4d	1.3043	0.0015
H2B	Hist1h2bk	1.2686	0.0015
H3	Hist1h3i	1.1831	0.0015
H2B	Hist1h2bg	1.1672	0.0015
H4	Hist1h4i	1.1225	0.0015
H4	Hist1h4b	1.1002	0.0015
H2A	Hist2h2ac	1.0897	0.0015
H2B	Hist1h2bl	1.0895	0.0015
H4	Hist2h4	1.0518	0.0015
H4	Hist1h4h	1.0499	0.0015
H2B	Hist1h2bm	1.0281	0.0015
H2A	Hist3h2a	0.9981	0.0015
H2A	Hist1h2ah	0.9973	0.0055
H2B	Hist1h2be	0.9929	0.0015
H3	Hist1h3f	0.9824	0.0015
H2B	Hist1h2bj	0.9806	0.0015
H3	Hist1h3a	0.9728	0.0015
H3	Hist1h3c	0.9416	0.0015
H2A	Hist1h2ak	0.9298	0.0015
H4	Hist4h4	0.916	0.0015
H2B	Hist1h2bf	0.8984	0.0015
H3	Hist2h3b	0.8816	0.0095
H2B	Hist3h2bb-ps	0.8594	0.0015
H4	Hist1h4c	0.8594	0.0015
H2A	Hist1h2ai	0.8042	0.008
H3	Hist1h3g	0.7957	0.0015
H3	Hist1h3h	0.7068	0.0015
H2B	Hist1h2bp	0.6818	0.0015

H2B	Hist3h2ba	0.6661	0.0015
H3	Hist1h3d	0.5921	0.0015
H2A	Hist1h2ac	0.5881	0.02
H3	Hist1h3b	0.5487	0.0015
H1	Hist1h1b	0.5382	0.0015
H1	Hist1h1c	0.4263	0.0036
H2B	Hist2h2bb	0.4164	0.0055
H1	Hist1h1d	0.3362	0.0354
H2A.X	H2afx	-2.398	0.0015
H2A.Z	H2afz	-2.486	0.0015

Table 6.1: Histone mRNA levels significantly change following *Skiv2l2* knockdown in P19 cells. RNA-seq identified a significant proportion of replication dependent histone mRNAs as accumulating in *Skiv2l2* knockdown cells (q-value<0.05). Log_2fold change represents the fold change in *Skiv2l2* knockdown P19 cells compared to control P19 cells. Only two histone mRNAs are downregulated in *Skiv2l2* knockdown cells, H2afx and H2afz, which are both non-canonical histone mRNAs.

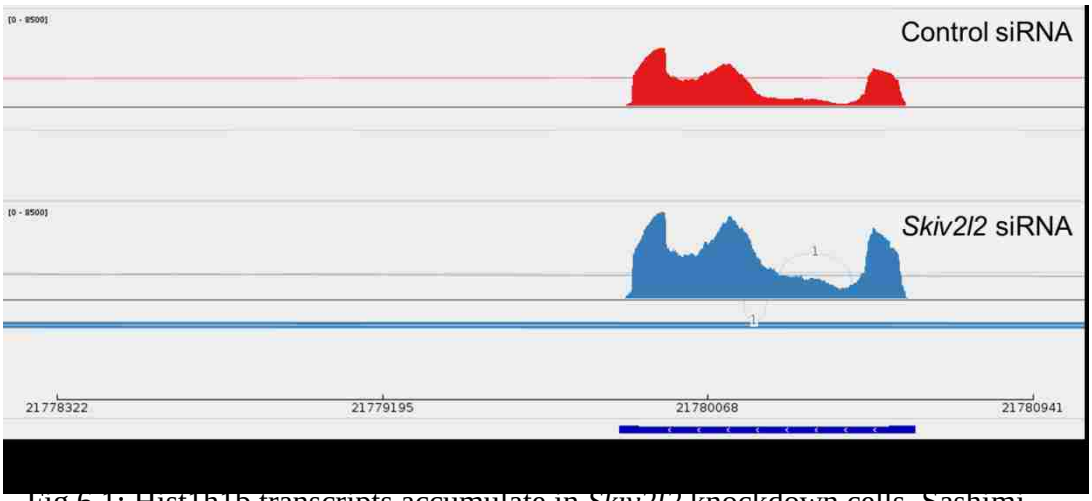

Fig 6.1: Hist1h1b transcripts accumulate in *Skiv2l2* knockdown cells. Sashimi plots generated from RNA-seq data from P19 cells show higher levels of the entire Hist1h1b transcript in *Skiv2l2* knockdown cells (blue) when compared to control cells (red).

A.

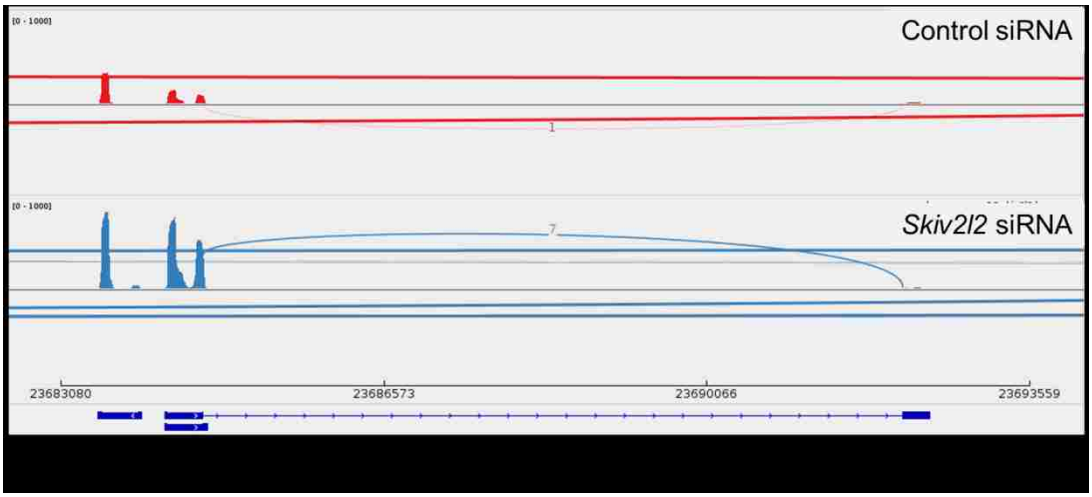

B.

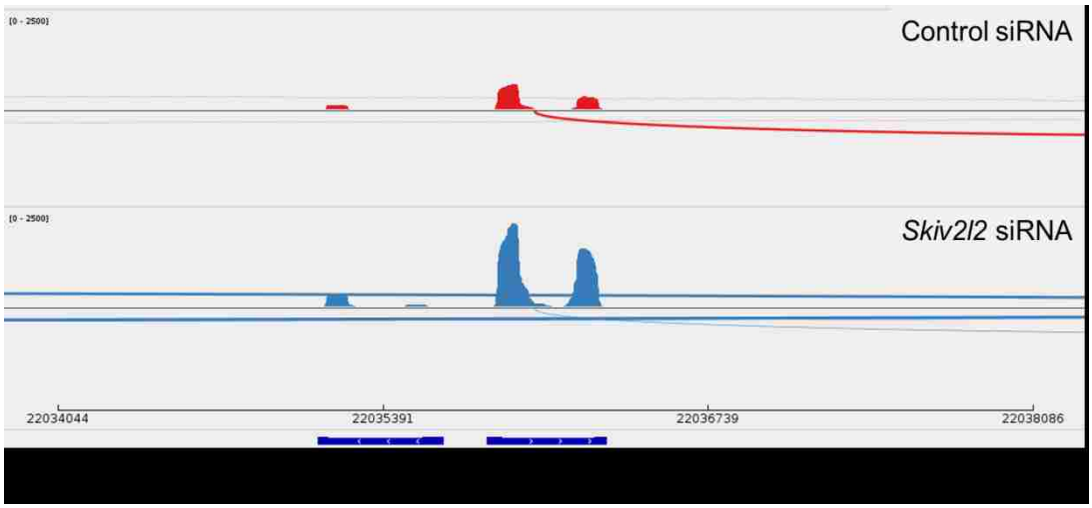

Fig 6.2: Clusters of H2A and H2B transcripts accumulate in *Skiv2l2* knockdown cells. A. Sashimi plots generated from RNA-seq data in P19 cells show higher levels of the entire Hist1h2ac and Hist1h2bc transcripts in *Skiv2l2* knockdown cells (blue) when compared to control cells (red). B. Sashimi plot of the Hist1h2ah and Hist1h2bk loci shows a similar mRNA accumulation upon *Skiv2l2* knockdown.

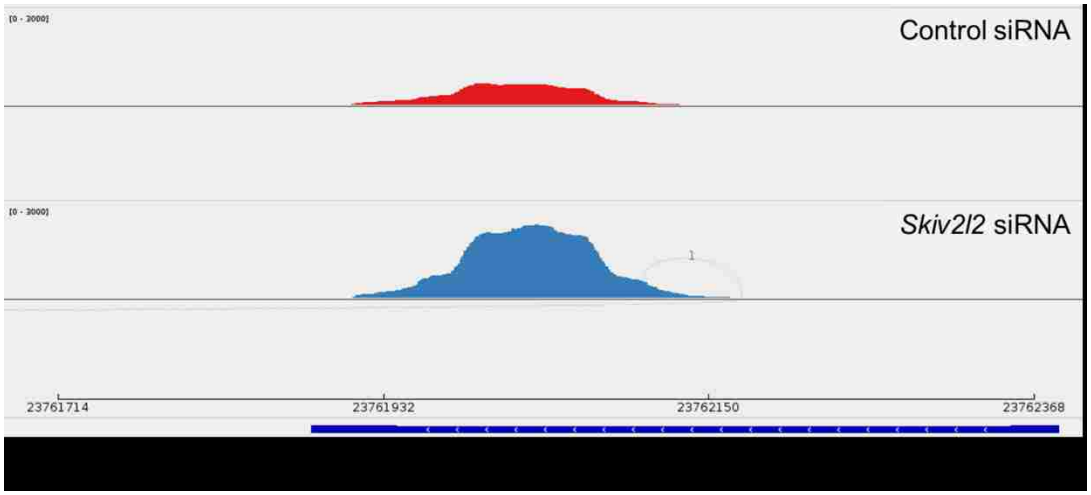

Fig 6.3:Hist1h3a transcripts accumulate in *Skiv2l2* knockdown cells. Sashimi plots generated from RNA-seq data in P19 cells show higher levels of the entire Hist1h3a transcript in *Skiv2l2* knockdown cells (blue) when compared to control cells (red).

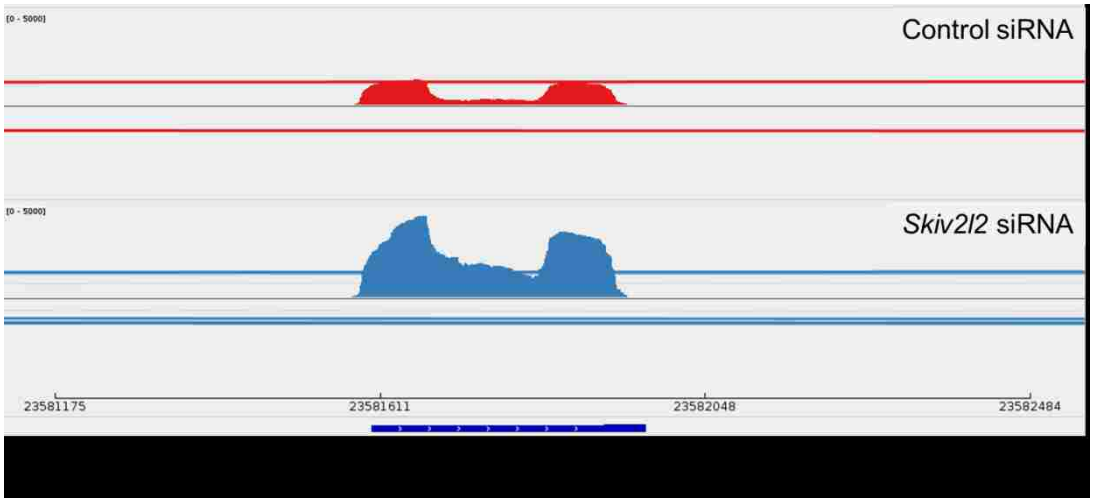

Fig 6.4: Hist1h4d transcripts accumulate in *Skiv2l2* knockdown cells. Sashimi plots generated from RNA-seq data in P19 cells show higher levels of the entire Hist1h4d transcript in *Skiv2l2* knockdown cells (blue) when compared to control cells (red).

To verify the accumulation calculated in the RNA-seq data and visualized in the Sashimi plotting of that data, qRT-PCR was performed to measure the overall abundance of replication-dependent histone mRNAs. The sequence similarity between mRNAs makes distinguishing between individual transcript variants difficult, so primers were designed to probe for replication-dependent histone mRNA levels for total H1, H2A, H2B, H3, and H4 mRNAs. qRT-PCR verified that the replication-dependent histone mRNAs H1, H2A, H2B, H3, and H4 were significantly elevated in both N2a cells and P19 cells following SKIV2L2 depletion (Fig 6.5, d, n=3, p-values all < 0.05). In N2a cells, H1, H2A, H2B, and H4 mRNAs all accumulated approximately 3-fold, with a large, but highly variable 12-fold increase in H3 mRNA. SKIV2L2 depletion in P19 cells yielded a similar accumulation of the replication-dependent histone mRNAs, with approximately a 2 to 3-fold increase in H1, H2A, H2B, and H4 mRNAs. Attempts to detect histones following reverse transcription with oligo-dT were unsuccessful, suggesting that the accumulating histones lack long poly-A-tails that efficiently prime using oligo-dT. Overall, qRT-PCR and RNA-seq data both corroborate replication-dependent histone mRNA accumulation following SKIV2L2 depletion.

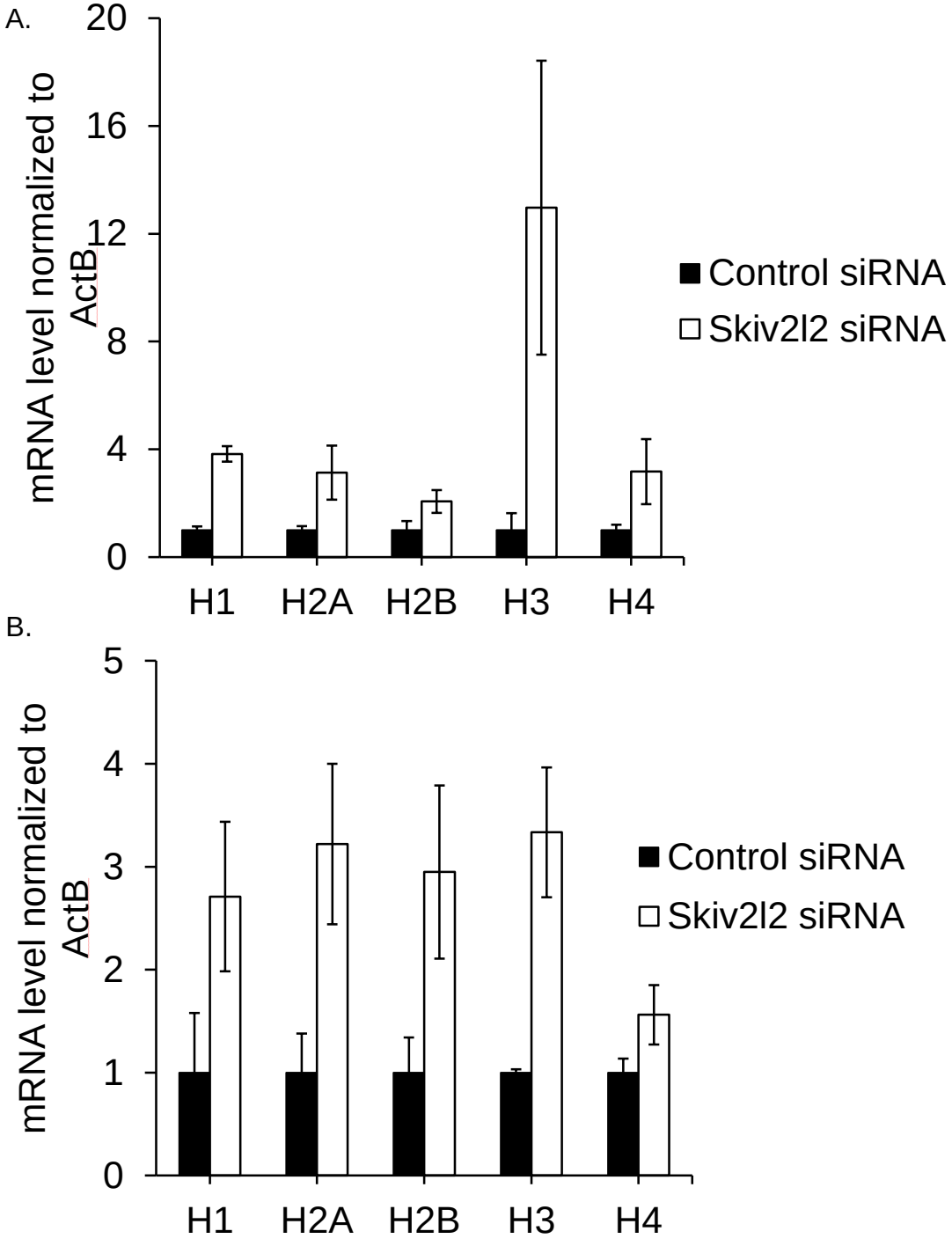

Fig 6.5: Histone transcripts accumulate with SKIV2L2 depletion in N2a and P19 cells. A. qRT-PCR of histone mRNAs in N2a cells. Expression levels of histone mRNAs were calculated using ΔCq values and normalized to ActB expression and control siRNA levels (error bars represent ±SD for n=3, p-values all <0.05). B. qRT-PCR of histone mRNAs in P19 cells. Expression levels of histone mRNAs were calculated using ΔCq values and normalized to ActB expression and control siRNA levels (error bars represent ±SD for n=3, p-values all < 0.05).

6.2.2 Histone mRNAs accumulate slightly in *Papd5* knockdown cells but not in *Zcchc8* knockdown cells

Confident that SKIV2L2 depletion results in histone mRNA accumulation, the next experiment addressed whether the TRAMP or the NEXT complex could be involved in histone mRNA turnover. Both PAPD5 and ZCCHC8 were depleted via siRNA in N2a cells, and qRT-PCR was again utilized to measure the abundance of H4 mRNA. H4 was probed for because it moderately but consistently increased with *Skiv2l2* knockdown. H4 mRNA levels were normalized to ActB and compared to control siRNA-treated cells (Fig 6.6). *Papd5* knockdown cells showed a very slight increase in H4 mRNA (1.18-fold increase), while *Zcchc*8 knockdown cells had no detectable accumulation in H4 mRNA. This effectively demonstrates that ZCCHC8 is not essential for histone turnover. While the increase in H4 mRNA following PAPD5 depletion was statistically significant (p-value< 0.0006), it did not replicate the 2-fold increase seen with SKIV2L2 depletion.

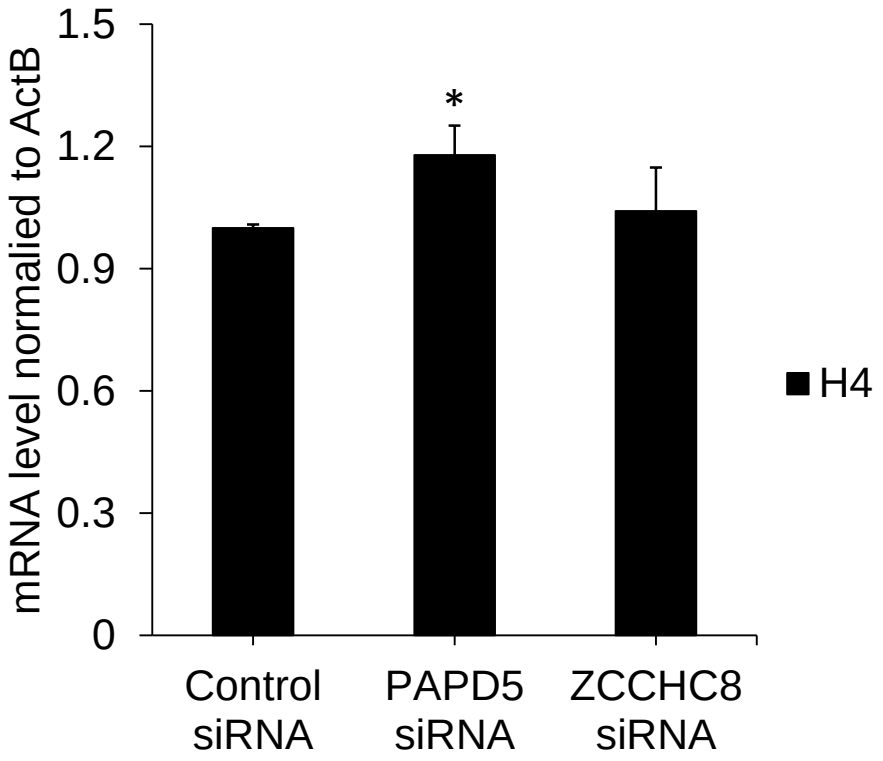

Fig 6.6: Histone H4 transcripts accumulate in *Papd5* knockdown cells. qRT-PCR measured histone H4 mRNAs in N2a cells following *Papd5*, *Zcchc8*, and control siRNA treatments. Expression levels of histone mRNAs were calculated using ΔCq values and normalized to ActB expression (error bars represent ±SD for n=3). A slight but statistically significant increase (denoted by asterisk, p-value< 0.05) in H4 mRNA was observed in *Papd5* knockdown cells but not *Zcchc8* knockdown cells.

6.2.3 Histone transcript accumulation with SKIV2L2 depletion correlates to an increase in at least one histone protein

Previous research in Drosophila found that histone mRNAs accumulate with loss of Rrp6, with no change in histone protein levels (Graham, 2009). To see if an increase in histone mRNA results in an increase in histone protein following SKIV2L2 depletion, total protein was recovered from control and *Skiv2l2* knockdown cells. The total protein was fractionated into nuclear and cytoplasmic fractions, and the nuclear fraction was acid-extracted to release histones from DNA. Western blotting was then used to detect histone H4 in the acid-extracted fractions and ActB in the cytoplasmic fractions for normalization. Histone H4 protein levels increased by an average of 2.9 fold ($n=3$, p-value< 0.03) in N2a cells and an average of 4.5 fold ($n=3$, p-value< 0.002) in P19 cells following *Skiv2l2* knockdown (Fig 6.7). This demonstrates that the increase in histone H4 mRNA transcripts following SKIV2L2 depletion correlates to an increase in H4 protein.

A.

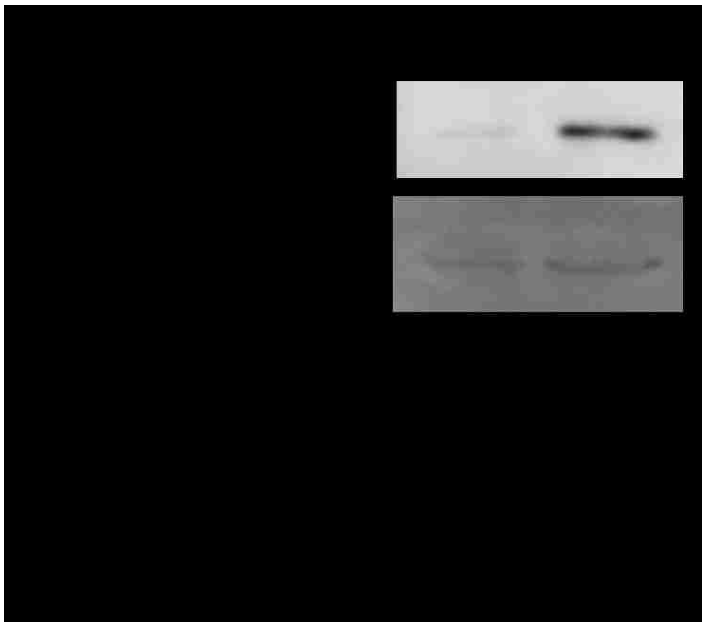

B.

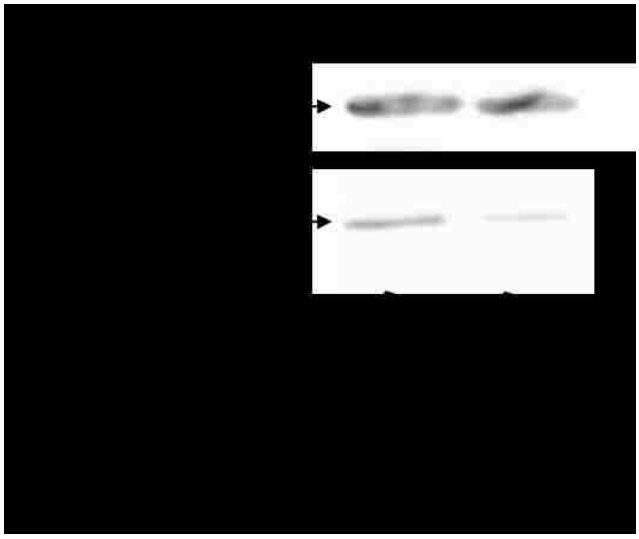

6.2.4 Histone accumulation with SKIV2L2 depletion may negatively impact chromatin compaction

Because both histone mRNAs and H4 protein were found to accumulate with SKIV2L2 depletion, it was hypothesized that these excess histones could affect chromatin compaction in *Skiv2l2* knockdown cells. During prophase, chromatin becomes tightly compacted to prepare for the attachment of kinetochores during prometaphase and metaphase. Excess free histones have been shown to inhibit this chromatin compaction and trigger mitotic arrest, particularly if the histone dimer pairs (H2A-H2B and H3-H4) are not expressed with the correct stoichiometry (Meeks-Wagner, 1986; Singh, 2010). The observed histone imbalance with SKIV2L2 depletion could prevent the compaction of chromatin, leading to the observed mitotic arrest. To test this hypothesis, micrococcal nuclease assays were performed to measure the overall compactness of the chromatin in control and *Skiv2l2* knockdown cells. Micrococcal nuclease cuts the DNA between histone octamers. When the chromatin is loose (euchromatin), the micrococcal nuclease will digest the DNA between histones, generating small fragments of DNA. If the chromatin is compact, histone octamers are spaced closer together, and the micrococcal nuclease cannot access the DNA. This leads to decreased digestion of the DNA, generating larger DNA fragments.

The micrococcal nuclease assays performed on chromatin isolated from N2A cells treated with control and *Skiv2l2* siRNA resulted in a qualitative assessment of overall chromatin compaction (Fig 6.8). As a control, isolated chromatin was digested with proteinase K to degrade histone proteins. The resulting naked DNA was then digested with micrococcal nuclease to verify that DNA digestion was complete in the absence of

histone proteins (Fig 6.8, lanes 2 and 3). No large DNA bands appeared on the gel, confirming that digestion was complete after 9 minutes of treatment with micrococcal nuclease. The intact chromatin from N2A cells was then digested in a similar manner (lanes 4-9). Each lane pair (4 and 5, 6 and 7, 8 and 9) represents a unique biological replicate. For chromatin extracted from control N2A cells, digestion generated mainly large DNA fragments and some small DNA fragments, generating a "smear" on the gel (lanes 4, 6, and 8). With SKIV2L2 depletion, chromatin digestion with micrococcal nuclease generates an increased number of smaller base pair fragments and fewer larger DNA fragments when compared to the control cells (lanes 5, 7, and 9). Lane 5 shows digestion to completion like with naked DNA, while lane 7 and 9 contain mainly smaller base pair fragments, effectively shifting the "smear" downward on the gel. This result suggests that the chromatin of control cells is compact, preventing the micrococcal nuclease from accessing the DNA and leading to increased distance between cut sites. This correlates to larger DNA fragments on the agarose gel. However, chromatin from *Skiv2l2* knockdown cells is digested more completely, visualized as smaller base pair fragments on the agarose gel. While this qualitative analysis is not definitive proof, the result suggests that the chromatin could be less compact following SKIV2L2 depletion, leading to increased digestion with micrococcal nuclease.

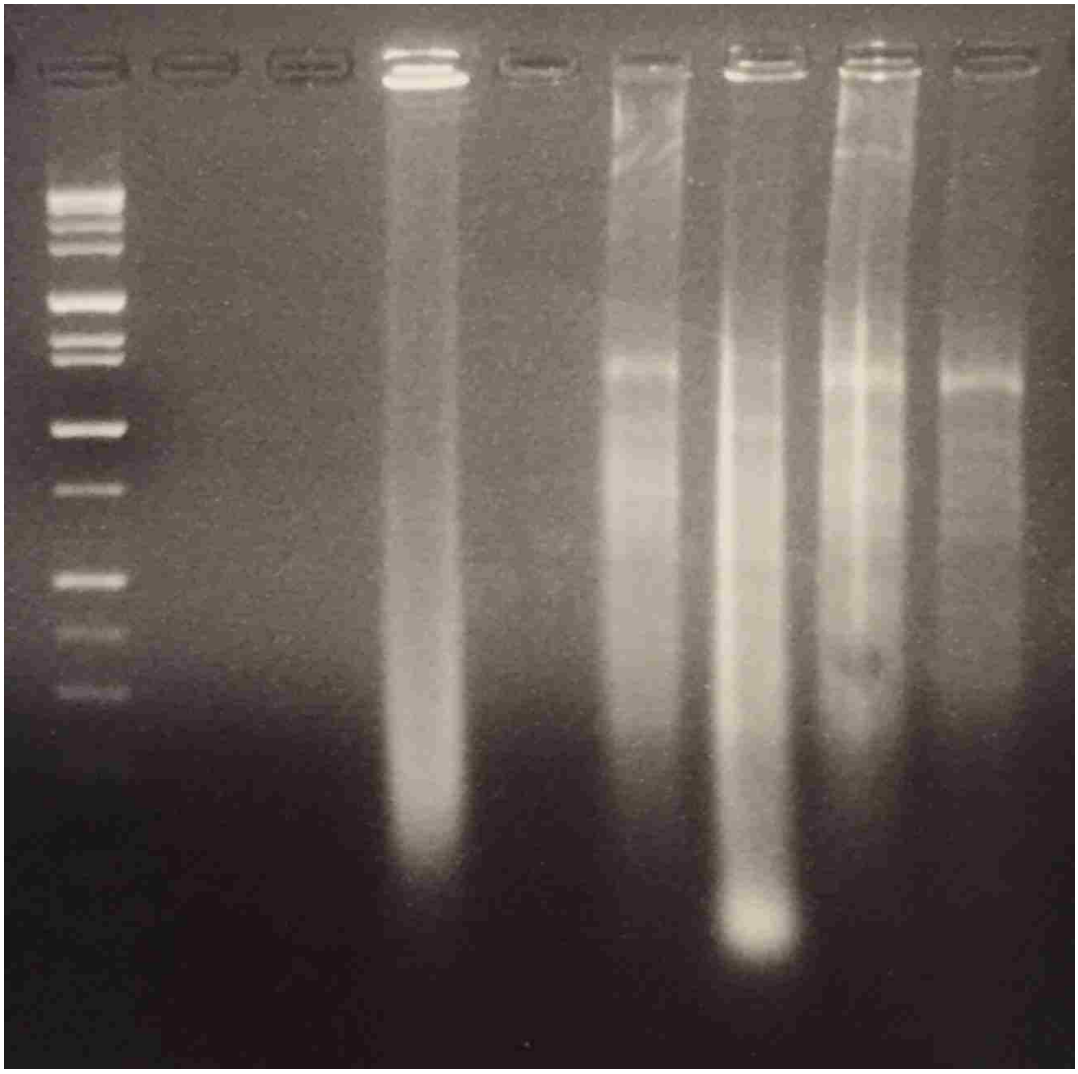

Fig 6.8: Micrococcal nuclease assays suggest chromatin compaction defects following SKIV2L2 depletion. Chromatin was digested with micrococcal nuclease and run on an agarose gel. Lane 1- 100 bp ladder; 2- naked DNA digested with micrococcal nuclease from control N2A cells; 3- naked DNA digested with micrococcal nuclease from *Skiv2l2* knockdown N2A cells; 4, 6, 8- chromatin digested with micrococcal nuclease from control N2A cells; 5, 7, 9- chromatin digested with micrococcal nuclease from *Skiv2l2* knockdown N2A cells. Smaller DNA fragments, particular noticeable in lane 7, indicate more complete digestion.

6.2.5 Histone mRNAs are detected among RNAs bound to the SKIV2L2 protein

In order to support the assertion that replication-dependent histone mRNA turnover requires SKIV2L2, experiments sought to demonstrate that SKIV2L2 binds histone mRNAs in vivo, thereby establishing a direct, physical link between SKIV2L2 and histone mRNA. To demonstrate that histone mRNAs directly associate with the nuclear-localized SKIV2L2 (Norbury, 2011; Lubas, 2011; Osman, 2011), cross-linked immunoprecipitation was performed to detect histone mRNAs bound to SKIV2L2. Both N2a and P19 cells were irradiated with UV light to crosslink RNA to protein, and proteins were bound to beads coated with antibodies directed against either SKIV2L2 or a negative control goat IgG. Western blots demonstrated that anti-SKIV2L2 successfully pulled down approximately 10% of cellular SKIV2L2, while no SKIV2L2 was detected in the eluate from control IgG (Fig 6.9a, Fig 6.10a).

RNAs immunoprecipitated with anti-SKIV2L2 were compared to those RNAs immunoprecipitated with the control antibody using qRT-PCR. Histone mRNA levels in immunoprecipitates were normalized against *Skiv2l2* and *Tubb3* mRNA, which both showed no binding to SKIV2L2. Compared to RNA immunoprecipitated with anti-goat IgG, replication dependent histone mRNAs (H1, H2A, H2B, H3, and H4) were elevated among RNAs immunoprecipitated with anti-SKIV2L2, as measured via qRT-PCR (Fig 6.9b,6.10b, all p-values< 0.05). In N2a cells, H1, H2A,H2B, and H4 were enriched among those RNAs pulled down with anti-SKIV2L2 by more than 5-fold, while H3 was found at levels 2-fold above the control (Fig 6.9b). Among those RNAs that immunoprecipitated with SKIV2L2, retro-Phgdh mRNA levels were not above those

seen in the control immunoprecipitate, suggesting that the protocol sufficiently distinguished between RNAs bound to SKIV2L2 and unbound RNA. P19 cells proved to yield a more dramatic result, with H1, H2A, and H3 being pulled down with anti-SKIV2L2 at levels 20-fold or greater above those seen in control cells, and H2B and H4 enriched in the immunoprecipitate approximately 10-fold about control levels (Fig 6.10b). Because close association is necessary to crosslink RNA to protein, these results demonstrate binding of SKIV2L2 to histone mRNAs in vivo in both N2a and P19 cells.

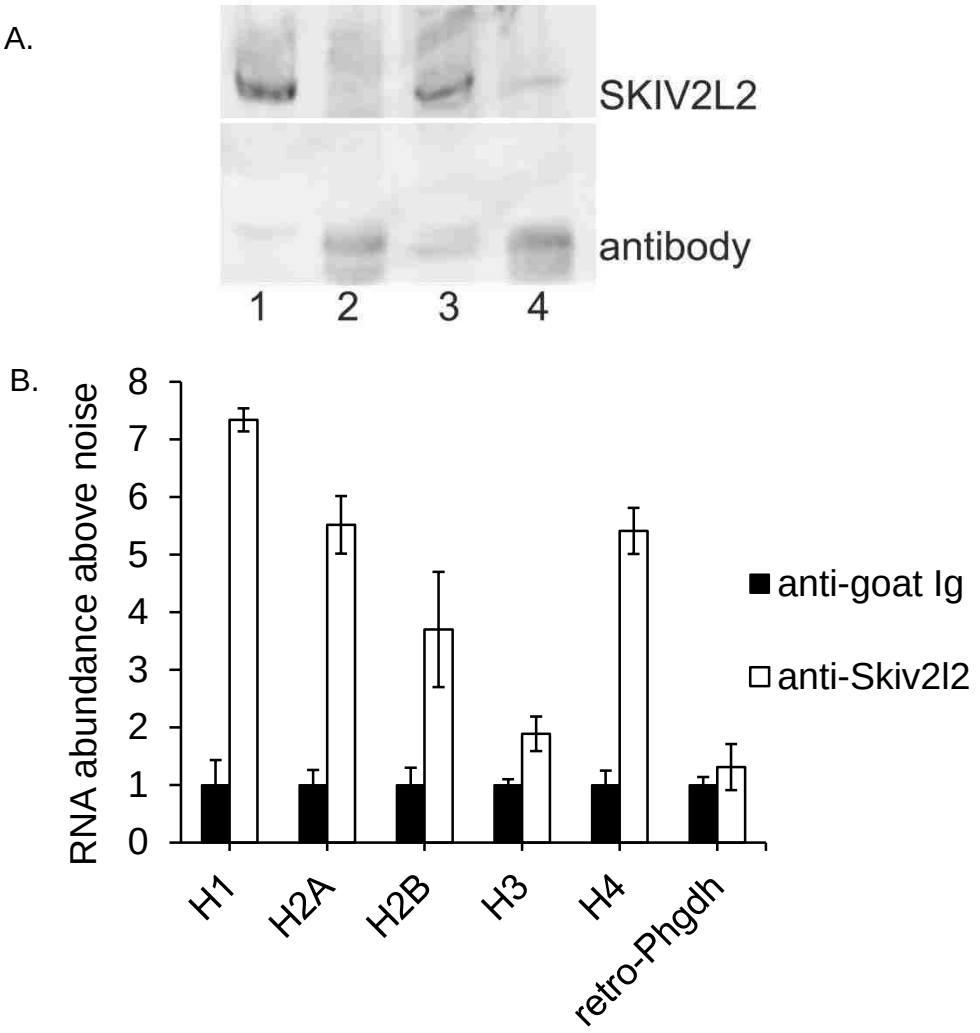

Fig 6.9: RNA immunoprecipitation demonstrates SKIV2L2 binding to histone mRNAs in N2a cells. A. Western blots against immunoprecipitated SKIV2L2. Lanes 1, 3-total cell lysate; lane 2-eluate following immunoprecipitation with anti-goat Ig; lane 4- eluate following immunoprecipitation with anti-SKIV2L2. Top band represents SKIV2L2, bottom band is the heavy chain of the antibody used for immunoprecipitation. B. qRT-PCR of histone RNAs bound to immunoprecipitated SKIV2L2 in N2a cells. Proteins were extracted from N2a cells irradiated with UV light, and SKIV2L2 was immunoprecipitated with its associated RNAs using anti-SKIV2L2. Anti-goat was used as a negative control, and RNA was isolated from both samples. Using qRT-PCR, RNA abundance levels of histone mRNAs immunoprecipitated in either sample were calculated using ΔCq values, and normalized for background noise based on the amplification of *Skiv2l2* mRNA transcript, which was unbound in both samples (error bars represent ±SD for n=3). Immunoprecipitated retro-Phgdh represents an RNA precipitated equally by anti-goat and anti-SKIV2L2.

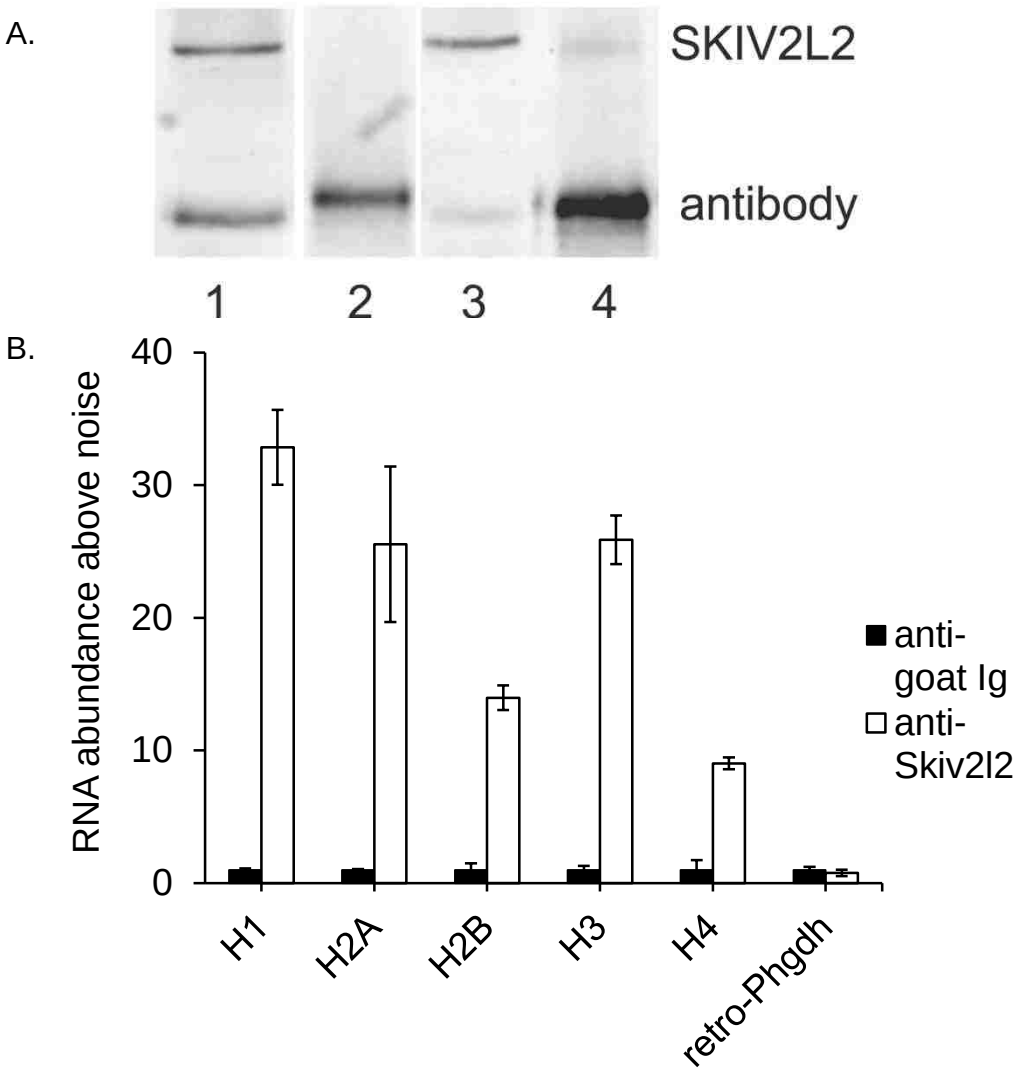

Fig 6.10: RNA immunoprecipitation demonstrates SKIV2L2 binding to histone mRNAs in P19 cells. A. Western blots against immunoprecipitated SKIV2L2. Lanes 1, 3-total cell lysate; lane 2-eluate following immunoprecipitation with anti-goat Ig; lane 4- eluate following immunoprecipitation with anti-SKIV2L2. Top band represents SKIV2L2, bottom band is the heavy chain antibody used for immunoprecipitation. B. qRT-PCR of histone RNAs bound to immunoprecipitated SKIV2L2 in P19 cells. Proteins were extracted from P19 cells irradiated with UV light, and SKIV2L2 was immunoprecipitated with its associated RNAs using anti-SKIV2L2. Anti-goat was used as a negative control, and RNA was isolated from both samples. Using qRT-PCR, RNA abundance levels of histone mRNAs immunoprecipitated in either sample were calculated using ΔCq values, and normalized for background noise based on the amplification of *Skiv2l2* mRNA transcript, which was unbound in both samples (error bars represent ±SD for n=3). Immunoprecipitated retro-Phgdh represents an RNA precipitated equally by anti-goat and anti-SKIV2L2.

6.2.6 The half-life of H4 mRNA increases following SKIV2L2 depletion

Given that histone mRNAs were found to accumulate with loss of SKIV2L2, and SKIV2L2 was found to directly bind to histone mRNAs, it was hypothesized that SKIV2L2 is necessary for the turnover of these histone mRNAs. To confirm this, experiments aimed to establish that SKIV2L2 depletion leads to a reduction in histone mRNA turnover and an increase in histone mRNA half-life. This evidence would further support the notion of SKIV2L2-mediated turnover of replication-dependent histone mRNAs. Histone mRNA turnover was assessed using Northern blotting. Following either *Skiv2l2* or control siRNA knockdown, N2a cells were treated with Dactinomycin, which inhibits RNA polymerase II transcription (Bensaude, 2011). At time points following Dactinomycin treatment, cells were harvested to isolate RNA, which was utilized in Northern blotting and probed for histone H4 mRNA. Since transcription was inhibited, any subsequent decrease in H4 mRNA would be due to turnover. RNA from *Skiv2l2* and control knockdown cells that were not treated with Dactinomycin was also probed for H4 mRNA. Northern blots confirmed the 1.9 fold increase (p-value< 0.04, $n=3$) in H4 mRNA observed in *Skiv2l2* knockdown cells (Fig 6.11). This demonstrated that Northern blotting was sensitive enough to discriminate differences in H4 mRNA levels after treatment with Dactinomycin. In a pilot experiment, H4 mRNA was not detected after 6 hours of Dactinomycin treatment. Therefore, the time points were selected to measure H4 mRNA for 4 hours after Dactinomycin treatment. In the first trial, samples were collected at 0, 1, 2, 3, and 4 hours. However, RNA yield was not of sufficient quality at the 0 and 1 hour time points in *Skiv2l2* knockdown cells, and no H4 mRNA was detected in control cells after 2 hours. Therefore, Northern blotting detected H4 mRNA at 0, 1, and 2 hours

in control N2a cells and at 2, 3, and 4 hours in *Skiv2l2* knockdown cells. While H4 mRNA was depleted after 2 hours in control cells, H4 mRNA remained in *Skiv2l2* knockdown cells at 4 hours (Fig 6.11a). While this did not allow for direct comparison at hour time points, the H4 mRNA levels were used to calculate mRNA half-life in both control cells and cells depleted of SKIV2L2.

To correct for issues in RNA quality in the first trial of this experiment, a second trial was performed. In control cells, H4 mRNA was depleted to negligible levels four hours after Dactinomycin treatment (Fig 6.11b). However, at four hours post Dactinomycin treatment, *Skiv2l2* knockdown cells retained higher levels of H4 mRNA (Fig 6.11b). This result was consistent with the first trial, suggesting that cells depleted of SKIV2L2 exhibit a decreased rate of H4 mRNA turnover. However, the second trial did reveal the appearance of two H4 mRNA bands. Both bands were found to decrease at identical rates in both control and *Skiv2l2* knockdown cells, so it is possible that the lower band corresponds to degradation intermediates or a transcript variant. Using the data from the first and second trials, the half-life of H4 mRNA was calculated. In control cells, the mRNA half-life was 34 minutes, while the half-life increased to 72 minutes following SKIV2L2 depletion (p-value< 0.04, $n=2$). For trial two, both the upper and lower band had identical half-lives. Given that Dactinomycin inhibited transcription in these samples, a slower rate of mRNA decay must be responsible for the increase in H4 mRNA half-life.

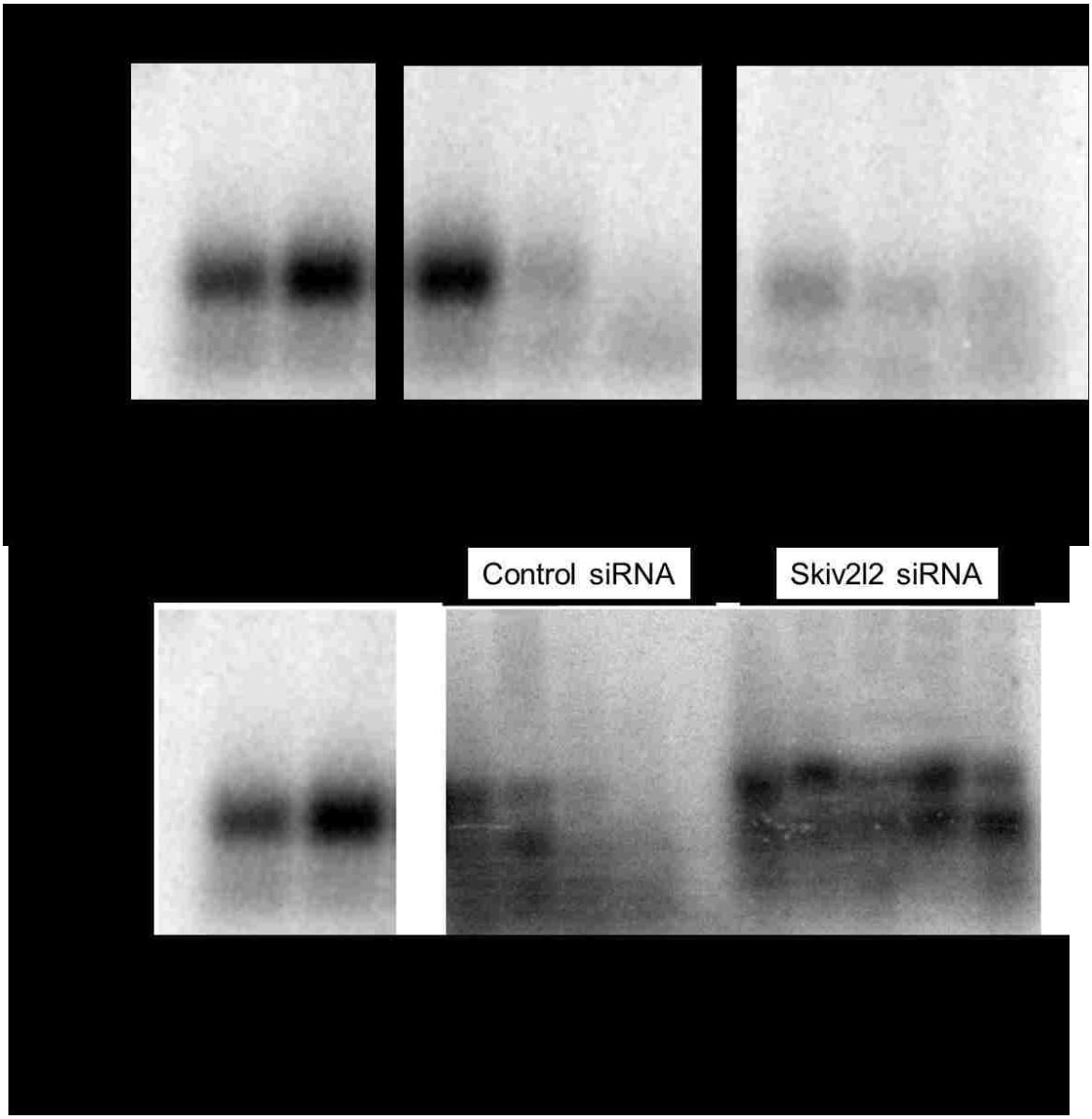

Fig 6.11: *Skiv2l2* knockdown impairs H4 histone mRNA turnover, doubling its mRNA half-life. Northern blots tracking H4 mRNA turnover following Dactinomycin treatment. RNA was extracted from control and *Skiv2l2* knockdown N2a cells following application of Dactinomycin at 1 hour timepoints. Northern blotting detected H4 mRNA, which was quantified and normalized to ActB mRNA levels to calculate half-life. A and B represent two unique biological replicates. In A, RNA quality for control siRNA at 3 hr and 4 hr and *Skiv2l2* siRNA 0 hr and 1 hr was low and excluded from analysis.

6.3 Discussion

Initial analysis of the RNA-seq data from P19 cells revealed that replication-dependent histone mRNAs accumulated with SKIV2L2 depletion. This accumulation was confirmed through qRT-PCR of histone mRNAs following SKIV2L2 depletion in both N2a and P19 cells. In light of this, replication dependent-histone mRNAs were hypothesized to be a potential SKIV2L2 target. To confirm histone mRNAs as a RNA surveillance target via SKIV2l2, experiments proved that SKIV2L2 depletion prevents histone mRNA turnover and that SKIV2L2 directly binds histone mRNAs. Because replication-dependent histone mRNAs immunoprecipitated with SKIV2L2 at high levels, these results conclusively demonstrate SKIV2L2 directly binds to histone mRNAs in vivo. Coupled with the doubling of H4 mRNA half-life following SKIV2L2 depletion, we conclude that SKIV2L2 directly aids in the turnover of replication-dependent histone mRNAs.

Sequencing data established that the majority of replication-dependent histone mRNAs accumulated with SKIV2L2 depletion, while the loss of nuclear RNA surveillance triggered downregulation of certain non-canonical histone mRNAs. Identification of the human NEXT complex demonstrated that two histone proteins, H2Bn and H2A.X, co-immunoprecipitated with human SKIV2L2 (Lubas, 2011). Looking at the corresponding mRNAs in mouse P19 cells, SKIV2L2 depletion led to the accumulation of Hist1h2bn mRNA and the downregulation of H2Afx mRNA. Additionally, *Skiv2l2* knockdown increased H4 protein levels, suggesting that SKIV2L2's role in histone mRNA turnover affects histone protein abundance. While not

definitive, micrococcal nuclease assays suggest that this increase in histone protein with SKIV2L2 depletion may negatively impact chromatin compaction. These findings allude to a possible role for SKIV2L2 in regulating histone levels that includes physical association with both histone mRNAs and proteins.

While results implicated SKIV2L2 in histone mRNA turnover, experiments could not definitively confirm the role of the TRAMP complex in this process. PAPD5 depletion led to a slight but significant increase in H4 mRNA. However, it is unclear whether the accumulation is due to the loss of PAPD5 or reduced SKIV2L2 protein levels, which were discussed previously. Even though the TRAMP complex was not proven to participate in histone mRNA turnover, the NEXT complex is not essential to the process, seeing as ZCCHC8 depletion had no effect on histone mRNA levels. This result agrees with experiments that demonstrate no change in histone mRNA levels with knockdown of the NEXT complex component Rbm7 (Mullen, 2008) but conflicts with reports that Rbm7 binds 3' extended histone mRNAs (Lubas, 2015). This hints at the possibility of a more complicated model for nuclear histone mRNA turnover, which may include different turnover pathways for both mature and aberrant transcripts. Previous experiments show that PAPD5 is dispensable for TRAMP complex function on certain RNA targets (Rammelt, 2011; Beaulieu, 2012), which could explain why loss of PAPD5 does not have a large effect on histone mRNA levels. Alternatively, the helicase SKIV2L2 could function independently to remove the 3' stem loop and proteins like SLBP that are bound to the stem loop. Indeed, other RNAs with highly structured 3' end require helicases to aid in turnover via the nuclear exosome (Schilders, 2007; Dominski, 2003).

In yeast, the TRAMP complex regulates the turnover and 3' end processing of the signal recognition particle RNA (SRP RNA) scR1 (Leung, 2014). SRP RNA is highly structured, and the protein La family protein, Lhp1, protects the mature 3'end from degradation and further processing. TRAMP degrades a subset of SRP RNA, but Lhp1 overexpression prevents this turnover, suggesting that TRAMP and Lhp1 compete for the 3' end of SRP RNA. Histone mRNAs could be turned over in a similar manner (Leung, 2014). SLBP binds to and protects the 3' end of histone mRNAs (Zhang, 2012). At the end of S-phase, SLBP is degraded through proteolysis (Koseoglu, 2008). In competition for the binding of the 3' end of histone mRNAs, SKIV2L2 might outcompete SLBP for histone mRNAs at the end of S phase, leading to mRNA turnover.

Overall, there is substantial evidence that SKIV2l2 aids in the turnover of replication-dependent histone mRNAs. Because all localization studies have documented SKIV2L2's location as nuclear and nucleolar (Osman, 2011; Lubas, 2011), this represents the first reported instance of nuclear histone mRNA turnover. Previous research has implicated Rrp6 and PAPD5 in mammalian histone mRNA turnover (Mullen, 2008), but these results were either assumed to occur in the cytoplasm or dismissed. By confirming that SKIV2L2 is necessary for histone mRNA turnover, a new model for nuclear histone mRNA turnover has emerged, one that includes Rrp6, SKIV2L2, and possibly PAPD5. We hypothesize that SKIV2L2 binds to histone mRNAs, displaces SLBP and other stem-loop binding proteins, unwinds the stem-loop, and feeds the histone mRNA into the nuclear exosome. This could occur as histone mRNAs are being transcribed at the end of S phase to quickly degrade histone mRNAs in the nucleus, while cytoplasmic histone mRNAs are uridylated and degraded (Kaygun, 2005ab,

Kaygun, 2006; Mullen, 2008). This model and its influence on cell cycle progression will be discussed in depth in the next chapter.

CHAPTER VII: FINAL CONCLUSIONS

In this dissertation, it was reported that SKIV2L2 is necessary to enhance proliferation and prevent differentiation in two murine cell lines. SKIV2L2 depletion in proliferative cells led to mitotic arrest, but it is unclear whether this phenotype is attributed to SKIV2L2 working independently or its function in the TRAMP complex. Given that SKIV2L2 targets RNAs for processing and turnover via the nuclear exosome, it was hypothesized that loss of SKIV2L2 leads to the accumulation of aberrant RNAs that trigger mitotic arrest. RNA-seq identified multiple RNAs targeted by SKIV2L2 for processing and degradation, including non-coding RNAs, intergenic RNAs, ribosomal protein mRNAs, and replication-dependent histone mRNAs. While the accumulation of many of these target RNAs could be responsible for the observed mitotic arrest with SKIV2L2 depletion, replication-dependent histone mRNAs were probed in further detail. It was found that SKIV2L2 directly binds histone mRNAs and that SKIV2L2 depletion doubles histone mRNA half-life. Together, this identified replication-dependent histone mRNAs as a definitive target of SKIV2L2-mediated RNA surveillance. Accumulation of histone mRNA and protein can hinder cell cycle progression, making histone mRNAs a viable SKIV2L2 target RNA capable of causing the mitotic arrest observed with SKIV2L2 depletion.

7.1 SKIV2L2 and its role in differentiation and proliferation

The experiments presented in this dissertation highlighted the phenotype associated with SKIV2L2 depletion. Following *Skiv2l2* knockdown via RNAi, cell proliferation slowed, pluripotency genes were downregulated, and differentiation genes

were upregulated. This phenotype occurred in both P19 and N2a cells, resulting in differentiation into both cardiac muscle and neurons. Neither knockdown of the TRAMP complex component PAPD5 nor the NEXT complex component ZCCHC8 could perfectly replicate the phenotype associated with SKIV2L2 depletion. This finding suggests that SKIV2L2 maintains cell proliferation and prevents differentiation through the turnover and processing of multiple RNA targets, either independently, in concert with the NEXT and TRAMP complexes, or a combination of these instances.

Because SKIV2L2 depletion led to decreased proliferation and increased differentiation, the cell cycle was examined to pinpoint a specific defect in cell growth or division. Increased cell death and apoptosis were not observed with SKIV2L2 depletion, which correlated well with the upregulation of anti-apoptotic genes according to the RNA-seq data. Usually, exit from the cell cycle at G1 precedes differentiation, which was visualized as G1 arrest in chemically differentiated N2a cells. Surprisingly, *Skiv2l2* knockdown reduced the percentage of cells in G1 phase. Instead, SKIV2L2 depletion triggered an accumulation of G2/M phase cells, mitotic arrest, and binucleation. A previous RNAi screen in HeLa cells corroborated this finding. *Skiv2l2* knockdown cells were reported as being binucleated, with no delay in the onset of mitosis (Neumann, 2010). Consistent with both datasets is a model where SKIV2L2 depletion primarily affects later stages of mitosis and cytokinesis, such as chromosome segregation, as opposed to regulating the timing of mitosis itself.

Interestingly, the study that identified the NEXT complex in humans lends insight into the role of SKIV2L2 in mitotic progression. Multiple proteins involved with proliferation and mitosis co-immunoprecipitate with SKIV2L2. SKIV2l2 associates with

the spliceosome and splicing factors for an unknown function (Lubas, 2011), and some of these splicing factors are necessary for mitotic progression. For example, ERH is required for proper splicing of the mRNA for the CENP-E gene, which encodes the kinesin motor protein localized to centromeres during mitotic chromosome segregation (Weng, 2013). In addition to ERH, the RNA processing gene Dhx9 also associates with SKIV2L2 (Lubas, 2011). The helicase Dhx9 functions in complex with other proteins to protect Myc mRNA from cytoplasmic decay (Weidensdorfer, 2009), and loss of Dhx9 triggers premature cellular senescence through p53 (Lee, 2014). In immortalized cancer cells like P19 and N2a, senescence leads to differentiation, hinting that the differentiation observed with SKIV2L2 depletion may be similar to the senescence associated with Dhx9 depletion and destabilization of Myc.

Also similar to Dhx9, SKIV2L2 is connected to the transcription factor Myc, which regulates multiple genes involved in cell growth, proliferation, and differentiation (Hirsch, 2015). In many cancers, Myc is constitutively activated, leading to constant upregulation of the cyclin genes and enhanced cell cycle progression (Mateyak, 1999). Myc is necessary to reprogram mouse embryonic fibroblasts into induced pluripotent stem cells (Takanashi, 2006). This reprogramming depends on Myc, in complex with SAGA, upregulating cell cycle and RNA processing genes (Hirsch, 2015). Interestingly, the Myc-SAGA complex binds to and activates *Skiv2l2* transcription during this reprogramming (Hirsch, 2015), further implicating SKIV2L2 as a factor necessary for stem cell formation and/or maintenance. The SAGA complex and Myc both are downregulated with differentiation through growth signaling (Hirsch, 2015), which could

account for the downregulation of *Skiv2l2* following chemically induced differentiation in P19 and N2a cells.

The downregulation of *Skiv2l2* during differentiation further cements the role for SKIV2L2 in maintaining stem cell proliferation and pluripotency but also raises questions about nuclear RNA surveillance in differentiated cells. RNA-seq studies have demonstrated the developmental downregulation of *Skiv2l2* as well (Cinghu, 2014), but the Human Protein Atlas documents medium to high SKIV2L2 expression levels in all human tissues, cell lines, and cancer cells (Uhlen, 2010). In zebrafish, *Skiv2l2* mutations are embryonic lethal, presumably due to underdevelopment in the brain and immune system (Yang, 2007; Hultman, 2010; Iwanami, 2009). This suggests that high levels of SKIV2L2 are necessary for development, and differentiated cells may require lower levels of nuclear RNA surveillance. It is unclear whether *Skiv2l2* is upregulated following differentiation or if differentiated cells function with less SKIV2L2 than stem cells despite how nuclear RNA surveillance is thought to be essential to cell health.

However, the experiments in this dissertation definitively link SKIV2L2 to proliferation in mouse cell lines. The increase in mitotic cells following SKIV2L2 depletion suggests that differentiation aberrantly occurs through a mechanism distinct from developmental or chemically-induced differentiation, particularly through mitotic slippage, followed by failed cytokinesis and the senescence and differentiation of binuclear 4N cells. Even though p53 does not regulate the spindle assembly checkpoint, p53-mediated apoptosis is activated when cells arrest in mitosis for prolonged periods of time (Orth, 2012). Without p53, these cells often undergo mitotic slippage and failed cytokinesis (Orth, 2012; Rieder, 2004). Because N2a and P19 cells lack p53, SKIV2L2

depletion results in mitotic arrest, binucleation following mitotic slippage, and possibly cellular senescence and differentiation. This phenotype could be unique to cancer cell lines, so further research must be conducted in primary cells, embryonic stem cells, and iPSCs to see how SKIV2L2 depletion affects proliferation when apoptotic pathways are intact.

7.2 SKIV2L2 mediates the turnover and processing of multiple classes of RNAs

Understanding how SKIV2L2 functions in both nuclear RNA surveillance and stem cell maintenance requires identifying SKIV2L2 target RNAs. Expanding on previous research, this dissertation presented a pipeline for identifying and verifying SKIV2L2 target RNAs. First, RNA-seq identifies RNAs accumulating in *Skiv2l2* knockdown cells, representing putative target RNAs. Then, this accumulation is verified through qRT-PCR, which can also be used to detect poly-A-tails through oligo-dT priming in certain cases. Next, RNA immunoprecipitation demonstrates SKIV2L2 binding to target RNAs. Performing qRT-PCR after RIP can monitor binding of individual putative target RNAs, while RIP followed by RNA-seq can be used to generate a list of all RNAs bound to SKIV2L2. Those RNAs found to both accumulate with SKIV2L2 depletion and bind to SKIV2L2 represent target RNAs. Finally, if the half-life of a particular target RNA increases with SKIV2L2 depletion and Dactinomycin treatment, then that RNA is a validated SKIV2L2 target whose turnover depends on SKIV2L2-mediated RNA surveillance. This pipeline can also be applied to PAPD5 and ZCCHC8 target RNAs to distinguish between TRAMP and NEXT complex targets.

Target RNAs identified through RNA-seq included lncRNAs, snoRNAs, intergenic RNAs, ribosomal protein mRNAs, and replication-dependent histone mRNAs. Of these, only replication-dependent histone mRNAs represent validated SKIV2L2 target RNAs based on the experiments presented in this dissertation. However, other studies have established that SKIV2L2 mediates lncRNA (Beaulieu, 2012), PROMPT (Tiedje, 2014), and snoRNA (Berndt, 2012; Lubas, 2015) processing and turnover. In the future, this pipeline can be used to validate unique SKIV2L2 target RNAs, such as ribosomal protein mRNAs and small RNAs arising from processed pseudogenes. Importantly, RNA-seq did highlight a previously established trend that links SKIV2L2 to the processing of spliced transcripts, such as snoRNAs and lncRNAs, and identify a novel role for SKIV2L2 in the turnover of two protein-coding RNAs: ribosomal protein mRNAs and replication-dependent histone mRNAs. While previous research attributed histone turnover to cytoplasmic NMD, this research has discovered a nuclear RNA surveillance pathway for histone mRNAs via the nuclear localized SKIV2L2 (Uhlen, 2010; Osman, 2011).

7.3 The accumulation and misprocessing of SKIV2L2 target RNAs may trigger mitotic arrest

Because SKIV2L2 depletion triggers mitotic arrest and leads to the accumulation of target RNAs, it reasons that one or a few of these targets RNAs cause the observed mitotic arrest. Intergenic RNAs, lncRNAs, snoRNAs, ribosomal protein mRNAs, and replication-dependent histone mRNAs all could contribute to slowed proliferation, and the accumulation of one or multiple RNAs could trigger mitotic arrest following SKIV2L2 depletion. In particular, spurious transcription from intergenic regions,

dysregulation of ribosome biogenesis, and increased free histone levels could lead to mitotic arrest in *Skiv2l2* knockdown cells (Fig 7.1).

The TRAMP complex is located in the nucleolus (Lubas, 2011), where ribosome biogenesis occurs, so it is not surprising that SKIV2L2 and the TRAMP complex are linked to ribosome biogenesis. Ribosome biogenesis requires rDNA transcription by RNA pol I and rRNA processing directed by snoRNAs and cofactors. Ribosomal proteins are imported into the nucleolus where the ribosome is assembled before export to the cytoplasm (Boisvert, 2007). Previous research demonstrated that SKIV2L2 mediates the processing of ribosomal RNA (Schilders, 2007; Lubas, 2015). Additionally, SKIV2L2 physically interacts with 61 out of 79 ribosomal proteins (Lubas, 2011). This dissertation presents a novel connection between SKIV2L2 and ribosome biogenesis. Ribosomal protein mRNAs were dysregulated with SKIV2L2 depletion. A substantial number of ribosomal protein mRNAs accumulate in *Skiv2l2* knockdown cells, while a few are downregulated. Given that SKIV2L2 mediates the processing of rRNA, promotes the turnover of ribosomal protein mRNAs, and associates with ribosomal proteins, SKIV2L2 plays an important role in ribosome biogenesis.

The ribosome is tightly linked to cell cycle control. As the cell grows, more ribosomes are assembled in the nucleolus to support increased translation. Before the cell can divide, it must double its number of ribosomes so that both daughter cells receive a sufficient number of ribosomes. (Boisvert, 2007) Proliferating cells require increased levels of rRNA transcription, and high levels of ribosomes prevent differentiation (Zhang, 2014). Therefore, ribosome biogenesis regulates the timing and progression of the cell cycle. For example, impaired ribosome biogenesis often triggers G1-S phase

arrest and apoptosis (Donati, 2012). In addition, the expression of certain ribosomal proteins like human L13a causes G2/M phase arrest and apoptosis (Chen, 1999). The transcription factor Myc serves as a master regulator of ribosome biogenesis and controls the transcription of multiple genes involved with the each step of ribosome biogenesis (van Riggelen, 2010), including *Skiv2l2* (Hirsch, 2015). In addition to SKIV2L2's function in rRNA processing and ribosomal protein mRNA turnover, the fact that Myc coordinates *Skiv2l2* expression and ribosome biogenesis may indicate that nuclear RNA surveillance plays a central role in regulating ribosome biogenesis. With SKIV2L2 depletion, ribosome biogenesis may be impaired, leading to cell cycle arrest, reduced proliferation, and ultimately differentiation. In support of this, replicative stress in stem cells leads to *Skiv2l2* downregulation, slowed rRNA processing, and cellular senescence (Nishimura, 2015).

While impaired ribosome biogenesis could trigger cell cycle arrest and differentiation, spurious transcription and excess histones also could account for the proliferation defects seen in *Skiv2l2* knockdown cells. Although not definitive in its conclusion, micrococcal nuclease digestion of chromatin following SKIV2L2 depletion suggests a defect in chromatin compaction may be responsible for the observed mitotic arrest. At the onset of mitosis, chromatin condenses, preventing certain transcription factors and RNA polymerase II from accessing the DNA (Chen, 2004). Proper spindle assembly and chromosome segregation requires transcriptional activation and silencing at proper regions (Chan, 2012; Pastor, 2016). Chromatin modifiers and transcription factors that can access the condensed chromatin silence the majority of the genome (Chen, 2004). Small areas of the genome are activated, particular genes necessary for mitosis,

such as cyclin-B1 (Sciortino, 2010) and small RNAs transcribed from the centromere to promote spindle attachment and activate the mitotic Aurora kinases (Chan, 2012). However, the majority of the genome is transcriptionally silenced. Spurious transcription from intergenic regions could either be responsible for or symptomatic of a more open chromatin environment. With SKIV2L2 depletion, small RNAs arising from intergenic regions accumulate. These intergenic RNAs, which include PROMPTs and processed pseudogenes, are transcribed from various regions on each chromosome, eliminating the possibility that these are RNAs at the centromere to promote mitosis. If spurious transcription occurs at these regions during mitosis, it could negatively impact spindle attachment and chromosome segregation. Analysis hints that a subset of the small RNAs transcribed from processed pseudogenes may be piRNAs, which play a role in transcriptional silencing and chromatin condensation during mitosis (Pek, 2011). SKIV2L2-mediated RNA surveillance may function in the turnover and transcriptional silencing of RNAs transcribed from intergenic regions, thereby promoting chromatin condensation and mitosis.

It is also probable that defects in chromatin condensation are result of histone imbalance. Replication-dependent histone mRNAs are a direct SKIV2L2 target whose accumulation could impair chromatin condensation and induce mitotic arrest. SKIV2L2 depletion leads to both an accumulation in histone mRNAs and at least one histone protein, H4. Cell cycle progression is sensitive to the level of histones in the cell, with both histone depletion and accumulation triggering cell cycle arrest in G2 or M phase (Günesdogan, 2014; Sullivan, 2001; Groth, 2005). In both cases, the cell cycle arrest is attributed to defects in chromatin compaction during mitosis, which leads to impaired

spindle assembly, improper chromosome segregation, non-disjunction, and DNA damage (Meeks-Wagner, 1986; Sullivan, 2001). In the case of excess histones, the positively-charged free histones inappropriately bind to negatively-charged DNA and RNA (Singh, 2010), which impairs proper chromatin compaction and leads to mitotic arrest (Meeks-Wagner, 1986). Additionally, excess histones titrate chromatin modifiers away from the chromatin (Singh, 2010). Without certain histone marks, the chromatin cannot condense during mitosis. For example, SIRT6 must deacetylate H3K18 to silence pericentric heterochromatin containing repetitive DNA (Pastor, 2016). In fact, histone deacetylase inhibitors replicate the phenotype seen with SKIV2L2 depletion: defects in chromatin condensation trigger mitotic arrest, mitotic slippage, and binucleation (Stevens, 2007).

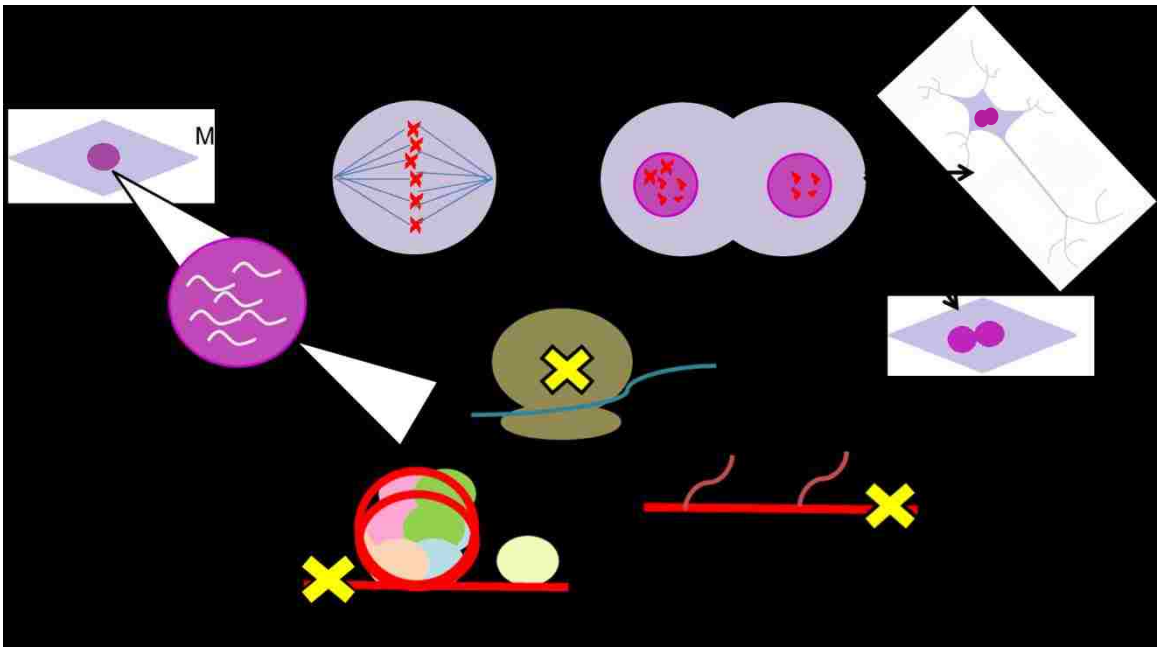

Fig 7.1: Hypothetical model for mitotic arrest phenotype observed with loss of SKIV2L2. Treatment with *Skiv2l2* siRNA in mouse cell lines results in an observable phenotype that includes increased differentiation, mitotic arrest, and binucleation. At a molecular level, loss of SKIV2L2 inhibits nuclear RNA turnover, leading to impaired ribosome biogenesis, spurious transcription from intergenic regions, and histone accumulation.

Given that excess free histones are known to cause mitotic arrest, it is hypothesized that SKIV2L2 promotes mitotic progression by degrading replication-dependent histone mRNAs in the nucleus at the end of G2. The turnover of these mRNAs would ensure that excess free histones do not interfere with chromatin condensation during mitosis.

7.4 Summary and significance of findings

This dissertation characterized the phenotype associated with the loss of SKIV2L2-mediated RNA surveillance, establishing a connection between RNA surveillance and cell cycle progression. With SKIV2L2 depletion triggering mitotic arrest and differentiation in two cell lines, it appears that SKIV2L2 is necessary for maintaining proliferation and pluripotency. While the exact function of SKIV2L2 in the cell cycle is unclear, an imbalance of SKIV2L2 target RNAs could be responsible for the defects in mitotic progression following SKIV2L2 depletion. Loss of SKIV2L2 prevents histone mRNAs from being efficiently degraded, and the presence of excess histone transcripts as the cell enters G2 phase could activate the spindle assembly checkpoint and trigger mitotic arrest. Alternatively, because SKIV2L2 facilitates the processing of mammalian pre-rRNAs and ribosomal protein mRNA turnover, SKIV2L2 may enhance the efficiency of rRNA processing and ribosome assembly, which are necessary to maintain cell proliferation in actively dividing cells. Experiments also implicated SKIV2L2-mediated RNA surveillance in snoRNA and miRNA biogenesis, lncRNA turnover, and degradation of transcripts arising from intergenic regions. Verifying and exploring these RNA surveillance targets will drive forward a better understanding of how RNA surveillance can influence RNA transcription and non-coding RNA biogenesis pathways on a more

global scale and lead to greater insight on the regulation of mammalian gene expression. The interconnectedness of SKIV2L2, RNA surveillance, and the cell cycle may lead to a greater understanding of SKIV2L2-associated diseases and stem cells.

CHAPTER VIII: MATERIALS AND METHODS

8.1 Cell culture

Neuro2A (N2a) cells were grown at 37°C in Dulbecco's Modified Eagle Medium (Sigma Aldrich #D6429) supplemented with 10% fetal bovine serum (FBS, Sigma Aldrich #12306C). Cells were plated on Greiner Bio-One Advanced TC™ 35 or 60 mm plates. The cells were split at 1:5 or 1:10 every 48 hours, and incubator conditions were held at 5% CO2 and 95% humidity. N2a cell differentiation was initiated by plating the cells in Dulbecco's Modified Eagle Medium supplemented with 2% FBS and 20μM all-trans retinoic acid (Sigma Aldrich #R2625). Cells were harvested after 48 hours by simple pipetting.

P19 cells were cultured in α-MEM growth medium (Sigma Aldrich # M8042) supplemented with 10% FBS (Sigma Aldrich #12306C). P19 cells were passaged every 48 hours at 1:5 or 1:10 and grown under incubator conditions of 37°C, 5% CO2, and 95% humidity. P19 cells were differentiated using α-MEM growth medium supplemented with 10% FBS and 0.1% dimethyl sulfoxide (Sigma Aldrich #D2438). Cells were harvested after 48 hours by simple pipetting.

8.2 Kinase inhibitor treatment

N2a and P19 cells were treated with various kinase inhibitors. Drugs were purchased from Cayman Chemical and dissolved in DMSO. Three replicate P60 plates were treated with each drug according to the concentrations listed in Table 2.1, with three

plates treated with 40 μL of DMSO as a vehicle control. Three hours after treatment, cells were harvested by simple pipetting for isolation of RNA and protein.

8.3 RNAi

Before RNAi knockdown, $3x10^5$ N2a cells or P19 cells were plated on 35 mm Advanced TC™ plates. When cells were at approximately 60% confluency (around 24 hours after plating), cells were transfected with the appropriate siRNA. *Skiv2l2* knockdowns were performed by transfecting cells with either 67 nM *Skiv2l2* Silencer® siRNA ID #177475 (ThermoFisher # AM16704/s90745), 3 nM PAPD5 Silencer Select® siRNA ID s103146, 67 nM ZCCHC8 Silencer® siRNA ID #163169, or 67 nM Negative Control Silencer® No. 1 siRNA by Ambion™ (ThermoFisher #AM4635). Knockdown was performed on five plates per siRNA. Delivery of siRNAs was accomplished with 1 mL of Opti-MEM (Thermo Fisher #31985) and 0.1% Lipofectamine RNAiMax® by invitrogen™ (ThermoFisher #13778) for N2a cells or 0.1% Lipofectamine 3000® by invitrogen™ (ThermoFisher #L300008) for P19 cells according to manufacturer's protocol. Cells treated with the siRNAs were grown for 48 hours at 37°C, 5% CO2, and 95% humidity. The cells were then harvested following RNAi using simple pipetting.

8.4 Neuronal Processes Quantification

Following RNAi, N2a cells were viewed under a simple compound microscope at 40x magnification. Random fields were selected on the plate, and the number of cells was counted in each field until 1000 cells were counted. In each field, individual cells that extended processes longer than twice the diameter of the cell body were counted as

differentiated. The number of cells extending processes longer than twice the diameter of the cell body was divided by the total number of cells to calculate the percent differentiated for each siRNA treatment. N2a cells were also counted in the same manner following treatment with the Neural Outgrowth Staining kit (Thermo Fisher # A15001) according to manufacturer's protocol. Cells were viewed on the Leica DMI6000 B inverted microscope with excitation at 495 nM and 555 nM for visualization of the cell viability stain (green) and the cell membrane stain (orange). Random fields were again selected, and 900 cells were scored for each siRNA treatment. Cells staining red only were counted as dead. Cells staining both orange and green (yellow overlay) with processes extending longer than twice the diameter of the cell body were counted as differentiated. The numbers of dead and differentiated cells were then divided by the total number of cells counted to obtain the percentage of dead and differentiated cells. Population statistics were calculated using the two proportion z-score. As the z-score becomes more negative, the probability of observing a smaller difference between the two proportions becomes less.

8.5 Protein Extraction

Harvested N2a and P19 cells were lysed on ice for 15 minutes with protein lysis buffer containing 1% Triton-X, 150mM sodium chloride, 50 mM Tris-HCl pH 8, and cOmplete™ EDTA-free proteinase inhibitor tablet (04693132001 Roche). Cells were then spun down at 16,000g at 4°C for 15 minutes, and the supernatant containing the protein was collected. Bradford Assays were performed to quantify total protein using

Bradford Reagent (Sigma Aldrich #B6916). Histone proteins were isolated by incubating the nuclear pellet with 0.2N HCl overnight at 4°C.

8.6 RNA Isolation

Cells were lysed in 1 mL TRI Reagent® (Sigma Aldrich #T9424) by pipetting up and down and incubating at 21°C for 5 minutes. 200 μL of chloroform was added to the lysed cell mixture, and the organic and aqueous phases were separated through centrifugation at 12,000 g at 4°C for 10 minutes. The aqueous phase was collected, added to 500μL isopropanol, and incubated at 21°C for 20 minutes. The mixture was then spun down at 12,000 g at 4°C for 20 minutes to pellet the RNA. The supernatant was poured off, and the pellet was washed twice in 75% ethanol in DEPC-treated water. The RNA pellet was resuspended in 20 μL DEPC-treated water and quantified using the NanoDrop 2000 instrument (Thermo Scientific) for RNA-40 values. The RNA was then DNase treated according to the TURBO DNA-free™ kit protocol (Ambion #AM1907) and re-quantified using the NanoDrop 2000. RNA isolated from P19 cells for sequencing was tested for RNA integrity using the RNA 6000 Nano Kit (Agilent #5067-1511) on the Agilent 2100 Bioanalyzer according to the manufacturer's protocol.

8.7 Western Blotting

Western blots were performed on the protein extracts from N2a and P19 cells to quantify SKIV2L2, ActB, Rrp6, H4, and H3 phospho-S10 protein levels. Laemmli buffer was added to total protein extracts, and the proteins were then run at 100V on a 10% acrylamide (37.5:1) SDS-PAGE gel. Proteins were then transferred onto BioTrace™

nitrocellulose membrane, 0.2 μm pore size (Pall Corporation #66485) at 4°C and 15V for 12 hours. The nitrocellulose membrane was blocked in 5% milk in PBS pH 7.5 with 0.1% NP-40 for one hour at 21°C. Following three 10 minute washes in PBS, 0.1% NP-40, the membrane was incubated in blotting milk containing polyclonal antibodies raised in rabbit against mouse SKIV2L2 (1:1000 dilution, Abcam® ab187884), beta-actin (1:50 dilution, Thermo Fisher #PA5-16914), Histone H4 (1:500 dilution, Bethyl Laboratories, Inc. Catalog #A300-646A-T), or H3 phospho-S10 (1:500 dilution, Abcam® ab5176). The Rrp6 antibody produced by the Anderson laboratory was used at a dilution of 1:500. Primary antibody incubation occurred for 16 hours at 4°C and was followed by three washes in PBS, 0.1% NP-40. The secondary antibody, goat anti-rabbit conjugated to horseradish peroxidase (1:5,000 dilution, Abcam® ab6721) was applied to the membrane in blotting milk for 1 hour at 21°C. Protein was detected using luminol, ρ-coumaric acid, and hydrogen peroxide and capturing chemiluminescence with the UVP Biospectrum System. SKIV2L2, Rrp6, H4, and H3 phospho-S10 protein levels were quantified by normalizing to ACTB and control levels using the ImageJ software provided by the NIH. Statistics were calculated using the student's t-test.

8.8 Quantitative RT-PCR

DNAse-treated RNA isolated from N2a and P19 cells was reversed transcribed using oligo-dT or gene-specific primers (primers listed in Table 8.1) according to M-MLV reverse transcriptase protocol (Promega #M1705). PCR cleanup (IBI Scientific, VWR #95039) was then carried out according to manufacturer's protocol, and the cDNA samples were diluted with DEPC-treated water by a factor of 10. Targets (primers listed

in Table 8.1) were amplified from the reverse transcription reactions using 12.5 μL of iQ SYBR® Green Supermix (BioRad #1708880) per 10 μL of target cDNA. Primers were added to a concentration of 60nM. Amplification was detected using the CFX Connect™ Real-Time PCR detection system, with annealing temperatures ranging from 52-58°C depending on primer melting temperature. Cycles 1-35 were analyzed using regression threshold analysis for samples with no amplification in control reactions without reverse transcriptase. Target expression was calculated using CFX Manager™ Software, where expression equals 2^(–(Cqtarget-CqActB)) with targets normalized to beta-actin and control treatment. Statistics were calculated using the student's t-test.

Target	Primer	Application
polyadenylated mRNAs	TTTTTTTTTTTTTTTTTTTT	oligo dT RT primer
ActB	TGAAGTGTGACGTTGACATCCG	forward qPCR primer
ActB	GTACTCCTGCTTGCTGATCCAC	reverse qPCR primer
ActB	GTA AAA CGC AGC TCA GTA ACA GTC CG	RT primer
H2An	GTGCTGGAGTACCTGACGG	forward qPCR primer
H2An	CTTGTTGAGCTCCTCGTCG	reverse qPCR primer, RT
Hist1h4d	CAAAGTTCTGCGCGACAAC	forward qPCR primer
Hist1h4d	AGGAACACCTTCAGCACAC	reverse qPCR primer
Hist1h4d	CCAAGCGCAAGACCGTC	RT primer
Hist1h3a	GTGCTCACCAGCTTGCTTTC	forward qPCR primer
Hist1h3a	CTTTGGTGGCTAGCTGCTTG	reverse qPCR primer
Hist1h3a	AGAGCCTTTGGTTAATTCCG	RT primer
Hist1h1b	CAAGAGTCTGGTGAGCAAGG	forward qPCR primer
Hist1h1b	GTTAAGCTTGAAGGAACCAGAG	reverse qPCR primer, RT
Nestin	TGAGAACTCTCGCTTGCAGACAC	forward qPCR primer
Nestin	GGTATCCCAAGGAAATGCAGC	reverse qPCR primer
ChAT	GAGCCACCTGAGATGTTCATG	forward qPCR primer
ChAT	CAGCAGAACATCTCCATGGTC	reverse qPCR primer
MAP2	GCTCACTTGACAATGCTCACCACG	forward qPCR primer
MAP2	GGGCCTTTGCATGCTCTCTGAAG	reverse qPCR primer
Fabp3	ACTCATCCATGTGCAGAAGTG	forward qPCR primer

Fabp3	CCTTCTCATAAGTCCGAGTGC	reverse qPCR primer
Desmin	GGGTTCTGAAGTCCATAC	forward qPCR primer
Desmin	CACTGAATTCCTGGCTTAC	reverse qPCR primer
GATA4	GCTGTCATCTCACTATGGGC	forward qPCR primer
GATA4	GGAGATGCATAGCCTTGTGG	reverse qPCR primer
Pax7	ACTGGCTACAGTGTGGACCCTG	forward qPCR primer
Pax7	CTTCATACGGCGCTGTGTGG	reverse qPCR primer
Sox2	CATGGGCTCTGTGGTCAAGTCC	forward qPCR primer
Sox2	TGCTGATCATGTCCCGGAGGTC	reverse qPCR primer
Tubb3	ACACCTATTCAGGCCCGACAAC	forward qPCR primer
Tubb3	CCGCACGACATCTAGGACTGAG	reverse qPCR primer
Skiv2l2	CAGTTGAAGGCTGCACACAT	forward qPCR primer
Skiv2l2	CACTGAATGGCTTCTCTTTGG	reverse qPCR primer
Nkx2.5	GACAGGTACGGCTGTTGCTT	forward qPCR primer
Nkx2.5	AGCCTACGGTGACCCTGAC	reverse qPCR primer
Nanog	AAAGGATGAAGTGCAAGCG	forward qPCR primer
Nanog	GGATGCTGGGATACTCCACT	reverse qPCR primer

Table 8.1: List of primers used in study. Annealing temperature was Tm−5°C for each qPCR primer and 42°C for each RT primer.

8.9 MTT Assay

Immediately following transfection of N2a or P19 cells with negative control siRNA or *Skiv2l2* siRNA, cells were harvested and transferred to a 96- well plate. 100 μL of cells were added to each well, and cells were grown at 37°C, 5% CO2, and 95% humidity. Thiazolyl blue tetrazolium bromide (MTT, Sigma Aldrich #M5655) was dissolved in 1X PBS to a concentration of 5 mg/mL and filtered through a .2 μm filter. 10 μL of 5 mg/mL MTT was added to each well at various time points, and the cells were incubated at 37°C for three hours. Media was removed, and cells were resuspended in 100 μL of isopropanol:DMSO. Absorbance of the suspension was measured at 570 nm (absorbance of purple formazan) and 630 nm (background protein absorbance) using a

spectrophotometer. 100 μL of isopropanol:DMSO was used as a negative control. Formazan absorbance was calculated by subtracting the absorbance at 630 nm from the absorbance at 570 nm for 10 wells per time point. Formazan absorbance was then used to calculate cell proliferation by dividing any given formazan absorbance by the initial formazan absorbance at the time of transfection.

8.10 Fluorescent Activated Cell Sorting

Following RNAi, knockdown cells were harvested and washed in PBS supplemented with 2% FBS and resuspended in 1 mL of PBS. For viability staining, cells were then incubated with 1 U RNaseA for 1 hour at 37° C. 100 μL of 1 mg/mL propidium iodide (Thermo Fisher # P3566) was added to the cells 20 minutes before cell sorting on the BD Accuri™ C6 cell sorter. Cells were excited with the 488 nm blue laser, and the filter was set to FL-2 to detect propidium iodide fluorescence. 50,000 cells were sorted for each sample on slow fluidics, debris and clumps were gated out, and the percentage of stained cells was calculated using the CFlow® Plus software.

For cell cycle analysis, cells were fixed in ice cold ethanol for 30 minutes, washed twice in PBS, and re-suspended in 1mL PBS. The fixed cells were then incubated with 1 U RNaseA for 1 hour at 37° C. 100 μL of 1 mg/mL propidium iodide (Thermo Fisher # P3566) was added to the fixed cells 20 minutes before cell sorting on the BD Accuri™ C6 cell sorter as stated above. The percentage of stained cells in G1, S, and G2/M phase was calculated using the CFlow® Plus software based on FL-2 detection (DNA content) and cell count.

For H3 phospho-S10 detection, fixed cells were incubated with the primary antibody against H3 phospho-S10 (1:1000 dilution, Abcam® ab5176) for 1 hour at 21°C. Cells were washed twice in PBS, 0.1% NP-40, pH 7.5 before incubation with the secondary antibody anti-rabbit conjugated to AlexaFluor® 488 (1:500 dilution, Thermo Fisher #A-11034) and 1 U RNaseA for 30 minutes at 37°C. Cells were then washed in PBS and treated with 100 µL of 1 mg/mL propidium iodide before analysis on the BD Accuri™ C6 cell sorter as stated above, with excitation at 488nm and detection using the FL-1 filter. The percentage of cells fluorescing was normalized to negative controls with primary antibody only and secondary antibody only, with the percentage of cells fluorescing calculated by the CFlow® Plus software.

8.11 Immunofluorescence Cell Imaging

Following RNAi treatment, harvested cells were washed in PBS, 2% FBS and fixed for 30 minutes in ice-cold ethanol. After washing in PBS, 0.1% NP-40, pH 7.5, cells were blocked for 60 minutes at 21°C in PBS, 2% FBS. Cells were then incubated with the primary antibody against H3 phospho-S10 (1:500 dilution, Abcam® ab5176), Rrp6 (1:100 dilution), or SKIV2L2 (1:100 dilution, ab187884) for 14 hours at 4°C. Cells were again washed before incubation with the secondary antibody anti-rabbit conjugated to AlexaFluor® 488 (1:500 dilution, Thermo Fisher #A-11034) for two hours at 21°C. Cells were washed and resuspended in 100 µL PBS and 100 µL of propidium iodide before viewing 100 µL of cells on slides. Cells were excited at 488nm and brightfield images, FL-1 filtered images, and FL-3 filtered images were captured on the Nikon Eclipse E600 microscope. For H3 phospho-S10 staining, one hundred cells per sample

were scored based on fluorescence intensity, with three biological replicates. For SKIV2L2 and Rrp6 staining, images were captured to detect protein localization relative to propidium iodide staining of nuclei.

8.12 RNA-seq

RNA was harvested from P19 cells as previously described on three biological replicates of control siRNA and *Skiv2l2* siRNA treated cells. Paired-end sequencing was performed at University of Wisconsin-Madison. FASTQ reads were trimmed and filtered to improve mapping quality before mapping to mm10 genomic build using Tophat, with a maximum of 2 mismatches allowed. Galaxy web based tools were used to perform cufflinks, and cuffdiff was run to determine differential transcripts, using the mm10 reference annotation as a guide. Transcripts either upregulated or downregulated 1.5 fold with a q-value less than 0.05 were considered to be differentially expressed in the *Skiv2l2* knockdown cells.

8.13 RNA-seq analysis

Go-Ontology was performed on the differentially expressed transcripts using the GO Enrichment Analysis online platform at http://geneontology.org/page/go-enrichment-analysis. Intergenic regions were identified using the UCSC genome browser on the mm10 genome build (http://genome.ucsc.edu/). The NCBI nucleotide database was used to identify genes names and their function. Significantly upregulated and downregulated mRNAs were then sorted by hand based on function specified at the NCBI database, with categories including: proliferation, DNA damage, chromatin remodeling, histones, ribosome, and RNA processing and turnover. Each category was then divided into

subcategories to identify genes involved with different aspects of the cell cycle. The phypher function in R was used for probability calculations.

8.14 Protein-RNA immunoprecipitation

After 48 hours of cell growth, untreated P19 and N2a cells from three P100 plates were irradiated at 254 nm (150 mJ/cm2) two times to crosslink proteins and RNA using the UVP Crosslinker CL-1000 model. Protein A conjugated Dynabeads® were prepared according to manufacturer's protocol using the Dynabeads® Protein A Immunoprecipitation Kit (Thermo Fisher # 10006D). Dynabeads were incubated with 12μL rabbit polyclonal antibody against SKIV2L2 (Abcam #ab70552) or incubated with 12 μL anti-goat Ig as a negative control. Cells from three plates were combined into one biological sample and were lysed as described previously. 500μL of cellular lysate prepared from UV irradiated cells was loaded onto the Dynabeads® and incubated according to kit protocol. Immunoprecipation of SKIV2L2 according to kit protocol was performed, and the protein-RNA complexes were eluted off the Dynabeads®. Eluate was treated with DNase and proteinase K. Samples were taken for Western blotting to verify recovery of SKIV2L2 protein, while RNA was isolated from eluate using Trizol extraction with chloroform as previously described. cDNA was prepared using reverse gene specific primers in Table 8.1 or oligo-dT, and qPCR reactions were performed on the prepared cDNA as mentioned previously.

8.15 3'UTR pMirGlo Assay

The 3'UTR of *Skiv2l2* (200 bp) was amplified from N2a cell DNA isolated through Trizol extraction and cloned into the pMirGlo Dual Luciferase miRNA target expression vector (Promega #E1330). A 200 bp sequence from the 5' end of yeast Mtr4 was amplified from yeast genomic DNA and cloned into a second pMirGlo vector as a negative control. This resulted in the firefly luciferase gene being fused to either the 3' UTR of *Skiv2l2* or yeast genomic DNA. Using 0.1% Lipofectamine 3000, N2a cells were transfected with either 20 ng of the pMirGlo vector containing the 3'UTR of *Skiv2l2* or 20 ng of the control vector containing yeast genomic DNA. Cells were then either grown in 10% FBS or 2% FBS with 20 μM retinoic acid. The cells were harvested after 24 hours and diluted in DMEM. The cells were lysed using the Dual-Glo® Luciferase Assay System kit (Promega #E2920). Using the Lumat LB tube luminometer, firefly luciferase luminescence was measured first followed by measurement of background Renilla luciferase luminescence according to manufacturer's protocol. Firefly luciferase expression was calculated by subtracting Renilla luciferase luminescence from the firefly luciferase luminescence.

8.16 RNA Decay Assay

Following 24 hours of control and *Skiv2l2* RNAi as previously described, N2a cells were treated with Actinomycin-D (Sigma #A1410) to a concentration of 5 μg/mL. Cells were harvested for RNA extraction at 0, 1, 2, 3, and 4 hours. RNA was quantified and 8μL of identical amounts of RNA (approximately 8 μg) were run on a 1.4% agarose

gel at 90V. RNA was transferred to a blotting membrane overnight in 20X SSC before being crosslinked to the membrane. The Northern blot was probed using primers against H4 and ActB labeled with ATP, [γ-32P]- 3000Ci/mmol 10mCi/ml EasyTide Lead (Perkin Elmer) ATP-using T4-polynucleotide kinase (NEB #M0201) according to manufacturer's protocol. Radiolabeled probes were incubated with the blot at 42°C for 16 hours and developed using phosphorimaging screens and the Storm™ PhosphorImager from GE Healthcare. Peak quantification for ActD and H4 mRNA was performed on Image J software, and H4 mRNA levels were normalized to ActD or rRNA levels as appropriate. The decay constant was calculated using the equation $\ln(C/C_0)=-k_{decay}t$, where t= time, k_{decay}=decay constant, C=RNA level at t, and C_0= RNA level at t=0. H4 half-life ($t_{1/2}$) was found by solving for t at ln(.5). The student's t-test was performed on the H4 half-life calculated for three distinct trials.

8.17 Poly-A-tail Length Assay

RNA was isolate from N2A cells following *Skiv2l2* knockdown as previously described. RNA was digested using RNAseH (NEB #M0297), and primers annealing to the 5' end of the RNA according to manufacturer's protocol. 150-200 bp RNA fragments were extracted with phenol-chloroform according to laboratory protocol to remove RNAseH. RNA was circularly ligated with T4 RNA ligase according to manufacturer's protocol (NEB #M0204). Circularly ligated RNA was reverse transcribed with a gene specific primer for 2 hours at Tm-5°C. DNA was then amplified with PCR using Taq DNA polymerase in ThermoPol® Buffer according to manufacturer's protocol (NEB #M0267). DNA fragment was cloned into pGEM®-T Easy using the Promega kit

(Promega #A1360). BL21 Escherichia coli were then transformed with the pGEM®-T Easy vector with insert according to chemically competent BL21 protocol (NEB #C2530H) and plated on ampicillin plates with X-Gal for 16 hours at 37°C. White colonies were selected, and plasmids were purified using the Wizard® Plus SV Minipreps DNA Purification System according to manufacturer's protocol (Promega #A1330).

8.18 Micrococcal Nuclease Assay

Nuclei were isolated from P19 and N2A cells lysed with 0.1% Triton X-100 after control siRNA or Skiv2l2 siRNA transfection. The nuclei were then treated with micrococcal nuclease (Sigma Aldrich N3755) and digested for 9 minutes at 20°C. Nuclei were digested with Proteinase K and RNase A for one hour at 37°C to remove proteins and RNA from DNA fragments. Hi-Lo loading buffer was added to reactions and DNA was run on 1% agarose gels with .001% ethidium bromide at 100V for 1 hour. DNA was detected using the UVP™ GelDoc-IT^2 310 Imaging System.

CHAPTER IX: RNA-SEQ DATA TABLES

9.1 RefSeq genes dysregulated following *Skiv2l2* knockdown in P19 cells

Gene ID	Gene Symbol	Locus	M	q
NR_015517	5930412G12Rik	chr5:128579129-128600687	-0.85177	0.005539
NM_001013608	Ercc6l2	chr13:63815319-63900301	-0.79391	0.001451
NR_015601	Fam120aos	chr13:48968111-48969905	0.839344	0.002615
NM_178182	Hist1h2ai	chr13:21716411-21716859	0.804162	0.007984
NM_175656	Hist1h4i	chr13:22040959-22041362	1.12245	0.001451
NM_026821	Lurap1l	chr4:80910685-80954301	-1.19847	0.001451
NM_009538	Plagl1	chr10:13090787-13131695	-1.16881	0.001451
NM_144912	Rad9b	chr5:122325507-122354195	-0.73071	0.023577
NR_028515	Snora78	chr17:24719530-24719965	1.65325	0.001451
NM_026738	Card19	chr13:49202950-49216026	0.623596	0.001451
NM_001033145	1190002N15Rik	chr9:94517863-94538081	-1.09564	0.001451
NR_015476	1500011K16Rik	chr2:127791376-127792488	0.749772	0.023031
NR_029432	1500015A07Rik	chr18:61726389-61728253	1.13436	0.001451
NR_029440	2010320M18Rik	chr8:70776861-70777606	0.736332	0.006305
NM_001001881	2510009E07Rik	chr16:21649044-21694665	-2.04653	0.001451
NR_028428	2610005L07Rik	chr8:20385781-20424814	-0.61171	0.012253
NM_183287	2610318N02Rik	chr16:17113397-17125106	0.738631	0.001451
NM_029818	2700049A03Rik	chr12:71136847-71243303	-1.3526	0.001451
NR_033780	2810001G20Rik	chr11:64079483-64083259	0.608595	0.035448
NR_045268	2810013P06Rik	chr8:123042574-123044602	1.08102	0.001451
NR_029441	2810454H06Rik	chr6:134897960-134900785	0.678476	0.007984
NR_033215	3000002C10Rik	chr9:109830153-109831431	0.730317	0.046147
NR_015510	4632427E13Rik	chr7:92740705-92741459	0.638455	0.002615
NM_028934	4930452B06Rik	chr14:8431171-8666290	-0.85158	0.001451
NR_033601	4930519F09Rik	chr10:28921962-28923507	0.968532	0.031973
NM_026296	4930548H24Rik	chr5:31485858-31488262	0.955223	0.029723
NR_015555	4933404O12Rik	chr5:136919145-136937109	-0.67445	0.001451
NR_036602	4933421O10Rik	chr4:33027138-33031323	1.09842	0.001451
NR_040469	5031425E22Rik	chr5:23431807-23434353	0.665507	0.001451
NR_015552	5330434G04Rik	chrX:105372993-105391754	0.776201	0.004643
NM_001162537	9330159F19Rik	chr10:29211642-29230779	-0.76028	0.001451
NM_001081963	9430020K01Rik	chr18:4634928-4682869	-0.59852	0.001451
NR_027446	A230072C01Rik	chrX:20951664-20987349	1.02958	0.023031

NM_001160370	A830018L16Rik	chr1:11414104-11975902	-1.00424	0.001451
NR_002142	Rpph1	chr14:50807446-50807771	1.04795	0.001451
NR_015488	A930003A15Rik	chr16:19876567-19884274	-1.38304	0.001451
NR_028376	A930004D18Rik	chr2:18025188-18037741	0.891504	0.045018
NM_172961	Abat	chr16:8513428-8621567	-1.36166	0.001451
NM_011075	Abcb1b	chr5:8798146-8866314	-0.66127	0.001451
NM_001033336	Abcc4	chr14:118482691-118706219	-0.58801	0.007984
NM_013790	Abcc5	chr16:20331303-20426394	-0.66933	0.001451
NM_007435	Abcd1	chrX:73716596-73738287	-0.79438	0.001451
NM_011994	Abcd2	chr15:91145870-91191807	-0.72012	0.001451
NM_009593	Abcg1	chr17:31057693-31117981	-1.08434	0.001451
NM_145421	Abhd17a	chr10:80583648-80590341	0.676096	0.008818
NM_025341	Abhd6	chr14:8002901-8056555	-1.0291	0.014141
NM_009595	Abl2	chr1:156558786-156649619	-0.63119	0.005539
NM_028037	Acad10	chr5:121621028-121660510	-0.59944	0.025833
NM_025408	Acer3	chr7:98213659-98309527	-0.60026	0.004643
NM_022816	Acot10	chr15:20665213-20666750	0.646105	0.011607
NM_025590	Acot11	chr4:106733914-106799831	-0.76832	0.011607
NM_015729	Acox1	chr11:116171882-116215318	0.589957	0.005539
NM_207625	Acsl4	chrX:142317992-142390535	-0.72736	0.001451
NM_080575	Acss1	chr2:150618110-150668932	-1.21089	0.001451
NM_007392	Acta2	chr19:34240335-34255373	1.03603	0.001451
NM_009609	Actg1	chr11:120345689-120348484	-0.58144	0.001451
NM_007498	Atf3	chr1:191170296-191183333	0.851031	0.001451
NM_001291890	Adam19	chr11:46054501-46147347	-1.09343	0.001451
NM_009621	Adamts1	chr16:85793827-85803115	0.643524	0.001451
NM_029967	Adamtsl1	chr4:86053914-86428382	-0.6252	0.013563
NM_019822	Adrm1	chr2:180171587-180176283	1.20408	0.023918
NM_026531	Aen	chr7:78895926-78908833	0.724787	0.030628
NM_133919	Aff1	chr5:103754161-103855322	-0.83578	0.001451
NM_153403	Ago1	chr4:126435012-126468421	-0.78951	0.001451
NM_016661	Ahcy	chr2:155059311-155074497	-0.67955	0.007984
NM_001162970	Aim1l	chr4:134068451-134092504	0.897542	0.010258
NM_001199270	Aldoart1	chr4:72850582-72852634	0.784181	0.001451
NM_008537	Amacr	chr15:10981755-10996624	-0.58883	0.018937
NM_001164602	Amigo2	chr15:97244073-97385691	-1.3001	0.020957
NM_173405	Amz1	chr5:140724126-140753312	1.1413	0.035448
NM_001252193	Amz2	chr11:109425945-109438148	-0.89148	0.039437
NM_019764	Amotl2	chr9:102717803-102733417	0.970163	0.001451
NM_027480	Ankrd24	chr10:81628539-81647612	-0.71059	0.01595
NM_008486	Anpep	chr7:79821802-79842352	-1.11325	0.001451

NM_021492	Ap3b2	chr7:81460398-81493925	-0.98739	0.001451
NM_018758	Apba3	chr10:81268171-81291581	0.769216	0.003645
NM_007462	Apc	chr18:34207774-34322190	-0.65079	0.001451
NM_133237	Apcdd1	chr18:62922326-62953195	-0.98482	0.001451
NM_001297554	Apela	chr8:65028416-65037336	-0.86277	0.001451
NM_013912	Apln	chrX:48025145-48034852	-0.95207	0.001451
NM_001289687	Arhgef3	chr14:27143992-27403911	0.964467	0.002615
NM_025404	Arl4d	chr11:101665540-101667832	-0.82126	0.005539
NM_207231	Arl5c	chr11:97989579-97996173	-0.78756	0.047777
NM_001166379	Armcx1	chrX:134717937-134721912	-1.5474	0.006305
NM_027560	Arrdc2	chr8:70835137-70839720	0.61483	0.031539
NM_028710	Arsg	chr11:109440077-109573329	-0.70753	0.032882
NM_133346	Asb6	chr2:30823097-30828300	0.587319	0.017725
NM_026937	Ascc1	chr10:59987908-60099990	-0.60955	0.040659
NM_178662	Atcay	chr10:81194690-81230779	0.743805	0.001451
NM_178405	Atp1a2	chr1:172271708-172298064	-1.29012	0.001451
NM_026094	Atp8b3	chr10:80519584-80539124	0.838981	0.004643
NM_001289446	Atp9a	chr2:168634437-168742136	-0.79311	0.005539
NM_001033532	AW554918	chr18:25169019-25467321	-0.58659	0.001451
NM_015732	Axin2	chr11:108920348-108950781	-0.94668	0.001451
NR_028263	B130006D01Rik	chr11:95723585-95726773	-0.93014	0.003645
NM_001080935	B230217C12Rik	chr11:97840779-97843043	0.82094	0.026781
NR_030695	B330016D10Rik	chr4:141546161-141548313	1.12611	0.001451
NM_133234	Bbc3	chr7:16309582-16318334	1.0077	0.02001
NM_001033328	Tmem185a	chrX:70460055-70477043	-0.73287	0.001451
NR_030677	BC025920	chr10:81606307-81609836	1.15783	0.001451
NM_029410	Bcl2l12	chr7:44986899-44997579	0.804035	0.034184
NM_177235	Bend6	chr1:33852051-33907621	-0.82651	0.023031
NM_026512	Bphl	chr13:34037640-34074074	-0.68139	0.008818
NM_007557	Bmp7	chr2:172868011-172940321	-1.01801	0.001451
NM_172870	Bnc2	chr4:84272541-84675086	-0.7047	0.010947
NM_028055	Btbd17	chr11:114790668-114795892	0.819902	0.023577
NR_024078	Btbd19	chr4:117119217-117125725	0.867965	0.001451
NM_001037758	Btrc	chr19:45363733-45533343	-0.63459	0.031973
NR_027987	C030016D13Rik	chr19:27430036-27432631	1.81803	0.001451
NR_026848	C030034I22Rik	chr17:69416446-69419192	0.784575	0.004643
NM_013484	C2	chr17:34862601-34882100	-1.29889	0.001451
NR_027923	C630043F03Rik	chr4:72201243-72203930	0.994274	0.001451
NM_001146287	Cables1	chr18:11821087-11945627	-2.04232	0.001451
NM_027381	Cactin	chr10:81321102-81326251	0.640942	0.002615
NM_053199	Cadm3	chr1:173334253-173367695	-0.63969	0.011607

NM_144817	Camk1g	chr1:193346345-193370282	-0.63039	0.022563
NM_009800	Car11	chr7:45699966-45704661	-0.96743	0.007175
NM_010828	Cited2	chr10:17723227-17725674	-0.84435	0.001451
NM_001076789	Cbx5	chr15:103191545-103239816	-0.67472	0.001451
NM_145970	Cc2d1a	chr8:84132827-84147753	0.75623	0.001451
NM_001293560	Kyat3	chr3:142701047-142744911	-0.58782	0.007175
NM_026964	Ccdc124	chr8:70868226-70873490	0.728343	0.001451
NM_172428	Ccdc134	chr15:82127921-82142202	0.596359	0.006305
NM_001195672	Ccdc170	chr10:4509871-4561111	-0.86799	0.046988
NM_028381	Ccdc94	chr17:55952622-55967951	0.811028	0.001451
NM_025725	Ccdc96	chr5:36484587-36488171	0.983034	0.001451
NM_146014	Ccm2	chr11:6546886-6596761	0.65293	0.001451
NM_007630	Ccnb2	chr9:70407688-70421554	-0.63783	0.001451
NM_009829	Ccnd2	chr6:127125708-127212419	-0.69289	0.001451
NM_009831	Ccng1	chr11:40748551-40755286	0.640568	0.001451
NM_001045530	Ccnjl	chr11:43528748-43586999	-0.71086	0.002615
NM_001039151	Cd44	chr2:102811141-102901665	-1.16429	0.001451
NM_009865	Cdh10	chr15:18820328-19014234	-0.92773	0.001451
NM_019707	Cdh13	chr8:118283754-119323448	-0.66781	0.016521
NM_033037	Cdo1	chr18:46713204-46728342	-1.90239	0.022563
NM_009734	Cep131	chr11:120064429-120086827	0.73183	0.001451
NM_027559	Cfap43	chr19:47736856-47837361	-0.81559	0.001451
NM_026929	Chac1	chr2:119351241-119354327	1.58486	0.001451
NM_021350	Chml	chr1:175662420-175692632	0.606073	0.001451
NM_031258	Chrdl1	chrX:143285673-143394262	-0.77846	0.001451
NM_015730	Chrna4	chr2:181022310-181039177	-0.75624	0.001451
NM_018763	Chst2	chr9:95400925-95407270	-0.61947	0.001451
NM_001033302	Ciart	chr3:95871521-95891930	0.663316	0.026333
NM_001085500	Cisd3	chr11:97685951-97688625	-0.75114	0.010947
NM_028870	Cltb	chr13:54592938-54611272	0.775639	0.029213
NM_009131	Clec11a	chr7:44303765-44306959	0.707745	0.029723
NM_053109	Clec2d	chr6:129180614-129186535	-0.58727	0.005539
NM_172469	Clic6	chr16:92498146-92541241	-0.7698	0.002615
NM_001039162	Clip2	chr5:134489382-134552434	0.638823	0.031973
NM_001033175	Cln6	chr9:62838786-62875917	-0.59123	0.006305
NM_001102471	Cnnm2	chr19:46761608-46878580	-1.379	0.038705
NM_175651	Cnpy1	chr5:28205462-28237873	1.05426	0.017725
NM_175275	Cntln	chr4:84884308-85131921	-0.58761	0.007175
NM_053185	Col4a6	chrX:141165402-141474076	-0.83748	0.001451
NM_130449	Colec12	chr18:9707647-9877995	-0.80878	0.001451
NM_147778	Commd3	chr2:18672461-18676216	0.612389	0.010258

NM_001039710	Coq10b	chr1:55052769-55072702	0.835201	0.001451
NM_009898	Coro1a	chr7:126699773-126704816	0.92625	0.002615
NM_146067	Cpped1	chr16:11803720-11930594	-0.67858	0.010947
NM_176073	Cpq	chr15:33083128-33653436	-0.64717	0.028252
NM_021273	Ckb	chr12:111669354-111672338	1.00512	0.001451
NM_133930	Creld1	chr6:113483568-113493338	0.610899	0.001451
NM_024223	Crip2	chr12:113140235-113145506	0.910495	0.001451
NR_033641	Crnde	chr8:92326030-92356120	-0.88086	0.024425
NM_019922	Crtap	chr9:114368323-114390712	0.811066	0.019402
NM_007770	Crx	chr7:15865946-15879955	0.913287	0.006305
NM_009965	Cryba1	chr11:77718731-77725293	-1.19805	0.023918
NM_153076	Crygn	chr5:24751001-24757843	-0.7814	0.024857
NM_027945	Csl	chr10:99757704-99759658	-0.64491	0.002615
NM_153409	Csrnp3	chr2:65845766-66031546	-1.88083	0.001451
NM_145953	Cth	chr3:157894247-157925063	0.646348	0.001451
NM_007801	Ctsh	chr9:90054266-90076095	-1.06494	0.035448
NM_001291234	Cux1	chr5:136248134-136567490	-1.06126	0.017111
NM_021704	Cxcl12	chr6:117168534-117181368	-0.85014	0.002615
NM_001012477	Cxcl12	chr6:117168534-117181368	-1.13871	0.001451
NM_013655	Cxcl12	chr6:117168534-117181368	-1.14089	0.002615
NM_009911	Cxcr4	chr1:128588198-128592299	-0.61332	0.001451
NM_001004367	Cxxc4	chr3:134236494-134262089	-1.07338	0.001451
NM_007811	Cyp26a1	chr19:37697807-37701536	0.735006	0.001451
NM_010516	Cyr61	chr3:145646970-145649985	0.859053	0.001451
NR_028421	D430020J02Rik	chr12:116401946-116405161	0.598397	0.001451
NM_194061	D630045J12Rik	chr6:38048482-38254009	-0.81213	0.001451
NR_027958	D930048N14Rik	chr11:51643088-51657681	0.939226	0.017725
NM_001190474	Dapk3	chr10:81183006-81193197	0.675098	0.009538
NM_027490	Dcp2	chr18:44380499-44424969	-0.77572	0.001451
NM_026993	Ddah1	chr3:145758691-145894277	-0.79472	0.001451
NM_030143	Ddit4l	chr3:137623671-137628332	-0.6201	0.005539
NM_172962	Ddr1	chr17:35681566-35704139	0.6732	0.001451
NM_013932	Ddx25	chr9:35541847-35558470	-0.60009	0.001451
NM_026500	Ddx59	chr1:136411915-136440220	-0.58886	0.003645
NM_181324	Ddx6	chr9:44604891-44640731	-0.59378	0.045495
NM_145470	Deptor	chr15:55099916-55259273	-0.83282	0.001451
NM_001037938	Dhrs4	chr14:55478757-55490340	-0.63668	0.002615
NM_001033326	Dhrsx	chr4_GL456216_random:15880-36213	-0.62977	0.039437
NM_001033548	Dnaaf3	chr7:4522956-4532442	0.863737	0.001451
NM_198412	Dnajc6	chr4:101496647-101642799	-2.27332	0.012963
NM_133964	Dohh	chr10:81384427-81388352	0.75188	0.001451

NM_025675	Dph6	chr2:114516417-114654928	-0.8041	0.001451
NM_026767	Dpm3	chr3:89266460-89267079	0.907552	0.010947
NM_033606	Dqx1	chr6:83057843-83067219	0.638118	0.014681
NM_025853	Dsn1	chr2:156995061-157007075	-0.67744	0.001451
NM_009342	Dynlt1b	chr17:6430111-6436295	-0.79283	0.008818
NM_025943	Dzip1	chr14:118875519-118925470	-0.67729	0.001451
NR_040708	E130102H24Rik	chr4:101346523-101399185	0.832681	0.001451
NR_038037	E130307A14Rik	chr10:39612933-39732007	-0.72414	0.034591
NM_001291105	E2f1	chr2:154559399-154569892	0.989853	0.004643
NM_033270	E2f6	chr12:16810964-16826752	-0.80704	0.014681
NM_010023	Eci1	chr17:24426682-24439316	-0.60942	0.003645
NM_001110331	Eci2	chr13:34977747-34994144	-1.01705	0.001451
NM_010100	Edar	chr10:58600787-58675696	-1.02699	0.009538
NM_021519	Edf1	chr2:25557899-25562082	0.770002	0.001451
NM_027974	Efhc1	chr1:20951625-20990841	-1.20103	0.001451
NM_020578	Ehd3	chr17:73804840-73832093	-0.72624	0.001451
NM_198425	Eid2	chr7:28267880-28269168	-0.70312	0.001451
NM_001177427	Eid2b	chr7:28277705-28280129	-0.72295	0.002615
NM_144958	Eif4a1	chr11:69666935-69672423	-1.17147	0.01595
NM_013506	Eif4a2	chr16:23107467-23127730	-1.41013	0.014681
NM_010487	Elavl3	chr9:22015004-22052023	0.693958	0.001451
NM_080288	Elmo1	chr13:20090506-20608356	-0.87566	0.001451
NM_001253692	Elmod3	chr6:72565921-72598413	-1.0245	0.001451
NM_001043336	Eml1	chr12:108371152-108702306	-0.70668	0.001451
NM_199466	Eml4	chr17:83350930-83480359	-0.90435	0.036345
NM_172573	Engase	chr11:118476959-118489198	0.596771	0.014681
NM_015744	Enpp2	chr15:54838678-54920146	-1.06961	0.001451
NM_134005	Enpp3	chr10:24773813-24836195	-0.63271	0.001451
NM_010139	Epha2	chr4:141301220-141329384	0.791182	0.001451
NM_001122889	Epha7	chr4:28813130-28967503	1.35026	0.025833
NM_030711	Erap1	chr13:74639871-74691875	-0.96831	0.001451
NM_011843	Esyt1	chr10:128510249-128525859	0.590776	0.005539
NM_008815	Etv4	chr11:101769741-101785310	0.943731	0.014681
NM_145920	Evc2	chr5:37338477-37425054	-0.72143	0.043378
NM_175399	Exosc4	chr15:76327396-76330670	0.690836	0.001451
NM_010164	Eya1	chr1:14168957-14310199	-1.27045	0.049716
NM_007970	Ezh1	chr11:101191114-101226463	-0.69164	0.001451
NM_001166213	Fam129c	chr8:71597645-71608149	-0.73895	0.046988
NM_173395	Fam132b	chr1:91366429-91374217	0.892481	0.001451
NM_027342	Fam162a	chr16:36043843-36071515	-0.72433	0.001451
NM_199200	Fam171a2	chr11:102436980-102447663	0.588976	0.011607

NM_001114174	Fam189a2	chr19:23972749-24031019	-1.56449	0.001451
NM_001025382	Fam196b	chr11:34226820-34783905	0.850402	0.001451
NM_177233	Fam19a4	chr6:96831208-97060411	-0.83872	0.035898
NM_007991	Fbl	chr7:28169747-28179269	-0.64919	0.012963
NM_001033312	Fbxl18	chr5:142871788-142895238	0.835289	0.002615
NM_025386	Fbxo36	chr1:84839840-84900486	-1.56789	0.001451
NM_176982	Fbxo48	chr11:16951409-16954772	0.586972	0.018345
NM_010203	Fgf5	chr5:98254183-98277033	1.81829	0.002615
NM_008013	Fgl2	chr5:21292960-21424677	-0.76476	0.002615
NM_001110329	Fiz1	chr7:5007055-5014728	1.42803	0.004643
NM_008019	Fkbp1a	chr2:151542482-151561691	-0.87757	0.001451
NM_013902	Fkbp3	chr12:65036333-65073938	-0.88211	0.001451
NM_201411	Flrt1	chr19:7056767-7198062	-0.71766	0.046988
NM_001301375	Fst	chr13:114452261-114458951	-0.8606	0.029723
NM_010425	Foxd3	chr4:99656298-99658671	0.714189	0.009538
NM_019739	Foxo1	chr3:52268336-52350109	-0.59029	0.003645
NM_175473	Fras1	chr5:96373954-96784728	-0.66351	0.001451
NM_145148	Frmd4b	chr6:97286866-97617657	-0.71275	0.001451
NM_172673	Frmd5	chr2:121545528-121807057	-0.70758	0.001451
NM_001195284	Fsd1l	chr4:53631470-53707009	-0.85621	0.001451
NM_001301373	Fst	chr13:114452261-114458951	-0.83147	0.001451
NM_021356	Gab1	chr8:80764430-80880519	-0.90908	0.048741
NM_008078	Gad2	chr2:22622326-22693877	-2.1367	0.001451
NM_001081421	Galnt16	chr12:80518989-80603896	-0.74836	0.001451
NM_008086	Gas1	chr13:60174404-60177535	-0.6767	0.001451
NM_010258	Gata6	chr18:11042036-11085635	-1.01435	0.001451
NM_013526	Gdf6	chr4:9844371-9862345	-1.82012	0.001451
NM_201352	Gdpd5	chr7:99381548-99460984	0.876064	0.001451
NM_027450	Glipr2	chr4:43957701-43979118	0.851218	0.001451
NM_053108	Glrx	chr13:75839885-75850151	-0.65482	0.001451
NR_033595	Gm13498	chr2:50909683-50911846	1.30957	0.001451
NR_004442	Gm15421	chr5:22486488-22550331	-0.78532	0.001451
NM_001033248	Gm266	chr12:111484608-111485823	-1.43469	0.024857
NR_033619	Gm6623	chr17:36178776-36181364	0.705313	0.04692
NR_045618	Gm9958	chr5:90366996-90368488	1.34624	0.001451
NM_198101	Gmip	chr8:69808686-69821870	0.667856	0.032882
NM_001113384	Gnao1	chr8:93810837-93969388	-0.78072	0.001451
NM_010316	Gng3	chr19:8836928-8848683	0.581008	0.020957
NM_010318	Gng5	chr3:146499835-146505543	1.53371	0.001451
NM_145965	Gphn	chr12:78226654-78684769	-0.58314	0.007175
NM_010338	Gpr37	chr6:25668522-25689980	-0.79998	0.001451

NM_008160	Gpx1	chr9:108339079-108340344	0.999232	0.001451
NM_001083628	Greb1l	chr18:10325178-10562941	-0.63197	0.001451
NM_016886	Gria3	chrX:41401300-41678601	-0.88117	0.049405
NM_001291045	Grm4	chr17:27422387-27503533	-0.62935	0.031539
NM_010345	Grb10	chr11:11930498-12037420	1.42927	0.001451
NM_026672	Gstm7	chr3:107926333-107931745	-0.72887	0.001451
NM_008185	Gstt1	chr10:75783812-75798584	-0.75688	0.039858
NM_010363	Gstz1	chr12:87106865-87164723	-0.68513	0.020957
NR_027009	Gt(ROSA)26Sor	chr6:113046326-113077244	0.795253	0.04735
NM_053266	Gtf2ird2	chr5:134184037-134218143	-0.74592	0.020957
NM_001033322	Gucy1a2	chr9:3532348-3905787	-0.83139	0.001451
NM_178747	Gulo	chr14:65986786-66009210	-0.73376	0.011607
NM_172670	Gyltl1b	chr2:92365045-92371057	-1.0279	0.001451
NM_177688	H2afj	chr6:136808247-136810074	0.855991	0.001451
NM_016750	H2afz	chr3:137864486-137866922	-0.6071	0.001451
NM_008216	Has2	chr15:56665626-56694546	-1.31155	0.001451
NM_027382	Hdac8	chrX:102284639-102505148	-0.58885	0.022043
NM_001163471	Hectd2	chr19:36554638-36689479	-1.52125	0.041324
NM_022331	Herpud1	chr8:94386499-94395358	0.612819	0.001451
NM_020259	Hhip	chr8:79965850-80058008	1.94527	0.001451
NM_145567	Hibadh	chr6:52546229-52640300	-0.67793	0.001451
NM_175454	Hid1	chr11:115347708-115367719	0.740602	0.027823
NM_001162950	Hif3a	chr7:17030992-17062427	-1.00065	0.003645
NM_010433	Hipk2	chr6:38697839-38876190	-0.83333	0.015282
NM_178189	Hist1h2ac	chr13:23683472-23683959	0.588116	0.02001
NM_175659	Hist1h2ah	chr13:22035121-22035643	0.997338	0.005539
NM_178183	Hist1h2ak	chr13:21753376-21753912	0.929831	0.001451
NM_178184	Hist1h2an	chr13:21786771-21787218	1.39517	0.001451
NM_001290380	Hist1h2bc	chr13:23684198-23692480	1.72254	0.001451
NM_001290530	Hist1h2be	chr13:23583669-23621124	0.992899	0.001451
NM_178195	Hist1h2bf	chr13:23573759-23574190	0.898411	0.001451
NM_178196	Hist1h2bg	chr13:23571399-23571863	1.16721	0.001451
NM_178197	Hist1h2bh	chr13:23542922-23543444	1.4328	0.001451
NM_178198	Hist1h2bj	chr13:22043229-22043658	0.98064	0.001451
NM_175665	Hist1h2bk	chr13:22035820-22036320	1.26857	0.001451
NM_178199	Hist1h2bl	chr13:21715712-21716143	1.08947	0.001451
NM_178200	Hist1h2bm	chr13:21722043-21722526	1.02812	0.001451
NM_178201	Hist1h2bn	chr13:21754122-21754553	1.54492	0.001451
NM_001290466	Hist1h2bp	chr13:21787487-21789213	0.681751	0.001451
NM_013550	Hist1h3a	chr13:23761884-23762386	0.97277	0.001451
NM_175653	Hist1h3c	chr13:23745041-23745521	0.941578	0.001451

NM_178204	Hist1h3d	chr13:23575762-23576266	0.5921	0.001451
NM_013548	Hist1h3f	chr13:23544051-23544954	0.982357	0.001451
NM_013548	Hist1h3f	chr13:23544051-23544954	0.982357	0.001451
NM_145073	Hist1h3g	chr13:23535417-23535909	0.795682	0.001451
NM_178206	Hist1h3h	chr13:21717627-21718115	0.706797	0.001451
NM_178207	Hist1h3i	chr13:21782914-21783397	1.18313	0.001451
NM_178192	Hist1h4a	chr13:23760794-23761249	1.60444	0.001451
NM_178193	Hist1h4b	chr13:23756936-23757386	1.10022	0.001451
NM_178208	Hist1h4c	chr13:23698083-23698458	0.859387	0.001451
NM_175654	Hist1h4d	chr13:23581601-23581969	1.30428	0.001451
NM_175655	Hist1h4f	chr13:23551285-23551643	1.31757	0.001451
NM_153173	Hist1h4h	chr13:23531043-23531478	1.04986	0.001451
NM_178210	Hist1h4j	chr13:21735095-21735407	2.49915	0.005539
NM_178211	Hist1h4k	chr13:21750144-21750553	1.31433	0.001451
NM_175662	Hist2h2ac	chr3:96220412-96220880	1.08966	0.001451
NM_178215	Hist2h3b	chr3:96268653-96269155	0.881644	0.009538
NM_033596	Hist2h4	chr3:96262933-96263317	1.05178	0.001451
NM_178218	Hist3h2a	chr11:58954684-58955192	0.998117	0.001451
NM_030082	Hist3h2ba	chr11:58948910-58949372	0.666109	0.001451
NM_175652	Hist4h4	chr6:136803992-136804431	0.915953	0.001451
NM_206882	-	chr11:58954047-58954512	0.859444	0.001451
NM_010420	Hesx1	chr14:27000361-27002325	1.37467	0.001451
NM_146256	Hpdl	chr4:116819906-116821508	1.01682	0.012253
NM_011828	Hs2st1	chr3:144431106-144570216	-0.59104	0.001451
NM_153571	Hscb	chr5:110829069-110839777	-0.95979	0.001451
NM_013558	Hspa1l	chr17:34972702-34979228	0.866197	0.006305
NM_030704	Hspb8	chr5:116408490-116422864	-0.65297	0.002615
NM_031166	Id4	chr13:48044230-48264036	-0.6833	0.001451
NM_001112715	Ifitm1	chr7:140967428-140969827	-1.19295	0.001451
NM_008988	Igdcc3	chr9:65141188-65185870	-0.75362	0.001451
NM_010518	Igfbp5	chr1:72858064-72874865	-0.6407	0.001451
NM_177591	Igsf1	chrX:49782536-49797745	-0.97211	0.002615
NM_018738	Igtp	chr11:58199555-58207592	-0.93694	0.001451
NM_011772	Ikzf4	chr10:128632414-128645993	-0.98324	0.001451
NM_008349	Il10rb	chr16:91406234-91425834	-1.00229	0.010258
NM_172786	Il20ra	chr10:19712586-19760053	0.686806	0.013563
NM_001164528	Ildr2	chr1:166254138-166316832	-0.89211	0.001451
NM_011830	Impdh2	chr9:108560500-108565566	0.65436	0.010258
NM_001136270	Inafm1	chr7:16272012-16273692	0.981794	0.008818
NM_175515	Intu	chr3:40540766-40704774	-0.69049	0.001451
NM_008393	Irx3	chr8:91798510-91801654	-1.10608	0.001451

NM_018826	Irx5	chr8:92357795-92361456	-1.10616	0.001451
NM_010588	Jag2	chr12:112908589-112929495	0.683042	0.003645
NM_010591	Jun	chr4:95049035-95052222	0.648298	0.001451
NM_152923	Kcnq3	chr15:65994914-66286224	-0.77391	0.002615
NM_001039472	Kif21b	chr1:136131400-136178014	0.6251	0.001451
NM_008447	Kif5a	chr10:127225694-127263363	1.61143	0.001451
NM_033563	Klf7	chr1:64035670-64121389	0.687312	0.001451
NM_026167	Klhl13	chrX:23219270-23365082	-0.60127	0.001451
NM_029436	Klhl24	chr16:20097553-20127744	-0.59553	0.001451
NM_001163020	Klhl32	chr4:24617272-24851086	-1.02064	0.004643
NM_001083322	Klrk1	chr6:129610322-129623864	-0.61138	0.009538
NM_026412	Knstrn	chr2:118814002-118836212	-0.63751	0.001451
NM_024291	Ky	chr9:102506137-102546239	0.991254	0.001451
NM_026038	L3hypdh	chr12:72073427-72085313	-1.07399	0.019402
NM_008482	Lamb1	chr12:31265293-31329639	-0.58562	0.001451
NM_177356	Lamp3	chr16:19653380-19706365	0.977188	0.001451
NM_033521	Laptm4b	chr15:34238025-34284295	-0.70194	0.001451
NR_038063	Rplp2-ps1	chr12:75630593-75669537	0.588396	0.001451
NM_153168	Lars2	chr9:123366939-123462664	0.712285	0.001451
NM_001276402	Lef1	chr3:131110296-131224357	-1.26171	0.001451
NM_134093	Letmd1	chr15:100469033-100479252	-0.69564	0.001451
NM_008499	Lhx5	chr5:120431885-120441457	0.738453	0.001451
NM_010720	Lipg	chr18:74939321-74961263	1.06835	0.001451
NM_145438	Llgl2	chr11:115824057-115855780	0.72233	0.023031
NM_020295	Lmbr1	chr5:29229801-29378390	-0.8475	0.001451
NM_028050	Lmntd2	chr7:141194129-141214080	-0.99499	0.047777
NM_001142335	Lmo2	chr2:103957994-103981878	-0.66398	0.023918
NM_010725	Lmx1b	chr2:33564535-33640511	-0.98519	0.049405
NM_033325	Loxl2	chr14:69609475-69695834	-0.67025	0.001451
NM_008509	Lpl	chr8:68880554-68906932	-0.90333	0.001451
NM_146164	Lrch4	chr5:137629122-137642902	0.746265	0.008818
NM_028886	Lrguk	chr6:34029447-34134034	-0.96163	0.002615
NM_029044	Lrrc48	chr11:60353379-60394333	-1.08917	0.013563
NM_133897	Lrrc8c	chr5:105519470-105608954	-0.61585	0.002615
NM_017405	Lsr	chr7:30957769-30973469	1.70253	0.023918
NM_146006	Lss	chr10:76531604-76562226	0.624592	0.001451
NM_010756	Mafg	chr11:120628350-120633547	0.621452	0.001451
NM_010757	Mafk	chr5:139791535-139802652	0.661288	0.004643
NM_001013813	Maml2	chr9:13619988-13709533	-0.86023	0.001451
NM_027288	Manba	chr3:135485610-135571403	-0.58616	0.001451
NM_022012	Map3k11	chr19:5689130-5702864	0.592452	0.005539

NM_001048167	Map6	chr7:99267446-99337137	1.00769	0.001451
NM_198599	Map6d1	chr16:20233308-20241358	-0.65067	0.030178
NM_001045483	Mapk1ip1	chr7:138835817-138846267	0.676809	0.004643
NM_011841	Mapk7	chr11:61488811-61494266	0.701916	0.009538
NM_011162	Mapk8ip1	chr2:92383675-92401263	0.596152	0.006305
NM_016762	Matn2	chr15:34306680-34436240	-0.77468	0.001451
NM_001306143	Mbd3	chr10:80392538-80399531	0.951823	0.007984
NM_001025245	Mbp	chr18:82475122-82585637	-0.74582	0.001451
NM_001085374	Mcc	chr18:44425059-44812182	-0.79696	0.008818
NM_001024703	Mctp2	chr7:72077829-72306595	1.13506	0.001451
NM_001033259	Mcu	chr10:59446983-59616692	-0.62005	0.006305
NM_010783	Mdfi	chr17:47815327-47834691	0.866976	0.001451
NM_010786	Mdm2	chr10:117688874-117710758	-0.60026	0.031973
NM_001081979	Mecp2	chrX:74026591-74085690	-0.83667	0.016521
NM_001045484	Mef2b	chr8:70152777-70167488	0.89741	0.036345
NM_145128	Mgat5	chr1:127204985-127482972	-0.72303	0.001451
NM_019394	Mia	chr7:27179740-27181149	-1.06465	0.046518
NM_026524	Mid1ip1	chrX:10717364-10719702	0.786363	0.001451
NR_030711	Mir22hg	chr11:75461538-75466690	1.04915	0.017725
NR_030451	Mir682	chr13:75645045-75645141	3.63846	0.001451
NR_030484	Mir703	chr5:98329303-98802019	3.18442	0.001451
NM_177595	Mkx	chr18:6934965-7004779	-0.70546	0.022563
NM_027326	Mllt3	chr4:87769924-88033407	-0.73479	0.001451
NM_025962	Mmachc	chr4:116702433-116708385	-0.62013	0.001451
NM_175217	Mmd2	chr5:142563480-142608752	-1.02964	0.010258
NM_011900	Mpdu1	chr11:69655036-69662649	-0.84261	0.001451
NR_102690	Mphosph9	chr5:124250958-124327972	-0.89529	0.017111
NM_008624	Mras	chr9:99385419-99436712	-0.69322	0.041324
NM_001005423	Mreg	chr1:72159232-72212307	-1.09925	0.001451
NM_013601	Msx2	chr13:53466880-53472780	-0.78201	0.012253
NM_029104	Mss51	chr14:20482863-20496901	-0.67742	0.048741
NM_008638	Mthfd2	chr6:83305703-83317604	0.916797	0.001451
NM_001081285	Mup6	chr4:60003548-60006214	-1.1367	0.001451
NM_133250	Mutyh	chr4:116807733-116819431	0.669184	0.024857
NM_138656	Mvd	chr8:122433595-122443422	0.732202	0.001451
NM_026280	Mxra7	chr11:116803399-116828046	-0.94294	0.001451
NM_001198914	Myb	chr10:21124929-21160984	-0.69304	0.024425
NM_010848	Myb	chr10:21124929-21160984	-1.17101	0.001451
NM_010860	Myl6	chr10:128490860-128493825	0.900494	0.001451
NM_148413	Myo3a	chr2:22227502-22423370	-1.30699	0.002615
NM_001177965	Naa10	chrX:73916869-73921944	0.601453	0.013563

NM_013608	Naca	chr10:128035345-128048637	0.901187	0.005539
NM_028016	Nanog	chr6:122707488-122714633	-1.04467	0.001451
NM_008671	Nap1l2	chrX:103184058-103186664	0.867887	0.004643
NM_183276	Nbeal2	chr9:110624788-110654161	0.615838	0.015282
NM_011986	Ncdn	chr4:126743749-126753429	0.635131	0.001451
NM_178772	Nceh1	chr3:27183003-27244911	-0.89574	0.001451
NM_030729	Nckipsd	chr9:108808379-108818366	1.02171	0.001451
NM_172495	Ncoa7	chr10:30645581-30803107	-0.66906	0.001451
NM_026614	Ndufa5	chr6:24518665-24527687	-0.67824	0.001451
NM_025843	Ndufb7	chr8:83566757-83571623	0.754608	0.001451
NR_131212	Neat1	chr19:5824709-5845480	-0.60987	0.009538
NM_010896	Neurog1	chr13:56250497-56252163	-1.1792	0.003645
NM_009719	Neurog3	chr10:62133089-62134763	-2.13204	0.035448
NM_182716	Nfasc	chr1:132564689-132741797	-0.63519	0.023031
NM_013610	Ninj1	chr13:49187546-49196251	0.773791	0.001451
NM_023456	Npy	chr6:49822728-49829505	-0.85517	0.001451
NM_008173	Nr3c1	chr18:39410544-39487245	-0.77515	0.001451
NM_015743	Nr4a3	chr4:48045304-48086446	-0.62853	0.004643
NM_001146031	Nrcam	chr12:44328884-44601846	-0.69916	0.001451
NM_008744	Ntn1	chr11:68209363-68386826	-0.68339	0.001451
NM_182809	Ntrk3	chr7:78192113-78577838	-1.01237	0.001451
NM_027722	Nudt4	chr10:95547006-95564167	-0.73383	0.001451
NM_001136075	Numb	chr12:83794033-83921934	0.898536	0.027823
NM_001134457	Nxpe3	chr16:55839952-55895279	-0.66164	0.003645
NM_177215	Ocrl	chrX:47912455-47965866	-0.84414	0.001451
NM_025909	Oma1	chr4:103313845-103366428	-0.6543	0.005539
NM_026580	Otub2	chr12:103376893-103406350	0.679657	0.001451
NM_130880	Otud7a	chr7:63444771-63759027	1.1083	0.009538
NM_144841	Otx2	chr14:48657676-48667644	-0.677	0.016521
NM_007696	Ovgp1	chr3:105973801-105987423	-0.89346	0.001451
NM_011035	Pak1	chr7:97842938-97912381	-0.59513	0.001451
NM_181402	Parp11	chr6:127453722-127494239	-0.58677	0.001451
NM_001291508	Pbx1	chr1:168119363-168432169	-0.78006	0.049158
NM_025273	Pcbd1	chr10:61089330-61094329	-0.73705	0.036345
NM_025835	Pccb	chr9:100982037-101034875	-0.59621	0.013563
NM_028994	Pck2	chr14:55540265-55550017	0.984571	0.001451
NM_172832	Pcyox1l	chr18:61696836-61707635	0.763693	0.001451
NM_024229	Pcyt2	chr11:120610086-120617890	0.6282	0.001451
NM_133667	Pdk2	chr11:95026257-95041371	-0.82151	0.006305
NM_001114088	Pdlim7	chr13:55497486-55513446	0.614648	0.030178
NM_018884	Pdzrn3	chr6:101149606-101377897	-0.64294	0.001451

NM_026441	Pef1	chr4:130107555-130128134	-0.60893	0.002615
NM_011066	Per2	chr1:91415981-91459328	1.83775	0.001451
NM_023418	Pgam1	chr19:41911870-41918665	-0.59915	0.001451
NM_001161797	Phactr4	chr4:132355924-132422446	-0.60023	0.029213
NM_001109691	Phf21a	chr2:92184181-92364666	-0.77591	0.033356
NM_027949	Phf7	chr14:31237695-31251218	-0.85642	0.001451
NM_016966	Phgdh	chr3:98313170-98339969	0.595831	0.001451
NM_008832	Phka1	chrX:102513974-102644246	-0.74368	0.001451
NM_021501	Pias4	chr10:81153965-81167720	0.678756	0.001451
NM_001039485	Piezo2	chr18:63010212-63387183	-0.74156	0.001451
NM_025662	Pigk	chr3:152714099-152789013	-0.59899	0.001451
NM_001039536	Pigl	chr11:62458459-62513900	-0.82655	0.001451
NM_027153	Pir	chrX:164269430-164373013	-0.68056	0.01595
NM_134117	Pkdcc	chr17:83215282-83225069	0.645349	0.001451
NM_013737	Pla2g7	chr17:43568450-43612201	-0.79687	0.001451
NM_013829	Plcb4	chr2:135741829-136013068	-0.88177	0.001451
NM_172285	Plcg2	chr8:117498290-117635142	-0.61934	0.001451
NM_146030	Plekhh3	chr11:101162679-101171302	0.818677	0.011607
NM_001033150	Plekhm2	chr4:141625733-141664115	0.709805	0.003645
NM_013807	Plk3	chr4:117126812-117133952	0.583309	0.009538
NM_026162	Plxdc2	chr2:16356303-16755839	-0.60575	0.001451
NM_026784	Pmvk	chr3:89459117-89469009	0.64029	0.001451
NM_054088	Pnpla3	chr15:84167815-84189521	0.658739	0.003645
NM_025593	Polr2l	chr7:141471859-141475153	0.827479	0.007175
NM_026398	Pop5	chr5:115235850-115240970	-0.60881	0.002615
NM_029741	Ppfia3	chr7:45339125-45370564	0.831715	0.004643
NM_001110218	Ppm1h	chr10:122678761-122945793	-0.74186	0.001451
NM_013636	Ppp1cc	chr5:122158278-122175269	0.58589	0.028252
NM_033371	Ppp1r16a	chr15:76671679-76694915	0.667704	0.001451
NM_199149	Ppp1r37	chr7:19530966-19562398	0.679085	0.003645
NM_016854	Ppp1r3c	chr19:36731730-36736604	-0.85818	0.001451
NM_008924	Prkar2a	chr9:108692142-108749511	-0.6269	0.001451
NM_011158	Prkar2b	chr12:31958478-32061279	-0.63597	0.001451
NM_016979	Prkx	chrX:77762029-77795960	0.720997	0.001451
NM_011173	Pros1	chr16:62854333-62929340	-0.65183	0.002615
NM_175485	Prtg	chr9:72807273-72917307	-0.66621	0.001451
NM_177698	Psd3	chr8:67689081-67974574	-0.60862	0.019402
NM_013640	Psmb10	chr8:105935727-105938392	0.700649	0.020957
NM_025604	Psmg3	chr5:139823593-139826843	0.947122	0.001451
NM_133900	Psph	chr5:129765557-129787253	0.61375	0.001451
NM_022415	Ptges	chr2:30889470-30903297	-0.6409	0.026781

NM_008982	Ptprj	chr2:90429755-90580647	-0.86895	0.001451
NM_008985	Ptprn	chr1:75247040-75264208	0.683393	0.034591
NM_001098233	Purg	chr8:33386324-33417469	-0.70958	0.023918
NM_011224	Pygm	chr19:6384428-6398459	0.770995	0.046988
NM_026111	Qpctl	chr7:19140216-19149196	0.588919	0.036874
NR_045289	Rab26os	chr17:24528250-24528744	0.974891	0.001451
NM_175122	Rab39b	chrX:75572044-75578231	1.15471	0.001451
NM_173781	Rab6b	chr9:103112073-103185270	-0.77684	0.001451
NM_013862	Rabgap1l	chr1:160219173-160792938	-0.6667	0.023577
NM_001038621	Rabgap1l	chr1:160219173-160792938	-0.72522	0.015282
NM_009014	Rad51b	chr12:79297281-79814690	-0.62213	0.041698
NM_019444	Ramp2	chr11:101246333-101248250	-0.77239	0.012963
NM_028238	Rab38	chr7:88430272-88491572	-1.33228	0.001451
NM_029182	Rasd2	chr8:75213943-75224113	0.666243	0.031539
NM_001013386	Rasl10b	chr11:83410071-83421038	-0.66979	0.039043
NM_178045	Rassf4	chr6:116633007-116673836	-0.76871	0.001451
NM_019711	Rbms2	chr10:128129469-128180297	-0.80459	0.001451
NM_025654	Rdm1	chr11:101627948-101636081	-0.75331	0.001451
NM_011261	Reln	chr5:21884453-22344705	-0.61762	0.001451
NM_177073	Relt	chr7:100845847-100863413	0.585365	0.043378
NM_080726	Rem2	chr14:54476099-54480434	0.762426	0.022563
NM_001085492	Rere	chr4:150281915-150621966	-0.73275	0.001451
NM_001025388	Eno1b	chr4:150237196-150248873	1.02201	0.001451
NM_028713	Rftn2	chr1:55170159-55226782	-0.97699	0.001451
NM_178615	Rgmb	chr17:15806252-15826586	-0.59034	0.001451
NM_001291210	Rgs19	chr2:181688418-181693977	-1.74472	0.048168
NM_139228	Rhbdl3	chr11:80300911-80355986	-0.73955	0.001451
NM_007483	Rhob	chr12:8497758-8499985	0.984946	0.001451
NM_182929	Rims3	chr4:120877868-120891560	0.690133	0.016521
NM_009066	Ring1	chr17:34020791-34024680	0.677998	0.002615
NR_001460	Rmrp	chr4:43492784-43493059	0.839268	0.001451
NR_046233	Rn45s	chr17:39842996-39848829	1.4549	0.001451
NM_207623	Rnf138	chr18:21001299-21028224	0.7866	0.006305
NR_004432	Rnu12	chr15:83149644-83149794	0.767094	0.001451
NM_013845	Ror1	chr4:100095790-100442545	-1.5786	0.001451
NM_016738	Rpl13	chr8:123102349-123105242	-0.64125	0.001451
NM_025586	Rpl15	chr14:18267822-18270986	-0.59677	0.001451
NM_009077	Rpl18	chr7:45718070-45720835	0.833382	0.001451
NM_026517	Rpl22l1	chr3:28805510-28807415	-0.66835	0.001451
NM_022891	Rpl23	chr11:97777525-97782439	0.721106	0.001451
NM_025592	Rpl35	chr2:38998308-39005131	1.50758	0.001451

NM_018730	Rpl36	chr17:56613394-56614246	1.89609	0.017111
NM_019865	Rpl36a	chrX:134585653-134588062	1.54295	0.041324
NM_001271590	Rpl37rt	chr5:115102921-115110268	0.779787	0.010258
NM_001048057	Rpl38	chr11:114344525-114757886	2.22584	0.014681
NM_023372	Rpl38	chr11:114344525-114757886	1.28024	0.026333
NM_016980	Rpl5	chr5:107900527-107987077	-0.69064	0.001451
NM_011290	Rpl6	chr5:121204500-121209241	1.13705	0.001451
NM_018853	Rplp1	chr9:61913282-61914510	1.50091	0.001451
NM_026020	Rplp2	chr7:141447649-141451342	0.899075	0.001451
NM_026308	Rpp21	chr17:36255672-36257846	-0.66464	0.003645
NR_024198	Rprl3	chr8:3803124-3803361	1.78531	0.001451
NM_025963	Rps10	chr17:27630428-27635242	0.867204	0.005539
NM_025587	Rps21	chr2:180257378-180258444	1.06018	0.001451
NM_013765	Rps26	chr10:128624528-128626506	0.846086	0.001451
NM_016959	Rps3a1	chr3:86137939-86142668	1.02828	0.019402
NM_011300	Rps7	chr12:28630846-28635953	0.917797	0.006305
NM_001039521	Rrn3	chr16:13780698-13814841	-0.70166	0.001451
NM_145620	Rrp9	chr9:106477308-106485415	0.633676	0.001451
NM_028351	Rspo3	chr10:29453106-29535867	-0.87311	0.001451
NM_053076	Rtn3	chr19:7417624-7483291	-0.6637	0.001451
NM_001083807	Rusc1	chr3:89083978-89093363	0.746244	0.045806
NM_016924	Rwdd2b	chr16:87433330-87440592	-0.90352	0.001451
NM_001033288	Sbspon	chr1:15853861-15892722	-1.05281	0.001451
NM_172769	Sc5d	chr9:42254176-42264300	0.599921	0.001451
NM_133199	Scn4a	chr11:106318592-106349390	-0.92056	0.001451
NM_025468	Sec11c	chr18:65800577-65817657	0.659179	0.006305
NM_025483	Senp7	chr16:56075403-56190031	-0.85755	0.001451
NM_028800	Stk40	chr4:126103956-126141029	0.782848	0.001451
NM_144907	Sesn2	chr4:132492806-132510456	0.93953	0.001451
NM_001204875	Set	chr2:30061995-30072577	-0.61497	0.007984
NM_013834	Sfrp1	chr8:23411501-23449632	-0.99608	0.001451
NM_011361	Sgk1	chr10:21882183-21999902	-0.80874	0.001451
NM_019989	Sh3bgrl	chrX:109095406-109162467	-0.68736	0.001451
NM_017400	Sh3gl3	chr7:82259907-82307420	-1.3727	0.003645
NM_001135727	Sh3kbp1	chrX:159627271-159975920	-0.67971	0.001451
NM_001033415	Shisa3	chr5:67607882-67613987	1.0298	0.001451
NM_001034874	Shisa6	chr11:66211724-66526126	-0.65868	0.001451
NM_011382	Six4	chr12:73100258-73113245	-0.61242	0.014141
NM_028151	Skiv2l2	chr13:112800776-112927380	-1.71634	0.001451
NM_009197	Slc16a2	chrX:103697413-103821988	-0.65199	0.001451
NM_001033167	Slc22a23	chr13:34179157-34345182	-0.65022	0.001451

NM_020520	Slc25a20	chr9:108662097-108684641	-0.60862	0.026781
NM_025877	Slc25a23	chr17:57043710-57059863	-0.6546	0.001451
NM_011989	Slc27a4	chr2:29802679-29817522	-0.58183	0.002615
NM_146257	Slc29a4	chr5:142702100-142722490	1.04559	0.001451
NM_172659	Slc2a6	chr2:27021364-27027998	0.777258	0.043378
NM_001033286	Slc30a10	chr1:185447115-185468761	-0.63632	0.038705
NM_177732	Slc35d1	chr4:103171717-103214884	-0.63582	0.038244
NM_029529	Slc35d3	chr10:19847916-19851459	0.705233	0.001451
NM_153142	Slc35e4	chr11:3907021-3914664	0.752319	0.022043
NM_001101483	Slc35g2	chr9:100552187-100571085	-1.65674	0.001451
NM_172479	Slc38a5	chrX:8271380-8280176	-0.69201	0.04692
NM_001135150	Slc39a8	chr3:135825278-135888572	-0.67724	0.041324
NM_008577	Slc3a2	chr19:8706881-8723369	0.727574	0.001451
NM_177388	Slc41a2	chr10:83231138-83337817	-0.6261	0.001451
NM_001177628	Slc45a3	chr1:131962914-131982972	-0.82108	0.001451
NM_027872	Slc46a3	chr5:147878440-147894802	-0.58904	0.003645
NM_053248	Slc5a5	chr8:70882888-70892757	1.6118	0.010258
NM_178703	Slc6a1	chr6:114282634-114317525	-0.85411	0.001451
NM_008135	Slc6a9	chr4:117835257-117872470	0.753468	0.002615
NM_011404	Slc7a5	chr8:121881145-121907686	0.908661	0.001451
NM_177353	Slc9a7	chrX:20105754-20291764	-0.82088	0.014681
NM_001161431	Slitrk2	chrX:66649317-66661402	1.08592	0.024857
NM_198864	Slitrk3	chr3:73048124-73056943	1.80073	0.001451
NM_025891	Smarcd3	chr5:24592621-24602002	-0.95324	0.031073
NM_020618	Smarce1	chr11:99209047-99231017	-0.62992	0.001451
NM_133214	Smco4	chr9:15505494-15545259	-0.84828	0.006305
NM_138743	Smim11	chr16:92301302-92313041	-0.58627	0.031973
NM_027885	Smug1	chr15:103153289-103163284	-0.63976	0.001451
NR_027059	Snhg20	chr11:117076782-117078955	1.20416	0.001451
NR_003270	Snhg3	chr4:132351932-132353686	0.669058	0.001451
NR_024068	Snhg7	chr2:26637175-26640244	0.673014	0.001451
NR_028078	Snora21	chr11:97777525-97782439	2.09124	0.001451
NR_002897	Snora64	chr17:24720062-24721927	1.22966	0.001451
NR_002899	Snora70	chrX:74270815-74273135	1.93401	0.001451
NR_004445	Snord22	chr19:8723486-8726326	0.809997	0.026781
NR_002898	Snora65	chr2:32961711-32964045	3.85619	0.001451
NM_001291077	Snph	chr2:151590548-151632593	-0.7538	0.012253
NM_027246	Snrpf	chr10:93540631-93605245	0.599943	0.023918
NM_172951	Sntg2	chr12:30174556-30373375	-1.14183	0.001451
NM_029655	Snx7	chr3:117781496-117868936	-0.89998	0.031973
NM_175407	Sobp	chr10:43002499-43174530	-0.67377	0.003645

NM_172752	Sorbs2	chr8:45507787-45827906	-1.40107	0.007984
NM_009233	Sox1	chr8:12385770-12436732	-0.82657	0.001451
NM_011440	Sox14	chr9:99874105-99876170	-1.41483	0.001451
NM_011448	Sox9	chr11:112782209-112787757	-0.67911	0.002615
NM_001033277	Spryd3	chr15:102116527-102136215	0.852993	0.001451
NM_029035	Spsb1	chr4:149896283-149955006	0.671107	0.028252
NM_013675	Sptb	chr12:76580487-76710547	-0.6252	0.014681
NM_177710	Ssh2	chr11:77216424-77460219	-0.91432	0.014681
NM_020491	Sssca1	chr19:5730305-5731732	0.650989	0.011607
NM_138744	Ssx2ip	chr3:146404641-146440137	1.1569	0.001451
NM_001252505	St6gal1	chr16:23224739-23360350	-1.29952	0.001451
NM_011491	Stc2	chr11:31359440-31370061	0.598009	0.001451
NM_011505	Stxbp4	chr11:90476492-90638108	-0.67637	0.001451
NM_001198565	Sulf1	chr1:12692429-12860372	-0.74488	0.001451
NM_178652	Supt3	chr17:44495986-45119284	-0.61936	0.009538
NM_201639	Synm	chr7:67730160-67759742	-1.12886	0.010258
NM_021441	Taf1c	chr8:119575234-119605240	0.650325	0.009538
NM_145968	Tagap	chr17:7925999-7934897	-0.59555	0.014141
NM_178598	Tagln2	chr1:172500245-172507375	0.652271	0.001451
NM_009317	Tal2	chr4:53779704-53786885	-0.92345	0.001451
NM_001111304	Tbc1d9	chr8:83165351-83272940	0.817801	0.001451
NM_134023	Tbc1d10a	chr11:4186832-4215505	0.636033	0.007175
NM_146236	Tceal1	chrX:136708064-136709866	0.638177	0.023918
NM_013736	Tceb3	chr4:136003369-136021649	-0.67177	0.001451
NM_183289	Tcerg1l	chr7:138208971-138397730	-0.79542	0.041698
NM_001253862	Tcf12	chr9:71844251-72111819	-0.67644	0.002615
NM_001083967	Tcf4	chr18:69344491-69687967	-0.66943	0.049405
NM_133986	Tcta	chr9:108302957-108305951	0.674032	0.012253
NM_001166585	Tead1	chr7:112679319-112906805	-0.6288	0.001451
NM_029464	Tex26	chr5:149439705-149470620	-0.59801	0.009538
NM_001113417	Thrb	chr14:17660959-18038088	-0.69475	0.001451
NM_001164805	Thsd7a	chr6:12311607-12749253	-0.98561	0.001451
NM_178646	Tigd5	chr15:75909734-75914535	0.782431	0.002615
NM_013895	Timm13	chr10:80879815-80900969	0.720606	0.001451
NM_011904	Tll2	chr19:41083980-41206774	-1.18843	0.001451
NM_145439	Tmc6	chr11:117765984-117780683	0.619196	0.004643
NM_028876	Tmed5	chr5:108121646-108132591	0.583891	0.001451
NM_153776	Tmem121	chr12:113185902-113189522	0.975739	0.034184
NM_026734	Tmem126b	chr7:90468828-90475995	0.663002	0.001451
NM_177735	Tmem130	chr5:144735914-144761578	-1.05168	0.009538
NM_001034863	Tmem136	chr9:43108652-43116570	-0.58431	0.007175

NM_183311	Tmem145	chr7:25306107-25316195	-0.87128	0.014141
NM_026938	Tmem160	chr7:16452778-16455490	0.935306	0.001451
NM_177592	Tmem164	chrX:142681399-142843494	-0.69429	0.001451
NM_025781	Tmem170	chr8:111864897-111876675	-0.61717	0.001451
NM_001142647	Nemp2	chr1:52630704-52651919	-0.81575	0.043705
NM_029881	Tmem200a	chr10:25991185-26079447	-0.66308	0.001451
NM_177344	Tmem203	chr2:25255438-25256352	0.729464	0.034591
NM_001304267	Tmem265	chr7:127561222-127565270	-0.71667	0.004643
NM_028053	Tmem38b	chr4:53826044-53862018	-0.90875	0.001451
NM_025284	Tmsb10	chr6:72957346-72958748	0.838554	0.001451
NM_001164155	Tnfrsf19	chr14:60963833-61046855	-0.9432	0.001451
NM_013869	Tnfrsf19	chr14:60963833-61046855	-1.4039	0.001451
NM_011613	Tnfsf11	chr14:78277445-78308043	0.87577	0.001451
NM_001163007	Tnik	chr3:28263213-28670585	-0.65381	0.013563
NM_001081260	Tnks1bp1	chr2:85050459-85073048	0.6225	0.001451
NM_144812	Tnrc6b	chr15:80711312-80941086	-0.93631	0.030178
NM_024214	Tomm20	chr8:126930663-126945921	-0.58939	0.001451
NM_016871	Tomm40	chr7:19701312-19715429	0.764291	0.001451
NM_009423	Traf4	chr11:78158422-78165550	0.704985	0.001451
NM_146140	Tram1l1	chr3:124321036-124323260	-1.05287	0.007175
NM_175093	Trib3	chr2:152337424-152344060	1.29086	0.001451
NM_053166	Trim7	chr11:48826137-48850195	1.02485	0.001451
NM_001024920	Trp53i13	chr11:77508098-77513273	1.09228	0.024857
NM_010286	Tsc22d3	chrX:140539528-140600522	1.54305	0.001451
NM_183180	Tspan18	chr2:93201759-93334487	-0.6342	0.031073
NM_030203	Tspyl4	chr10:34297420-34301320	0.683652	0.001451
NM_028341	Ttc39c	chr18:12643532-12737052	-0.69344	0.001451
NM_023279	Tubb3	chr8:123411563-123422010	1.19427	0.001451
NM_009450	Tubb2a	chr13:34074279-34078008	1.19477	0.001451
NM_001145162	Ube2ql1	chr13:69702831-69739897	-1.00183	0.003645
NM_011670	Uchl1	chr5:66626494-66687234	0.917756	0.001451
NM_001029873	Unc13a	chr8:71626711-71671757	0.646161	0.001451
NM_145628	Usp11	chrX:20703908-20720539	-0.67403	0.001451
NM_009482	Utf1	chr7:139943855-139945112	1.24914	0.001451
NM_020505	Vav3	chr3:109340682-109685694	-0.64204	0.015282
NM_001039385	Vgf	chr5:137030294-137033351	1.88523	0.046147
NM_011701	Vim	chr2:13574310-13582826	0.85631	0.001451
NM_146168	Vopp1	chr6:57752263-57825125	-0.64819	0.001451
NM_027906	Vwa8	chr14:78849177-79202310	-0.63111	0.04692
NM_001159527	Wdr35	chr12:8974000-9028847	-0.63148	0.001451
NM_146254	Wdr78	chr4:103038064-103114299	-0.65795	0.020957

NM_001163766	Wdr90	chr17:25838837-25861515	0.619682	0.005539
NM_001037927	Wdr93	chr7:79743162-79785950	-0.68421	0.013563
NM_011716	Wfs1	chr5:36966103-36988982	0.587721	0.014141
NM_026582	Wls	chr3:159839694-159935175	-0.6339	0.001451
NM_009290	Wnt8a	chr18:34542327-34548061	-1.10869	0.001451
NM_177618	Wscd1	chr11:71750702-71789646	-0.66894	0.006305
NM_023500	Xk	chrX:9272783-9313245	-0.83567	0.001451
NM_026940	Ydjc	chr16:17139063-17148857	0.754508	0.015282
NM_023871	Set	chr2:30061995-30072577	0.944805	0.04735
NM_001098723	Yy2	chrX:157547821-157598715	0.939965	0.001451
NM_181412	Zbed4	chr15:88751710-88784516	-0.66661	0.001451
NM_001098237	Zbtb3	chr19:8802495-8804854	0.828871	0.021454
NM_001034907	Zc3h12b	chrX:95711677-95927970	-0.77707	0.034184
NM_172467	Zc3hav1l	chr6:38287393-38299259	-0.98878	0.001451
NM_028673	Zdbf2	chr1:63182570-63314575	-1.37526	0.038705
NM_175358	Zdhhc15	chrX:104536969-104671064	-0.69514	0.001451
NM_007496	Zfhx3	chr8:108714643-108961636	0.668829	0.001451
NM_030708	Zfhx4	chr3:5177823-5415855	-0.86143	0.001451
NM_172918	Zfp317	chr9:19622090-19649731	-0.60932	0.001451
NM_172794	Zfp454	chr11:50872722-50887443	-0.58575	0.006305
NM_024215	Zfp593	chr4:134243305-134245873	0.587058	0.003645
NM_201609	Zfp652	chr11:95749066-95764713	-0.73182	0.001451
NM_026521	Zfp706	chr15:36997026-37007402	-0.66711	0.001451
NM_177747	Zfp711	chrX:112600525-112635062	0.589761	0.024857
NM_001002008	Zfp948	chr17:21567045-21588682	0.609054	0.001451
NM_009569	Zfpm1	chr8:122282140-122337247	1.00165	0.002615
NM_001145778	Zkscan3	chr13:21387003-21402755	-0.92365	0.043017
NM_001081329	Zkscan2	chr7:123478638-123500449	-1.07394	0.001451
NM_009517	Zmat3	chr3:32334793-32367438	-0.64369	0.001451
NM_177086	Zmat4	chr8:23669660-24063116	-0.71334	0.008818
NM_013859	Znhit2	chr19:6061206-6062468	0.745141	0.025833
NM_001290819	Zscan29	chr2:121158272-121171125	-0.61533	0.030178
NM_172503	Zswim4	chr8:84210941-84237042	0.618329	0.001451
NM_001029912	Zswim5	chr4:116877401-116989105	-0.71061	0.001451
NM_001167936	Zyg11a	chr4:108181933-108217922	-1.18457	0.001451

Table 9.1: List of statistically significant changes in annotated genes following *Skiv2l2* knockdown in P19 cells. Cuffdiff results in were filtered based on log2(fold_change) , denoted as M in table, and q-value (q in table). Annotated genes with M greater than .58 and q less than .05 were considered elevated. Annotated genes with M less than -.58 and q less than .05 were considered downregulated.

9.2 Intergenic transcripts dysregulated following *Skiv2l2* knockdown in P19 cells

gene	locus	log2(fold_change)	q_value
-	chr1:72236944-72284314	-6.92682	0.001103
-	chr4:85940115-85940936	-2.83531	0.045344
-	chr12:74331503-74332640	-2.0956	0.038943
-	chr2:16759633-16761414	-1.99871	0.03405
-	chr2:26245805-26249369	-1.88393	0.001103
-	chr18:49795350-49796733	-1.85991	0.002761
-	chr17:27422387-27513691	-1.77807	0.021093
-	chr1:121548071-121549638	-1.63827	0.018943
-	chr19:23199179-23200177	-1.59595	0.029356
-	chr5:76699048-76700997	-1.55665	0.003497
-	chrX:135909349-135911190	-1.52527	0.015721
-	chr9:13536467-13537932	-1.41724	0.048434
-	chr5:104802304-104807950	-1.40667	0.03405
-	chrX:101462310-101465148	-1.38315	0.004143
-	chr3:83357207-83359846	-1.34998	0.005924
-	chr18:7338138-7339976	-1.31332	0.036002
-	chr2:78927085-78928702	-1.3122	0.030571
-	chr4:136137200-136138729	-1.30077	0.026277
-	chr15:43783713-43786070	-1.26752	0.012039
-	chrX:81100675-81104325	-1.24812	0.004143
-	chr14:67671034-67672764	-1.22511	0.028115
-	chr13:115103375-115105227	-1.18968	0.043906
-	chr3:83238886-83300566	-1.17063	0.003497
-	chr7:59933198-59935315	-1.1705	0.01449
-	chr4:85869533-85871458	-1.12941	0.045635
-	chr1:93985685-93986178	-1.12677	0.040415
-	chr8:112916362-112921968	-1.12226	0.001103
-	chr9:13312678-13324261	-1.11505	0.001103
-	chr11:110516272-110523201	-1.11125	0.001103
-	chr8:20122306-20151685	-1.08932	0.001103
-	chr5:76704312-76707514	-1.08093	0.009141
-	chr8:89045569-89058258	-1.07925	0.001103
-	chr9:13498556-13503668	-1.05382	0.001103
-	chr5:58961128-58966274	-1.0289	0.001103
-	chr14:77819895-77823557	-1.02431	0.015296
-	chr5:76691303-76695019	-1.00875	0.004143

-	chr9:13453656-13463172	-1.00843	0.001103
-	chr17:75532137-75533053	-1.00482	0.033584
-	chr8:106867719-106870016	-1.00381	0.030839
-	chr6:28211588-28215374	-0.99831	0.003497
-	chr3:121823467-121827805	-0.995	0.001103
-	chr9:13423504-13427542	-0.99398	0.001103
-	chr9:13463643-13498457	-0.98166	0.001103
-	chr2:40557003-40557434	-0.97903	0.001103
-	chr6:90963979-90967574	-0.97659	0.020393
-	chr3:65393577-65396208	-0.97571	0.006501
-	chr1:17768830-17770890	-0.95537	0.038943
-	chr7:92839891-92843766	-0.95122	0.005364
-	chr5:109684721-109685869	-0.94966	0.047876
-	chr12:57498187-57499932	-0.93885	0.047044
-	chr14:18547759-18550506	-0.93634	0.018213
-	chr8:71823610-71842466	-0.91466	0.020734
-	chr8:112937820-112939230	-0.91045	0.045814
-	chr4:149143232-149143466	-0.9019	0.001103
-	chr15:59210894-59211169	-0.88609	0.001103
-	chr1:156424388-156425255	-0.88359	0.001103
-	chr9:32089863-32093108	-0.87011	0.0218
-	chr7:80706451-80709499	-0.85699	0.037903
-	chr1:59713908-59715219	-0.85512	0.001984
-	chr9:13296683-13312443	-0.85346	0.001103
-	chr5:58958633-58961039	-0.8479	0.022171
-	chr16:9567915-9571718	-0.83249	0.001984
-	chr5:58980552-58985853	-0.82958	0.001103
-	chr1:130232372-130253622	-0.82721	0.001103
-	chr13:119613525-119617644	-0.82568	0.001103
-	chr5:58974101-58980419	-0.82343	0.001103
-	chr7:39588901-39591534	-0.82267	0.008667
-	chr9:32074244-32076527	-0.82168	0.031428
-	chrX:134724023-134729224	-0.8089	0.002761
-	chr8:112939686-112944777	-0.80167	0.006501
-	chr3:121829800-121831333	-0.79054	0.013733
-	chr3:101306401-101307192	-0.78318	0.001984
-	chr11:17095521-17095680	-0.78278	0.030839
-	chr9:94541206-94546397	-0.75561	0.003497
-	chr9:92214270-92218587	-0.75489	0.001103
-	chr14:49678669-49679686	-0.75445	0.032233
-	chr18:63543929-63544365	-0.74615	0.001103

-	chr5:76684917-76690903	-0.73507	0.008178
-	chr17:15826638-15830661	-0.70561	0.001103
-	chr3:96460501-96467513	-0.70027	0.022438
-	chr5:76658199-76662815	-0.68756	0.013733
-	chr13:106475760-106476824	-0.67866	0.034803
-	chr8:71520119-71525693	-0.67819	0.047044
-	chrX:61405480-61412540	-0.67624	0.01449
-	chr15:31627162-31630305	-0.6725	0.046815
-	chr7:39570671-39573988	-0.67168	0.005924
-	chr3:121833340-121836420	-0.66939	0.002761
-	chr5:76665484-76670185	-0.65429	0.025296
-	chr9:123930060-123934453	-0.63462	0.001103
-	chr6:76284241-76284931	-0.6302	0.016151
-	chr14:49674364-49678586	-0.62442	0.009618
-	chr10:35710554-35711559	-0.6171	0.012039
-	chr12:52570588-52572261	-0.61553	0.03674
-	chr3:104933331-104940758	-0.61469	0.020734
-	chr14:18494286-18514427	-0.61289	0.001103
-	chr3:49185483-49190564	-0.60892	0.039831
-	chr4:85424804-85429767	-0.60717	0.032517
-	chr9:7214760-7221282	-0.60148	0.004143
-	chr9:32058967-32067138	-0.6002	0.007069
-	chr3:49381283-49382579	0.582099	0.004796
-	chr6:122761082-122764642	0.587207	0.03115
-	chr13:83832510-83833263	0.595626	0.001103
-	chr17:17345127-17346199	0.595902	0.001103
-	chrX:60045344-60045916	0.597235	0.044427
-	chr10:37139015-37151953	0.601783	0.029046
-	chr4:122008647-122009473	0.601995	0.001103
-	chr11:120762888-120763212	0.605785	0.001103
-	chr14:52368853-52369291	0.607691	0.027894
-	chr12:4782169-4783512	0.608779	0.005924
-	chr6:35926705-35927122	0.612033	0.032517
-	chr3:19881415-19881726	0.612894	0.018943
-	chr2:36807782-36808427	0.616275	0.001103
-	chr19:57403408-57404282	0.618511	0.009141
-	chrX:109389964-109390256	0.620435	0.007069
-	chr4:100567402-100568050	0.623381	0.002761
-	chr2:146834469-146839495	0.62509	0.016554
-	chr6:49218295-49222769	0.626367	0.019707
-	chr16:4880716-4884302	0.633972	0.01449

-	chr7:134660320-134660740	0.638849	0.007637
-	chr8:72156277-72160764	0.642191	0.019707
-	chr1:128520905-128521404	0.64267	0.001103
-	chr7:134661760-134662000	0.64679	0.030571
-	chr6:92087615-92091251	0.648465	0.032233
-	chr1:181282073-181282912	0.649351	0.040675
-	chr18:34954681-34957188	0.651491	0.001103
-	chr4:53791077-53791468	0.653268	0.001103
-	chr19:11958748-11958905	0.666639	0.019707
-	chr3:124385623-124385990	0.667669	0.001103
-	chrX:146599586-146601125	0.673414	0.014135
-	chr11:76600994-76601925	0.673721	0.001103
-	chrX:78856929-78857804	0.677579	0.035407
-	chr3:104752376-104752998	0.680913	0.001103
-	chr4:69854089-69854836	0.680928	0.025626
-	chr5:149660644-149661013	0.683345	0.001984
-	chr6:37805989-37807095	0.687369	0.025626
-	chr8:47675390-47685496	0.688199	0.043172
-	chr3:69314890-69316584	0.691437	0.046815
-	chr19:6152712-6153266	0.69182	0.013733
-	chr17:20661629-20662057	0.691874	0.008178
-	chr12:91590556-91592870	0.69331	0.028719
-	chr8:129263839-129265809	0.694904	0.045635
-	chr13:98613716-98614161	0.699812	0.009141
-	chr15:44282987-44284079	0.704103	0.001103
-	chr12:56189959-56190128	0.704297	0.03586
-	chr14:84758553-84758873	0.707711	0.006501
-	chr6:58017484-58017969	0.710819	0.001103
-	chr2:126677939-126679116	0.717697	0.042045
-	chr17:30576559-30579668	0.7244	0.014135
-	chr1:29737216-29737702	0.72486	0.024679
-	chr7:115172172-115172379	0.725564	0.001103
-	chr17:32852763-32852954	0.736313	0.001103
-	chr14:50978540-50978895	0.736734	0.011101
-	chrX:106283350-106284768	0.738619	0.044185
-	chr5:27860594-27861055	0.739064	0.026681
-	chr7:80990245-80992973	0.74085	0.022438
-	chr6:37686014-37686290	0.744235	0.001103
-	chr15:31531372-31534284	0.744263	0.009141
-	chr15:102397928-102401258	0.748521	0.002761
-	chr2:130284503-130288768	0.754375	0.028447

-	chr11:79336194-79339426	0.754526	0.03674
-	chr6:38545281-38545908	0.755505	0.032038
-	chr11:99932294-99933264	0.75727	0.001103
-	chr19:28773052-28773589	0.760004	0.017014
-	chr8:70010114-70011031	0.760958	0.001103
-	chr11:97188563-97191354	0.764144	0.001103
-	chr4:116874045-116876640	0.764429	0.005364
-	chr1:33100883-33101266	0.765155	0.034602
-	chr1:178299351-178299904	0.769144	0.004143
-	chr1:180814319-180817544	0.775863	0.040096
-	chrX:8038794-8039017	0.777078	0.001103
-	chr4:57956584-57966928	0.77927	0.049884
-	chr1:78783634-78784302	0.782275	0.001103
-	chr11:97884545-97885542	0.783795	0.001103
-	chr7:19226501-19228107	0.783818	0.036002
-	chr8:83477343-83477770	0.784305	0.001984
-	chr6:96032931-96033332	0.788598	0.001103
-	chr1:79957562-79958058	0.788979	0.005924
-	chr11:53300595-53301799	0.791706	0.040222
-	chr12:85453890-85455157	0.793197	0.03586
-	chr7:110059904-110061607	0.794218	0.029954
-	chr11:96007457-96012039	0.79518	0.001103
-	chr12:56373556-56373869	0.796783	0.001103
-	chr4:149457291-149457852	0.79813	0.001984
-	chr5:85963078-85966779	0.798534	0.023465
-	chr1:78967610-78968098	0.809539	0.042334
-	chr4:135853337-135855843	0.809789	0.036002
-	chr18:28188650-28189061	0.813861	0.001103
-	chr2:87563376-87563645	0.814539	0.009618
-	chr3:88509105-88510073	0.815134	0.03674
-	chr6:47431790-47433141	0.816384	0.012908
-	chr4:10439478-10439792	0.818542	0.001103
-	chr17:91547931-91548551	0.819418	0.033016
-	chr10:14567222-14567341	0.820002	0.009141
-	chr14:54424698-54426858	0.820402	0.005364
-	chr17:79933462-79933701	0.820839	0.001103
-	chr19:50030164-50030612	0.823044	0.001103
-	chr5:38561891-38564881	0.823637	0.006501
-	chr1:78784403-78784799	0.82591	0.007637
-	chr11:94160605-94162156	0.830475	0.020035
-	chr15:38990482-38990769	0.831446	0.030839

-	chr11:6476186-6478362	0.83382	0.018586
-	chr11:98200988-98202892	0.844757	0.032233
-	chr7:110119815-110121754	0.846933	0.029954
-	chr14:62540896-62541547	0.847845	0.001103
-	chr12:54622805-54623144	0.848247	0.001103
-	chr2:154087641-154087874	0.850868	0.002761
-	chr19:15193544-15194002	0.852217	0.001103
-	chr8:124949677-124951899	0.853062	0.044906
-	chr1:118387285-118388886	0.854728	0.009618
-	chr3:8563992-8566074	0.856383	0.027894
-	chr4:132272650-132274306	0.859961	0.028447
-	chr13:23529814-23530941	0.861986	0.033309
-	chr13:21720353-21721761	0.862479	0.04255
-	chr4:143671324-143671672	0.862625	0.012908
-	chr12:118302313-118307366	0.863562	0.001103
-	chr5:121546027-121549607	0.864746	0.014135
-	chr1:30949887-30952025	0.871771	0.032737
-	chr9:91402241-91403376	0.872392	0.001103
-	chr3:88522500-88531570	0.872699	0.02598
-	chr4:72542665-72543083	0.872842	0.022438
-	chr4:23517074-23517823	0.873314	0.048434
-	chr8:117156178-117157862	0.875816	0.040952
-	chr16:90284802-90286988	0.876603	0.013733
-	chr2:14056240-14058576	0.88131	0.0218
-	chr4:152156395-152156612	0.885776	0.029356
-	chr6:149140806-149141380	0.886837	0.037903
-	chr3:63170961-63171433	0.886943	0.01449
-	chr6:57485120-57665279	0.88882	0.001103
-	chr2:30159495-30159797	0.890694	0.011617
-	chr11:6781545-6782784	0.8924	0.012908
-	chr8:43289826-43290037	0.895211	0.001103
-	chr1:4688598-4689239	0.895662	0.001103
-	chr17:88070051-88073616	0.904108	0.008178
-	chr11:58067815-58069226	0.909327	0.04255
-	chr11:49712809-49715102	0.91156	0.011617
-	chr17:88066343-88069956	0.913303	0.001984
-	chr13:54499578-54499776	0.913793	0.001103
-	chr17:19422529-19422788	0.91421	0.009141
-	chrX:106281680-106282184	0.915294	0.011101
-	chr13:3139642-3140129	0.916118	0.001103
-	chr8:122841659-122841957	0.919063	0.039831

-	chr16:91513441-91513856	0.919722	0.014135
-	chr13:12679783-12680238	0.926215	0.001984
-	chr4:106908590-106911005	0.926389	0.004143
-	chr1:86486191-86487543	0.927312	0.040096
-	chr6:47787711-47788178	0.928957	0.008667
-	chr2:152399057-152400554	0.930795	0.043645
-	chr15:53346495-53348130	0.93085	0.037676
-	chr7:16399041-16400509	0.930884	0.03405
-	chr5:126025715-126026426	0.937069	0.023465
-	chr11:3193860-3202292	0.937896	0.001103
-	chr1:134093208-134094469	0.940171	0.010606
-	chr2:34769166-34771738	0.941337	0.013321
-	chr11:23304164-23306308	0.943051	0.008667
-	chr5:22471639-22472997	0.944528	0.001984
-	chr12:17346391-17348382	0.94485	0.031734
-	chr4:31961338-31963815	0.946377	0.001984
-	chr11:120633750-120634988	0.946748	0.003497
-	chr2:24179662-24179843	0.947308	0.004143
-	chr1:28800232-28800552	0.949103	0.043172
-	chr12:100744499-100744985	0.951354	0.001103
-	chr14:19985964-19988177	0.952156	0.04114
-	chr7:19318072-19320029	0.954358	0.002761
-	chr17:82539233-82539425	0.955557	0.03674
-	chrX:156442424-156442581	0.956942	0.001103
-	chr10:84308937-84309299	0.959166	0.001103
-	chr5:97822027-97839374	0.959793	0.017855
-	chr1:160213026-160214968	0.95988	0.001984
-	chr19:12796232-12797571	0.96063	0.025626
-	chr6:120663356-120665481	0.962747	0.027894
-	chr12:85374805-85376358	0.968673	0.012501
-	chr9:79760920-79761460	0.974468	0.002761
-	chr12:88334537-88334925	0.975405	0.037349
-	chr11:50325914-50329688	0.980412	0.001103
-	chr14:20641118-20643947	0.981322	0.001984
-	chr16:17734411-17734627	0.981753	0.001103
-	chr5:44405838-44406559	0.990446	0.001103
-	chr2:119477894-119478827	0.992611	0.040096
-	chr17:88856107-88856318	0.996236	0.033016
-	chr4:44234325-44237030	1.00176	0.024679
-	chr15:5464194-5464368	1.00261	0.012039
-	chr6:113045203-113046162	1.00306	0.038161

-	chr13:25582999-25583219	1.00563	0.001103
-	chr7:59225871-59228605	1.00584	0.001103
-	chr11:20332940-20334428	1.00592	0.024976
-	chr4:93544950-93545059	1.00594	0.03586
-	chr4:148590250-148591243	1.00708	0.01449
-	chr2:129378391-129378632	1.00819	0.034602
-	chr6:122341035-122341935	1.01015	0.005924
-	chr5:44226796-44243546	1.01269	0.009141
-	chr12:109528890-109530686	1.01747	0.022171
-	chr3:89963453-89966361	1.01812	0.004796
-	chr10:128057482-128058749	1.01851	0.033779
-	chr11:96830212-96831476	1.01924	0.026277
-	chr2:25356461-25357956	1.01944	0.03702
-	chr6:49215702-49217959	1.02088	0.001103
-	chr2:4700288-4700585	1.0217	0.001103
-	chr3:20055350-20057679	1.02486	0.020734
-	chr5:34572287-34573423	1.02883	0.042334
-	chr2:12082984-12083378	1.02887	0.001103
-	chr17:24469536-24470313	1.03428	0.013733
-	chr19:23136154-23138657	1.0354	0.001103
-	chr12:25125125-25126373	1.03624	0.0273
-	chr7:29930814-29965711	1.03671	0.019362
-	chr2:68830993-68831177	1.03992	0.001103
-	chr14:29962413-29968171	1.04022	0.001103
-	chr8:97164402-97164758	1.04299	0.011617
-	chr4:46389535-46390612	1.04328	0.034803
-	chr8:70897593-70899324	1.04389	0.018586
-	chr2:73892954-73893980	1.04591	0.022438
-	chr3:145650069-145653316	1.04685	0.035407
-	chr13:23745668-23746524	1.04964	0.017855
-	chr6:128759970-128760816	1.05321	0.043172
-	chr12:112829723-112831009	1.05444	0.012501
-	chr12:25099670-25100760	1.05544	0.001103
-	chr4:11484505-11484932	1.06036	0.003497
-	chr18:10262478-10262663	1.06065	0.001103
-	chr13:63812854-63815128	1.06097	0.005364
-	chr13:98489476-98489815	1.06289	0.001103
-	chr8:35053276-35053454	1.06295	0.004796
-	chr12:100185542-100187488	1.065	0.001103
-	chr14:52369468-52369869	1.066	0.001103
-	chr2:129379125-129379332	1.06677	0.001103

-	chr5:125393209-125394451	1.06789	0.001103
-	chr11:98025471-98026643	1.0746	0.033309
-	chr4:10438710-10439017	1.07754	0.001103
-	chr6:70328013-70328194	1.0784	0.008667
-	chr8:121850150-121852644	1.08195	0.005364
-	chr18:24020906-24022155	1.08523	0.026277
-	chr19:5846023-5846482	1.08623	0.035667
-	chr2:22894325-22895394	1.08718	0.040222
-	chr11:20541122-20542526	1.08774	0.026277
-	chr1:133129861-133131057	1.08915	0.018213
-	chr4:48041128-48042901	1.09407	0.014135
-	chr1:159229837-159231748	1.09417	0.030571
-	chr2:157566486-157568177	1.09508	0.01449
-	chr9:62339512-62340953	1.09628	0.042334
-	chr8:120101771-120105300	1.09884	0.001103
-	chr8:6937971-6939941	1.10194	0.030839
-	chr19:32754613-32755989	1.10248	0.035407
-	chr3:138578274-138578480	1.10514	0.001103
-	chr19:5400229-5401494	1.10783	0.001103
-	chr9:77910954-77913008	1.10865	0.001984
-	chrX:11683921-11684080	1.10904	0.001103
-	chr11:52347846-52358700	1.11104	0.024679
-	chr5:93390553-93391060	1.11135	0.019707
-	chr15:98968808-98970319	1.11231	0.018943
-	chr1:86502438-86504056	1.11288	0.01449
-	chr15:96643094-96644256	1.11349	0.019707
-	chr15:59645894-59648071	1.11529	0.001103
-	chr15:86212961-86214357	1.11592	0.001103
-	chr10:116582101-116583644	1.11637	0.001984
-	chr18:66491581-66491873	1.1229	0.001984
-	chr12:32819134-32820061	1.12882	0.032233
-	chr4:133814405-133818067	1.13054	0.001103
-	chr18:75767108-75767295	1.13112	0.002761
-	chrUn_GL456359:19943-20394	1.1314	0.043436
-	chr2:25365825-25366428	1.13413	0.006501
-	chr19:5325103-5325761	1.13448	0.032233
-	chr10:7956774-7959886	1.13461	0.016554
-	chr15:3217270-3217485	1.1362	0.001103
-	chr8:75108044-75109314	1.13838	0.021093
-	chr1:134059764-134062648	1.14504	0.006501
-	chr3:157888553-157888902	1.14536	0.001103

-	chr1:71714248-71714422	1.14752	0.001103
-	chr17:34604327-34605721	1.14793	0.035407
-	chr1:44463842-44464291	1.14873	0.001103
-	chrX:89806465-89806715	1.15022	0.006501
-	chr15:45979752-45980025	1.15148	0.001103
-	chr17:25183201-25184437	1.15156	0.001103
-	chr11:62545140-62550979	1.15287	0.001103
-	chrX:13346008-13347851	1.15344	0.004796
-	chr15:96710198-96711822	1.15716	0.049647
-	chr12:76931278-76931901	1.15738	0.009141
-	chr4:11015494-11015883	1.16038	0.0273
-	chr3:128954961-128955124	1.16279	0.009618
-	chr4:115240444-115240671	1.16686	0.001103
-	chr11:75458668-75461398	1.17266	0.001103
-	chrX:120178941-120179109	1.17361	0.001103
-	chr5:105697072-105699772	1.1752	0.001103
-	chr2:168850787-168851045	1.17635	0.034803
-	chr8:4040071-4040371	1.1773	0.001103
-	chr5:137928153-137928435	1.17862	0.001103
-	chr15:95775824-95775965	1.17974	0.019707
-	chr2:34871128-34872979	1.18279	0.004796
-	chr5:132542611-132542864	1.18327	0.048434
-	chr17:35165105-35167474	1.18397	0.001103
-	chr17:4992836-4994106	1.18417	0.016554
-	chr8:12502712-12504370	1.18643	0.033016
-	chr1:74848341-74851814	1.18844	0.003497
-	chr13:34872738-34874361	1.18927	0.025626
-	chr2:27540404-27542005	1.20427	0.017855
-	chr13:8128310-8128700	1.20732	0.009618
-	chr11:88046242-88047241	1.21079	0.003497
-	chr3:122984765-122988331	1.21296	0.001103
-	chr2:39005290-39007991	1.21444	0.001103
-	chr2:125825782-125827116	1.2155	0.043906
-	chr7:111083325-111084931	1.21866	0.008667
-	chr1:134091888-134093017	1.22194	0.048287
-	chr6:38548663-38551237	1.22463	0.004796
-	chr6:47780490-47780885	1.22697	0.030241
-	chr9:72660515-72662155	1.23167	0.005924
-	chr19:36833234-36834122	1.23287	0.011617
-	chr2:34801438-34802217	1.23497	0.001984
-	chr3:88914049-88915269	1.23613	0.03702

-	chr1:177259122-177260696	1.23966	0.028115
-	chr17:24462410-24464543	1.2405	0.001103
-	chr11:102297363-102298663	1.24108	0.021461
-	chr9:108822347-108825179	1.24148	0.001103
-	chr1:146938859-146938982	1.24381	0.020734
-	chr17:37131127-37131345	1.24628	0.001103
-	chr16:16198057-16198222	1.24632	0.001103
-	chr5:34306935-34307226	1.24674	0.018586
-	chr1:10876876-10878406	1.24827	0.032737
-	chr9:96117938-96119196	1.24827	0.03405
-	chr12:106174153-106176220	1.24957	0.024976
-	chr2:146549006-146550386	1.25296	0.017855
-	chr4:106839250-106840027	1.2544	0.03586
-	chr11:11809051-11811288	1.25516	0.001103
-	chr11:69069786-69070727	1.2569	0.036239
-	chr1:43888225-43888419	1.25691	0.001103
-	chr7:73615872-73618176	1.2573	0.001103
-	chr4:127076684-127077226	1.25916	0.001103
-	chr5:57261577-57261711	1.26086	0.001103
-	chr15:3218688-3218895	1.26128	0.001103
-	chr3:157946203-157947205	1.26315	0.033779
-	chr5:113771756-113772424	1.26534	0.005364
-	chr1:58390941-58392724	1.26764	0.003497
-	chr19:6045127-6046399	1.26841	0.003497
-	chr11:33039125-33039696	1.26911	0.001103
-	chr1:10880171-10882321	1.26941	0.044427
-	chr6:148831556-148834106	1.27084	0.001103
-	chr13:5859533-5861133	1.27303	0.001103
-	chr9:123924944-123925311	1.27475	0.005364
-	chr11:85140451-85141471	1.27754	0.032737
-	chr2:22068576-22068938	1.27755	0.019707
-	chr1:152903330-152904699	1.27926	0.003497
-	chr9:53884116-53884468	1.28285	0.002761
-	chr12:19646419-19646575	1.28312	0.023465
-	chrX:153783428-153783538	1.28417	0.001984
-	chr19:28012022-28013167	1.28529	0.028115
-	chrX:77509347-77510607	1.2874	0.007637
-	chr15:98953755-98955023	1.28778	0.024679
-	chr8:18845027-18846147	1.29832	0.039212
-	chr12:20353270-20353384	1.29994	0.020035
-	chr4:118437479-118438771	1.30978	0.032517

-	chr11:74724631-74726418	1.31186	0.004143
-	chr7:144940118-144941475	1.31357	0.023186
-	chr2:136678918-136680030	1.31391	0.001103
-	chr16:46497757-46499278	1.31589	0.023186
-	chr5:33532782-33534404	1.31917	0.023465
-	chr15:48888065-48888180	1.31986	0.002761
-	chr7:19665165-19666743	1.31996	0.002761
-	chr4:40117011-40117138	1.31999	0.025296
-	chr12:86885058-86885861	1.32676	0.049647
-	chr6:117879662-117881237	1.336	0.013321
-	chr2:30717350-30718458	1.33646	0.04943
-	chr3:116424236-116425499	1.337	0.006501
-	chr6:7669591-7671610	1.34104	0.001103
-	chr7:128461954-128462922	1.34201	0.01449
-	chr6:149101752-149102646	1.3435	0.048434
-	chr6:122809889-122811223	1.34374	0.001984
-	chr12:72758192-72760835	1.34719	0.001103
-	chr11:62602461-62602708	1.35021	0.045144
-	chr9:110117700-110120078	1.35104	0.001103
-	chrX:154774625-154774889	1.35163	0.022438
-	chr6:87851226-87852254	1.35283	0.038723
-	chr11:31370294-31371289	1.35288	0.016151
-	chrX:151793695-151793879	1.35411	0.007637
-	chr11:60879090-60879808	1.35756	0.009618
-	chr6:128838780-128839831	1.35877	0.001103
-	chr16:22266095-22267077	1.36069	0.021093
-	chr6:148896419-148898621	1.36121	0.006501
-	chr8:31149344-31149965	1.36142	0.001103
-	chr1:19330964-19331325	1.36619	0.011617
-	chr13:23762631-23763567	1.36641	0.008178
-	chr5:9164834-9165077	1.367	0.001103
-	chr4:150912874-150914277	1.36897	0.017014
-	chr4:137387268-137388382	1.37195	0.001103
-	chr5:33530876-33532729	1.37333	0.008667
-	chr8:71745108-71745665	1.37363	0.030571
-	chr4:132513619-132515513	1.37368	0.002761
-	chr7:45016443-45017361	1.37425	0.022438
-	chr13:68156433-68156597	1.37869	0.003497
-	chr7:109516700-109518979	1.37917	0.001103
-	chrX:60046040-60046246	1.37924	0.010606
-	chr7:14304774-14304976	1.38	0.002761

-	chr5:108311679-108312722	1.38372	0.005924
-	chrX:91886978-91887347	1.38616	0.044906
-	chr15:12203285-12204792	1.38835	0.023465
-	chr4:39895980-39896124	1.38854	0.03586
-	chr18:10262877-10263285	1.39401	0.006501
-	chr9:77909439-77910481	1.39492	0.031734
-	chr14:56811988-56814751	1.39513	0.001103
-	chr15:37007522-37018719	1.39904	0.001103
-	chr19:53521186-53521871	1.40054	0.002761
-	chr5:149219755-149220590	1.40079	0.033584
-	chr4:105374416-105374606	1.40197	0.001103
-	chr1:134454283-134455284	1.40264	0.030839
-	chr8:47714352-47715456	1.40313	0.018213
-	chr5:28069870-28071078	1.40332	0.004143
-	chr10:119240297-119241300	1.40423	0.031734
-	chr18:61553896-61555050	1.40551	0.009618
-	chr4:73498015-73498180	1.40577	0.001103
-	chr5:121709519-121711344	1.40619	0.001103
-	chr6:43766968-43767287	1.41165	0.005364
-	chr3:90291502-90292900	1.41685	0.024679
-	chr5:57461495-57461592	1.41968	0.03586
-	chr3:131469833-131470922	1.41982	0.023186
-	chrX:95966880-95967753	1.42106	0.040222
-	chr19:44387353-44388542	1.42122	0.017855
-	chr4:108999334-109000448	1.42434	0.009141
-	chr8:19536088-19536264	1.42479	0.001103
-	chr6:37686390-37686574	1.42552	0.001103
-	chr6:145338298-145340731	1.42751	0.001103
-	chr18:61537271-61537668	1.42993	0.003497
-	chr8:97876199-97876479	1.43524	0.001103
-	chr8:84190728-84192651	1.43546	0.001103
-	chr6:136804545-136805655	1.43927	0.011101
-	chr11:94677625-94678698	1.43996	0.036555
-	chr9:102494703-102496925	1.44003	0.006501
-	chr13:58668616-58668799	1.4414	0.001103
-	chr15:81521785-81523271	1.44181	0.002761
-	chr2:164305491-164305599	1.44258	0.040952
-	chrX:157598831-157601173	1.4447	0.008178
-	chr12:87765976-87766294	1.4456	0.024679
-	chr10:31249788-31250028	1.44799	0.001103
-	chr5:64801878-64802809	1.44816	0.009141

-	chr2:136677222-136678696	1.45069	0.001984
-	chr8:12439382-12441627	1.45518	0.018213
-	chr2:94158336-94159005	1.4581	0.025296
-	chr15:48889852-48890016	1.4591	0.001103
-	chr15:37170881-37171061	1.46221	0.010123
-	chr5:21056281-21058481	1.46244	0.002761
-	chr2:111183579-111183892	1.46247	0.001984
-	chr18:23953442-23954566	1.4653	0.036239
-	chr15:102672240-102674467	1.46582	0.001103
-	chr1:51940695-51941080	1.46638	0.001103
-	chr7:24529216-24530409	1.46787	0.039212
-	chr14:55539334-55540175	1.46906	0.045814
-	chr2:59610111-59610488	1.47049	0.001103
-	chr1:64122003-64123564	1.47455	0.001103
-	chr7:73618649-73620525	1.47774	0.001103
-	chr2:144165679-144166901	1.48283	0.007637
-	chr5:31220766-31223386	1.49542	0.001103
-	chr11:83471224-83472998	1.49917	0.001984
-	chr1:180849089-180850843	1.50265	0.001984
-	chr4:126102395-126103898	1.50827	0.001103
-	chr3:108911864-108913111	1.5101	0.007069
-	chr17:45164025-45164172	1.51697	0.007069
-	chr2:69591416-69592652	1.52037	0.029708
-	chr5:111329116-111330544	1.52148	0.009141
-	chr9:7837193-7839336	1.52181	0.001103
-	chr13:17805508-17806582	1.52294	0.005924
-	chrX:165680375-165680531	1.52871	0.001103
-	chr18:20549002-20549169	1.53	0.001103
-	chr15:34080426-34082594	1.53327	0.005924
-	chr15:38198586-38199718	1.53541	0.042045
-	chr5:95974094-95974432	1.54059	0.001103
-	chr8:83606578-83607929	1.54259	0.022438
-	chr13:75648132-75648399	1.54338	0.001103
-	chr8:85025603-85026740	1.54911	0.004143
-	chr6:4359402-4359551	1.5523	0.013321
-	chr13:98613419-98613598	1.55268	0.001103
-	chr4:10854928-10855270	1.55697	0.001984
-	chr5:16981096-16981303	1.55746	0.001103
-	chr4:95052749-95054049	1.55816	0.004143
-	chr13:44728888-44729647	1.55862	0.020393
-	chr9:20606302-20607244	1.5608	0.012039

-	chr9:95512086-95514174	1.56472	0.001103
-	chr13:77669042-77669145	1.5668	0.001103
-	chr5:129018130-129019671	1.56895	0.012039
-	chr1:152729964-152730573	1.57326	0.001103
-	chr6:149353380-149353524	1.58094	0.001103
-	chr2:129196827-129198378	1.58443	0.001103
-	chr1:111805193-111805325	1.58744	0.001103
-	chr3:35536972-35537272	1.58765	0.001103
-	chr2:167777555-167781230	1.59014	0.001103
-	chr17:10333853-10336091	1.59521	0.011101
-	chr4:34940964-34941217	1.59606	0.005924
-	chr7:16048439-16049238	1.60049	0.010606
-	chr1:134362092-134363207	1.60191	0.027585
-	chr16:91647049-91647663	1.6026	0.040096
-	chr13:14039690-14041342	1.60282	0.003497
-	chr9:115310988-115311923	1.60718	0.023465
-	chr1:52112861-52113711	1.61006	0.008667
-	chr13:64703156-64703444	1.61073	0.001103
-	chr3:32395569-32396888	1.61357	0.046084
-	chr7:43506924-43507344	1.61854	0.001103
-	chr15:76523566-76526378	1.62129	0.001103
-	chr11:97782501-97783650	1.62692	0.008667
-	chr2:55404880-55405814	1.62974	0.004143
-	chrX:131037596-131038757	1.63019	0.008667
-	chr15:81858434-81859136	1.6307	0.023804
-	chr7:16615534-16618539	1.6317	0.001103
-	chr6:29346611-29347736	1.63262	0.001103
-	chr11:83290674-83291555	1.63847	0.027894
-	chr6:72900384-72902704	1.63885	0.001103
-	chr14:62540394-62540795	1.64009	0.001103
-	chr19:32867483-32868534	1.64387	0.001103
-	chr11:20113466-20114320	1.64489	0.010606
-	chr11:72688844-72689884	1.64562	0.009618
-	chr13:91808227-91809273	1.64753	0.027585
-	chr2:104821159-104821712	1.65033	0.001103
-	chr2:140066888-140068595	1.65264	0.004796
-	chr5:125392240-125393149	1.65801	0.048636
-	chr6:58091565-58091712	1.66405	0.005364
-	chr5:142821739-142822382	1.66434	0.01449
-	chr2:32271913-32272184	1.66486	0.001103
-	chr1:72805184-72806125	1.66498	0.001103

-	chr13:3139114-3139519	1.66754	0.010123
-	chr1:77066639-77066794	1.66762	0.001103
-	chr10:73202534-73202853	1.66866	0.001103
-	chr1:151520598-151520757	1.6751	0.001103
-	chr12:110696838-110697507	1.67514	0.032233
-	chr2:69721600-69722761	1.67575	0.009618
-	chr5:29194265-29195776	1.678	0.001984
-	chr18:50208988-50209147	1.67813	0.001103
-	chr15:77971146-77972271	1.68563	0.004143
-	chrX:78855464-78855874	1.69385	0.004796
-	chr5:43948235-43949246	1.69581	0.023804
-	chr16:91513952-91514128	1.70455	0.001103
-	chr3:108240241-108241886	1.70458	0.034803
-	chr19:24901586-24902761	1.7057	0.013733
-	chrX:74007122-74007375	1.70815	0.001103
-	chr2:86325790-86325927	1.71169	0.001103
-	chr13:77670296-77670434	1.71973	0.001103
-	chr1:101386086-101386353	1.72035	0.001103
-	chr6:47813776-47815102	1.72118	0.002761
-	chr16:65793764-65793927	1.7212	0.004143
-	chr10:91171965-91172725	1.72144	0.002761
-	chr2:104820276-104820437	1.72207	0.001103
-	chr11:33163353-33164543	1.7305	0.004143
-	chr4:70535357-70536542	1.73734	0.005924
-	chr2:28477092-28477578	1.74066	0.001103
-	chr1:71709715-71709870	1.74227	0.001103
-	chrX:20528302-20528459	1.74447	0.001103
-	chr7:97370845-97371523	1.74451	0.015721
-	chr16:30061984-30063254	1.76014	0.04114
-	chr12:80114478-80115351	1.76691	0.04943
-	chr4:140698617-140701273	1.76746	0.001103
-	chr3:63173128-63173326	1.7764	0.001103
-	chr12:31018684-31018811	1.77886	0.001103
-	chr11:100318622-100319722	1.78112	0.010123
-	chr19:36924394-36926015	1.7853	0.003497
-	chr14:19351418-19351601	1.79327	0.001103
-	chr18:57119793-57119920	1.79483	0.036002
-	chr1:17399372-17399560	1.79613	0.007069
-	chr2:92055601-92056507	1.7994	0.04812
-	chr5:65698470-65699588	1.79963	0.007069
-	chrX:60426185-60426362	1.80354	0.001103

-	chr13:58129100-58130292	1.80425	0.001103
-	chr11:111276052-111276182	1.80549	0.001103
-	chr14:13902040-13902289	1.81552	0.001103
-	chr10:59952077-59952755	1.81646	0.018213
-	chr17:65614090-65615151	1.81657	0.045814
-	chr16:17735140-17735267	1.81717	0.046566
-	chr1:51478629-51479824	1.81793	0.002761
-	chrX:141982126-141982292	1.82536	0.001103
-	chr9:42264458-42265918	1.82897	0.006501
-	chr17:80207477-80208593	1.83148	0.043172
-	chr7:55793043-55794043	1.84908	0.021461
-	chr1:144312256-144312408	1.85537	0.001103
-	chr1:33101498-33101671	1.85773	0.001103
-	chr2:4833302-4833707	1.85789	0.001103
-	chr15:81464585-81466068	1.86061	0.011101
-	chr11:100528156-100528998	1.86956	0.042942
-	chr3:27013326-27013467	1.87225	0.017014
-	chr4:137388456-137389409	1.87292	0.042942
-	chrX:114857959-114858093	1.87544	0.001103
-	chr11:94742017-94742558	1.87771	0.001103
-	chr14:62331106-62331996	1.87889	0.044185
-	chr3:104753112-104753274	1.88201	0.001103
-	chrX:89802985-89803141	1.89893	0.001103
-	chr12:25100874-25102109	1.90264	0.045144
-	chr17:53361057-53361333	1.90414	0.03115
-	chr9:14274506-14276159	1.90423	0.040222
-	chr6:39591337-39592449	1.90683	0.016554
-	chr3:95015595-95016479	1.91411	0.035407
-	chr1:4687876-4688186	1.91633	0.001103
-	chr18:84658884-84659051	1.91805	0.001103
-	chrX:116886923-116887191	1.92294	0.004796
-	chr7:144894160-144895774	1.92561	0.001103
-	chr2:107011179-107011322	1.92633	0.012908
-	chr3:123508637-123509188	1.9286	0.036239
-	chr11:52230813-52231897	1.94267	0.03513
-	chrX:36806413-36807961	1.94291	0.001103
-	chr2:24179967-24180109	1.94421	0.001103
-	chr1:164247775-164248734	1.94551	0.017448
-	chr18:38360161-38360416	1.94668	0.004143
-	chr19:28763373-28763519	1.94756	0.001103
-	chr18:64288501-64288782	1.95683	0.001103

-	chr17:45163689-45163967	1.96373	0.038723
-	chr11:96248600-96248779	1.96822	0.001103
-	chr6:73528918-73529064	1.96897	0.001103
-	chr9:105545549-105545762	1.96967	0.001103
-	chr6:38365720-38365900	1.97559	0.032737
-	chr11:93995085-93995852	1.9781	0.038161
-	chr5:117059357-117059535	1.9788	0.001103
-	chr5:142367863-142368559	2.01278	0.024418
-	chr6:39558469-39559022	2.0203	0.009618
-	chr9:95636483-95637305	2.02126	0.043645
-	chr11:78550958-78551907	2.02175	0.008178
-	chrX:68319699-68319841	2.03223	0.001103
-	chr2:109889268-109890699	2.03709	0.029046
-	chr2:15128339-15128527	2.03746	0.001103
-	chr7:41335381-41335486	2.04956	0.01449
-	chr9:114844323-114844761	2.06786	0.045344
-	chr11:20115857-20117101	2.07571	0.007069
-	chr1:60901276-60901437	2.08523	0.001103
-	chr15:89766659-89766782	2.109	0.001103
-	chr5:146831946-146832743	2.12287	0.022171
-	chr4:146944232-146944332	2.12623	0.001103
-	chrX:90744663-90744820	2.14101	0.001103
-	chr13:8030821-8030986	2.14347	0.001103
-	chr11:79905989-79906125	2.14453	0.001103
-	chr5:123058253-123059066	2.15079	0.038943
-	chr13:119791383-119791762	2.16542	0.038943
-	chr10:51414802-51415267	2.16855	0.038943
-	chr4:73498312-73498504	2.17309	0.001103
-	chr10:5792106-5792260	2.17657	0.001103
-	chr15:99898389-99898496	2.18291	0.001103
-	chr7:7097434-7097688	2.18452	0.001103
-	chrX:140797524-140797770	2.20347	0.007637
-	chrX:77757246-77757342	2.20916	0.023465
-	chrX:106282534-106282674	2.21024	0.001103
-	chrX:94775205-94775348	2.23636	0.001103
-	chr12:24828390-24830858	2.24061	0.001103
-	chr11:6414143-6415657	2.24858	0.001103
-	chr8:4391967-4392147	2.25204	0.001103
-	chr4:52361743-52361891	2.27493	0.001103
-	chr10:59952823-59953467	2.27513	0.033016
-	chr5:46855978-46857025	2.27696	0.040415

-	chr2:4832532-4832716	2.29292	0.001103
-	chr13:78953973-78954125	2.30384	0.006501
-	chr19:37784277-37784384	2.3096	0.001103
-	chr7:104692862-104693074	2.31044	0.001103
-	chr7:116598243-116598423	2.31537	0.001103
-	chr8:19536642-19536753	2.31574	0.001103
-	chr6:7194539-7194665	2.32097	0.001103
-	chr6:71829311-71830655	2.32918	0.033779
-	chr4:148068374-148068534	2.33227	0.001103
-	chr11:100243257-100243667	2.34043	0.029356
-	chr18:79935418-79935557	2.35807	0.001984
-	chr4:98922125-98922839	2.36514	0.02598
-	chr3:37599507-37599697	2.37228	0.010123
-	chr9:99946596-99946764	2.37342	0.018213
-	chr5:142852772-142853150	2.374	0.040675
-	chr1:33372847-33372987	2.3792	0.004143
-	chrX:60483598-60807993	2.38083	0.001103
-	chr15:45979397-45979548	2.38899	0.001103
-	chr4:119294918-119295766	2.39199	0.019362
-	chr17:50227661-50227831	2.39392	0.001103
-	chr11:83299062-83299530	2.39576	0.022171
-	chrX:91887838-91887950	2.40122	0.001103
-	chr2:149356923-149357034	2.40145	0.001103
-	chr7:99358898-99360254	2.41427	0.037349
-	chr17:20570374-20570535	2.44155	0.038161
-	chr5:62004383-62004524	2.44335	0.001103
-	chr7:14307862-14307987	2.46089	0.036555
-	chr7:11845276-11845387	2.50775	0.001103
-	chr2:71367648-71389077	2.51586	0.047876
-	chr11:15049205-15049321	2.52981	0.001103
-	chrX:77757531-77757759	2.53286	0.014135
-	chr16:23718457-23718572	2.53476	0.018586
-	chrX:76919952-76920072	2.53666	0.001103
-	chr7:17686166-17686304	2.54056	0.001103
-	chrX:48010008-48010193	2.55573	0.001103
-	chr2:111182621-111182780	2.55629	0.010123
-	chr17:73870713-73870846	2.56105	0.003497
-	chrX:108893479-108893585	2.57209	0.015296
-	chr15:71310413-71310564	2.57362	0.026681
-	chrX:91887583-91887695	2.585	0.001984
-	chr15:37171394-37171632	2.58566	0.001103

-	chr1:24595238-24595420	2.58719	0.001103
-	chr3:67607454-67607779	2.62348	0.0273
-	chr16:51363678-51363879	2.63384	0.001103
-	chr2:86328167-86328318	2.63519	0.009141
-	chr8:19537774-19537962	2.63669	0.001103
-	chr10:119090817-119090917	2.64469	0.016554
-	chr18:28188358-28188503	2.64987	0.001103
-	chrX:60483598-60807993	2.67167	0.001103
-	chr3:69716974-69717133	2.69908	0.001103
-	chrX:13302244-13302402	2.72137	0.001103
-	chr15:37172172-37172286	2.73691	0.011101
-	chrX:36213541-36213680	2.75248	0.001103
-	chr3:65968898-65968995	2.75457	0.019362
-	chr16:28951309-28951415	2.75626	0.001984
-	chr18:4485104-4485214	2.76269	0.005924
-	chr17:37842327-37842446	2.76587	0.001103
-	chr17:15846395-15846507	2.77806	0.005924
-	chr13:74533833-74533948	2.77915	0.001103
-	chr14:33213263-33213364	2.78397	0.001103
-	chr10:58757362-58757485	2.7987	0.005924
-	chr5:142622654-142622779	2.82212	0.001103
-	chr3:59431738-59431880	2.82982	0.001103
-	chr9:3495535-3495677	2.83013	0.015296
-	chr12:25099127-25099454	2.83913	0.04628
-	chr16:93630112-93630226	2.84453	0.020734
-	chr18:84659678-84659834	2.84691	0.001103
-	chr8:40855573-40855699	2.85104	0.04943
-	chr9:26960904-26961022	2.92627	0.005364
-	chr1:191992848-191992991	2.93307	0.001103
-	chr3:57362598-57362733	2.9421	0.001103
-	chr3:107631854-107632599	2.96617	0.04628
-	chr16:45205370-45205504	2.97082	0.049647
-	chr12:109540174-109540814	2.98365	0.04628
-	chr14:60141337-60141461	3.00512	0.001103
-	chr8:104845665-104845769	3.01518	0.013321
-	chr11:48996959-48997061	3.02097	0.01449
-	chr14:74297967-74298075	3.02396	0.001103
-	chr11:34833740-34835895	3.02928	0.002761
-	chr1:55127977-55128115	3.08939	0.013321
-	chrX:13303919-13304067	3.09451	0.001103
-	chr2:110209294-110209437	3.09829	0.001103

-	chr12:70823882-70824985	3.1017	0.040675
-	chr4:10853714-10853889	3.10531	0.001103
-	chr1:89049087-89049199	3.12271	0.013321
-	chr3:65613855-65614075	3.12736	0.009618
-	chr13:3138930-3139041	3.15054	0.013321
-	chr2:142577083-142577252	3.20222	0.038943
-	chr4:143460099-143460212	3.23329	0.001103
-	chr2:87333831-87333952	3.25181	0.044631
-	chr6:79541406-79541541	3.27795	0.049211
-	chr6:7194971-7195086	3.27853	0.049884
-	chr17:37842030-37842141	3.32808	0.009618
-	chr2:147642931-147643032	3.33003	0.001103
-	chr16:23050623-23050746	3.34296	0.001103
-	chr7:52755408-52755509	3.34362	0.009141
-	chr13:58546281-58546384	3.381	0.001103
-	chr14:120713290-120713427	3.39064	0.001103
-	chr1:27991041-27991195	3.39678	0.001103
-	chr5:100513237-100513368	3.41181	0.034803
-	chrX:109390401-109390496	3.42242	0.008178
-	chr6:117473188-117473309	3.43593	0.036002
-	chr9:3497050-3497157	3.436	0.001103
-	chrX:60045122-60045236	3.4454	0.028719
-	chr13:97015008-97015134	3.52559	0.001984
-	chr19:11438294-11438491	3.53981	0.008667
-	chr4:10946588-10946687	3.68159	0.008178
-	chr7:25792722-25792845	3.69701	0.005364
-	chr1:43887989-43888102	3.70033	0.001103
-	chr4:52900649-52900764	3.70393	0.001103
-	chr1:14550776-14550883	3.7342	0.032737
-	chr11:58097119-58097236	3.75938	0.032737
-	chrX:85793229-85793452	3.7595	0.024418
-	chr17:50228085-50228197	3.78372	0.005364
-	chr5:137928628-137928767	3.78918	0.007069
-	chr7:41326383-41326504	3.81308	0.027585
-	chr15:56414802-56414905	3.81341	0.004796
-	chr2:50522888-50523003	3.83666	0.005364
-	chr18:20548675-20548788	3.8378	0.001103
-	chr2:172100871-172100996	3.87478	0.005364
-	chr3:90760929-90761046	3.90302	0.004143
-	chr7:41048716-41048822	3.94659	0.024418
-	chr4:59162886-59163008	3.96784	0.001103

-	chr13:101349017-101349118	4.01117	0.001103
-	chr3:98821083-98821190	4.04647	0.002761
-	chr7:125547973-125548172	4.0624	0.002761
-	chr15:37171878-37171989	4.17182	0.024152
-	chr6:109126188-109126284	4.21118	0.024152
-	chr9:79346923-79347034	4.25135	0.001103
-	chr17:41102021-41102121	4.38416	0.024152
-	chr15:44281892-44282061	4.44334	0.033779
-	chr11:60816475-60816570	1000	0.001103
-	chr17:53196690-53196823	1000	0.001103
-	chr2:154789851-154790396	1000	0.001103
-	chr3:57963314-57963411	1000	0.001103
-	chr4:56643774-56644303	1000	0.001103
-	chr5:125465001-125465663	1000	0.001103
-	chr9:32369156-32369533	1000	0.001103

Table 9.2: List of statistically significant changes in intergenic regions following *Skiv2l2* knockdown in P19 cells. Cuffdiff results were filtered based on M and q. Intergenic regions (loci with no geneID) with M greater than .58 and q-values less than .05 were considered elevated. Intergenic regions (loci with no geneID) with M or less than -.58 and q less than .05 were considered downregulated.

9.3 Transcripts of interest dysregulated following *Skiv2l2* knockdown in P19 cells

Gene ID	Gene Symbol	RNA levels in Skiv2l2 knockdown cells
NR_035500	mir1983	accumulating
NR_030451	mir681	accumulating
NR_024198	RPRl3	accumulating
NR_030484	Mir703	accumulating
NR_002898	snoRNA65	accumulating
NR_033595	Gm13498	accumulating
NR_002899	snoRNA70	accumulating
NR_046233	Rn45s	accumulating
NR_002142	A930003A15Rik	accumulating
NR_028515	Snora78	accumulating
NR_001460	Rmrp	accumulating
NR_002897	Snora64	accumulating
NR_045268	2810013P06Rik	accumulating
NR_029432	1500015A07Rik	accumulating
NR_027059	Snhg20	accumulating
NR_045618	Gm9958	accumulating

NR_028078	Snora21	accumulating
NR_045289	RAB26	accumulating
NR_027923	C630043F03Rik	accumulating
NR_036602	4933421O10Rik	accumulating
NR_027987	C030016D13Rik	accumulating
NR_030677	BC025920	accumulating
NR_004432	Rnu12	accumulating
NR_040469	5031425E22Rik	accumulating
NR_030695	B330016D10Rik	accumulating
NR_003363	Gm6548	accumulating
NR_040708	E130102H24Rik	accumulating
NR_024078	Btbd19	accumulating
NR_024068	Snhg7	accumulating
NR_015601	Fam120aos	accumulating
NR_028421	D430020J02Rik	accumulating
NR_015552	5330434G04Rik	accumulating
NR_026848	C030034I22Rik	accumulating
NR_015510	4632427E13Rik	accumulating
NR_029440	2010320M18Rik	accumulating
NR_029441	2810454H06Rik	accumulating
NR_003964	Tubb2a-ps2	accumulating
NR_004445	Snord22	accumulating
NR_030711	Mir22hg	accumulating
NR_027446	A230072C01Rik	accumulating
NR_027958	D930048N14Rik	accumulating
NR_015476	1500011K16Rik	accumulating
NR_033601	4930519F09Rik	accumulating
NR_033599	Gm6682	accumulating
NR_027009	Gt(ROSA)26Sor	accumulating
NR_033215	3000002C10Rik	accumulating
NR_033780	2810001G20Rik	accumulating
NR_033619	Gm6623	accumulating
NR_130973	H19	downregulated
NR_038037	E130307A14Rik	downregulated
NR_040286	Gm11627	downregulated
NR_033641	Crnde	downregulated
NR_028428	2610005L07Rik	downregulated
NR_102690	M-phase phosphoprotein 9 (Mphosph9)	downregulated
NR_131212	Neat1	downregulated
NR_015517	5930412G12Rik	downregulated
NR_028263	B130006D01Rik	downregulated

NR_015555	4933404O12Rik	downregulated
NR_004442	Gm15421	downregulated
NR_015488	A930003A15Rik	downregulated

Table 9.3: Non-coding RNAs dysregulated in P19 cells following *Skiv2l2* knockdown. RNA levels were deemed as accumulating if M>0.3 and downregulated if M<-0.3. For all M values, q <0.05.

Gene ID	Gene Symbol	RNA levels in Skiv2l2 knockdown cells
NM_018853	Rplp1	upregulated
NM_011290	Rpl6	upregulated
NM_025587	Rps21	upregulated
NM_025592	Rpl35	upregulated
NM_013765	Rps26	upregulated
NM_009077	Rpl18	upregulated
NM_022891	Rpl23	upregulated
NM_013721	Rpl7a	upregulated
NM_001048057	Rpl38	upregulated
NR_038063	Rplp2-ps1	upregulated
NM_026020	Rplp2	upregulated
NM_018730	Rpl36	upregulated
NM_011300	Rps7	upregulated
NM_020600	Rps14	upregulated
NM_025963	Rps10	upregulated
NM_016959	Rps3a1	upregulated
NM_001271590	Rpl37rt	upregulated
NM_023372	Rpl38	upregulated
NM_019865	Rpl36a	upregulated
NM_007475	Rplp0	upregulated
NM_023133	Rps19	upregulated
NM_026768	Mrps18a	upregulated
NM_026055	Rpl39	downregulated
NM_009096	Rps6	downregulated
NM_016980	Rpl5	downregulated
NM_025586	Rpl15	downregulated
NM_016738	Rpl13	downregulated
NM_026517	Rpl22l1	downregulated

Table 9.4: Ribosomal protein mRNAs dysregulated in P19 cells following *Skiv2l2* knockdown. RNA levels were deemed as accumulating if M>0.3 and downregulated if M<-0.3. For all M values, q <0.05.

CHAPTER X: BIBLIOGRAPHY

Akamatsu S, Wyatt AW, Lin D, Lysakowski S, Zhang F, Kim S, Tse C, et al. The Placental Gene PEG10 Promotes Progression of Neuroendocrine Prostate Cancer. Cell Reports. 12.6 (2015): 922-936.

Allmang C, Petfalski E, Podtelejnikov A, Mann M, Tollervey D, Mitchell P. The yeast exosome and human PM-Scl are related complexes of 3'→5′ exonucleases. Genes and Development.13.16(1999): 2148–2158.

Andersen K, T. H. Jensen, and D. E. Brodersen. Take the A Tail--Quality Control of Ribosomal and Transfer RNA. Biochimica et biophysica acta 1779.9 (2008): 532-7.

Anokye-Danso F, et al. Highly Efficient miRNA-Mediated Reprogramming of Mouse and Human Somatic Cells to Pluripotency. Cell stem cell 8.4 (2011): 376-88.

Baciu C, et al. The LO-BaFL Method and ALS Microarray Expression Analysis. BMC bioinformatics 13 (2012): 244,2105-13-244.

Barre A, De La. Core Histone N-termini Play an Essential Role in Mitotic Chromosome Condensation. The EMBO Journal 19.3 (2000): 379-91.

Bartel, D. P. MicroRNAs: Genomics, Biogenesis, Mechanism, and Function. Cell 116.2 (2004): 281-97.

Beaulieu, Y. B., et al. Polyadenylation-Dependent Control of Long Noncoding RNA Expression by the Poly(A)-Binding Protein Nuclear 1. PLoS genetics 8.11 (2012): e1003078.

Bensaude O. Inhibiting eukaryotic transcription. Transcription. 2.3 (2011): 103-108.

Berndt, H., et al. Maturation of Mammalian H/ACA Box snoRNAs: PAPD5-Dependent Adenylation and PARN-Dependent Trimming. RNA (New York, N.Y.) 18.5 (2012): 958-72.

Bird, A. Perceptions of Epigenetics. Nature 447.7143 (2007): 396-8.

Boele, J., et al. PAPD5-Mediated 3' Adenylation and Subsequent Degradation of miR-21 is Disrupted in Proliferative Disease. Proceedings of the National Academy of Sciences of the United States of America 111.31 (2014): 11467-72.

Bohnsack, MT, Tollervey D. and Granneman S. Identification of RNA helicase target sites by UV crosslinking and analysis of cDNA (CRAC). Meth. Enz. 511 (2012): 275-288.

Boisvert, F. M., et al. The Multifunctional Nucleolus. Nature reviews. Molecular cell biology 8.7 (2007): 574-85.

Bühler M, Spies N, Bartel DP, Moazed D. TRAMP-mediated RNA surveillance prevents spurious entry of RNAs into the Schizosaccharomyces pombe siRNA pathway. Nature Structural and Molecular Biology. 15(2008): 1015 – 1023.

Bustin S and Nolan T. Pitfalls of quantitative Real-time reverse-transcription Polymerase Chain Reaction. Journal of Molecular Biotechnology.15.3 (2004): 155-166.

Callahan KP, Butler JS. TRAMP Complex Enhances RNA Degradation by the Nuclear Exosome Component Rrp6. Journal of Biological Chemistry. 285.6 (2009): 3540-3547.

Canavan R, Bond U. Deletion of the nuclear exosome component RRP6 leads to continued accumulation of the histone mRNA HTB1 in S-phase of the cell cycle in Saccharomyces cerevisiae. Nucleic Acids Research. 35.18 (2007): 6268-6279.

Chan FL, Marshall OJ, Saffery R, et al. Active transcription and essential role of RNA polymerase II at the centromere during mitosis. *Proceedings of the National Academy of Sciences of the United States of America*. 109.6 (2012):1979-1984.

Chang G, Miao YL, Zhang Y, Liu S, Kou Z, Ding J, et al. Linking Incomplete Reprogramming to the Improved Pluripotency of Murine Embryonal Carcinoma Cell-Derived Pluripotent Stem Cells. PLoS ONE. 5.4 (2010): e10320.

Chang YF, Imam JS, and MF Wilkinson. The nonsense-mediated decay pathway. Annual Review of Biochemistry. 76 (2007):51-74.

Chen D, Dundr M, Wang C, Leung A, Lamond A, et al. Condensed mitotic chromatin is accessible to transcription factors and chromatin structural proteins. The Journal of Cell Biology. 168.1 (2004): 41.

Chen FW, Ioannou YA. Ribosomal proteins in cell proliferation and apoptosis. International reviews of Immunology. 18.5-6 (1999): 429-38.

Chen X, Xu H, Yuan P, Fang F, Huss M, Vega VB, et al. Integration of External Signaling Pathways with the Core Transcriptional Network in Embryonic Stem Cells. Cell. 133.6 (2008): 1106-1117.

Choi, E., E. Choi, and K. C. Hwang. MicroRNAs as Novel Regulators of Stem Cell Fate. World journal of stem cells 5.4 (2013): 172-87.

Choi SC, Yoon J, Shim WJ, Ro YM, Lim DS. 5-azacytidine induces cardiac differentiation of P19 embryonic stem cells. Experimental & Molecular Medicine, 2004. 36(6): p. 515-523.

Ciais, D. B. The mRNA encoding the yeast ARE-binding protein Cth2 is generated by a novel 3′ processing pathway. Nucleic Acids Research. (2008): 3075–3084.

Cinghu, S., et al. Integrative Framework for Identification of Key Cell Identity Genes Uncovers Determinants of ES Cell Identity and Homeostasis. Proceedings of the National Academy of Sciences of the United States of America 111.16 (2014): E1581-90.

Costa Y, Ding J, Theunissen TW, Faiola F, Hore TA, Shliaha PV, Fidalgo M, Saunders A, et al.NANOG-dependent function of TET1 and TET2 in establishment of pluripotency. Nature. 495.7441 (2013): 370-4.

Cox, J. A., et al. A Zebrafish SKIV2L2-Enhancer Trap Line Provides a Useful Tool for the Study of Peripheral Sensory Circuit Development. Gene expression patterns: GEP 11.7 (2011): 409-14.

Cox, J. L., et al. The SOX2-Interactome in Brain Cancer Cells Identifies the Requirement of MSI2 and USP9X for the Growth of Brain Tumor Cells. PloS one 8.5 (2013): e62857.

Costa, Yael, Junjun Ding, Thorold W. Theunissen, Francesco Faiola, Timothy A. Hore, Pavel V. Shliaha, Miguel Fidalgo, Arven Saunders, Moyra Lawrence, Sabine Dietmann, Satyabrata Das, Dana N. Levasseur, Zhe Li, Mingjiang Xu, Wolf Reik, José C. R. Silva, and Jianlong Wang. NANOG-dependent Function of TET1 and TET2 in Establishment of Pluripotency. Nature 495.7441 (2013): 370-74.44.

Crosio C, Fimia GM, Loury R, Kimura M, Okano Y, Zhou H, et al. Mitotic Phosphorylation of Histone H3: Spatio-Temporal Regulation by Mammalian Aurora Kinases. Molecular and Cellular Biology. 22.3 (2002): 874-885.

de la Cruz J, Kressler D, Tollervey D, Linder P. Dob1p (Mtr4p) is a putative ATP-dependent RNA helicase required for the 3' end formation of 5.8S rRNA in Saccharomyces cerevisiae. The EMBO Journal. 17.4 (1998): 1128-1140.

Dey BK, Gagan J, Dutta A. miR-206 and -486 Induce Myoblast Differentiation by Downregulating Pax7. Molecular and Cellular Biology. 31.1 (2010): 203-214.

Dikovskaya D, Cole JJ, Mason SM, Nixon C, Karim SA, McGarry L, et al. Mitotic Stress Is an Integral Part of the Oncogene-Induced Senescence Program that

Promotes Multinucleation and Cell Cycle Arrest. Cell Reports. 12.9 (2015): 1483-1496.

Dominski Z, Yang XC, Kaygun H, Dadlez M, Marzluff WF. A 3′ Exonuclease that Specifically Interacts with the 3′ End of Histone mRNA. Molecular Cell. 12.2 (2003): 295-305.

Donati G, Montanaro L, Derenzini M. Ribosome Biogenesis and Control of Cell Proliferation: p53 Is Not Alone. Cancer Research. 72.7 (2012): 1602-1607.

Dong D, Meng L, Yu Q, Tan G, Ding M, Tan Y. Stable Expression of FoxA1 Promotes Pluripotent P19 Embryonal Carcinoma Cells to Be Neural Stem-Like Cells. gene expr. 15.4 (2012): 153-162.

Dorweiler JE, Ni T, Zhu J, Munroe SH, Anderson JT. Certain Adenylated Non-Coding RNAs, Including 5′ Leader Sequences of Primary MicroRNA Transcripts, Accumulate in Mouse Cells following Depletion of the RNA Helicase MTR4. PLoS ONE. 9.6 (2014): e99430.

Eberle AB, Jordán-Pla A, Gañez-Zapater A, Hessle V, Silberberg G, von Euler A, et al. An Interaction between RRP6 and SU(VAR)3-9 Targets RRP6 to Heterochromatin and Contributes to Heterochromatin Maintenance in Drosophila melanogaster. PLOS Genetics. 2015.

Engelen E, Akinci U, Bryne JC, Hou J, Gontan, C, et al. Sox2 cooperates with Chd7 to regulate genes that are mutated in human syndromes. Nature Genetics. 43 (2011): 607-611.

Farhy, C, et al. Pax6 is required for normal cell-cycle exit and the differentiation kinetics of retinal progenitor cells. PLoS One (2013): 8, 9, e76489.

Fazzio, T. G., J. T. Huff, and B. Panning. An RNAi Screen of Chromatin Proteins Identifies Tip60-p400 as a Regulator of Embryonic Stem Cell Identity. Cell 134.1 (2008): 162-74.

Fei, T., et al. Genome-Wide Mapping of SMAD Target Genes Reveals the Role of BMP Signaling in Embryonic Stem Cell Fate Determination. Genome research 20.1 (2010): 36-44.

Fujiwara N, Shigemoto M, Masuda S. A Dual function of MPP6 to stimulate the nuclear exosome. Poster presentation at RNA Meeting 2016. Kyoto, Japan, 2016.

Freije A, Molinuevo R, Ceballos L, Cagigas M, Alonso-Lecue P, Rodriguez R, et al. Inactivation of p53 in Human Keratinocytes Leads to Squamous Differentiation and Shedding via Replication Stress and Mitotic Slippage. Cell Reports. 9.4 (2014): 1349-1360.

Graham AC, Kiss DL, Andrulis ED. Core Exosome-independent Roles for Rrp6 in Cell Cycle Progression. Molecular Biology of the Cell. 20.8 (2009): 2242-2253.

Ghosal, S., S. Das, and J. Chakrabarti. Long Noncoding RNAs: New Players in the Molecular Mechanism for Maintenance and Differentiation of Pluripotent Stem Cells. Stem cells and development 22.16 (2013): 2240-53.

Groth, Anja, Dominique Ray-Gallet, Jean-Pierre Quivy, Jiri Lukas, Jiri Bartek, and Geneviève Almouzni. Human Asf1 Regulates the Flow of S Phase Histones during Replicational Stress. Molecular Cell 17.2 (2005): 301-11.

Gui MC, Chen B, Yu SS, Bu BT. Effects of suppressed autophagy on mitochondrial dynamics and cell cycle of N2a cells. Journal of Huazhong University of Science and Technology [Medical Sciences]. 34.2 (2014): 157-160.

Günesdogan U, Jäckle H, Herzig A. Histone supply regulates S phase timing and cell cycle progression. eLife, 2014.

Gunjan, Akash, Johanna Paik, and Alain Verreault. Regulation of Histone Synthesis and Nucleosome Assembly. Biochimie 87.7 (2005): 625-35.

Gunjan, Akash, and Alain Verreault. A Rad53 Kinase-Dependent Surveillance Mechanism That Regulates Histone Protein Levels in S. Cerevisiae. Cell, 2003. 115.5: 537-49.

Guo, Y., et al. Quantitative Proteomics Analysis of the cAMP/protein Kinase A Signaling Pathway. Biochemistry. 51.46 (2012): 9323-32.

Gustafson, M. P., et al. Zcchc8 is a Glycogen Synthase Kinase-3 Substrate that Interacts with RNA-Binding Proteins. Biochemical and biophysical research communications. 338.3(2005): 1359-67.

Guttman, M, et al. lincRNAs act in the circuitry controlling pluripotency and differentiation. Nature. 477(2011): 295-200.

Hawkins PG, Morris KV. Transcriptional regulation of Oct4 by a long non-coding RNA antisense to Oct4-pseudogene 5.Transcr. 1(2010):165–175.

He S, Nakada D, Morrison SJ. Mechanisms of Stem Cell Self-Renewal. Annual Review of Cell and Developmental Biology. 25(2009): 377-406.

Heras, Sara R., Sara Macias, Javier F. Cáceres, and Jose L. Garcia-Perez. Control of Mammalian Retrotransposons by Cellular RNA Processing Activities. Mobile Genetic Elements. 4.2(2014).

Hiriart E, Vavasseur A, Touat-Todeschini L, Yamashita A, Gilquin B, et al. Mmi1RNA surveillance machinery directs RNAi complex RITS to specific meiotic genes in fission yeast. The EMBO Journal. 31.10 (2012):2296-308.

Hirsch CL, Akdemir C, Wang L, Javakumaran G, Trcka D, Weiss A, et al. Myc and SAGA rewire an alternative splicing network during early somatic cell reprogramming. Genes and Development. 29.8 (2015): 803-816.

Houseley, J., J. LaCava, and D. Tollervey. RNA-Quality Control by the Exosome. Nature reviews. Molecular cell biology 7.7 (2006): 529-39.

Hu, M., et al. Using Poisson Mixed-Effects Model to Quantify Transcript-Level Gene Expression in RNA-Seq. Bioinformatics (Oxford, England) 28.1 (2012): 63-8.

Hultman, K. A., and S. L. Johnson. Differential Contribution of Direct-Developing and Stem Cell-Derived Melanocytes to the Zebrafish Larval Pigment Pattern. Developmental biology 337.2 (2010): 425-31.

Hutchins AP, Poulain S, Miranda-Saavedra D. Genome-wide analysis of STAT3 binding in vivo predicts effectors of the anti-inflammatory response in macrophages. Blood, 2012. 119(13): e110-e119.

Iwanami, N., et al. Ethylnitrosourea-Induced Thymus-Defective Mutants Identify Roles of KIAA1440, TRRAP, and SKIV2L2 in Teleost Organ Development. European journal of immunology 39.9 (2009): 2606-16.

Jackson, R. N., et al. The Crystal Structure of Mtr4 Reveals a Novel Arch Domain Required for rRNA Processing. The EMBO journal 29.13 (2010): 2205-16.

Jarmoskaite I, Russell R. DEAD-box proteins as RNA helicases and chaperones. *Wiley interdisciplinary reviews RNA*. 2.1 (2011):135-152.

Jasmin DC, Spray DC, Campos de Carvalho AC, Mendez-Otero R. Chemical Induction of Cardiac Differentiation in P19 Embryonal Carcinoma Stem Cells. Stem Cells and Development. 19.3 (2010): 403-412.

Jeon, W. B., et al. Functional Enhancement of Neuronal Cell Behaviors and Differentiation by Elastin-Mimetic Recombinant Protein Presenting Arg-Gly-Asp Peptides. BMC biotechnology 12 (2012): 61,6750-12-61.

Jia H, Wang X, Anderson JT, Jankowsky E. RNA unwinding by the Trf4/Air2/Mtr4 polyadenylation (TRAMP) complex. Proceedings of the National Academy of Sciences. 109.19 (2012): 7292-7297.

Jia H, Wang X, Liu F, Guenther UP, Srinivasan S, Anderson JT, Jankowsky E. The RNA Helicase Mtr4p Modulates Polyadenylation in the TRAMP Complex. Cell. 145 (2011):890–901.

Johnson SJ, Jackson RN. Ski2-like RNA helicase structures: Common themes and complex assemblies. RNA Biology.10.1 (2013):33-43.

Jonkers J, Korswagen HC, Acton D, Breuer M, Berns A. Activation of a novel proto-oncogene, Frat1, contributes to progression of mouse T-cell lymphomas. The EMBO Journal.16.3 (1997):441-450.

Kadaba S, Krueger A, Trice T, Krecic AM, Hinnebusch AG, Anderson J. Nuclear surveillance and degradation of hypomodified initiator tRNAMet in S. cerevisiae. Genes and Development. 18.11 (2004):1227-40.

Kallen AN, Zhou XB, Xu J, Qiao C, Ma J, Yan L, Lu L, Liu C, Yi JS, Zhang H, Min W, Bennett AM, Gregory RI, Ding Y, Huang Y. The imprinted H19 lncRNA antagonizes let-7 microRNAs. Molecular Cell. 52.1(2014): 101-12.

Kaygun H, Marzluff WF. Regulated degradation of replication-dependent histone mRNAs requires both ATR and Upf1. Nat Struct Mol Biol. 12.9 (2005): 794-800.

Kaygun H, Marzluff WF. Translation Termination Is Involved in Histone mRNA Degradation when DNA Replication Is Inhibited. Molecular and Cellular Biology. 25.16 (2005): 6879-6888.

Kaygun H., Marzluff W.F. Upf1 functions in regulation of mammalian histone mRNA decay. In: Maquat L.E., editor. Landes Bioscience; Georgetown, TX (2006): 237–252.

Kimura SH, Ikawa M, Ito A, Okabe M, Nojima H. Cyclin G1 is involved in G2/M arrest in response to DNA damage and in growth control after damage recovery. Oncogene. 20.25 (2001): 3290-3300.

Kong KY, T. H. Cotranscriptional recruitment of yeast TRAMP complex to intronic sequences promotes optimal pre-mRNA splicing. Nucleic Acids Research. (2014): 643-60.

Koseoglu MM, Graves LM, Marzluff WF. Phosphorylation of threonine 61 by cyclin a/Cdk1 triggers degradation of stem-loop binding protein at the end of S phase. Molecular Cell Biology. 28.14 (2008): 4469-79.

Krishan A. Rapid flow cytofluorometric analysis of mammalian cell cycle by propidium iodide staining. *The Journal of Cell Biology*. 66.1(1975): 188-193.

LaCava, J., et al. RNA Degradation by the Exosome is Promoted by a Nuclear Polyadenylation Complex. Cell. 121.5(2005): 713-24.

Lange H, Sement FM, Gagliardi D. MTR4, a putative RNA helicase and exosome co-factor, is required for proper biogenesis and development in Arabidopsis thaliana. The Plant Journal. 68(2011): 51-63.

Lam, M. T., et al. Enhancer RNAs and Regulated Transcriptional Programs. Trends in biochemical sciences. 39.4 (2014) : 170-82.

Lanzotti DJ, Kaygun H, Yang X, Duronio RJ, Marzluff WF. Developmental Control of Histone mRNA and dSLBP Synthesis during Drosophila Embryogenesis and the Role of dSLBP in Histone mRNA 3' End Pr ocessing In Vivo. Molecular and Cellular Biology. 22.7 (2002): 2267-2282.

Lee, N. N., et al. Mtr4-Like Protein Coordinates Nuclear RNA Processing for Heterochromatin Assembly and for Telomere Maintenance, Cell. 2013. 155.5: 1061-74.

Lee T, Di Paola D, Malina A, Mills JR, Kreps A, et al. Suppression of the DHX9 Helicase Induces Premature Senescence in Human Diploid Fibroblasts in a p53-dependent Manner. The Journal of Biological Chemistry, 2014. 289, 22798-22814.

Lima, RM, Alvarez LD, Costa MF, Costa SL, Clarêncio J, El-Bachá RS. Cytotoxic effects of catechol to neuroblastoma N2a cells. General physiology and biophysics. 27.4 (2008): 306-14.

Lejeune F, Li X, Maquat LE. Nonsense-mediated mRNA decay in mammalian cells involves decapping, deadenylating, and exonucleolytic activities. Molecular Cell. 12.3 (2003):675-87.

Lesiak A, Pelz C, Ando H, Zhu M, Davare M, Lambert TJ, et al. A Genome-Wide Screen of CREB Occupancy Identifies the RhoA Inhibitors Par6C and Rnd3 as Regulators of BDNF-Induced Synaptogenesis. PLoS ONE. 8.6 (2013): e64658.

Leung, E. C. Integrity of SRP RNA is ensured by La and the nuclear RNA quality control machinery. Nucleic Acids Research. (2014): 10698–10710.

Li, T, Shi Y, Wang P, Guachalla LM, Sun B, Joerss T, et al.Smg6/Est1 licenses embryonic stem cell differentiation via nonsense-mediated mRNA decay. The EMBO Journal. 34.12 (2015):1630-47.

Liu A, Yu X, Liu S. Pluripotency transcription factors and cancer stem cells: small genes make a big difference. Chinese Journal of Cancer. 32.9 (2013):483-487.

Liu K, Lin B, Zhao M, Yang X, Chen M, Gao A, et al. The multiple roles for Sox2 in stem cell maintenance and tumorigenesis. Cellular Signalling. 25.5 (2013): 1264-1271.

Lou C-H, Dumdie J, Goetz A, et al. Nonsense-Mediated RNA Decay Influences Human Embryonic Stem Cell Fate. Stem Cell Reports. 6.6 (2016):844-857.

Lubas M, Andersen PR, Schein A, Dzeimbowski A, Kudla G, Jensen TH. The Human Nuclear Exosome Targeting Complex Is Loaded onto Newly Synthesized RNA to Direct Early Ribonucleolysis. Cell Reports. 10.2 (2015): 178-192.

Lubas M, Christensen MS, Kristiansen MS, Domanski M, Falkenby LG, Lykke-Andersen S, et al. Interaction Profiling Identifies the Human Nuclear Exosome Targeting Complex. Molecular Cell. 43.4 (2011): 624-637.

Lykke-Andersen J, Bennett EJ. Protecting the Proteome: Eukaryotic Cotranslational Quality Control Pathways. JCB, 2014.

Lykke-Andersen, S., D. E. Brodersen, and T. H. Jensen. Origins and Activities of the Eukaryotic Exosome. Journal of cell science 122.10 (2009): 1487-94.

Maden, M. Retinoic Acid in the Development, Regeneration and Maintenance of the Nervous System. Nature reviews. Neuroscience 8.10 (2007): 755-65.

Madon-Simon M, Cowley M, Garfield AS, Moorwood K, Bauer SR, Ward A. Antagonistic roles in fetal development and adult physiology for the oppositely imprinted Grb10 and Dlk1 genes. BMC Biology. 12(2014): 771.

Marzluff WF, Gongidi P, Woods KR, Jin J, Maltais LJ. The human and mouse replication dependent histone genes. Genomics. 80.5 (2002):487-98.

Marzluff WF, Wagner EJ, Duronio RJ. Metabolism and regulation of canonical histone mRNAs: life without a poly(A) tail. Nat Rev Genet. 9.11 (2008): 843-854.

Mateyak MK, Obaya AJ, Sedivy JM. c-Myc Regulates Cyclin D-Cdk4 and -Cdk6 Activity but Affects Cell Cycle Progression at Multiple Independent Points. Molecular and Cellular Biology. 19.7 (1999): 4672-4683.

Matsuura I, Denissova NG, Wang G, He D, Long J, Liu F. Cyclin-dependent kinases regulate the antiproliferative function of Smads. Nature. 430.6996 (2004): 226-231.

Meeks-Wagner D, Hartwell L. Normal stoichiometry of histone dimer sets is necessary for high fidelity of mitotic chromosome transmission. Cell. 44(1986): 43-52.

Meola N and Jensen TH. Identification of a decay pathway for processed transcripts within human nuclei. Poster presentation at RNA Meeting 2016. Kyoto, Japan, 2016.

Meza-Sosa, K. F., G. Pedraza-Alva, and L. Perez-Martinez. MicroRNAs: Key Triggers of Neuronal Cell Fate. Frontiers in cellular neuroscience 8 (2014): 175.

Milligan, L. T. A nuclear surveillance pathway for mRNAs with defective polyadenylation. Molecular Cell. (2005): 624–637.

Montagner A, Yart A, Dance M, Perret B, Salles J, Raynal P. A Novel Role for Gab1 and SHP2 in Epidermal Growth Factor-induced Ras Activation. The Journal of Biological Chemistry. 280(2005): 5350-5360.

Morrison SJ, Spradling AC. Stem cells and niches: mechanisms that promote stem cell maintenance throughout life. Cell. 132.4 (2008):598-611.

Mortazavi, A., et al. Mapping and Quantifying Mammalian Transcriptomes by RNA-Seq. Nature methods 5.7 (2008): 621-8.

Mullen TE, Marzluff WF. Degradation of histone mRNA requires oligouridylation followed by decapping and simultaneous degradation of the mRNA both 5' to 3' and 3' to 5'. Genes & Development. 22.1 (2008): 50-65.

Murillo-Pineda, M., M. J. Cabello-Lobato, M. Clemente-Ruiz, F. Monje-Casas, and F. Prado. Defective Histone Supply Causes Condensin-dependent Chromatin Alterations, SAC Activation and Chromosome Decatenation Impairment. Nucleic Acids Research 42.20 (2014): 12469-2482.

Nag, A., and J. A. Steitz. Tri-snRNP-Associated Proteins Interact with Subunits of the TRAMP and Nuclear Exosome Complexes, Linking RNA Decay and Pre-mRNA Splicing. RNA biology 9.3 (2012): 334-42.

Nagahama, M., et al. The AAA-ATPase NVL2 is a Component of Pre-Ribosomal Particles that Interacts with the DExD/H-Box RNA Helicase DOB1. Biochemical and biophysical research communications 346.3 (2006): 1075-82.

Narendrula R, Mispel-Beyer K, Guo B, Parissenti AM, et al. RNA disruption is associated with response to multiple classes of chemotherapy drugs in tumor cell lines. BMC Cancer. 16(2016):146.

Neumann B, Walter T, Hériché JK, Bulkescher J, Erfle H, Conrad C, et al. Phenotypic profiling of the human genome by time-lapse microscopy reveals cell division genes. Nature. 464.7289 (2010): p. 721-727.

Nilbratt M, Porras O, Marutle A, Hovatta O, Nordberg A. Neurotrophic factors promote cholinergic differentiation in human embryonic stem cell-derived neurons. Journal of Cellular and Molecular Medicine. 14.6b (2009): 1476-1484.

Nishimura K, Kumazawa T, Kuroda T, Katagiri N, Tsuchiya M, et al. Perturbation of ribosome biogenesis drives cells into senescence through 5S RNP-mediated p53 activation. Cell reports. 10.8 (2015):1310-23.

Norbury CJ. Regional Specialization: The NEXT Big Thing in Nuclear RNA Turnover. Molecular Cell. 43.4 (2011): p. 502-504.

Orth JD, Loewer A, Lahav G, Mitchison TJ. Prolonged mitotic arrest triggers partial activation of apoptosis, resulting in DNA damage and p53 induction. Doxsey S, ed. Molecular Biology of the Cell. 23.4 (2012):567-576.

Osman, B. A., et al. Localization of a Novel RNA-Binding Protein, SKIV2L2, to the Nucleus in the Round Spermatids of Mice. The Journal of reproduction and development 57.4 (2011): 457-67.

Parlato, R., and G. Kreiner. Nucleolar Activity in Neurodegenerative Diseases: A Missing Piece of the Puzzle? Journal of Molecular Medicine (Berlin, Germany) 91.5 (2013): 541-7.

Parikh, Shan. Changes in miRNA Expression in a Model of Microcephaly. Honors Scholar Theses University of Connecticut, 2010. Storrs: CT.

Pastor BM, Mostoslavky R. SIRT6: a new guardian of mitosis. Nature Structural & Molecular Biology. 23(2016): 360-362.

Pek JW, Kai T. A role for Vasa in regulating chromatin condensation in Drosophila. Current Biology. 21.1 (2011): 39-44.

Phadwal, K., A. S. Watson, and A. K. Simon. Tightrope Act: Autophagy in Stem Cell Renewal, Differentiation, Proliferation, and Aging. Cellular and molecular life sciences: CMLS 70.1 (2013): 89-103.

Phillips A, Jones CJ, Blaydes JP. The mechanisms of regulation of Hdm2 protein level by serum growth factors. FEBS Letters. 580.1 (2006): 300-304.

Pink RC, Wicks K, Caley DP, Punch EP, Jacobs L, Carter DRF. Pseudogenes: Pseudo-functional or key regulators in health and disease? RNA. 17.5(2011): 792–798.

Piskounova E, Polytarchou C, Thornton JE, LaPierre RJ, Pothoulakis C, Hagan JP, Iliopoulos D, Gregory RI. Lin28A and Lin28B inhibit let-7 microRNA biogenesis by distinct mechanisms. Cell. 147.5 (2011):1066-79.

Preker, P., et al. PROMoter uPstream Transcripts Share Characteristics with mRNAs and are Produced Upstream of all Three Major Types of Mammalian Promoters. Nucleic acids research 39.16 (2011): 7179-93.

Qureshi, I. A., and M. F. Mehler. Emerging Roles of Non-Coding RNAs in Brain Evoluction, Development, Plasticity and Disease. Nature reviews.Neuroscience 13.8 (2012): 528-41.

Rammelt C, Bilen B, Zavolan M, Keller W. PAPD5, a noncanonical poly(A) polymerase with an unusual RNA-binding motif. RNA. 17.9 (2011): 1737-1746.

Reis CC, Campbell JL. Contribution of Trf4/5 and the Nuclear Exosome to Genome Stability Through Regulation of Histone mRNA Levels in Saccharomyces cerevisiae. Genetics. 175.3 (2006): 993-1010.

Rieder CL, Maiato H. Stuck in Division or Passing through. Developmental Cell. 7.5 (2004): 637-651.

Rotenberg, M. O., M. Moritz, and J. L. Woolford Jr. Depletion of Saccharomyces Cerevisiae Ribosomal Protein L16 Causes a Decrease in 60S Ribosomal Subunits and Formation of Half-Mer Polyribosomes. Genes & development 2.2 (1988): 160-72.

Sabò A, Kress TR, Pelizzola M, de Pretis S, Gorski MM, et al. Selective transcriptional regulation by Myc in cellular growth control and lymphomagenesis. Nature. 511.7510 (2014): 488-492.

Salton, S. R., D. J. Fischberg, and K. W. Dong. Structure of the Gene Encoding VGF, a Nervous System-Specific mRNA that is Rapidly and Selectively Induced by Nerve Growth Factor in PC12 Cells. Molecular and cellular biology 11.5 (1991): 2335-49.

Sato, Noboru, Kazuhiko Hotta, Satoshi Waguri, Tohru Nitatori, Koujiro Tohyama, Yoshihide Tsujimoto, and Yasuo Uchiyama. Neuronal Differentiation of PC12 Cells as a Result of Prevention of Cell Death Bybcl-2. Journal of Neurobiology J. Neurobiol. 25.10 (1994): 1227-234.

Sanvitale, C. E., et al. A New Class of Small Molecule Inhibitor of BMP Signaling. PloS one 8.4 (2013): e62721.

Schilders G, van Dijk E, Pruijn GJM. C1D and hMtr4p associate with the human exosome subunit PM/Scl-100 and are involved in pre-rRNA processing. Nucleic Acids Research. 35.8 (2007): 2564-2572.

Schmidt K, Butler JS. Nuclear RNA surveillance: role of TRAMP in controlling exosome specificity. Wiley Interdisciplinary Reviews: RNA. 4.2(2013): 217-231.7.

Schmidt MJ, West S, Norbury CJ. The human cytoplasmic RNA terminal U-transferase ZCCHC11 targets histone mRNAs for degradation. RNA. 17.1 (2010): 39-44.

Sciortino S, Gurtner A, Manni I, et al. The *cyclin B1* gene is actively transcribed during mitosis in HeLa cells. EMBO Reports. 2.11 (2001):1018-1023.

Shcherbik, N., et al. Polyadenylation and Degradation of Incomplete RNA Polymerase I Transcripts in Mammalian Cells. EMBO reports 11.2 (2010): 106-11.

Shore D, Langowski J, Baldwin RL. DNA flexibility studied by covalent closure of short fragments into circles. PNAs. 78.8 (1981) 4833-4837.

Sidiropoulou E, Sachana M, Flaskos J, Harris W, Hargreaves AJ, Woldehiwet Z. Diazinon oxon affects the differentiation of mouse N2a neuroblastoma cells. Archives of Toxicology. 83.4 (2008): 373-380.

Singh RK, Liang D, Gajjalaiahvari UR, Kabbaj MH, Paik J, Gunjan A. Excess histone levels mediate cytotoxicity via multiple mechanisms. Cell Cycle. 9.20 (2010): 4236-4244.

Sloan, K. E., et al. The Roles of SSU Processome Components and Surveillance Factors in the Initial Processing of Human Ribosomal RNA. RNA (New York, N.Y.) 20.4 (2014): 540-50.

Slomovic, S., et al. Addition of Poly(A) and Poly(A)-Rich Tails during RNA Degradation in the Cytoplasm of Human Cells. Proceedings of the National Academy of Sciences of the United States of America 107.16 (2010): 7407-12.

Smith SB, Kiss DL, Turk E, Tartakoff AM, Andrulis ED. Pronounced and extensive microtubule defects in a Saccharomyces cerevisiae DIS3 mutant. Yeast. 28.11 (2011): 755-769.

Smith TK, Nylander KD, Schor NF. The roles of mitotic arrest and protein synthesis in induction of apoptosis and differentiation in neuroblastoma cells in culture. Developmental Brain Research, 1998. 105(2): 175-180.

Stevens FE, Beamish H, Warrener R, Gabrielli B. Histone deacetylase inhibitors induce mitotic slippage. Oncogene. 27.10 (2007): 1345-1354.

Sullivan, E. Drosophila Stem Loop Binding Protein Coordinates Accumulation of Mature Histone MRNA with Cell Cycle Progression. Genes & Development 15.2 (2001): 173-87.

Sullivan KD, Steiniger M, Marzluff WF. A core complex of CPSF73, CPSF100, and Symplekin may form two different cleavage factors for processing of poly(A) and histone mRNAS. Molecular Cell. 34.3 (2009): 322-32.

Sun, Y. J., et al. Effects of Avermectins on Neurite Outgrowth in Differentiating Mouse Neuroblastoma N2a Cells. Toxicology letters 192.2 (2010): 206-11.

Sundaram MV. Canonical RTK-Ras-ERK signaling and related alternative pathways. WormBook. (2013): 1-38.

Takahashi, K and S Yamanaka. Induction of pluripotent stem cells from mouse embryonic and adult fibroblast cultures by defined factors. Cell 126 (2006): 663-76.

Tam OH, Aravin AA, Stein P, Girard A, Murchison EP, Cheloufi S, Hodges E, Anger M, Sachidanandam R, Schultz RM, et al. Pseudogene-derived small interfering RNAs regulate gene expression in mouse oocytes. Nature.453(2008):534–538.

Tani, H., M. Torimura, and N. Akimitsu. The RNA Degradation Pathway Regulates the Function of GAS5 a Non-Coding RNA in Mammalian Cells. PloS one 8.1 (2013): e55684.

Tanenbaum, Marvin E., Noam Stern-Ginossar, Jonathan S. Weissman, and Ronald D. Vale. Regulation of MRNA Translation during Mitosis. ELife 4 (2015).

Thiebaut M, Kisseleva-Romanova E, Rougemaille M, Boulay J, Libri D. Transcription Termination and Nuclear Degradation of Cryptic Unstable Transcripts: A Role for the Nrd1-Nab3 Pathway in Genome Surveillance. Molecular Cell. 23.6 (2006): 853-864.

Tiedje C, Lubas M, Tehrani M, Menon MB, Ronkina N, Roussesau S, et al. p38MAPK/MK2-mediated phosphorylation of RBM7 regulates the human nuclear exosome targeting complex. RNA. 21.2 (2014): 262-278.

Tinguely A, Chemin G, Péron S, Sirac C, Reynaud S, Cogné M, Delpy L. Cross talk between immunoglobin heavy-chain transcription and RNA surveillance during B cell development. Molecular and cellular biology. 32.1 (2012): 107-17.

Tremblay RG, Sikorska M, Sandhu JK, Lantheir P, Ribecco-Lutkiewicz M, Bani-Yaghoub M. Differentiation of mouse Neuro 2A cells into dopamine neurons. Journal of Neuroscience Methods. 186.1 (2010): 60-67.

Tsai RY. Turning a new page on nucleostemin and self-renewal. Journal of Cell Science. 127.18 (2014): 3885-3891.

Tuck, Alex Charles, and David Tollervey. A Transcriptome-wide Atlas of RNP Composition Reveals Diverse Classes of MRNAs and LncRNAs. Cell 154.5 (2013): 996-1009.

Uhlen M, Oksvold P, Fagerberg E, Jonasson K, Forsberg M, et al. Towards a knowledge-based Human Protein Atlas. Nature Biotechnology. 28(2010): 1248-1250.

van Riggelen J, Yetil A, Felsher DW. MYC as a regulator of ribosome biogenesis and protein synthesis. Nature Reviews Cancer. 10(2010): 301-309.

Wang, L., et al. Retinoic Acid Induces CDK Inhibitors and Growth Arrest Specific (Gas) Genes in Neural Crest Cells. Development, growth & differentiation 47.3 (2005): 119-30.

Wang, M. L., S. H. Chiou, and C. W. Wu. Targeting Cancer Stem Cells: Emerging Role of Nanog Transcription Factor. OncoTargets and therapy 6 (2013): 1207-20.

Wang P, Wu T, Zhou H, Jin Q, He G, Yu H,et al. Long non-coding RNA Neat1promotes laryngeal squamous cell cancer through regulating miR-107/CDK6 pathway. Journal of experimental & clinical cancer research. 35(2016): 22.

Wang, S. W., et al. Global Role for Polyadenylation-Assisted Nuclear RNA Degradation in Posttranscriptional Gene Silencing. Molecular and cellular biology 28.2 (2008): 656-72.

Wang, Xiaoxing. Discovery of Metastatic Breast Cancer Suppressor Genes using Functional Genome Analysis. ADA566871 Vol. Boston: DANA-FARBER CANCER INST BOSTON MA, 2012.

Wang X, Jia H, Jankowsky E, Anderson JT. Degradation of hypomodified tRNAiMet in vivo involves RNA-dependent ATPase activity of the DExH helicase Mtr4p. RNA. 14.1(2007): 107-116

Wang, Y., et al. Embryonic Stem Cell-Specific microRNAs Regulate the G1-S Transition and Promote Rapid Proliferation. Nature genetics 40.12 (2008): 1478-83.

Wang Y, Medvid R, Melton C, Jaenisch R, Blelloch R. DGCR8 is essential for microRNA biogenesis and silencing of embryonic stem cell self-renewal. Nature Genetics. 39.3(2007): 380-385.

Wang ZF, K. T. Characterization of the mouse histone gene cluster on chromosome 13: 45 histone genes in three patches spread over 1Mb. Genome Research. (1996): 688-701.

Weidensdorfer D, Stöhr N, Baude A, et al. Control of c-myc mRNA stability by IGF2BP1-associated cytoplasmic RNPs. RNA. 15.1 (2009):104-115.

Weir JR, Bonneau F, Hentschel J, Conti E. Structural analysis reveals the characteristic features of Mtr4, a DExH helicase involved in nuclear RNA processing and

surveillance. Proceedings of the National Academy of Sciences. 107.27 (2010): 12139-12144.

Weng MT, Luo J. The enigmatic ERH protein: its role in cell cycle, RNA splicing and cancer. Protein Cell. 4.11 (2013): 807-12.

Wesley UV, Hatcher J, Dempsey RJ. Sphingomyelin synthase 1 regulates Neuro-2a cell proliferation and cell cycle progression through modulation of p27 expression and Akt signaling. Molecular Neurobiology. 51.3 (2015): 1530–1541.

Watanabe T, Totoki Y, Toyoda A, Kaneda M, Kuramochi-Miyagawa S, Obata Y, Chiba H, Kohara Y, Kono T, Nakano T, et al. Endogenous siRNAs from naturally formed dsRNAs regulate transcripts in mouse oocytes. Nature. 453(2008): 539–543.

Wlotzka W, Kudla G, Granneman S, Tollervey D. The nuclear RNA polymerase II surveillance system targets polymerase III transcripts. The EMBO journal.30(2011): 1790–1803.

Wu T, Zhang X, Huang X, Yang Y, Hua X. Regulation of cyclin B2 expression and cell cycle G2/M transition by menin. Journal of Biological Chemistry. 285.24 (2010): jbc.M110.106575.

Xie, Z., G. Tan, M. Ding, D. Dong, T. Chen, X. Meng, X. Huang, and Y. Tan. Foxm1 Transcription Factor Is Required for Maintenance of Pluripotency of P19 Embryonal Carcinoma Cells. Nucleic Acids Research 38.22 (2010): 8027-038.

Xu, K., et al. MiR-297 Modulates Multidrug Resistance in Human Colorectal Carcinoma by Down-Regulating MRP-2. The Biochemical journal 446.2 (2012): 291-300.

Yang, A., et al. Nucleolin Maintains Embryonic Stem Cell Self-Renewal by Suppression of p53 Protein-Dependent Pathway. The Journal of biological chemistry 286.50 (2011): 43370-82.

Yang CT, Hindes AE, Hultman KA, Johnson SL. Mutations in gfpt1 and skiv2l2 Cause Distinct Stage-Specific Defects in Larval Melanocyte Regeneration in Zebrafish. PLoS Genetics. 3.6 (2007): e88.

Yang R, Niepel M, Mitchison T, Sorger P. Dissecting Variability in Responses to Cancer Chemotherapy Through Systems Pharmacology. *Clinical pharmacology and therapeutics*. 88.1 (2010):34-38. doi:10.1038/clpt.2010.96.

Zanet, J, et al. A mitosis block links active cell cycle with human epidermal differentiation and results in endoreplication. PLoS one (2010).

Zanier, Katia, Ingrid Luyten, Catriona Crombie, Berndt Mueller, Daniel Schuemperli, Jens P. Linge, Michael Nilges, and Michael Sattler. Structure of the Histone MRNA Hairpin Required for Cell Cycle Regulation of Histone Gene Expression. Rna 8.1 (2002): 29-46.

Zhang M, Lam TT, Tonelli M, Marzluff WF, Thapar R. Interaction of the Histone mRNA Hairpin with Stem–Loop Binding Protein (SLBP) and Regulation of the SLBP–RNA Complex by Phosphorylation and Proline Isomerization. Biochemistry. 51.15 (2012): 3215-3231.

Zhao J, Kennedy BK, Lawrence BD, Barbie DA, Matera AG, Fletcher JA, Harlow E. NPAT links cyclin E-Cdk2 to the regulation of replication-dependent histone gene transcription. Genes and Development. 14.18 (2002): 2283-97.

Zhao X, McKillop-Smith S, Müller B. The human histone gene expression regulator HBP/SLBP is required for histone and DNA synthesis, cell cycle progression and cell proliferation in mitotic cells. Journal of Cell Science. 117.25 (2004): 6043-6051.

Zhang Q, Shalaby NA, Buszczak M. Changes in rRNA transcription influence proliferation and cell fate within a stem cell lineage. *Science*. 343.6168 (2014): 298-301.

Zhi F, Gong G, Xu Y, Zhu Y, Hu D, Yang Y, et al. Activated β-catenin Forces N2A Cell-derived Neurons Back to Tumor-like Neuroblasts and Positively Correlates with a Risk for Human Neuroblastoma. Int. J. Biol. Sci. 8.2 (2012): 289-297.

Zhu C, Hu DL, Liu YQ, Zhang QJ, Chen FK, Kong XQ, et al. Fabp3 Inhibits Proliferation and Promotes Apoptosis of Embryonic Myocardial Cells. Cell Biochem Biophys. 60.3 (2011): 259-266.